Appendix G: Posttest Data Correction

G.1 Data Uncertainty

Before a discussion of gage uncertainty can begin, the terms accuracy, precision, and uncertainty must be defined. As per standard practice, accuracy is defined as the deviation of an instrument's reading from a known input. Precision indicates an instrument's ability to reproduce a certain reading with a given accuracy. Uncertainty is defined as the plus or minus deviation range of a reading from the true value. In many experimental situations (certainly in the PCCV experiments), this true value is not known, however, the fairly high confidence exists in the uncertainty range.

Each gage used on the PCCV model had an associated uncertainty. Efforts were made to ensure that the level of uncertainty associated with each gage was appropriate for the magnitude of the expected data. This was done to avoid losing meaningful data because of relatively high inaccuracies of instruments.

G.2 Post Test Data Conversion and Correction

After the high pressure PCCV test was conducted, the data collected by the DAS during this final test was subjected to conversion and correction. The purpose of the conversion was to convert the data from raw form (usually volts) into engineering units. The purpose of the corrections was to correct the data for any offsets or external effects such as temperature. The specific details per instrument type are detailed in the sections below.

G.2.1 Corrections Made to Strain Gage Raw Data

Basic strain data reduction was accomplished through two major steps: 1) firmware reduction from measurements of the bridge-balancing voltages to values of strain and 2) post-test data corrections to compensate for various effects (i.e. temperature effects, transverse strain, etc.).

The first step will not be discussed here except to note that the data acquisition firmware automatically converts the voltages received from the strain gages to strain data. Therefore, for the PCCV test, the raw data from strain gages was in microstrain. The last steps (referred to here as the data corrections) are discussed in the following sections.

The least count requirement for the strain gages used in this test will be ± 0.01 % strain. The data acquisition system used in the PCCV high pressure test recorded seven significant digits for each data point. This is not meant to imply that the data was believed to be accurate to that extent. A study on the uncertainty of the data from the various instruments was performed.

The strain gage raw data obtained during the PCCV High Pressure Test was in the units of microstrain. Three types of data correction were done to the raw strain gage data. These are: corrections for gage specific gage factors, corrections for temperature effects, and corrections for transverse sensitivity.

G.2.1.1 *Instrument Specific Gage Factor Correction*

The data acquisition system (DAS) used in the PCCV High Pressure Test assumed a single gage factor for all strain gages. This factor (2.089) was determined by taking the average value of the gage factors of the strain gages used in the test. The standard practice in data acquisition is to use the value 2.0 for the gage factor while acquiring data. This value was used in the internal firmware of the DAS hardware to determine the strain values output by the system. However, each strain gage has associated with it a *specific* gage factor that is identified and provided by the manufacturer. The data from each gage was corrected, posttest, to reflect the correct GFAC for that gage.

To output strain gage readings in units of strain, the firmware must convert from the output voltage. The following equations were used.

$$\varepsilon = \frac{-4\,V_R}{GFAC(1+2V_R)} \qquad \text{(G-1)}$$

where $$V_R = \left(\frac{V_{out}}{V_S}\right)_{strained} - \left(\frac{V_{out}}{V_S}\right)_{unstrained}$$

ε = "raw" strain

Vout = output voltage of gage bridge

Vs = bridge excitation voltage

As stated above, during the acquisition of the PCCV High Pressure Test data, a single GFAC was input into Equation G-1 for all strain gages.

Post test, the gage specific GFAC for each gage was used to correct the raw data. Equation 2 below was used to accomplish this.

$$\varepsilon' = \varepsilon\left(\frac{GFAC_{general}}{GFAC_{specific}}\right) \qquad \text{(G-2)}$$

G.2.1.2 Corrections for Wire Length Change in Resistance

Because of the long lead wire lengths required for the instrumentation of the PCCV, consideration was given to correcting for changes in the GFACs due to the slight change in resistance. It was decided that this was not necessary because the strain gages were wired in a three-wire configuration, which effectively reduces lead wire resistance effects by 50% over a two-wire configuration, reducing the error to a very small value.

G.2.1.3 Corrections for Temperature Effects on the Lead Wires

Corrections to account for changes in lead wire resistance due to temperature changes over the test duration were also considered, but rejected for the reason mentioned above.

G.2.1.4 Corrections for Temperature Effects on the Strain Gages

There are two corrections that may be made for temperature effects on strain gages. The first is an adjustment of the strain gage data for apparent strain. Apparent strain is a value of strain that appears in the raw data as an artifact of the temperature at which the data was taken. This strain amount must be removed from the raw data to compensate for this effect. If the strain readings were taken at the temperature at which the strain gages were calibrated, there would be no apparent strain.

Correction for Apparent Strain

For the strain gages to be used in the PCCV test, the equation provided by the manufacturer for calculating apparent strain is a fourth order polynomial, shown below. The constants in this equation vary depending on the lot number of each strain gage.

$$\varepsilon_{apparent} = A_0 + A_1T + A_2T^2 + A_3T^3 + A_4T^4 \qquad \text{(G-3)}$$

where T = testing temperature at time data point was taken, in Celsius.

This value is then subtracted from the correction 1 value.

$$\varepsilon'' = \varepsilon' - \varepsilon_{apparent} \tag{G-4}$$

Although the strain of interest in the PCCV High Pressure Test will be that strain caused by pressure induced expansion of the model, no attempt was made to eliminate from the strain data the amount of strain caused by thermal expansion of the model.

Corrections for GFAC Temperature Effects

A correction to adjust the gage specific gage factor (GFAC) for temperature, was not done. The manufacturer provides a GFAC for each gage. This factor is determined at a temperature of 24°C. The GFAC value will change with temperature. For the temperature changes during the PCCV test, this correction affected GFAC values by much less than 1%. Therefore, although the impact of this correction was assessed post-test, this correction was not performed on the data.

G.2.1.5 Corrections for Transverse Strain Sensitivity

The final set of corrections to the strain gage data involved correcting for transverse strain sensitivity. These corrections were performed only on the rosette gage data, the strip gage data and data from any hoop/meridional gage pairs. For the strip gages, data from previously identified cross axis gages (of the type SSGH) were used in these corrections. Transverse sensitivity refers to the response of the gages due to cross axis strain.

The strip gages and hoop/meridional gage pairs were treated as a 90°, two element rosette gage. The equation used to correct for transverse sensitivity for these is:

$$\varepsilon_{corr} = \frac{(1 - \nu_o K_t)(\varepsilon'' - K_t \varepsilon''_{cross-axis})}{1 - K_t^2} \tag{G-5}$$

where ν_0 = Poisson's ratio of the material on which the manufacturer's gage factor was measured, usually 0.285

K_t = transverse sensitivity coefficient which is supplied by the gage manufacturer.

$\varepsilon''_{cross-axis}$ = the strain reading from the cross-axis gage taken at the same time as ε''. (This reading must have been corrected with the previously discussed corrections before being used here.)

G.2.1.6 Transverse Sensitivity Corrections for Rosette Gages

For the rosette gages, the following equations were used. Consider a three-gage rectangular rosette with the gage elements numbered consecutively. Elements 1 and 3 correspond to the elements that are 90° apart and element 2 is the center 45° gage.

$$\varepsilon_{1corr} = \frac{(1 - \nu_o K_t)(\varepsilon''_1 - K_t \varepsilon''_3)}{1 - K_t^2}$$

$$\varepsilon_{2corr} = \frac{(1 - \nu_o K_t)(\varepsilon''_2 - K_t(\varepsilon''_1 + \varepsilon''_3 - \varepsilon''_2))}{1 - K_t^2} \tag{G-6}$$

$$\varepsilon_{3_{corr}} = \frac{(1 - \nu_o K_t)(\varepsilon_3'' - K_t \varepsilon_1'')}{1 - K_t^2}$$

When these corrections were applied to a selected group of gages in areas of liner strain concentration, it was observed that the difference between the uncorrected and the corrected data was very small, on the order of 1%, for strains of approximately 2%. The difference becomes larger as the strains become smaller and is considerably greater for strains on the order of .05%. Because the difference is very small for the larger strains, the correction was not done.

G.2.1.8 Corrections to Rebar Strain Gages

One final correction was investigated for the strain data from gages installed on rebar. During the gage installation process, a small portion of the rebar must be ground flat to provide a suitable installation surface. This changes the cross-sectional area of the rebar at that location and the strain data should be compensated for this. A correction factor to account for this was considered, but later rejected because of inconsistent and non-reproducible results in lab experiments

G.2.2 Corrections Made to LVDT Raw Data

Linear Variable Displacement Transducers (LVDTs) output raw data that vary linearly with displacement. Data reduction for the LVDTs starts with the conversion of the raw signal (in volts) to displacement (in inches). The following single step reduction will provide the displacement of the device, either positive or negative, from its **null** (not necessarily original) position.

$$D_{null} = V_{raw_{time=t}} \left[\frac{1}{CF_{LVDT}} \right] \qquad \text{(G-7)}$$

where D_{nul} = displacement from the null position (in),

V_{raw} = raw signal from gage at time t (V),

CF_{LVDT} = LVDT calibration factor (V/in).

Note that the polarity of the output voltage is important for these measurements as the device reads in either direction around the null point that represents zero output voltage. The device will be initially spring loaded.

As shown below, for each LVDT location, the initial displacement reading ($V_{time=0}$) will be algebraically combined with each subsequent reading. The initial reading will be considered an offset. Thus, for each reading, the determination of the actual displacement of the LVDT with respect to the ***initial displacement*** is obtained as follows.

$$D = \left(V_{raw_{time=t}} - V_{raw_{time=0}} \right) \left[\frac{1}{CF_{LVDT}} \right] \qquad \text{(G-8)}$$

where D = displacement from original position (in),

V_{raw} = raw signal from gage at time indicated (V).

Figure G.1 illustrates the layout.

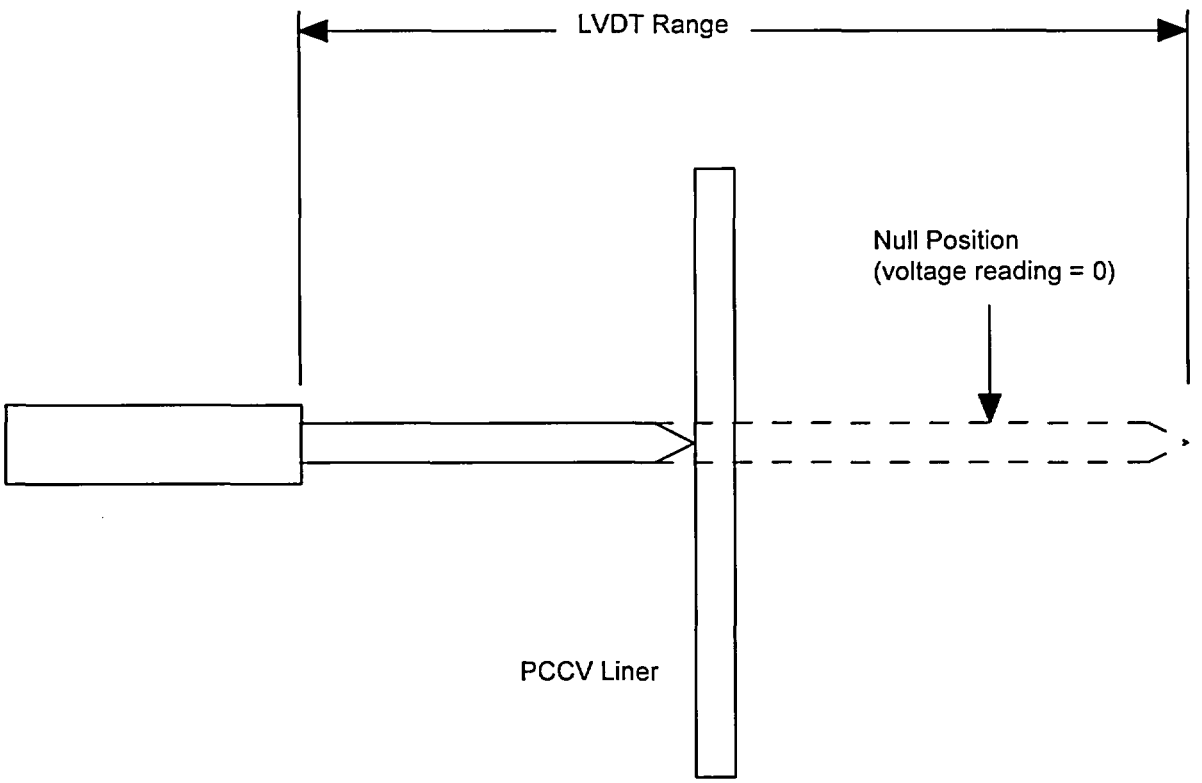

Figure G.1 Geometry for LVDT Measurements

Most of the LVDTs were mounted to the internal framework inside the PCCV model. Because the motion of the internal frame during the tests could affect the measurements, the corrections for motion would be similar to those specified for CPOTs (see G.2.6).

G.2.3 Corrections Made to Inclinometer Raw Data

Conversion of the inclinometer tilt data is accomplished by subtracting the initial raw data point value (in volts) from the current raw data point value (volts) and dividing the result by the calibration factor. This will remove the initial offset angle and provide as final results only the change in angle at any time or pressure.

$$\text{Change in Tilt Angle (°)} = \frac{\text{Raw Data}_{\text{time}=t}\,(\text{V}) - \text{Raw Data}_{\text{time}=0}\,(\text{V})}{\text{Calibration Factor (volts/°)}} \qquad \text{(G-9)}$$

G.2.4 Corrections Made to Thermocouple and RTD Raw Data

All temperature sensor measurements, including both thermocouples and RTDs, are entirely reduced through firmware calculations. Thus, no post-test data reduction is needed. The "raw data" is in the units of °C.

G.2.5 Corrections Made to Pressure Transducer Raw Data

The pressure transducers are voltage type devices and will be factory and SNL calibrated to provide a pressure value (in psia) given a voltage output from the transducers. The following data reduction were used:

$$P(psia) = [Signal(V)]\left[CalibrationFactor\frac{(psia)}{(mV)}\right]\left[1000\left(\frac{mV}{V}\right)\right] \quad \text{(G-10)}$$

To convert the pressure readings into psig, the initial pressure gage reading was subtracted from subsequent readings.

$$P(psig) = [Signal(V) - Signal_{initial}(V)]\left[CalibrationFactor\frac{(psia)}{(mV)}\right]\left[1000\left(\frac{mV}{V}\right)\right] \quad \text{(G-11)}$$

As the final desired pressure units are MPa, the pressure data in psig was then converted to MPa and reported as gage pressure.

G.2.6 Corrections Made to Cable Potentiometers

G.2.6.1 General Corrections

The cable potentiometers (CPOTs) each have a sensitivity factor. This sensitivity is of the form *mV/(V*in*). The signal in mV is normalized by the excitation voltage and divided by the sensitivity factor to obtain the CPOT length in inches. It is necessary to monitor the excitation voltage used for each measurement.

The first step in the reduction uses Equation G-12 below.

$$length(in) = [Signal(V)]\left[\frac{1}{Sens.Factor}\frac{(V-in)}{(mV)}\right]\left[\frac{1000(mV)}{(V)}\right]\left[\frac{1}{V_{excit.}(V)}\right] \quad \text{(G-12)}$$

For each cable potentiometer location, the ***initial length reading*** was algebraically combined with each subsequent reading to provide the differential displacement throughout the experiment. This operation is shown in Equation G-13.

$$Displacement(in) = [length]_{current} - [length]_{initial} \quad \text{(G-13)}$$

The geometry showing the use of Equation G-13 is shown in Figure G.2. Note that this assumes that the angle between the cable's original horizontal line and its displaced line is small so that the true horizontal and vertical components of the displacement are equal to the indicated displacement.

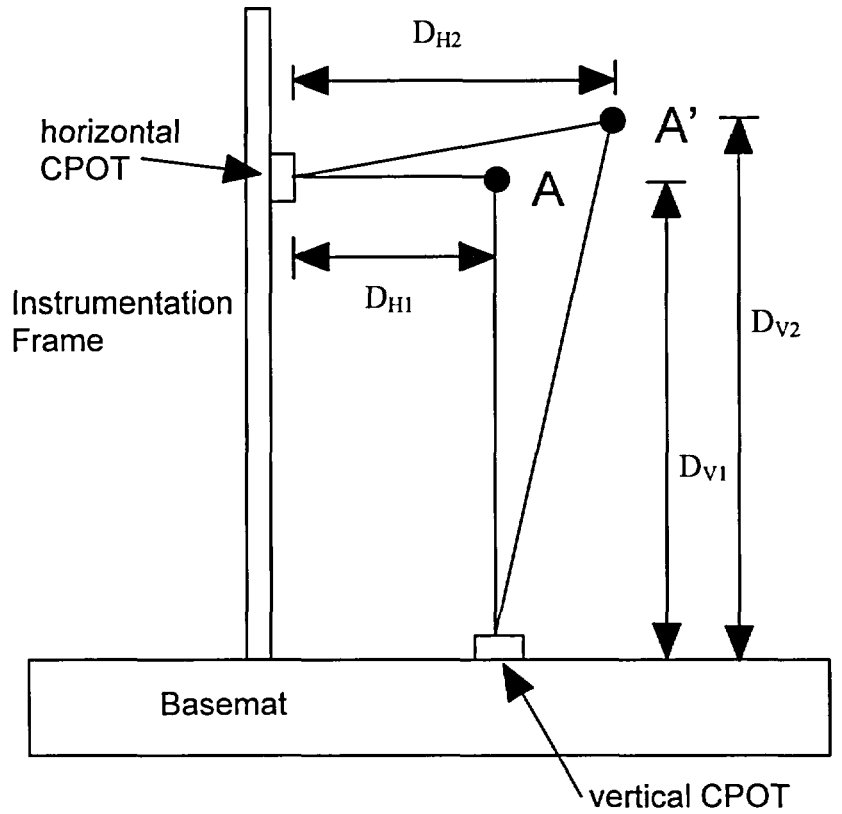

Figure G.2 **Displacement Measurements (Showing Offset Subtraction)**
horizontal displacement = $D_{H2} - D_{H1}$
vertical displacement = $D_{V2} - D_{V1}$

G.2.6.2 Corrections for Movement of Instrumentation Frame

For the PCCV model tests, there was the possibility of instrumentation frame movement caused by thermal expansion. The PCCV high pressure test duration was more than one day. The effect of thermal cycling from day to night temperature changes was characterized, and it was determined that the movement of the frame affected the measurements by a very small amount and no corrections were performed.

G.2.6.3 Correction in Horizontal Displacement Measurements for Vertical Translations

A sketch of the geometry for this case is shown in Figure G.3. Note that the liner motion imparts a vertical component of elongation of the cable-type displacement transducer. Vertical displacement measurements of the liner attachment point would be required to resolve the purely horizontal movement. Several of the CPOT attachment locations on the PCCV liner had both horizontally and vertically aligned gages. Thus, the true horizontal and vertical motions of those points was resolved.

The vertical displacements were corrected in a similar manner for horizontal translations.

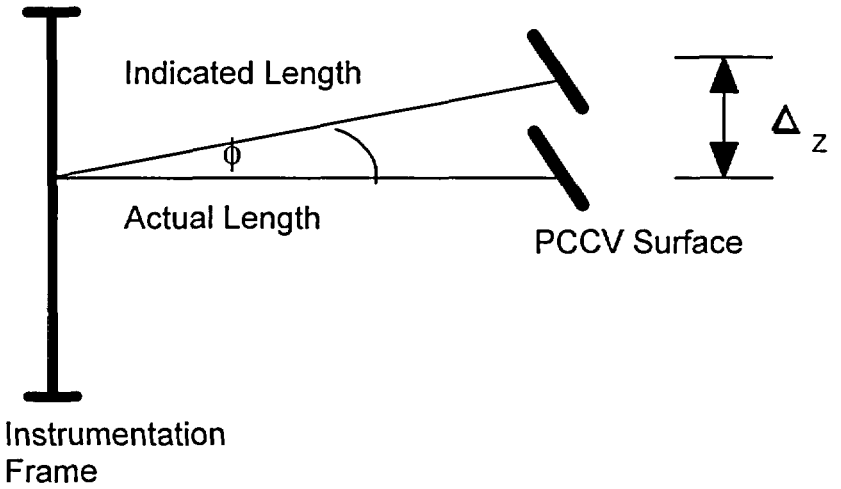

Figure G.3 Geometry for Vertical Movement of Liner at Horizontal Gage Locations

Appendix H: SFMT Instrumentation List

Displacement Instrumentation List

Labeling	Azimuthal	Vertical	Radial	Transducer	Location	Details	Initial	Modified	Comnts	Calibration
I D	Angle	Elevation	Distance	Designation	Drawing #	Drawing #	Offset	Mark #		
(name)	(deg)	(in)	(in)			D-SN-P-				
DL-R-B5-05	30	184.0	211.0		P-131	N/A	-4.5	LVDT-10	Disp	
DL-R-D5-05	90	184.0	211.0		P-131	N/A	-4.5	LVDT-10	Radial	
DL-R-Z2-05	135	10.0	211.0	GCD-121-500	P-131	N/A	-0.3	LVDT-1		
DL-R-Z3-05	135	56.0	211.0	GCD-121-2000-1283	P-131	N/A	-1.5	LVDT-4		
DL-R-Z4-05	135	104.0	211.0	GCD-121-2000-1283	P-131	N/A	-1.5	LVDT-4		
DL-R-Z5-05	135	184.0	211.0		P-131	N/A	-4.5	LVDT-10		
DL-R-Z6-05	135	244.0	211.0		P-131	N/A	-4.5	LVDT-10		
DL-R-Z7-05	135	304.0	211.0		P-131	N/A	-4.5	LVDT-10		
DL-R-Z9-05	135	423.0	211.0	GCD-121-2000-1283	P-131	N/A	-1.5	LVDT-4		
DL-R-G5-05	180	184.0	211.0		P-131	N/A	-4.5	LVDT-10		
DL-R-I5-05	240	184.0	211.0		P-131	N/A	-4.5	LVDT-10		
DL-R-J5-05	270	184.0	211.0		P-131	N/A	-4.5	LVDT-10		
DL-R-L2-05	324	10.0	211.0	GCD-121-500	P-131	N/A	-0.3	LVDT-1		
DL-R-L5-05	334	184.0	200.0		P-131	N/A	-4.5	LVDT-10		
DL-R-L6-05	324	244.0	211.0		P-131	N/A	-4.5	LVDT-10		
DL-R-L7-05	324	304.0	211.0		P-131	N/A	-4.5	LVDT-10		
DL-R-L9-05	324	423.0	211.0	GCD-121-2000-1283	P-131	N/A	-1.5	LVDT-4		
DL-M-Z9-05	135	423.0	211.0	GCD-121-2000-1283	P-131	N/A	-1.5	LVDT-4	Disp.	
DL-M-Z13-05	-	635.0	0.0		P-131	N/A	-2.5	LVDT-6	Vert	
DL-M-L9-05	324	423.0	211.0	GCD-121-2000-1283	P-131	N/A	-1.5	LVDT-4		

PreCal - Calibration was preformed on this instrument prior to model testing only
PostOK - Calibration was performed on this instrument Before and After model testing and remained within tolerance
PostOUT - Calibration was performed on this instrument Before and After model testing and difference was Out-of Tolerance

Rebar Strain Instrumentation List

Labeling	Azimuthal	Vertical	Radial	Transducer	Location	Details	Basic	Modified	Comnts	Calibration
I D	Angle	Elevation	Distance	Designation	Drawing #	Drawing #	Mark #	Mark #		
(name)	(deg)	(in)	(in)			D-SN-P-				
GB-M-A1-04	350	12.3	214.0	EP-08-062AQ-350	124/(A)	124/(1)	-	G15A1A	Gage	NoCal
GB-M-A1-08	350	7.9	217.2	EP-08-062AQ-350	124/(A)	124/(1)	-	G15A1B	Bars	NoCal
GB-M-A1-12	350	3.4	220.4	EP-08-062AQ-350	124/(A)	124/(1)	-	G15A1C		NoCal
GB-M-A1-14	350	12.3	220.4	EP-08-062AQ-350	124/(A)	124/(1)	-	G15A1C		NoCal
GB-M-A1-17	350	3.4	223.6	EP-08-062AQ-350	124/(A)	124/(1)	-	G15A1D		NoCal
GB-M-A1-19	350	12.3	223.6	EP-08-062AQ-350	124/(A)	124/(1)	-	G15A1D		NoCal
GB-M-A1-20	350	16.8	223.6	EP-08-062AQ-350	124/(A)	124/(1)	-	G15A1D		NoCal
GB-M-A1-21	351	-1.0	223.6	EP-08-062AQ-350	TBD	TBD	-	G15A1E	Added	NoCal
GB-M-A1-22	351	3.4	223.6	EP-08-062AQ-350	TBD	TBD	-	G15A1E	Added	NoCal
GB-M-D1-08	90	7.9	220.0	EP-08-062AQ-350	124/(A)	124/(1)	-	G15D1B		NoCal
GB-M-D1-13	90	7.9	226.0	EP-08-062AQ-350	124/(A)	124/(1)	-	G15D1C		NoCal
GB-M-D1-14	90	12.3	226.0	EP-08-062AQ-350	124/(A)	124/(1)	-	G15D1C		NoCal
GB-M-D1-15	90	16.8	226.0	EP-08-062AQ-350	124/(A)	124/(1)	-	G15D1C		NoCal
GB-M-D1-19	90	12.3	232.0	EP-08-062AQ-350	124/(A)	124/(1)	-	G15D1D		NoCal
GB-M-D1-20	90	16.8	232.0	EP-08-062AQ-350	124/(A)	124/(1)	-	G15D1D		NoCal
GB-M-Z1-03	135	7.9	214.0	EP-08-062AQ-350	124/(A)	124/(1)	-	G15Z1A		NoCal
GB-M-Z1-05	135	16.8	214.0	EP-08-062AQ-350	124/(A)	124/(1)	-	G15Z1A		NoCal
GB-M-Z1-09	135	12.3	217.2	EP-08-062AQ-350	124/(A)	124/(1)	-	G15Z1B		NoCal
GB-M-Z1-10	135	16.8	217.2	EP-08-062AQ-350	124/(A)	124/(1)	-	G15Z1B		NoCal
GB-M-Z1-13	135	7.9	220.4	EP-08-062AQ-350	124/(A)	124/(1)	-	G15Z1C		NoCal
GB-M-Z1-14	135	12.3	220.4	EP-08-062AQ-350	124/(A)	124/(1)	-	G15Z1C		NoCal
GB-M-Z1-17	135	3.4	223.6	EP-08-062AQ-350	124/(A)	124/(1)	-	G15Z1D		NoCal
GB-M-Z1-18	135	7.9	223.6	EP-08-062AQ-350	124/(A)	124/(1)	-	G15Z1D		NoCal
GB-M-Z1-19	135	12.3	223.6	EP-08-062AQ-350	124/(A)	124/(1)	-	G15Z1D		NoCal
GB-M-Z1-20	135	16.8	223.6	EP-08-062AQ-350	124/(A)	124/(1)	-	G15Z1D		NoCal
GB-M-Z1-21	136	-1.0	223.6	EP-08-062AQ-350	TBD	TBD	-	G15Z1E	Added	NoCal
GB-M-Z1-22	136	3.4	223.6	EP-08-062AQ-350	TBD	TBD	-	G15Z1E	Added	NoCal
RS-M-A1-01	0	2.0	214.0	EP-08-250BF-350	PCCV-S-2i	102/(5)	S2V002	S2V002A	SOL	NoCal
RS-M-A1-02	0	2.0	221.5	EP-08-250BF-350	PCCV-S-6i	102/(9)	S6V002	S6V002A	&	NoCal
RS-M-A2-01	0	10.0	214.0	EP-08-250BF-350	PCCV-S-2i	102/(5)	S2V002	S2V002A	Vert	NoCal
RS-M-D1-01	90	2.0	214.0	EP-08-250BF-350	PCCV-S-1i	102/(3)	S1VA02	S1VA02A	Wall	NoCal
RS-M-D1-02	89	2.0	230.0	EP-08-250BF-350	PCCV-SB-1i	102/(11)	SB1VA04	SB1VA04A	Base	NoCal
RS-M-D2-01	90	10.0	214.0	EP-08-250BF-350	PCCV-S-1i	102/(3)	S1VA02	S1VA02A		NoCal
RS-M-D2-02	89	10.0	230.0	EP-08-250BF-350	PCCV-SB-1i	102/(11)	SB1VA04	SB1VA04A		NoCal
RS-M-D6-02	89.5	244.0	230.0	EP-08-250BF-350	PCCV-SB-2i	108/(12)	SB2V002	SB2V002A		NoCal
RS-M-Z1-01	135	2.0	214.0	EP-08-250BF-350	PCCV-S-1i	102/(4)	S1VA02	S1VA02B		NoCal
RS-M-Z1-02	135	2.0	221.5	EP-08-250BF-350	PCCV-S-5i	102/(8)	S5VA03	S5VA03A		NoCal
RS-M-Z2-01	135	10.0	214.0	EP-08-250BF-350	PCCV-S-1i	102/(4)	S1VA02	S1VA02B		NoCal
RS-M-Z2-02	135	10.0	221.5	EP-08-250BF-350	PCCV-S-5i	102/(8)	S5VA03	S5VA03A		NoCal
RS-M-Z3-01	135	56.0	214.0	EP-08-250BF-350	PCCV-S-1i	104/(2)	S1VA03	S1VA03A		NoCal
RS-M-Z3-02	135	56.0	221.5	EP-08-250BF-350	PCCV-S-5i	106/(5)	S5VB03	S5VB03A		NoCal
RS-M-Z6-02	135	244.0	221.5	EP-08-250BF-350	PCCV-S-5i	106/(12)	S5VA07	S5VA07A		NoCal
RS-M-Z9-01	135	423.0	214.0	EP-08-250BF-350	PCCV-S-1i	104/(12)	S1V005	S1V005B		NoCal
RS-M-Z9-02	135	423.0	221.5	EP-08-250BF-350	PCCV-S-5i	106/(11)	S5V007	S5V007A		NoCal
RS-M-Z9-03	135	423.0	214.0	EP-08-250BF-350	PCCV-S-1i	104/(12)	S1V005	S1V005B		NoCal
RS-M-Z9-04	135	423.0	221.5	EP-08-250BF-350	PCCV-S-5i	106/(11)	S5V007	S5V007A		NoCal
RS-M-Z11-01	135	573.0	152.0	EP-08-250BF-350	PCCV-D-1i	117/(2)	D1V003	D1V003A		NoCal
RS-M-Z11-02	135	573.0	162.0	EP-08-250BF-350	PCCV-D-4i	117/(11)	D4VA03	D4VA03A		NoCal
RS-M-Z11-03	135	573.0	152.0	EP-08-250BF-350	PCCV-D-1i	117/(2)	D1V003	D1V003A		NoCal
RS-M-Z11-04	135	573.0	162.0	EP-08-250BF-350	PCCV-D-4i	117/(11)	D4VA03	D4VA03A		NoCal
RS-M-J1-01	270	2.0	214.0	EP-08-250BF-350	PCCV-S-2i	102/(6)	S2V002	S2V002B		NoCal
RS-M-J2-01	270	10.0	214.0	EP-08-250BF-350	PCCV-S-2i	102/(6)	S2V002	S2V002B		NoCal
RS-M-J2-02	269	10.0	230.0	EP-08-250BF-350	PCCV-SB-1i	102/(12)	SB1V004	SB1V004B		NoCal
RS-M-L1-01	324	2.0	214.0	EP-08-250BF-350	PCCV-S-2i	102/(7)	S2VA02	S2VA02A		NoCal
RS-M-L1-02	324	2.0	221.5	EP-08-250BF-350	PCCV-S-6i	102/(10)	S6V002	S6V002B		NoCal
RS-M-L2-01	324	10.0	214.0	EP-08-250BF-350	PCCV-S-2i	102/(7)	S2VA02	S2VA02A		NoCal
RS-M-L2-02	324	10.0	221.5	EP-08-250BF-350	PCCV-S-6i	102/(10)	S6V002	S6V002B		NoCal
RS-C-D6-02	90	246.0	223.0	EP-08-250BF-350	PCCV-S-8i	115/(9)	S8H033	S8H033A		NoCal
RS-C-Z6-01	135	246.0	215.0	EP-08-250BF-350	PCCV-S-3i	110/(10)	S3H026	S3H026A		NoCal
RS-C-Z6-02	135	246.0	223.0	EP-08-250BF-350	PCCV-S-7i	113/(2)	S7H031	S7H031A		NoCal
RS-C-Z9-02	135	423.0	223.0	EP-08-250BF-350	PCCV-S-7i	113/(4)	S7H036	S7H036B		NoCal
RS-C-Z11-02	135	573.0	163.0	EP-08-250BF-350	PCCV-D-6i	116/(11)	D6H048	D6H048B		NoCal

Liner Strain Instrumentation List

Labeling	Azimuthal	Vertical	Radial	Transducer	Location	Details	Basic	Modified	Comnts	Calibration
I D	Angle	Elevation	Distance	Designation	Drawing #	Drawing #	Mark #	Mark #		
(name)	(deg)	(in)	(in)			D-SN-P-				
LSO-C-A7-01	1.8	305.3	211.7	EP-08-125AC-350	ZCD1007Ai	209/(a.1)	4-1B	4-1B	Vert.	NoCal
LSO-C-Z5-01	137.5	216.2	211.7	EP-08-125AC-350	ZCD1008Ai	209/(a.2)	3-6B	3-6B	Weld	NoCal
LSO-C-Z6-01	137.5	229.7	211.7	EP-08-125AC-350	ZCD1008Ai	209/(a.3)	3-6B	3-6B		NoCal
LSO-C-D7-01	95.8	305.3	211.7	EP-08-125AC-350	ZCD1009Ai	209/(a.4)	4-3B	4-3B		NoCal
LSO-C-D7-02	95.8	291.5	211.7	EP-08-125AC-350	ZCD1009Ai	209/(a.5)	4-3B	4-3B		NoCal
LSO-M-A1-03	0	0.4	211.7	EP-08-125MW-120	ZCD1002Ai	208/(c.1)	1-12C	1-12C	Wall	NoCal
LSO-M-A1-04	0	0.5	211.7	EP-08-125MW-120	ZCD1002Ai	208/(c.1)	1-12C	1-12C	Base	NoCal
LSO-M-D1-01	89.6	-0.7	211.7	EP-08-125MW-120	ZCD1002Ai	208/(c.2)	1-3C	1-3C		NoCal
LSO-M-D1-02	89.6	-0.2	211.7	EP-08-125MW-120	ZCD1002Ai	208/(c.2)	1-3C	1-3C		NoCal
LSO-M-D1-03	89.6	0.4	211.7	EP-08-125MW-120	ZCD1002Ai	208/(c.2)	1-3C	1-3C		NoCal
LSO-M-D1-05	88.9	-0.7	211.7	EP-08-125MW-120	ZCD1002Ai	207/(c.3)	1-3C	1-3C		NoCal
LSO-M-I1-01	239.4	-0.7	211.7	EP-08-125MW-120	ZCD1002Ai	207/(c.6)	1-8C	1-8C		NoCal
LSO-M-I1-02	239.4	-0.2	211.7	EP-08-125MW-120	ZCD1002Ai	207/(c.6)	1-8C	1-8C		NoCal
LSO-M-L1-03	324.6	0.4	211.7	EP-08-125MW-120	ZCD1002Ai	208/(c.7)	1-11C	1-11C		NoCal
LSO-M-L1-04	324.6	0.5	211.7	EP-08-125MW-120	ZCD1002Ai	208/(c.7)	1-11C	1-11C		NoCal

Tendon Instrumentation List

Labeling	Azimuthal	Vertical	Radial	Transducer	Location	Details	Basic	Modified	Comnts	Calibration
I D	Angle	Elevation	Distance	Designation	Drawing #	Drawing #	Mark #	Mark #		
(name)	(deg)	(in)	(in)			D-SN-P-				
TT-M-Z6-01	135	244.0	218.0	TENSMEG-120	120/(2)	121/(1)	V46	V46-1	Tensmeg	NoCal
TT-M-Z9-01	135	380.0	218.0	TENSMEG-120	120/(2)	121/(1)	V46	V46-1		NoCal
TT-M-E10-01	121	537.0	178.0	TENSMEG-120	120/(2)	121/(1)	V46	V46-1		NoCal
TT-M-D11-01	90	580.0	141.0	TENSMEG-120	120/(2)	121/(1)	V46	V46-1		NoCal
TT-M-I3-01	241	64.0	218.0	TENSMEG-120	120/(1)	121/(2)	V37	V37-1		NoCal
TT-M-I3-02	241	90.0	218.0	TENSMEG-120	120/(1)	121/(2)	V37	V37-2		NoCal
TT-M-I9-01	241	380.0	218.0	TENSMEG-120	120/(1)	121/(2)	V37	V37-1		NoCal
TT-M-I9-02	241	406.0	218.0	TENSMEG-120	120/(1)	121/(2)	V37	V37-2		NoCal
TT-M-I9-03	241	354.0	218.0	TENSMEG-120	120/(1)	121/(2)	V37	V37-3		NoCal
TT-M-G12-01	180	615.0	87.0	TENSMEG-120	120/(1)	121/(1)	V37	V37-1		NoCal
TT-M-L9-03	325	354.0	218.0	TENSMEG-120	120/(3)	122/(6)	V85	V85-3		NoCal
TT-M-J11-01	270	588.0	132.0	TENSMEG-120	120/(3)	121/(1)	V85	V85-1		NoCal
TT-C-D3-01	90	73.0	220.0	TENSMEG-120	119/(1)	121/(1)	H11	H11-1		NoCal
TT-C-G3-01	180	73.0	220.0	TENSMEG-120	119/(1)	121/(1)	H11	H11-1		NoCal
TT-C-A5-01	0	180.0	220.0	TENSMEG-120	119/(2)	122/(6)	H35	H35-1		NoCal
TT-C-A5-02	7	180.0	220.0	TENSMEG-120	119/(2)	122/(6)	H35	H35-2		NoCal
TT-C-G5-01	180	174.0	220.0	TENSMEG-120	119/(2)	121/(1)	H35	H35-1		NoCal
TT-C-K5-03	278	180.0	220.0	TENSMEG-120	119/(2)	122/(6)	H35	H35-3		NoCal
TT-C-D6-01	90	259.0	220.0	TENSMEG-120	119/(3)	121/(2)	H53	H53-1		NoCal
TT-C-D6-03	97	259.0	220.0	TENSMEG-120	119/(3)	121/(2)	H53	H53-3		NoCal
TF-M-Z6-01	135	244.0	218.0	EP-08-062AQ-350	120/(2)	121/(1)	V46	V46-1	WSG	NoCal
TF-M-Z6-02	135	244.0	218.0	EP-08-062AQ-350	120/(2)	121/(1)	V46	V46-1		NoCal
TF-M-Z9-01	135	380.0	218.0	EP-08-062AQ-350	120/(2)	121/(1)	V46	V46-1		NoCal
TF-M-Z9-02	135	380.0	218.0	EP-08-062AQ-350	120/(2)	121/(1)	V46	V46-1		NoCal
TF-M-E10-01	121	537.0	178.0	EP-08-062AQ-350	120/(2)	121/(1)	V46	V46-1		NoCal
TF-M-E10-02	121	537.0	178.0	EP-08-062AQ-350	120/(2)	121/(1)	V46	V46-1		NoCal
TF-M-D11-01	90	580.0	141.0	EP-08-062AQ-350	120/(2)	121/(1)	V46	V46-1		NoCal
TF-M-D11-02	90	580.0	141.0	EP-08-062AQ-350	120/(2)	121/(1)	V46	V46-1		NoCal
TF-M-I3-01	241	64.0	218.0	EP-08-062AQ-350	120/(1)	121/(2)	V37	V37-1		NoCal
TF-M-I3-02	241	64.0	218.0	EP-08-062AQ-350	120/(1)	121/(2)	V37	V37-1		NoCal
TF-M-I3-03	241	90.0	218.0	EP-08-062AQ-350	120/(1)	121/(2)	V37	V37-2		NoCal
TF-M-I3-04	241	90.0	218.0	EP-08-062AQ-350	120/(1)	121/(2)	V37	V37-2		NoCal
TF-M-I3-05	241	38.0	218.0	EP-08-062AQ-350	120/(1)	121/(2)	V37	V37-3		NoCal
TF-M-I9-01	241	380.0	218.0	EP-08-062AQ-350	120/(1)	121/(2)	V37	V37-1		NoCal
TF-M-I9-02	241	380.0	218.0	EP-08-062AQ-350	120/(1)	121/(2)	V37	V37-1		NoCal
TF-M-I9-03	241	406.0	218.0	EP-08-062AQ-350	120/(1)	121/(2)	V37	V37-2		NoCal
TF-M-I9-04	241	406.0	218.0	EP-08-062AQ-350	120/(1)	121/(2)	V37	V37-2		NoCal
TF-M-I9-05	241	354.0	218.0	EP-08-062AQ-350	120/(1)	121/(2)	V37	V37-3		NoCal
TF-M-I9-06	241	354.0	218.0	EP-08-062AQ-350	120/(1)	121/(2)	V37	V37-3		NoCal
TF-M-G12-01	180	615.0	87.0	EP-08-062AQ-350	120/(1)	121/(1)	V37	V37-1		NoCal
TF-M-G12-02	180	615.0	87.0	EP-08-062AQ-350	120/(1)	121/(1)	V37	V37-1		NoCal
TF-M-L9-01	325	380.0	218.0	EP-08-062AQ-350	120/(3)	122/(6)	V85	V85-1		NoCal
TF-M-L9-02	325	380.0	218.0	EP-08-062AQ-350	120/(3)	122/(6)	V85	V85-1		NoCal
TF-M-L9-03	325	380.0	218.0	EP-08-062AQ-350	120/(3)	122/(6)	V85	V85-1		NoCal
TF-M-L9-07	325	354.0	218.0	EP-08-062AQ-350	120/(3)	122/(6)	V85	V85-3		NoCal
TF-M-L9-08	325	354.0	218.0	EP-08-062AQ-350	120/(3)	122/(6)	V85	V85-3		NoCal
TF-M-L9-09	325	354.0	218.0	EP-08-062AQ-350	120/(3)	122/(6)	V85	V85-3		NoCal
TF-M-J11-01	270	588.0	132.0	EP-08-062AQ-350	120/(3)	121/(1)	V85	V85-1		NoCal
TF-M-J11-02	270	588.0	132.0	EP-08-062AQ-350	120/(3)	121/(1)	V85	V85-1		NoCal
TF-C-D3-01	90	73.0	220.0	EP-08-062AQ-350	119/(1)	121/(1)	H11	H11-1		NoCal
TF-C-D3-02	90	73.0	220.0	EP-08-062AQ-350	119/(1)	121/(1)	H11	H11-1		NoCal
TF-C-G3-02	180	73.0	220.0	EP-08-062AQ-350	119/(1)	121/(1)	H11	H11-1		NoCal
TF-C-I3-01	260	73.0	220.0	EP-08-062AQ-350	119/(1)	121/(1)	H11	H11-1		NoCal
TF-C-I3-02	260	73.0	220.0	EP-08-062AQ-350	119/(1)	121/(1)	H11	H11-1		NoCal
TF-C-I3-03	260	73.0	220.0	EP-08-062AQ-350	119/(1)	121/(1)	H11	H11-1		NoCal
TF-C-A5-01	0	180.0	220.0	EP-08-062AQ-350	119/(2)	122/(6)	H35	H35-1		NoCal

Tendon Instrumentation List

Labeling	Azimuthal	Vertical	Radial	Transducer	Location	Details	Basic	Modified	Comnts	Calibration
I D	Angle	Elevation	Distance	Designation	Drawing #	Drawing #	Mark #	Mark #		
(name)	(deg)	(in)	(in)			D-SN-P-				
TF-C-A5-02	0	180.0	220.0	EP-08-062AQ-350	119/(2)	122/(6)	H35	H35-1		NoCal
TF-C-A5-03	0	180.0	220.0	EP-08-062AQ-350	119/(2)	122/(6)	H35	H35-1		NoCal
TF-C-A5-04	7	180.0	220.0	EP-08-062AQ-350	119/(2)	122/(6)	H35	H35-2		NoCal
TF-C-A5-05	7	180.0	220.0	EP-08-062AQ-350	119/(2)	122/(6)	H35	H35-2		NoCal
TF-C-A5-06	7	180.0	220.0	EP-08-062AQ-350	119/(2)	122/(6)	H35	H35-2		NoCal
TF-C-G5-01	180	174.0	220.0	EP-08-062AQ-350	119/(2)	121/(1)	H35	H35-1		NoCal
TF-C-G5-02	180	174.0	220.0	EP-08-062AQ-350	119/(2)	121/(1)	H35	H35-1		NoCal
TF-C-K5-07	278	180.0	220.0	EP-08-062AQ-350	119/(2)	122/(6)	H35	H35-3		NoCal
TF-C-K5-08	278	180.0	220.0	EP-08-062AQ-350	119/(2)	122/(6)	H35	H35-3		NoCal
TF-C-K5-09	278	180.0	220.0	EP-08-062AQ-350	119/(2)	122/(6)	H35	H35-3		NoCal
TF-C-D6-01	90	259.0	220.0	EP-08-062AQ-350	119/(3)	121/(2)	H53	H53-1		NoCal
TF-C-D6-02	90	259.0	220.0	EP-08-062AQ-350	119/(3)	121/(2)	H53	H53-1		NoCal
TF-C-D6-05	97	259.0	220.0	EP-08-062AQ-350	119/(3)	121/(2)	H53	H53-3		NoCal
TF-C-D6-06	97	259.0	220.0	EP-08-062AQ-350	119/(3)	121/(2)	H53	H53-3		NoCal
TF-C-K6-03	280	259.0	220.0	EP-08-062AQ-350	119/(3)	122/(5)	H53	H53-1		NoCal
TF-C-A7-01	0	321.0	220.0	EP-08-062AQ-350	119/(4)	121/(3)	H67	H67-1		NoCal
TF-C-A7-02	0	321.0	220.0	EP-08-062AQ-350	119/(4)	121/(3)	H67	H67-1		NoCal
TF-C-A7-03	0	321.0	220.0	EP-08-062AQ-350	119/(4)	121/(3)	H67	H67-1		NoCal
TF-C-D7-01	90	321.0	220.0	EP-08-062AQ-350	119/(4)	121/(3)	H67	H67-1		NoCal
TF-C-D7-02	90	321.0	220.0	EP-08-062AQ-350	119/(4)	121/(3)	H67	H67-1		NoCal
TF-C-D7-03	90	321.0	220.0	EP-08-062AQ-350	119/(4)	121/(3)	H67	H67-1		NoCal
TF-C-Z7-01	135	321.0	220.0	EP-08-062AQ-350	119/(4)	121/(3)	H67	H67-1		NoCal
TF-C-K7-01	280	321.0	220.0	EP-08-062AQ-350	119/(4)	121/(3)	H67	H67-1		NoCal
TF-C-K7-02	280	321.0	220.0	EP-08-062AQ-350	119/(4)	121/(3)	H67	H67-1		NoCal
TF-C-K7-03	280	321.0	220.0	EP-08-062AQ-350	119/(4)	121/(3)	H67	H67-1		NoCal
TF-C-E8-03	105	326.0	220.0	EP-08-062AQ-350	119/(5)	121/(4)	H68	H68-1		NoCal
TF-C-E8-07	98	326.0	220.0	EP-08-062AQ-350	119/(5)	121/(4)	H68	H68-3		NoCal
TF-C-E8-08	98	326.0	220.0	EP-08-062AQ-350	119/(5)	121/(4)	H68	H68-3		NoCal
TF-C-E8-09	98	326.0	220.0	EP-08-062AQ-350	119/(5)	121/(4)	H68	H68-3		NoCal
TF-C-Z8-01	135	326.0	220.0	EP-08-062AQ-350	119/(5)	121/(3)	H68	H68-1		NoCal
TF-C-Z8-03	135	326.0	220.0	EP-08-062AQ-350	119/(5)	121/(3)	H68	H68-1		NoCal
TF-C-G8-02	180	326.0	220.0	EP-08-062AQ-350	119/(5)	121/(3)	H68	H68-1		NoCal
TF-C-G8-03	180	326.0	220.0	EP-08-062AQ-350	119/(5)	121/(3)	H68	H68-1		NoCal
TF-C-J8-01	270	326.0	220.0	EP-08-062AQ-350	119/(5)	121/(4)	H68	H68-1		NoCal
TF-C-J8-02	270	326.0	220.0	EP-08-062AQ-350	119/(5)	121/(4)	H68	H68-1		NoCal
TF-C-J8-03	270	326.0	220.0	EP-08-062AQ-350	119/(5)	121/(4)	H68	H68-1		NoCal
TF-C-J8-07	277	326.0	220.0	EP-08-062AQ-350	119/(5)	121/(4)	H68	H68-3		NoCal
TF-C-J8-08	277	326.0	220.0	EP-08-062AQ-350	119/(5)	121/(4)	H68	H68-3		NoCal
TF-C-J8-09	277	326.0	220.0	EP-08-062AQ-350	119/(5)	121/(4)	H68	H68-3		NoCal
TL-M-A0-03	1	-46.0	218.0	GK-3000-200-2.0	-QCON-06i	N/A	V67	V67	Vert.	PreCal
TL-M-A0-05	13	-46.0	218.0	GK-3000-200-2.0	-QCON-06i	N/A	V61	V61	Load	PreCal
TL-M-B0-02	25	-46.0	218.0	GK-3000-200-2.0	-QCON-06i	N/A	V55	V55	Cells	PreCal
TL-M-B0-04	37	-46.0	218.0	GK-3000-200-2.0	-QCON-06i	N/A	V49	V49		PreCal
TL-M-B0-05	43	-46.0	218.0	GK-3000-200-2.0	-QCON-06i	N/A	V46	V46		PreCal
TL-M-C0-01	45	-46.0	218.0	GK-3000-200-2.0	-QCON-06i	N/A	V1	V1		PreCal
TL-M-C0-03	57	-46.0	218.0	GK-3000-200-2.0	-QCON-06i	N/A	V7	V7		PreCal
TL-M-C0-05	69	-46.0	218.0	GK-3000-200-2.0	-QCON-06i	N/A	V13	V13		PreCal
TL-M-D0-02	81	-46.0	218.0	GK-3000-200-2.0	-QCON-06i	N/A	V19	V19		PreCal
TL-M-D0-04	93	-46.0	218.0	GK-3000-200-2.0	-QCON-05i	N/A	V25	V25		PreCal
TL-M-E0-01	105	-46.0	218.0	GK-3000-200-2.0	-QCON-05i	N/A	V31	V31		PreCal
TL-M-E0-03	117	-46.0	218.0	GK-3000-200-2.0	-QCON-05i	N/A	V37	V37		PreCal
TL-M-Z0-01	129	-46.0	218.0	GK-3000-200-2.0	-QCON-05i	N/A	V43	V43		PreCal
TL-M-Z0-02	135	-46.0	218.0	HBM-C6-100t	-QCON-05i	N/A	V46	V46		PreCal
TL-M-Z0-03	141	-46.0	218.0	GK-3000-200-2.0	-QCON-05i	N/A	V49	V49		PreCal
TL-M-F0-02	153	-46.0	218.0	GK-3000-200-2.0	-QCON-05i	N/A	V55	V55		PreCal
TL-M-G0-01	165	-46.0	218.0	GK-3000-200-2.0	-QCON-05i	N/A	V61	V61		PreCal
TL-M-G0-03	177	-46.0	218.0	GK-3000-200-2.0	-QCON-05i	N/A	V67	V67		PreCal

Tendon Instrumentation List

Labeling	Azimuthal	Vertical	Radial	Transducer	Location	Details	Basic	Modified	Comnts	Calibration
I D	Angle	Elevation	Distance	Designation	Drawing #	Drawing #	Mark #	Mark #		
(name)	(deg)	(in)	(in)			D-SN-P-				
TL-M-G0-05	189	-46.0	218.0	GK-3000-200-2.0	-QCON-05i	N/A	V73	V73		PreCal
TL-M-H0-02	201	-46.0	218.0	GK-3000-200-2.0	-QCON-05i	N/A	V79	V79		PreCal
TL-M-H0-04	213	-46.0	218.0	GK-3000-200-2.0	-QCON-05i	N/A	V85	V85		PreCal
TL-M-I0-01	229	-46.0	218.0	GK-3000-200-2.0	-QCON-05i	N/A	V43	V43		PreCal
TL-M-I0-03	241	-46.0	218.0	HBM-C6-100t	-QCON-05i	N/A	V37	V37		PreCal
TL-M-I0-05	253	-46.0	218.0	GK-3000-200-2.0	-QCON-05i	N/A	V31	V31		PreCal
TL-M-J0-02	265	-46.0	218.0	GK-3000-200-2.0	-QCON-05i	N/A	V25	V25		PreCal
TL-M-J0-04	277	-46.0	218.0	GK-3000-200-2.0	-QCON-06i	N/A	V19	V19		PreCal
TL-M-K0-01	289	-46.0	218.0	GK-3000-200-2.0	-QCON-06i	N/A	V13	V13		PreCal
TL-M-K0-03	301	-46.0	218.0	GK-3000-200-2.0	-QCON-06i	N/A	V7	V7		PreCal
TL-M-K0-05	313	-46.0	218.0	GK-3000-200-2.0	-QCON-06i	N/A	V1	V1		PreCal
TL-M-L0-02	325	-46.0	218.0	HBM-C6-100t	-QCON-06i	N/A	V85	V85		PreCal
TL-M-L0-04	337	-46.0	218.0	GK-3000-200-2.0	-QCON-06i	N/A	V79	V79		PreCal
TL-M-A0-01	349	-46.0	218.0	GK-3000-200-2.0	-QCON-06i	N/A	V73	V73		PreCal
TL-C-D3-01	85	44.0	230.0	GK-3000-200-2.0	-QCON-06i	N/A	H4	H4	Hoop	PreCal
TL-C-D3-02	95	41.0	230.0	GK-3000-200-2.0	-QCON-05i	N/A	H4	H4	Load	PreCal
TL-C-D4-01	85	106.0	230.0	GK-3000-200-2.0	-QCON-06i	N/A	H18	H18	Cells	PreCal
TL-C-D4-02	95	103.0	230.0	GK-3000-200-2.0	-QCON-05i	N/A	H18	H18	90 Deg.	PreCal
TL-C-D5-01	85	159.0	230.0	GK-3000-200-2.0	-QCON-06i	N/A	H30	H30		PreCal
TL-C-D5-02	95	156.0	230.0	GK-3000-200-2.0	-QCON-05i	N/A	H30	H30		PreCal
TL-C-D5-03	85	203.0	230.0	GK-3000-200-2.0	-QCON-06i	N/A	H40	H40		PreCal
TL-C-D5-04	95	200.0	230.0	GK-3000-200-2.0	-QCON-05i	N/A	H40	H40		PreCal
TL-C-D6-01	85	230.0	230.0	GK-3000-200-2.0	-QCON-06i	N/A	H46	H46		PreCal
TL-C-D6-02	95	227.0	230.0	GK-3000-200-2.0	-QCON-05i	N/A	H46	H46		PreCal
TL-C-D7-01	85	283.0	230.0	GK-3000-200-2.0	-QCON-06i	N/A	H58	H58		PreCal
TL-C-D7-02	95	280.0	230.0	GK-3000-200-2.0	-QCON-05i	N/A	H58	H58		PreCal
TL-C-D8-01	85	327.0	230.0	HBM-C6-100t	-QCON-06i	N/A	H68	H68		PreCal
TL-C-D8-02	95	324.0	230.0	HBM-C6-100t	-QCON-05i	N/A	H68	H68		PreCal
TL-C-D9-01	85	389.0	230.0	GK-3000-200-2.0	-QCON-06i	N/A	H82	H82		PreCal
TL-C-D9-02	95	386.0	230.0	GK-3000-200-2.0	-QCON-05i	N/A	H82	H82		PreCal
TL-C-D10-01	85	481.0	230.0	GK-3000-200-2.0	-QCON-06i	N/A	H96	H96		PreCal
TL-C-D10-02	95	478.0	230.0	GK-3000-200-2.0	-QCON-05i	N/A	H96	H96		PreCal
TL-C-J3-01	265	75.0	230.0	GK-3000-200-2.0	-QCON-05i	N/A	H11	H11	Hoop	PreCal
TL-C-J3-02	275	72.0	230.0	HBM-C6-100t	-QCON-06i	N/A	H11	H11	Load	PreCal
TL-C-J4-01	265	137.0	230.0	GK-3000-200-2.0	-QCON-05i	N/A	H25	H25	Cells	PreCal
TL-C-J4-02	275	134.0	230.0	GK-3000-200-2.0	-QCON-06i	N/A	H25	H25	270 Deg	PreCal
TL-C-J5-01	265	181.0	230.0	HBM-C6-100t	-QCON-05i	N/A	H35	H35		PreCal
TL-C-J5-02	275	178.0	230.0	HBM-C6-100t	-QCON-06i	N/A	H35	H35		PreCal
TL-C-J6-01	265	261.0	230.0	HBM-C6-100t	-QCON-05i	N/A	H53	H53		PreCal
TL-C-J6-02	275	258.0	230.0	GK-3000-200-2.0	-QCON-06i	N/A	H53	H53		PreCal
TL-C-J7-01	265	305.0	230.0	GK-3000-200-2.0	-QCON-05i	N/A	H63	H63		PreCal
TL-C-J7-02	275	302.0	230.0	GK-3000-200-2.0	-QCON-06i	N/A	H63	H63		PreCal
TL-C-J7-03	265	323.0	230.0	HBM-C6-100t	-QCON-05i	N/A	H67	H67		PreCal
TL-C-J7-04	275	320.0	230.0	HBM-C6-100t	-QCON-06i	N/A	H67	H67		PreCal
TL-C-J8-01	265	358.0	230.0	GK-3000-200-2.0	-QCON-05i	N/A	H75	H75		PreCal
TL-C-J8-02	275	355.0	230.0	GK-3000-200-2.0	-QCON-06i	N/A	H75	H75		PreCal
TL-C-J9-01	265	420.0	230.0	GK-3000-200-2.0	-QCON-05i	N/A	H89	H89		PreCal
TL-C-J9-02	275	417.0	230.0	GK-3000-200-2.0	-QCON-06i	N/A	H89	H89		PreCal
TL-C-J10-01	265	543.0	230.0	GK-3000-200-2.0	-QCON-05i	N/A	H103	H103		PreCal
TL-C-J10-02	275	540.0	230.0	GK-3000-200-2.0	-QCON-06i	N/A	H103	H103		PreCal

NoCal - No calibration was performed on this instrument before or after model testing
PreCal - Calibration was preformed on this instrument prior to model testing only

Other Instrumentation List

Labeling	Azimuthal	Vertical	Radial	Transducer	Location	Details	Basic	Modified	Comnts	Calibration
I D	Angle	Elevation	Distance	Designation	Drawing #	Drawing #	Mark #	Mark #		
(name)	(deg)	(in)	(in)			D-SN-P-				
TC-R-D0-01	90	-134.0	48.0	K-24-2-505	PCCV-F-1i	N/A	N/A	N/A	(Thermoc.	NoCal
TC-R-D0-02	90	-104.0	48.0	K-24-2-505	PCCV-F-1i	N/A	N/A	N/A	embedded	NoCal
TC-R-D0-03	90	-104.0	200.0	K-24-2-505	PCCV-F-1i	N/A	N/A	N/A	basemat)	NoCal
TC-R-D0-04	90	-6.0	48.0	CASS-116U-240	PCCV-F-8i	N/A	N/A	N/A		NoCal
TC-R-D0-05	90	-36.0	214.0	CASS-116U-240	PCCV-F-5i	N/A	N/A	N/A		NoCal
TC-R-Z0-01	135	-36.0	214.0	CASS-116U-240	PCCV-F-5i	N/A	N/A	N/A		NoCal
TW-R-A2-01	0	10.0	218.0	TQSS-116U-180	PCCV-S-8ii	N/A	N/A	N/A	(Thermoc.	NoCal
TW-R-A4-01	0	104.0	218.0	TQSS-116U-72	PCCV-S-8ii	N/A	N/A	N/A	embedded	NoCal
TW-R-A5-01	0	184.0	218.0	TQSS-116U-72	PCCV-S-8ii	N/A	N/A	N/A	cylinder	NoCal
TW-R-A5-02	349	184.0	218.0	TQSS-116U-72	PCCV-S-8ii	N/A	N/A	N/A	& dome)	NoCal
TW-R-A6-01	0	244.0	218.0	TQSS-116U-72	PCCV-S-8ii	N/A	N/A	N/A		NoCal
TW-R-A7-01	0	304.0	218.0	TQSS-116U-72	PCCV-S-8ii	N/A	N/A	N/A		NoCal
TW-R-A9-01	0	423.0	218.0	TQSS-116U-72	PCCV-S-8ii	N/A	N/A	N/A		NoCal
TW-R-A11-01	0	573.0	158.0	TQSS-116U-240	PCCV-D-6ii	N/A	N/A	N/A		NoCal
TW-R-C5-01	44	184.0	218.0	TQSS-116U-96	PCCV-S-8ii	N/A	N/A	N/A		NoCal
TW-R-C5-02	62	125.0	218.0	TQSS-116U-96	PCCV-S-8ii	N/A	N/A	N/A		NoCal
TW-R-C5-03	62	230.0	218.0	TQSS-116U-96	PCCV-S-8ii	N/A	N/A	N/A		NoCal
TW-R-C5-04	80	184.0	218.0	TQSS-116U-96	PCCV-S-8ii	N/A	N/A	N/A		NoCal
TW-R-D2-01	90	10.0	222.0	TQSS-116U-180	PCCV-S-8ii	N/A	N/A	N/A		NoCal
TW-R-D4-01	90	104.0	222.0	TQSS-116U-96	PCCV-S-8ii	N/A	N/A	N/A		NoCal
TW-R-D5-01	90	184.0	222.0	TQSS-116U-96	PCCV-S-8ii	N/A	N/A	N/A		NoCal
TW-R-D7-01	90	304.0	222.0	TQSS-116U-96	PCCV-S-8ii	N/A	N/A	N/A		NoCal
TW-R-D9-01	90	423.0	222.0	TQSS-116U-72	PCCV-S-8ii	N/A	N/A	N/A		NoCal
TW-R-D11-01	62	180.0	220.0	TQSS-116U-240	PCCV-D-6ii	N/A	N/A	N/A	A/L	NoCal
TW-R-Z2-01	135	10.0	218.0	TQSS-116U-180	PCCV-S-7ii	N/A	N/A	N/A		NoCal
TW-R-Z4-01	135	104.0	218.0	TQSS-116U-72	PCCV-S-7ii	N/A	N/A	N/A		NoCal
TW-R-Z5-01	135	184.0	218.0	TQSS-116U-96	PCCV-S-7ii	N/A	N/A	N/A		NoCal
TW-R-Z6-01	135	244.0	218.0	TQSS-116U-96	PCCV-S-7ii	N/A	N/A	N/A		NoCal
TW-R-Z7-01	135	304.0	218.0	TQSS-116U-96	PCCV-S-7ii	N/A	N/A	N/A		NoCal
TW-R-Z9-01	135	423.0	218.0	TQSS-116U-72	PCCV-S-7ii	N/A	N/A	N/A		NoCal
TW-R-Z11-01	135	573.0	158.0	TQSS-116U-240	PCCV-D-6ii	N/A	N/A	N/A		NoCal
TW-R-Z13-01	-	640.0	0.0	TQSS-116U-480	PCCV-D-6ii	N/A	N/A	N/A		NoCal
TW-R-G5-01	180	184.0	218.0	TQSS-116U-96	PCCV-S-7ii	N/A	N/A	N/A		NoCal
TW-R-I2-01	240	10.0	218.0	TQSS-116U-180	PCCV-S-7ii	N/A	N/A	N/A		NoCal
TW-R-I5-01	240	184.0	218.0	TQSS-116U-96	PCCV-S-7ii	N/A	N/A	N/A		NoCal
TW-R-I9-01	240	423.0	218.0	TQSS-116U-72	PCCV-S-7ii	N/A	N/A	N/A		NoCal
TW-R-I11-01	324	184.0	220.0	TQSS-116U-240	PCCV-D-6ii	N/A	N/A	N/A	E/H	NoCal
TW-R-K5-01	299	184.0	218.0	TQSS-116U-96	PCCV-S-8ii	N/A	N/A	N/A		NoCal
TW-R-L2-01	324	10.0	218.0	TQSS-116U-180	PCCV-S-8ii	N/A	N/A	N/A		NoCal
TW-R-L4-01	324	79.0	218.0	TQSS-116U-96	PCCV-S-8ii	N/A	N/A	N/A		NoCal
TW-R-L7-01	324	289.0	218.0	TQSS-116U-96	PCCV-S-8ii	N/A	N/A	N/A		NoCal
TW-R-L9-01	324	423.0	218.0	TQSS-116U-72	PCCV-S-8ii	N/A	N/A	N/A		NoCal
TW-R-L11-01	324	573.0	158.0	TQSS-116U-240	PCCV-D-6ii	N/A	N/A	N/A		NoCal
RT-M-A3-01	0	40.0	150.0	RTD-805	TBD	N/A	N/A	N/A	(RTD	NoCal
RT-M-A5-01	0	170.0	150.0	RTD-805	TBD	N/A	N/A	N/A	inside	NoCal
RT-M-A7-01	0	290.0	150.0	RTD-805	TBD	N/A	N/A	N/A	air	NoCal
RT-M-A9-01	0	423.0	150.0	RTD-805	TBD	N/A	N/A	N/A	Temp.)	NoCal
RT-M-A10-01	0	533.0	120.0	RTD-805	TBD	N/A	N/A	N/A		NoCal
RT-M-D3-01	90	40.0	150.0	RTD-805	TBD	N/A	N/A	N/A		NoCal
RT-M-D5-01	90	170.0	150.0	RTD-805	TBD	N/A	N/A	N/A		NoCal
RT-M-D7-01	90	290.0	150.0	RTD-805	TBD	N/A	N/A	N/A		NoCal
RT-M-D9-01	90	423.0	150.0	RTD-805	TBD	N/A	N/A	N/A		NoCal

Other Instrumentation List

Labeling	Azimuthal	Vertical	Radial	Transducer	Location	Details	Basic	Modified	Comnts	Calibration
I D	Angle	Elevation	Distance	Designation	Drawing #	Drawing #	Mark #	Mark #		
(name)	(deg)	(in)	(in)			D-SN-P-				
RT-M-D10-01	90	533.0	120.0	RTD-805	TBD	N/A	N/A	N/A		NoCal
RT-M-Z12-01	-	608.0	0.0	RTD-805	TBD	N/A	N/A	N/A		NoCal
RT-M-G3-01	180	40.0	150.0	RTD-805	TBD	N/A	N/A	N/A		NoCal
RT-M-G5-01	180	170.0	150.0	RTD-805	TBD	N/A	N/A	N/A		NoCal
RT-M-G7-01	180	290.0	150.0	RTD-805	TBD	N/A	N/A	N/A		NoCal
RT-M-G9-01	180	423.0	150.0	RTD-805	TBD	N/A	N/A	N/A		NoCal
RT-M-G10-01	180	533.0	120.0	RTD-805	TBD	N/A	N/A	N/A		NoCal
RT-M-J3-01	270	40.0	150.0	RTD-805	TBD	N/A	N/A	N/A		NoCal
RT-M-J5-01	270	170.0	150.0	RTD-805	TBD	N/A	N/A	N/A		NoCal
RT-M-J7-01	270	290.0	150.0	RTD-805	TBD	N/A	N/A	N/A		NoCal
RT-M-J9-01	270	423.0	150.0	RTD-805	TBD	N/A	N/A	N/A		NoCal
RT-M-J10-01	270	533.0	120.0	RTD-805	TBD	N/A	N/A	N/A		NoCal
RT-R-G0-01	180	-60.0	400.0	RTD-805	TBD	N/A	N/A	N/A	Outside	NoCal
PG-R-G4-01	180	96.5	230.0	4040	N/A	N/A	N/A	N/A	(pressure	PostOK
PG-R-G4-02	180	96.5	230.0	4040	N/A	N/A	N/A	N/A	gages)	PostOK
PG-R-G2-01	180	5.0	200.0						Hydro	
PG-R-G6-01	180	210.0	200.0						Pressure	
PG-R-G9-01	180	423.0	200.0						Gages	
CE-M-Z2-01	135	10.0	214.0	SOFO-500	TBD	N/A	684	684	(fiber	NoCal
CE-M-Z2-02	135	10.0	221.0	SOFO-500	TBD	N/A	683	683	optic	NoCal
CE-M-A6-01	0	244.0	214.0	SOFO-500	TBD	N/A	682	682	concrete	NoCal
CE-M-A6-02	0	244.0	221.0	SOFO-500	TBD	N/A	738	738	gages)	NoCal
CE-C-Z6-01	135	244.0	214.0	SOFO-500	TBD	N/A	685	685		NoCal
CE-C-Z6-02	135	244.0	221.0	SOFO-500	TBD	N/A	687	687		NoCal
CE-C-Z11-01	135	573.0	157.0	SOFO-500	TBD	N/A	776	776		NoCal
A00	0	423.0	224.0						Acoustic	PreCal
A01	0	304.0	224.0						Sensors	PreCal
A02	0	184.0	224.0						(Ext)	PreCal
A03	0	10.0	224.0							PreCal
A04	0	-79.0	206.0							PreCal
A05	62	423.0	224.0							PreCal
A06	62	304.0	224.0							PreCal
A07	60	10.0	224.0							PreCal
A08	60	-79.0	206.0							PreCal
A09	90	580.0	170.0							PreCal
A10	90	423.0	230.0							PreCal
A11	90	244.0	230.0							PreCal
A12	90	127.0	230.0							PreCal
A13	90	10.0	230.0							PreCal
A14	120	-79.0	206.0							PreCal
A15	150	423.0	224.0							PreCal
A16	150	304.0	224.0							PreCal
A17	150	184.0	224.0							PreCal
A18	150	10.0	224.0							PreCal
A19	180	644.0	0.0							PreCal
A20	180	184.0	224.0							PreCal
A21	180	10.0	224.0							PreCal
A22	180	-79.0	206.0							PreCal
A23	210	423.0	224.0							PreCal
A24	210	304.0	224.0							PreCal
A25	210	184.0	224.0							PreCal
A26	210	10.0	224.0							PreCal
A27	240	-79.0	206.0							PreCal
A28	270	580.0	170.0							PreCal
A29	270	423.0	230.0							PreCal

Other Instrumentation List

Labeling	Azimuthal	Vertical	Radial	Transducer	Location	Details	Basic	Modified	Comnts	Calibration
I D	Angle	Elevation	Distance	Designation	Drawing #	Drawing #	Mark #	Mark #		
(name)	(deg)	(in)	(in)			D-SN-P-				
A30	270	244.0	230.0							PreCal
A31	270	127.0	230.0							PreCal
A32	270	10.0	230.0							PreCal
A33	285	304.0	224.0							PreCal
A34	285	56.0	224.0							PreCal
A35	300	-79.0	206.0							PreCal
A36	318	423.0	224.0							PreCal
A37	324	10.0	224.0							PreCal

NoCal - No calibration was performed on this instrument before or after model testing
PreCal - Calibration was preformed on this instrument prior to model testing only
PostOK - Calibration was performed on this instrument Before and After model testing and remained within tolerance

Appendix I: Data File Index

Converted Data

01. BPS (Before Prestressing)

DISP_CVTD_DOR_BPS.xls
DISP_CVTD_DYN_BPS.xls
GBST_CVTD_DOR_BPS.xls
GBST_CVTD_DYN_BPS.xls
LINST_CVTD_DOR_BPS.xls
LINST_CVTD_DYN_BPS.xls
PRES_CVTD_DOR_BPS.xls
PRES_CVTD_DYN_BPS.xls
REBST_CVTD_DOR_BPS.xls
REBST_CVTD_DYN_BPS.xls
TEMP_CVTD_DOR_BPS.xls
TEMP_CVTD_DYN_BPS.xls
TENDON_CVTD_DOR_BPS.xls
TENDON_CVTD_DYN_BPS.xls

02. PS (Prestressing)

DISP_CVTD_DOR_PS.xls
DISP_CVTD_DYN_PS1.xls
DISP_CVTD_DYN_PS2.xls
DISP_CVTD_DYN_PS3.xls
GBST_CVTD_DOR_PS.xls
GBST_CVTD_DYN_PS1.xls
GBST_CVTD_DYN_PS2.xls
GBST_CVTD_DYN_PS3.xls
LINST_CVTD_DOR_PS.xls
LINST_CVTD_DYN_PS1.xls
LINST_CVTD_DYN_PS2.xls
LINST_CVTD_DYN_PS3.xls
PRES_CVTD_DOR_PS.xls
PRES_CVTD_DYN_PS1.xls
PRES_CVTD_DYN_PS2.xls
PRES_CVTD_DYN_PS3.xls
RBST_CVTD_DOR_PS.xls
RBST_CVTD_DYN_PS1.xls
RBST_CVTD_DYN_PS2.xls
RBST_CVTD_DYN_PS3.xls
TEMP_CVTD_DOR_PS.xls
TEMP_CVTD_DYN_PS1.xls
TEMP_CVTD_DYN_PS2.xls
TEMP_CVTD_DYN_PS3.xls
TENDON_CVTD_DOR_PS.xls
TENDON_CVTD_DYN_PS1.xls
TENDON_CVTD_DYN_PS2.xls
TENDON_CVTD_DYN_PS3.xls

03. PPS (Post-Prestressing)

DISP_CVTD_DYN_PPS.xls
GBST_CVTD_DYN_PPS.xls
LINST_CVTD_DYN_PPS.xls
PRES_CVTD_DYN_PPS.xls
REBST_CVTD_DYN_PPS.xls
REBST_CVTD_DYN_PPS.xls
SOFO_CVTD_DYN_PPS.xls
TENDON_CVTD_DYN_PPS.xls

04. SFT (System Functionality Test)

DISP_CVTD_DOR_SFT.xls
DISP_CVTD_DYN_SFT.xls
GBST_CVTD_DOR_SFT.xls
GBST_CVTD_DYN_SFT.xls
LINST_CVTD_DOR_SFT.xls
LINST_CVTD_DYN_SFT.xls
PRES_CVTD_DOR_SFT.xls
PRES_CVTD_DYN_SFT.xls
RBST_CVTD_DOR_SFT.xls
REBST_CVTD_DYN_SFT.xls
TEMP_CVTD_DOR_SFT.xls
TEMP_CVTD_DYN_SFT.xls
TENDON_CVTD_DOR_SFT.xls
TENDON_CVTD_DYN_SFT.xls

05. PSFT (Post-System Functionality Test)

DISP_CVTD_DYN_PSFT.xls
GBST_CVTD_DYN_PSFT.xls
LINST_CVTD_DYN_PSFT.xls
PRES_CVTD_DYN_PSFT.xls
REBST_CVTD_DYN_PSFT.xls
TEMP_CVTD_DYN_PSFT.xls
TENDON_CVTD_DYN_PSFT.xls

06. SITILRT (Structural Integrity Test/Integrated Leak Rate Test)

DISP_CVTD_DOR_SITILRT.xls
DISP_CVTD_DYN_SITILRT.xls
GBST_CVTD_DOR_SITILRT.xls
GBST_CVTD_DYN_SITILRT.xls
LINST_CVTD_DOR_SITILRT.xls
LINST_CVTD_DYN_SITILRT.xls
PRES_CVTD_DOR_SITILRT.xls
PRES_CVTD_DYN_SITILRT.xls
REBST_CVTD_DOR_SITILRT.xls
REBST_CVTD_DYN_SITILRT.xls
TEMP_CVTD_DOR_SITILRT.xls
TEMP_CVTD_DYN_SITILRT.xls
TENDON_CVTD_DOR_SITILRT.xls
TENDON_CVTD_DYN_SITILRT.xls

07. PSITILRT (Post-Structural Integrity Test/Integrated Leak Rate Test)

DISP_CVTD_DYN_PSITILRT.xls
GBST_CVTD_DYN_PSITILRT.xls
LINST_CVTD_DYN_PSITILRT.xls
PRES_CVTD_DYN_PSITILRT.xls
RBST_CVTD_DYN_PSITILRT.xls
TEMP_CVTD_DYN_PSITILRT.xls
TENDON_CVTD_DYN_PSITILRT.xls

08. LST (Limit State Test)

DISP_CVTD_DOR_LST.xls
DISP_CVTD_DYN_LST.xls
GBST_CVTD_DOR_LST.xls
GBST_CVTD_DYN_LST.xls
LINST_CVTD_DOR_LST.xls
LINST_CVTD_DYN_LST.xls
PRES_CVTD_DOR_LST.xls
PRES_CVTD_DYN_LST.xls
REBST_CVTD_DOR_LST.xls
REBST_CVTD_DYN_LST.xls
SOFO_CVTD_DOR_LST.xls
SOFO_CVTD_DYN_LST.xls
TEMP_CVTD_DOR_LST.xls
TEMP_CVTD_DYN_LST.xls
TENDON_CVTD_DOR_LST.xls
TENDON_CVTD_DYN_LST.xls

09. PLST (Post-Limit State Test)

DISP_CVTD_DYN_PLST.xls
GBST_CVTD_DYN_PLST.xls
LINST_CVTD_DYN_PLST.xls
PRES_CVTD_DYN_PLST.xls
REBST_CVTD_DYN_PLST.xls
SOFO_CVTD_DYN_PLST.xls
TEMP_CVTD_DYN_PLST.xls
TENDON_CVTD_DYN_PLST.xls

10. SFMT (Structural Failure Mode Test)

ACOUSTIC_SFMT.xls	Acoustic Event Times
DISP_CVTD_DYN_SFMT.xls	
GBST_CVTD_DYN_SFMT.xls	
LINST_CVTD_DYN_SFMT.xls	
PRES_CVTD_DYN_SFMT.xls	
REBST_CVTD_DYN_SFMT.xls	
SOFO_CVTD_DYN_SFMT.xls	
SOL_CVTD_SFMT.xls	LST/PLST and SFMT Dynamic Data for all Standard Output Locations
TENDON_CVTD_DYN_SFMT.xls	

Corrected Data (LST)

DISP_COR_DOR_LST.xls
DISP_COR_DYN_LST.xls
GBST_COR_DOR_LST.xls
GBST_COR_DYN_LST.xls
LINST_COR_DOR_LST.xls
LINST_COR_DYN_LST.xls
REBST_COR_DOR_LST.xls
REBST_COR_DYN_LST.xls
TENDON_COR_DOR_LST.xls
TENDON_COR_DYN_LST.xls

SFMT Video Files

PCCV_SFMT2.mpg

Appendix J: Data Correction for Ambient Thermal Response

J.1 Overview of Instrumentation

As part of the post-test analysis effort, ANATECH was also tasked with reviewing and standardizing the measurements taken during the Limit State Test (LST). There are a variety of factors that can influence gage read-outs so the goal of this standardization effort was to identify these factors and, to the extent that their influence is significant, adjust the raw data to produce a uniform data set.

Detailed presentation and discussion of the PCCV instrumentation is beyond the scope of this Appendix. The instrumentation measurements that were addressed in the "data correction" effort, and the effects and phenomena that were addressed, are listed in Table J.1.

Table J.1

Measurement	Name Abbreviation	Effects Considered for Correction
Displacement	DISP	Temp., Rigid Body Motion
Strains in Special Gaged Rebars	GBST	Temp., Strain Localization
Strains in Liner	LINST	Temp.
Pressure	PRES	--
Strains in Rebar	REBST	Temp., Strain Localization
Tendon Strains	TENDON	Temp.
Temperatures	TEMP	--

The data acquisition system was installed and activated more than seven months prior to the LST. Gage measurements taken at various time intervals throughout this seven moths have provided a vast database of the model's response to changes in temperature. Since the goal of the "data correction" effort is to create a standardized set of data that is free of temperature effects, two sets of this history data were extracted from the data base to calibrate a correction formula for each individual gage. These two datasets are the following: 1) March X - March Y, Before Prestressing (BPS) and 2) August 7-9, Post System Functionality Test, PSFT. The datasets are also designated as "dynamic" data (DYN) and "data of record" (DOR). The dynamic data represents nearly continuous scanning of data, at every frequent intervals, regardless of whether strain and displacement readings have stabilized, and the DOR are scanned only at pressure holds (during the LST) after gage readings have reached a stability criteria. The filenames for the data, therefore, are as listed in Table J.2 below.

Table J-2. Gage Data Filename Matrix

Data Type	DYN_BPS	DYN_PSFT	DYN_LST	DOR_LST
DISP_CVTD	X	X	X	X
GBST_CVTD	X	X	X	X
LINST_CVTD	X	X	X	X
PRES_CVTD			X	X
REBST_CVTD	X	X	X	X
TEDON_CVTD	X	X	X	X
TEMP_CVTD	X	X	X	X

The "DYN_BPS" and DYN_PSFT" data are used to develop the correction algorithms and the "DYN_LST" and "DOR_LST" are the data that are corrected. ANATECH was also tasked with correcting SOL_CVTD_LST_PLST, the standard output location data file.

J.2 Temperature Effects on Measurements

Change in temperature has a direct influence on the strains and displacements of a free-standing structure. Further, temperature changes have secondary effects on the voltage readouts of strain gages. Both of these effects have been considered and quantified in the data correction effort, the former being calibrated by direct observation of the model response during the two calibration periods and the latter being provided by the gage manufacturer. To correct for either phenomena, first requires that the temperature be known at every gage, or in effect, at all possible locations within the PCCV. This information has been obtained by developing a temperature mapping algorithm based on interpolation between the matrix of temperature gages. Development of this algorithm is described below.

J.2.1 Temperature Measurements

The matrix of temperature measuring gages in the PCCV is shown in Figure J-1. Temperature Gages exist on the inside surface of the liner and at certain locations embedded in the concrete wall. Since the matrix of gages has gaps (no gage) at certain elevations and certain azimuths, the interpolation mapping was done in three steps as follows:

1. Extrapolation of Temperature Readings For Liner Inside Surface

   (TI-C-##-##) and the Liner Outside Surface (TW-R-##-##) at Azimuth

   Locations (0° 90°, 135°, 240°, 324°).

2. Compute the thermal gradients at the inside of liner wall.

3. Produce a temperature reading at all strain gage locations using the extrapolated temperature readings and thermal gradients.

Procedure Followed:

1. Read in the Temperature Data for the DOR and the Temperature for the Dynamic Record.

2. Data is read into an array

   a. Gage = G (1D array)

   b. Azimuth = AZ (1D array)

   c. Elevation = EL (1D array)

   d. Radial Distance = RA (1D array)

   e. Temperature Readings = TEMP (2D array)

3. Output a new array

   a. Gage = GB (1D array)

   b. Azimuth = AZN (1D array)

   c. Elevation = ELN (1D array)

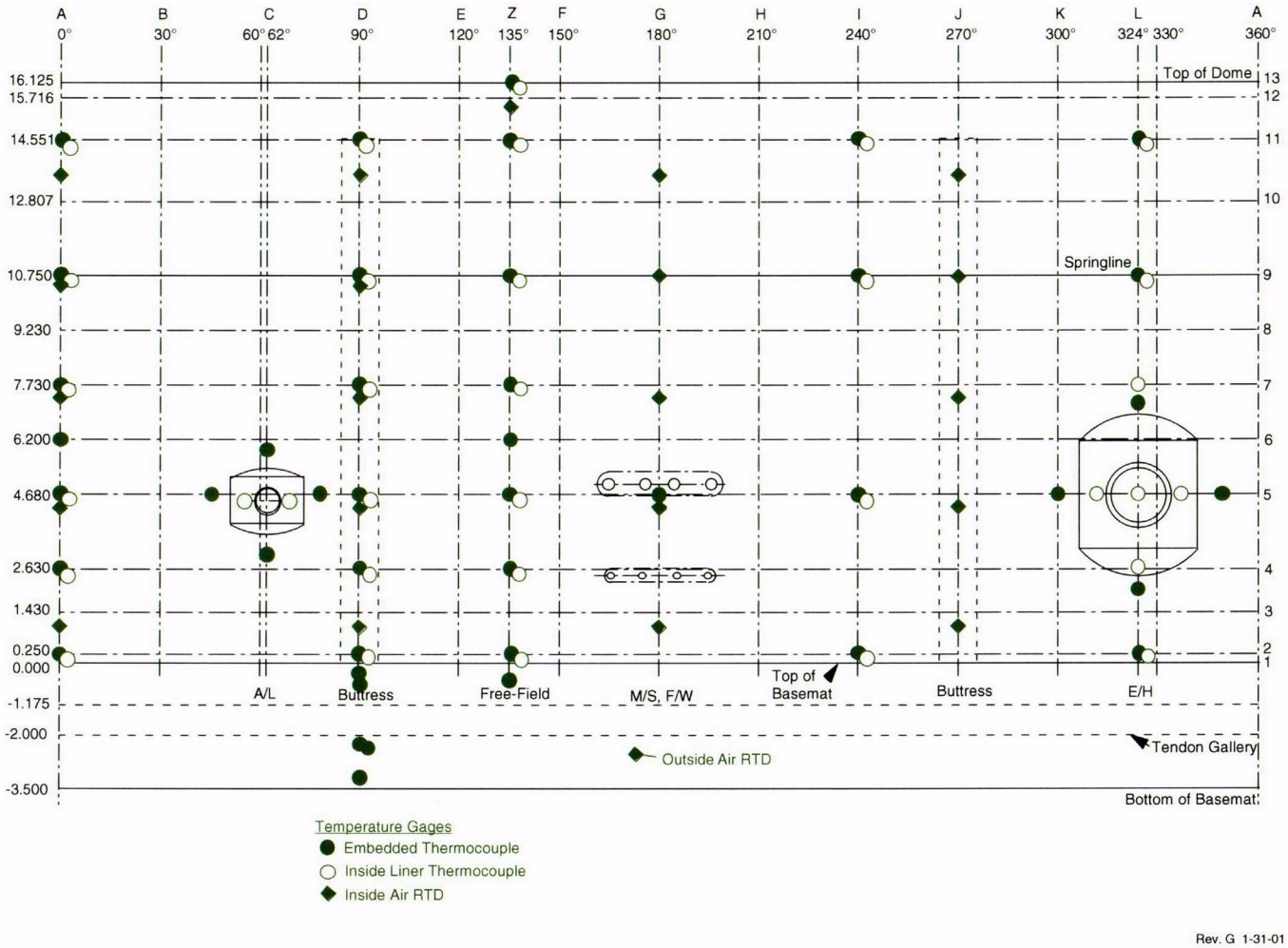

Figure J.1 Temperature Instrumentation Locations

C127

d. Radial Distance = RAN (1D array)

e. Temperature Readings = R(i , j) (2D array)

4. Output the Thermal Gradients of Inside Liner Location

a. Formula used:

1 $T_{grad} = (T_{conc} - T_{liner})/ \Delta r$

where Δr = Rconc – Rliner

5. Data array of strain gage locations read into new program with corresponding temperature readings on the inner liner and middle thickness of wall. The Subprogram Inter produces a temperature corresponding to a given elevation, azimuth, and radial distance.

6. Output strain gage readings and temperature readings.

J.2.2 Temperature Interpolation

The FORTRAN program algorithms for this procedure and three illustrative examples are outlined below. These examples show the temperature interpolation at three specific points within the PCCV cylinder. It should be noted that no basemat temperature extrapolation was attempted due to the lack of detailed temperature information within the basemat. Basemat gages were all assumed to be the same as the temperature at the base of the wall.

Temperature Interpolation of the Absent Strain Gages

The following example shows how temperature is extrapolated to a "missing" location.

Gages on Line 0 Degree
Gage 1 - TW-R-A2-01
Gage 2 – TW-R-A3-01
Gage 3 – TW-R-A4-01

Given: Gage 1 – Given by TEMP_CVTD_DOR_LST
Gage 3 – Given by TEMP_CVTD_DOR_LST

Required: Extrapolation of Gage 2

$$X(1) = 1. - \frac{elev.\ (TW-R-A3-01) - elev.\ (TW-R-A2-01)}{elev.\ (TW-R-A4-01) - elev.\ (TW-R-A2-01)} = 1 - \left(\frac{1430-254}{2642-254}\right) = 0.50754$$

$$X(2) = 1. + \frac{(elev.(TW-R-A3-01) - elev.(TW-R-A4-01))}{elev.(TW-R-A4-01) - elev.(TW-R-A2-01)} = 1 + \left(\frac{1430-2642}{2642-254}\right) - = 0.4924$$

Temperature TW-R-A3-01 = Temperature (TW-R-A2-01)*X(1) + Temperature (TW-R-A4-01)*X(2)

Temperature TW-R-A3-01 = (13.864)*0.50754+16.294901*(0.4924) = 15.0601 @ Time = 03/03/00 11:47

Temperature placed into Data Array at Time "L"

Temperature Interpolation at a Specific Location

Given: Temperature reading on line (2,3,4,5,6,7,8,9,10,11,12,13) and on azimuth (0°, 90°, 135°, 240°, 324°)

Examples: Extrapolation of Temperatures for Following Locations

1. Location1: Elevation =1425 Azimuth 35 degree, Radius 5699.7mm
2. Location2: Elevation =9130 Azimuth 210 degree, Radius 5359.4mm
3. Location3: Elevation =12900 Azimuth 310degree, Radius 5780.95mm

Information entered for subroutine temperature extrapolation

1. Azimuth Data: data az / 0.0, 90.0, 135.0, 240.0, 324.0, 360.0 /

2. Elevation Data: data elev / 254.0, 1430.0, 2642.0, 4674.0,
6200.0, 7722.0, 9230.0,10744.0,12807.0,
14554.0,15716.0,16125.0 /

3. Radial Data: data ra / 5359.4, 5537.2, 5638.8 /
where, data ra / inner liner radius, middle wall radius (except on line D), middle wall radius on line D /

Example 1.

(a) Search on Azimuth Location
First Azimuth Location = 0° (a)
Second Azimuth Location = 90° (a+1)

(b) Search on Elevation Location
First Elevation Location = 250.0 (e)
Second Elevation Location = 1430.0 (e+1)

(c) Search for Radial location

1. Since the gage is located at 35 degrees
- If radius of wall temperature is located at 0° then Radius = 5537.2 mm
- If radius of wall temperature is located at 90° then Radius = 5638.8 mm
5638.8 mm - 5537.2 mm = 101.6 mm

Therefore, radius of the wall for the example 1 gage location:
Formula: (liner radius + (wall radius on Line D) - (wall radius on Line A)

$$\left(\frac{(Az.(2)-Az.(gage)}{Az.(2)-Az.(1)}\right)$$

Value for Wall Radius:

$$5537.2 \text{ mm (liner radius)} + (5537.2 \text{ mm})\left(\frac{(90-35)}{90-0}\right) = 5599.29 \ mm$$

(d) Temperature is interpolated for Vertical Elevation

fact1=(elev(e+1)-EL1(i))/(elev(e+1)-elev(e)) = (1430.0-1425)/(1430.0 – 254.0) = 0.00425
fact2=(EL1(i)-elev(e))/(elev(e+1)-elev(e)) = (1425-254)/(1430-254) = 0.99575

1. LINER Temperature taken as % from 1st loc. + % from 2nd loc. data temperature at 1st elev., 1st az, 1st rad. loc. and 2nd elev.,1st az,1st rad. loc.

temp(1,ii)=fact1* temp. liner(254mm, 0°, 1-34) + fact2* temp. liner(1430mm, 0°, 1-34)
temp(1,2) = 0.00425*20.1455 + 0.99575 * 19.616 =19.6183

2. LINER Temperature taken as % from 1st loc. + % from 2nd loc.
   1st elev., 2nd az, 1st rad. loc.to 2nd elev.,2nd az,1st rad. loc.

temp(2,ii)=fact1* temp. liner(254mm, 90°, 1-34)+fact2* temp. liner(1430mm, 90°, 1-34)
temp(2,2) = 0.00425*20.2373 + 0.99575 * 19.783 =19.7849

3. WALL Temperature taken as % from 1st loc. + % from 2nd loc.
   1st elev., 1st az, 2nd rad. loc.to 2nd elev.,1st az,2nd rad. loc.

temp(3,ii)=fact1* temp. wall(254mm, 0°, 1-34)+fact2* temp. wall(1430mm, 0°, 1-34)
temp(3,2) = 0.00425*19.2764 + 0.99575 * 18.519 =18.5222

4. WALL Temperature taken as % from 1st loc. + % from 2nd loc.
   1st elev., 2nd az, 2nd rad. loc.to 2nd elev.,2nd az,2nd rad. loc.

temp(4,ii)=fact1* temp. wall(254mm, 90°, 1-34)+fact2* temp. wall(1430mm, 90°, 1-34)
temp(4,2) = 0.00425*19.9335 + 0.99575 * 19.436 =19.4381

2. Interpolation along the azimuth

fact1=(az(a+1)-AZ1(i))/(az(a+1)-az(a)) = (90-35)/(90-0) = 0.611
fact2=(AZ1(i)-az(a))/(az(a+1)-az(a)) = (35-0)/(90-0)=0.3889
tempa(1,ii)=fact1* temp(1,ii)+fact2* temp(2,ii)
tempa(1,2) = 0.611*19.6183+ 0.3889 * 19.7849 =19.6811

tempa(2,ii)=fact1*temp(3,ii)+ fact2*temp(4,ii)
tempa(2,2) = 0.611*18.5222 + 0.3889 * 19.4381 =18.8764

3. Finally the interpolation through the thickness

fact1=(rm-RA1(i))/(rm-ra(1)) = (5599.29 mm -5699.7 mm)/(5599.29 mm-5359.4) = -0.4186
fact2=(RA1(i)-ra(1))/(rm-ra(1)) = (5699.7mm-5359.4)/(5599.29 mm-5359.4) = 1.4186

tempr(i,ii)=fact1*tempa(1,ii)+fact2*tempa(2,ii)
tempr(1,2) = -0.4186*19.6811+1.4186*18.8764 = 18.5396

Example 1 for DOR_LST @ 9/26/00 10:03

Example Pt.	*Gage 1*	*Temp.*	*Gage 2*	*Temp.*	*Gage 3*	*Temp.*	*Gage 4*	*Temp.*
Liner	TI – C-A2-01	20.146	TI – C-A3-01	19.62	TI – C-D2-01	20.237	TI – C-D3-01	19.7838
Outside	TW – R-A2-01	19.276	TW – R-A3-01	18.52	TW – R-D2-01	19.9335	TW – R-D3-01	19.4368
Final								18.5396

Example 2.

(a) Search on Azimuth Location
First Azimuth Location = 135° (a)
Second Azimuth Location = 240° (a+1)

(b) Search on Elevation Location
First Elevation Location = 7722.0 (e)

Second Elevation Location = 9230 (e+1)

(c) Search for Radial location

Since the gage is located at 200 degrees Radius of wall = 5537.2 mm
- If radius of wall temperature is located at 135° then Radius = 5537.2 mm
- If radius of wall temperature is located at 240° then Radius = 5537.2 mm
  5537.2 mm - 5537.2 mm = 0 mm

(d) Temperature is interpolated for Vertical Elevation

fact1=(elev(e+1)-EL1(i))/(elev(e+1)-elev(e)) = (9230.-9130)/(9230 – 7722.0) = 0.066313
fact2=(EL1(i)-elev(e))/(elev(e+1)-elev(e)) = (9130-7722.0)/(9230-7722.0) = 0.933687

1. LINER Temperature taken as % from 1st loc. + % from 2nd loc.
data temperature at 1st elev., 1st az, 1st rad. loc.and 2nd elev.,1st az,1st rad. loc.

temp(1,ii)=fact1* temp. liner(7722mm, 135°, 1-34) + fact2* temp. liner(9230mm, 135°, 1-34)
temp(1,2) = 0.066313*17.0938 + 0.933687 * 17.065506 =17.06738

2. LINER Temperature taken as % from 1st loc. + % from 2nd loc.
1st elev., 2nd az, 1st rad. loc.to 2nd elev.,2nd az,1st rad. loc.

temp(2,ii)= fact1* temp. liner(7722mm, 240°, 1-34) + fact2* temp.liner(9230mm, 240°, 1-34)
temp(2,2) = 0.066313*16.8714 + 0.933687 * 16.794495 =16.799594

3. WALL Temperature taken as % from 1st loc. + % from 2nd loc.
1st elev., 1st az, 2nd rad. loc.to 2nd elev.,1st az,2nd rad. loc.

temp(3,ii)=fact1* temp. wall(7722mm, 135°, 1-34) +fact2* temp. wall(9230mm, 135°, 1-34)
temp(3,2) = 0.066313*15.5703 + 0.933687 * 15.857828 =15.83876

4. WALL Temperature taken as % from 1st loc. + % from 2nd loc.
1st elev., 2nd az, 2nd rad. loc.to 2nd elev.,2nd az,2nd rad. loc.

temp(4,ii)=fact1* temp. wall(7722mm, 240°, 1-34)+fact2* temp. wall(9230mm, 240°, 1-34)
temp(4,2) = 0.066313*16.368855+ 0.933687 * 14.087605 =14.2388

(e) Interpolation along the azimuth

fact1=(az(a+1)-AZ1(i))/(az(a+1)-az(a)) = (240-210)/(240-135) = 0.2857
fact2=(AZ1(i)-az(a))/(az(a+1)-az(a)) = (210-135)/ (240-135)=0.71429
tempa(1,ii)=fact1* temp.(1,ii)+fact2* temp.(2,ii)
tempa(1,2) = 0.2857*17.06738+ 0.71429 * 16.799594 =16.87593

tempa(2,ii)=fact1*temp(3,ii)+ fact2*temp(4,ii)
tempa(2,2) = 0.2857*15.83876+ 0.71429 * 14.2388 =14.69577

(f) Finally the interpolation through the thickness

fact1=(rm-RA1(i))/(rm-ra(1)) = (5537.2mm-5359.4mm)/(5537.2mm -5359.4mm) = 1.0
fact2=(RA1(i)-ra(1))/(rm-ra(1)) = (5359.4mm-5359.4)/(5537.2mm -5359.4mm) = 0.0

tempr(i,ii)=fact1*tempa(1,ii)+fact2*tempa(2,ii)
tempr(1,2) = 1.0*16.87593+1.0*14.2388 = 16.87593

Example 2 for DOR_LST @ 9/26/00 10:03

Example Pt.	*Gage 1*	*Temp.*	*Gage 2*	*Temp.*	*Gage 3*	*Temp.*	*Gage 4*	*Temp.*
Liner	TI – C-Z7-01	17.094	TI – C-Z8-01	17.06551	TI – C-I7-01	16.87147	TI – C-I8-01	16.7945
Outside	TW – R–Z7-01	15.570	TW – R-Z8-01	15.8578	TW – R–I7-01	16.36885	TW – R-I8-01	14.08761
Final								16.87593

Example 3.

(a) Search on Azimuth Location
First Azimuth Location = 240° (a)
Second Azimuth Location = 324° (a+1)

(b) Search on Elevation Location
First Elevation Location = 12807.0 (e)
Second Elevation Location = 14554.0 (e+1)

(c) Search for Radial location

Since the gage is located at 310 degrees Radius of wall = 5537.2 mm
- If radius of wall temperature is located at 135° then Radius = 5537.2 mm
- If radius of wall temperature is located at 240° then Radius = 5537.2 mm
  5537.2 mm - 5537.2 mm = 0 mm

(d) Temperature is interpolated for Vertical Elevation

fact1=(elev(e+1)-EL1(i))/(elev(e+1)-elev(e)) = (14554.-12900)/(14554 – 12807.0)
= 0.9468
fact2=(EL1(i)-elev(e))/(elev(e+1)-elev(e)) = (12900-12807.0)/(14554-12807.0) = 0.05323

1. LINER Temperature taken as % from 1st loc. + % from 2nd loc.
data temperature at 1st elev., 1st az, 1st rad. loc.and 2nd elev.,1st az,1st rad. loc.

temp(1,ii)=fact1* temp. liner(12807mm, 240°, 1-34) + fact2* temp. liner(14554, 240°, 1-34)
temp(1,2) = 0.9468*16.584515 + 0.05323* 15.8984 =16.5485

2. LINER Temperature taken as % from 1st loc. + % from 2nd loc.
1st elev., 2nd az, 1st rad. loc.to 2nd elev.,2nd az,1st rad. loc.

temp(2,ii)= fact1* temp.liner(12807, 324°, 1-34) + fact2* temp.liner(14554, 324°, 1-34)
temp(2,2) = 0.9468 *17.45914 + 0.05323* 17.5098 =17.4624

3. WALL Temperature taken as % from 1st loc. + % from 2nd loc.
1st elev., 1st az, 2nd rad. loc.to 2nd elev.,1st az,2nd rad. loc.

temp(3,ii)=fact1* temp. wall(12807, 240°, 1-34) +fact2* temp. wall(14554, 240°, 1-34)
temp(3,2) = 0.9468 *15.976255 + 0.05323* 15.619388 =15.9577

4. WALL Temperature taken as % from 1st loc. + % from 2nd loc.
1st elev., 2nd az, 2nd rad. loc.to 2nd elev.,2nd az,2nd rad. loc.

temp(4,ii)=fact1* temp. wall(12807, 324°, 1-34)+fact2* temp. wall(14554, 324°, 1-34)
temp(4,2) = 0.9468 *18.13707+ 0.05323* 18.0732 =18.1342

(e) Interpolation along the azimuth

fact1=(az(a+1)-AZ1(i))/(az(a+1)-az(a)) = (324-310)/(324-240) = 0.1667
fact2=(AZ1(i)-az(a))/(az(a+1)-az(a)) = (310-240)/ (324-240)=0.8333
tempa(1,ii)=fact1* temp.(1,ii)+fact2* temp.(2,ii)
tempa(1,2) = 0.1667*16.5485+ 0.8333 * 17.4624=17.3101

tempa(2,ii)=fact1*temp(3,ii)+ fact2*temp(4,ii)
tempa(2,2) = 0.1667*15.9577+0.8333 * 18.1342 =17.7713

(f) Finally the interpolation through the thickness

fact1=(rm-RA1(i))/(rm-ra(1)) = (5537.2mm-5780.95mm)/(5537.2mm -5359.4mm) = -1.371
fact2=(RA1(i)-ra(1))/(rm-ra(1)) = (5780.95mm-5359.4)/(5537.2mm -5359.4mm) = 2.37

tempr(i,ii)=fact1*tempa(1,ii)+fact2*tempa(2,ii)
tempr(1,2) = -1.371*17.3101+2.371*17.7713 = 18.4195

Example 3 for DOR_LST @ 9/26/00 10:03

Example Pt.	*Gage 1*	*Temp.*	*Gage 2*	*Temp.*	*Gage 3*	*Temp.*	*Gage 4*	*Temp.*
Liner	TI – C-I10-01	16.584	TI – C-I11-01	15.8984	TI – C-L10-01	17.459	TI – C-L11-01	17.51
Outside	TW – R-I10-01	15.976	TW – R-I11-01	15.619	TW – R-L10 - 01	18.137	TW – R-L11-01	18.073
Final								18.4195

J.2.3 Direct Temperature Effects on Gages

The basic premise for the gate temperature corrections is to calculate, for each gage, a gage adjustment function that is a function only of the temperature at that gage. This premise accepts the simplification that the correction is only a function of the individual gage temperature, when in reality it may be a function of the complete temperature distribution caused structural interaction effects. Since these interactions are judged to be secondary effects compared to the direct thermal expansion occurring directly at each gage, these secondary effects are being ignored in the data correction. Further, since much of the temperature changes are caused by passage of the sum, it is likely that daytime temperature distributions will at least be similar to each other (i.e. the sun will never be shining on the north side of the model, regardless of the seasonal changes in solar apogy). It is also noted that by using the BPS and the PSFT datasets, temperature corrections at a range of different PCCV stress levels have been evaluated.

J.2.4 Secondary Temperature Effects on Strain Gages(Correction Terms)

These effects are provided directly from the gage manufacturer. The corrections are in the form of Lot Numbers, with corrections given in units of microstrain.

Lot Number R-A12BP25:

$\Sigma = 4.97 \times 10^{1} + 1.12 \times 10^{0}T - 2.81 \times 10^{-2}T^{2} + 6.18 \times 10^{-5}T^{3} - 3.11 \times 10^{-8}T^{4}$ (deg F)

$\Sigma = 5.87 \times 10^{1} - 8.93 \times 10^{-1}T - 7.24 \times 10^{-2}T^{2} + 3.37 \times 10^{-4}T^{3} - 3.26 \times 10^{-7}T^{4}$ (deg C)

Lot Numbers R-A19A595, R-A19AP58, R-A19AP61, R-A19AP75, R-A19AP81, R-A19AP82, R-A19AP83,

R-A19AP95, R-A19AP96, R-A19AP97:

$\Sigma = -3.81 \times 10^{1} + 2.74 \times 10^{0}T - 3.52 \times 10^{-2}T^2 + 7.64 \times 10^{-5}T^3 - 4.30 \times 10^{-8}T^4$ (deg F)

$\Sigma = 1.60 \times 10^{1} + 1.29 \times 10^{-0}T - 9.11 \times 10^{-2}T^2 + 4.13 \times 10^{-4}T^3 - 4.51 \times 10^{-7}T^4$ (deg C)

Lot Number R-A19BP02:

$\Sigma = -1.39 \times 10^{1} + 2.41 \times 10^{0}T - 3.51 \times 10^{-2}T^2 + 7.74 \times 10^{-5}T^3 - 4.62 \times 10^{-8}T^4$ (deg F)

$\Sigma = 2.99 \times 10^{1} + 7.17 \times 10^{-1}T - 9.06 \times 10^{-2}T^2 + 4.17 \times 10^{-4}T^3 - 4.85 \times 10^{-7}T^4$ (deg C)

Lot Numbers R-A42AP02, R-A42AP04, R-A42AP08:

$\Sigma = -1.50 \times 10^{2} + 4.44 \times 10^{0}T - 3.82 \times 10^{-2}T^2 + 7.93 \times 10^{-5}T^3 - 4.33 \times 10^{-8}T^4$ (deg F)

$\Sigma = -4.45 \times 10^{1} + 4.02 \times 10^{0}T - 1.00 \times 10^{-1}T^2 + 4.30 \times 10^{-4}T^3 - 4.54 \times 10^{-7}T^4$ (deg C)

J.3 Standardize Gage Measurements

The development of the algorithm for temperature correction proceeded as follows.

1. Compute a mean linearized temperature correction factor $\overline{A}_1$, and standard deviation, σ_{A1} for every gage from Data Set 1 (the BPS data).

Typical calculation

ε_{n_i} is a set of dynamic gage data for gage n and time/temperature i=1, 2, 3, ...

$\varepsilon^t_{n_i} = \varepsilon_{n_i} - \Sigma_{n_i}$ (where Σ is a polynomial correction from Section 3.2.4)

$$\varepsilon'_{n_i} = f_n\left(\varepsilon^t_{n_i}\right)$$

Where f_n is a non-temperature correction function defined only for certain gages; in most cases $\varepsilon'_{n_i} = \varepsilon^t_{n_i}$

$$\Delta\varepsilon'_{n_i} = \varepsilon'_{n_i} - \varepsilon'_{n_1}$$

$$\Delta^T_{n_i} = T_{n_i} - T_{n_1}$$

$$A_{i_n} = \frac{\Delta\varepsilon'_{n_i}}{\Delta T_{n_i}}$$

Calculate a weighted average A_n- weighted average because we want the data correction to be the most heavily influenced by strain-temperature observation data that causes the largest strains:

$$\bar{A}_n = \frac{\frac{1}{\bar{\Delta\varepsilon}'_{n_i}} \sum_{i=1}^{I} \Delta\varepsilon'_{n_i} \frac{\Delta\varepsilon'_{n_i}}{\Delta T_{n_i}}}{I}$$

Where I = number of temperature points and $\bar{\Delta\varepsilon}'_{n_i}$ is the average of $\Delta\varepsilon'_{n_i}$

Check σ_A (Criteria $\sigma_{A_n} < 0.2\bar{A}_n$)

The assumed basic correction formula is therefore: $\varepsilon^c_{n_i} = \varepsilon_{n_i} - \Sigma_{n_i} - \bar{A}_n \Delta T_{n_i}$

This should produce a set of "corrected" gage readings that have less than 20% variation from the reading at time 1 over the entire time period.

2. Repeat same procedure for $\bar{A}_2$ and σ_{A_2} for every gage from Data Set 2 (the PSFT data)

Let $\alpha_n = \frac{\bar{A}_{n_1} + \bar{A}_{n_2}}{2}$ (or some other combination using other parameters or judgment)

3. Apply the correction to the DYN_LST and DOR_LST data.

The data for comparison to analysis that is free of temperature effects the (DYN_LST and DOR_LST), cannot be simply "zeroed" at the start, because the strains and displacements associated with the prestressing load and dead weight of the structure are important. To make the data free of temperature effects, the temperature corrections must be applied to a certain reference temperature. Since the LST started in the early morning prior to solar heating of the PCCV (and of course, prior to any heating or cooling caused by pumped in nitrogen), the LST DOR point 1 (zero pressure) is used as the reference temperature at each gage. (These temperatures can be different at each gage.) Using this reference temperature, the final correction formula becomes

$$\varepsilon^c_{n_i} = f_n\left(\varepsilon_{n_i} - \Sigma_{n_i}\right) - \alpha_n\left(T_{n_i} - T_{n_i}\right) \qquad \text{(J-1)}$$

Note that the function f_n could cover other, non-temperature related correction terms and might only be defined for certain gages.

J.3.1 Correction Summaries by Gage Group

Displacements

For the displacement measurements, Equation J-1 is followed without further correction except for some of the vertical displacement measurements. For the vertical displacement, there may have also been some movement of a portion of the instrumentation frame that influenced the gage readings.

Rebar Strains

Equation J-1 is followed with no function f_n.

A typical bar area reduction as a result of the grinding is 1.019. Then it is assumed that for all strain ε, there is a unique stress, σ, according to the engineering stress-versus engineering strain data. Using the data for the SD390-D13 bars, averaged, the yield curve is approximately

ε	σ
.002	58 ksi
.009	60.9 ksi
.013	62.06 ksi
.015	63.075 ksi
.020	66.7 ksi

For $\varepsilon^t_{n_i}, \sigma^t_{n_i}$ is "looked-up" from the yield function

Then $\sigma^{'}_{n_i} = \sigma^t_{n_i}$ / (Area Ratio)

$\varepsilon^{'}_{\varepsilon_i}$ is then "looked-up" from the yield function.

Thus, function "f_n" for rebar strain is a two-step "look-up" function.

Liner Strains

Equation J-1 is followed with no function f_n.

Tendon Strains

Equation J-1 is followed with no function f_n.

Appendix K: Soundprint® Acoustic System Reports

SoundPrint™ Acoustic Monitoring Report
Sandia PCCV

LST Sept 26-27, 2001

SFMT November 14, 2001

Background

Acoustic monitoring captures acoustic data arriving at sensors distributed over the PCCV model. For the LST and SIT, fifty-four sensors were used, sixteen of which were indice the vessel on the steel liner, and thirty-eight were installed on the outside of the concrete surface. For the SFMT test, no sensors were remaining inside the model, and thirty-eight sensors remained on the outside of the vessel.

The output of the sensors was recorded as acoustic energy arrived. Post-processing of the recorded information was done to estimate the location and the nature of the source of each event. Event classifications used throughout the testing included:

- Concrete cracking
- Wire Breaks
- Other emissions from the tendons
- Nitrogen Flow
- Leaks

Summary of Results

Concrete cracking events were dominant in SIT and the LST, but were largely absent during the SFMT. During the LST, analysis of the signals from the sensors appear to have detected the appearance of leaks in the liner.

The nitrogen flow noise, wire breaks, and other events originating from the area of tendon anchorages were the dominant features of the SFMT. The classification "tendon pings" was used to describe emissions showing resonant peaks in the 4KHz. To 8 KHz band. The classifications "wire break" , "double wire break", and "multiple wire break", were used to describe emissions that had other characteristics consistent with the failure of one or more wires in a tendon.

Estimates were made of the amount of energy released by each event relative to a reference impact. These estimates are qualitative only, as increasing amounts of damage to the concrete affected the propagation of acoustic energy from the source to the sensors.

Streaming audio files were available in real time to assist in understanding the developments on the model during each phase of the test.

Detection of Concrete Cracking

Concrete cracking was detected during the stressing phase, during aging of the vessel, and during the pressurization phases. Some of the events recorded were confirmed by visual examination. The cracking was audible during pressurization as continuous Kaiser effect cracking as each new pressure plateau was realized.

Larger cracks affected a sufficient number of sensors that the position of the origin of the cracks could be estimated.

Detection of Leaks during the LST

Analysis of the output of the sensors during the pressurization of the LST was done in an attempt to determine the development of leaks, and to determine the location of the first leaks as they appeared. In observing the FFT of all of the internal sensors, anomalies started to appear at 2.4 Pd in the area around the equipment hatch. This appearance is illustrated below in Figures 1 to 3.

Graph of FFT of Internal Sensors at different pressures during LST

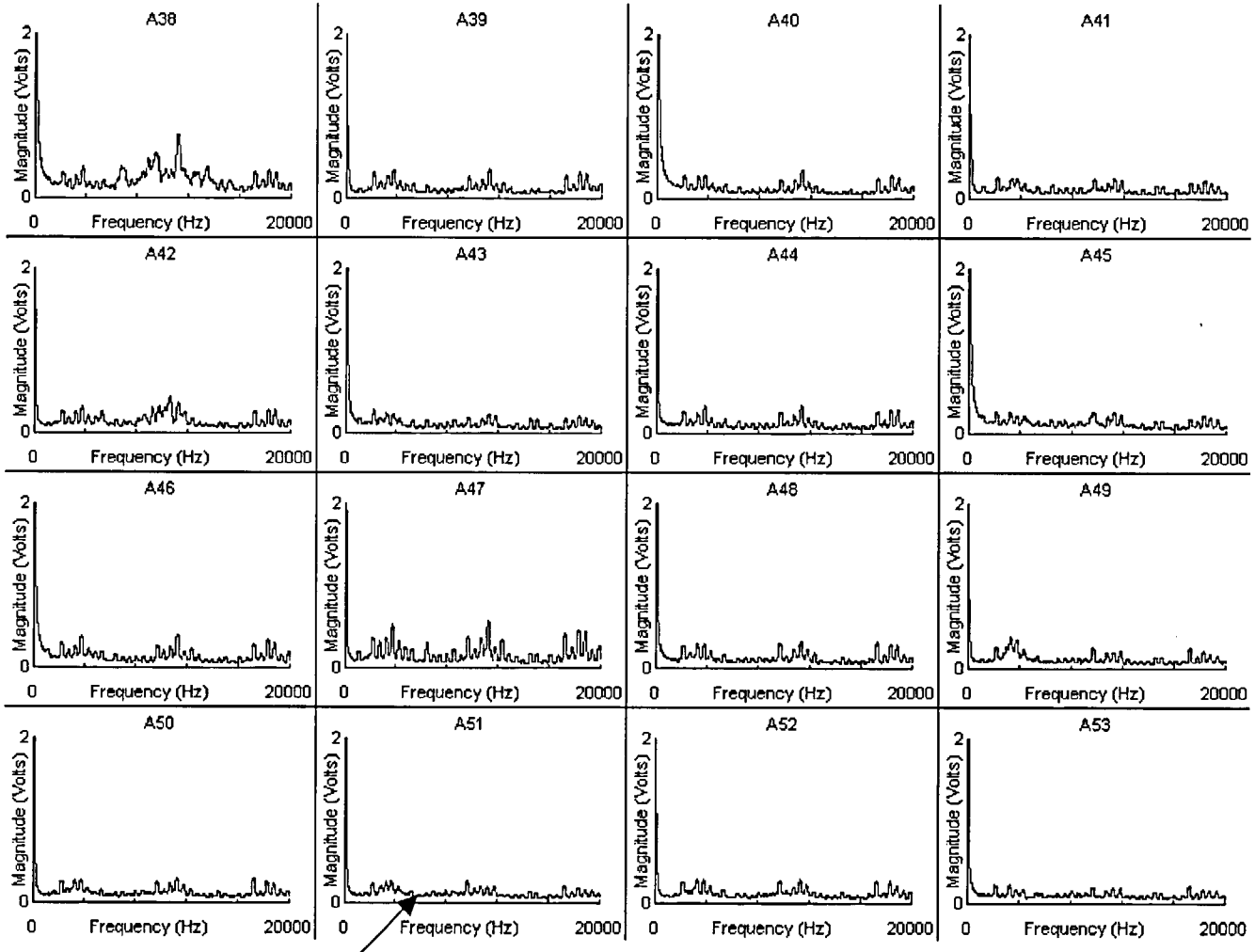

Figure 1: Internal Sensors (FFT) at 2.3 Pd

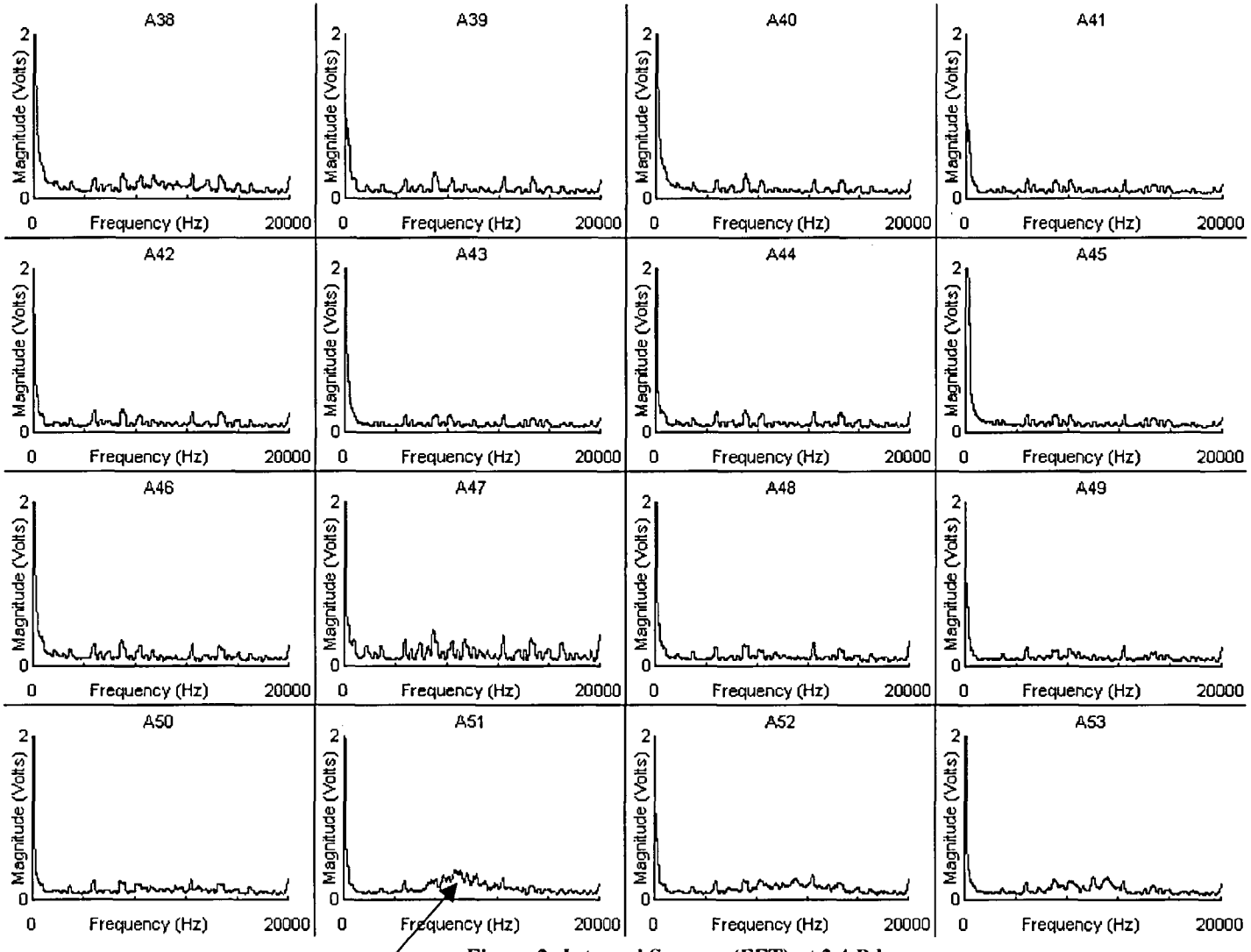

Figure 2: Internal Sensors (FFT) at 2.4 Pd

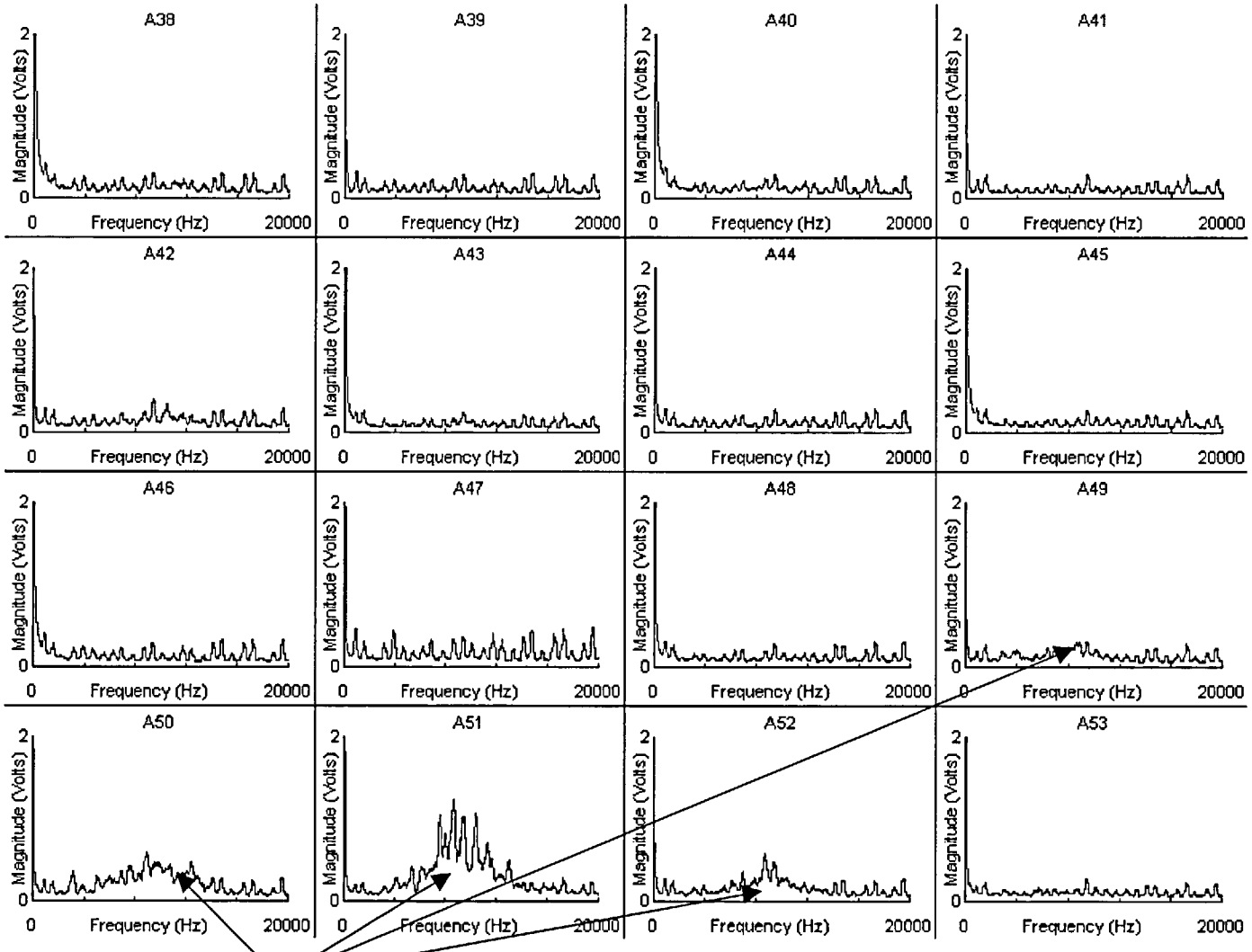

Figure 3: Internal Sensors (FFT) at 2.5 Pd

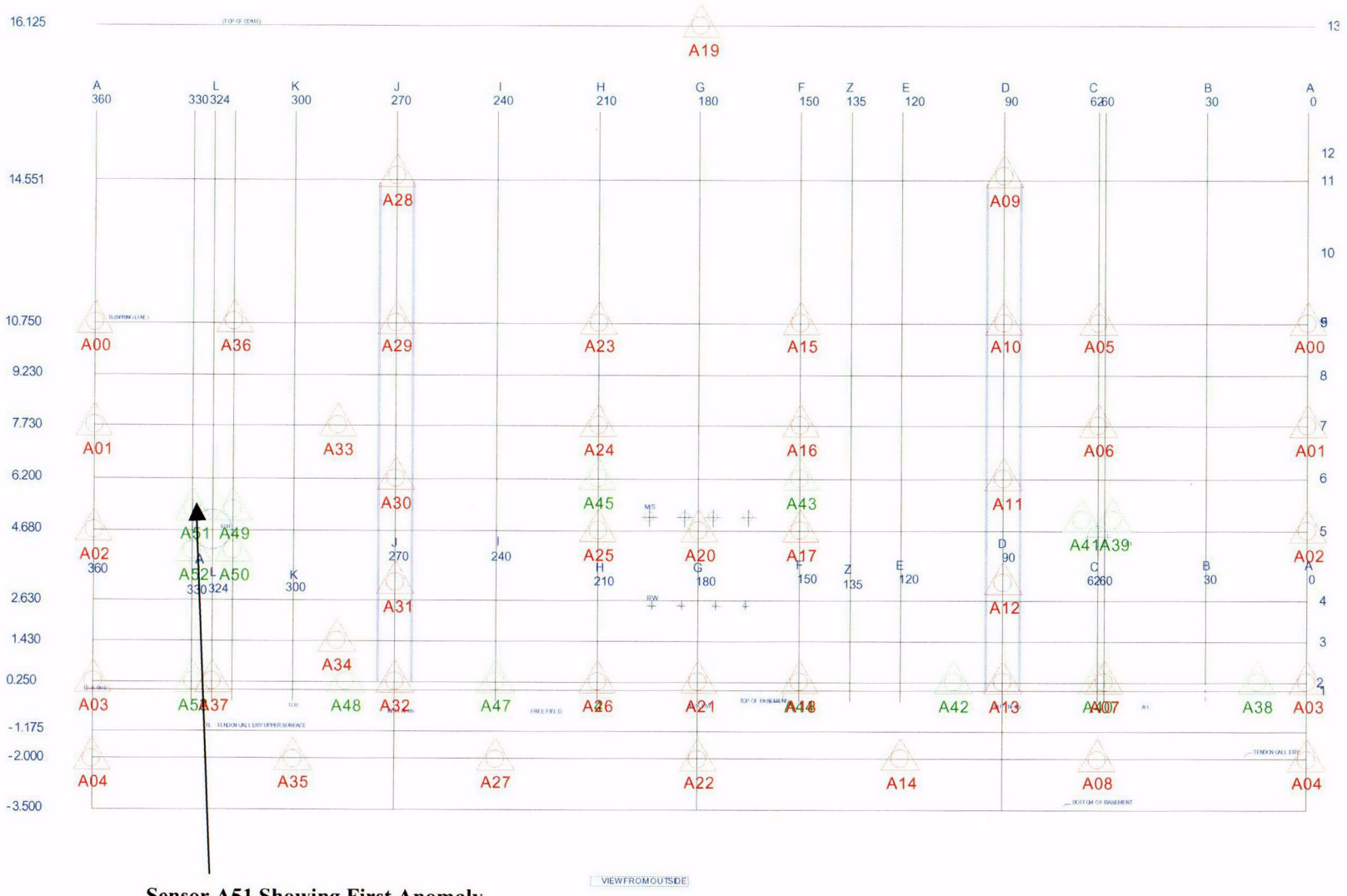

Sensor A51 Showing First Anomaly

Figure 4: Location of Sensor Detecting the first leak during LST

C128

Effect of Schmidt Hammer on PCCV

Use of a Sclerometer or Schmidt hammer allows the estimation of the size of an acoustic event. The Schmidt hammer generates about 1 Joule of energy. Below are two graphs showing the time domain and energy estimate of a Schmidt hammer impact on the PCCV wall.

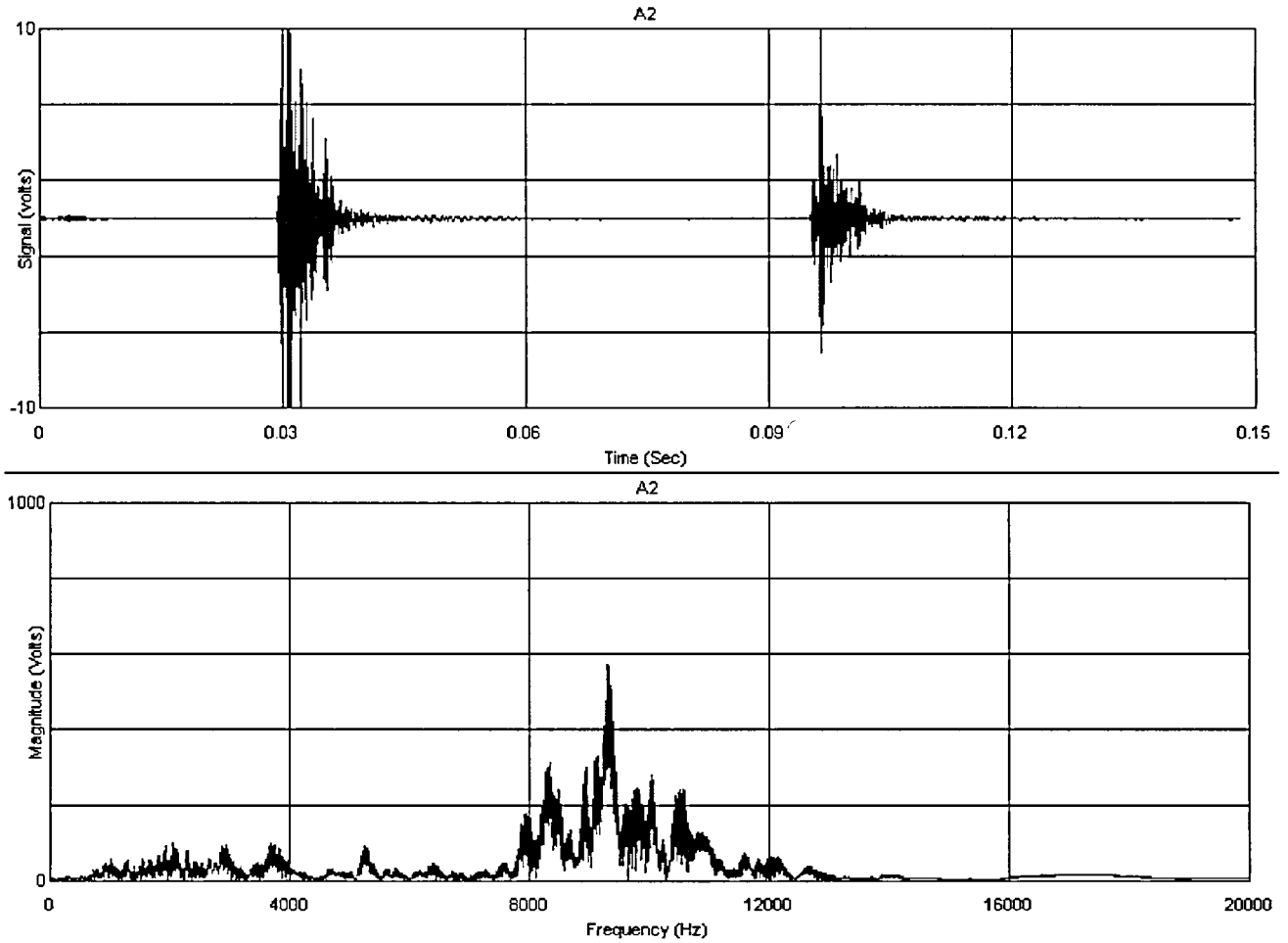

Fig 5: Time Domain and Frequency Domain of Schmidt Hammer Impact

Detection of "Tendon Pings during LST and SFMT

The phenomenon of "tendon pings" appeared during the LST. These emissions are characterized by a modest energy emission and a ringing sound, as if a taut string were plucked. Virtually all of these originated at or near the buttresses. The ringing manifests itself as a sharp peak in the FFT of the event. Below are two graphs showing the Time domain and Frequency domain graphs of a typical "Tendon Ping". These started occurring at a pressure of 1.7 Pd and continued to a pressure of 2.9 Pd during the LST

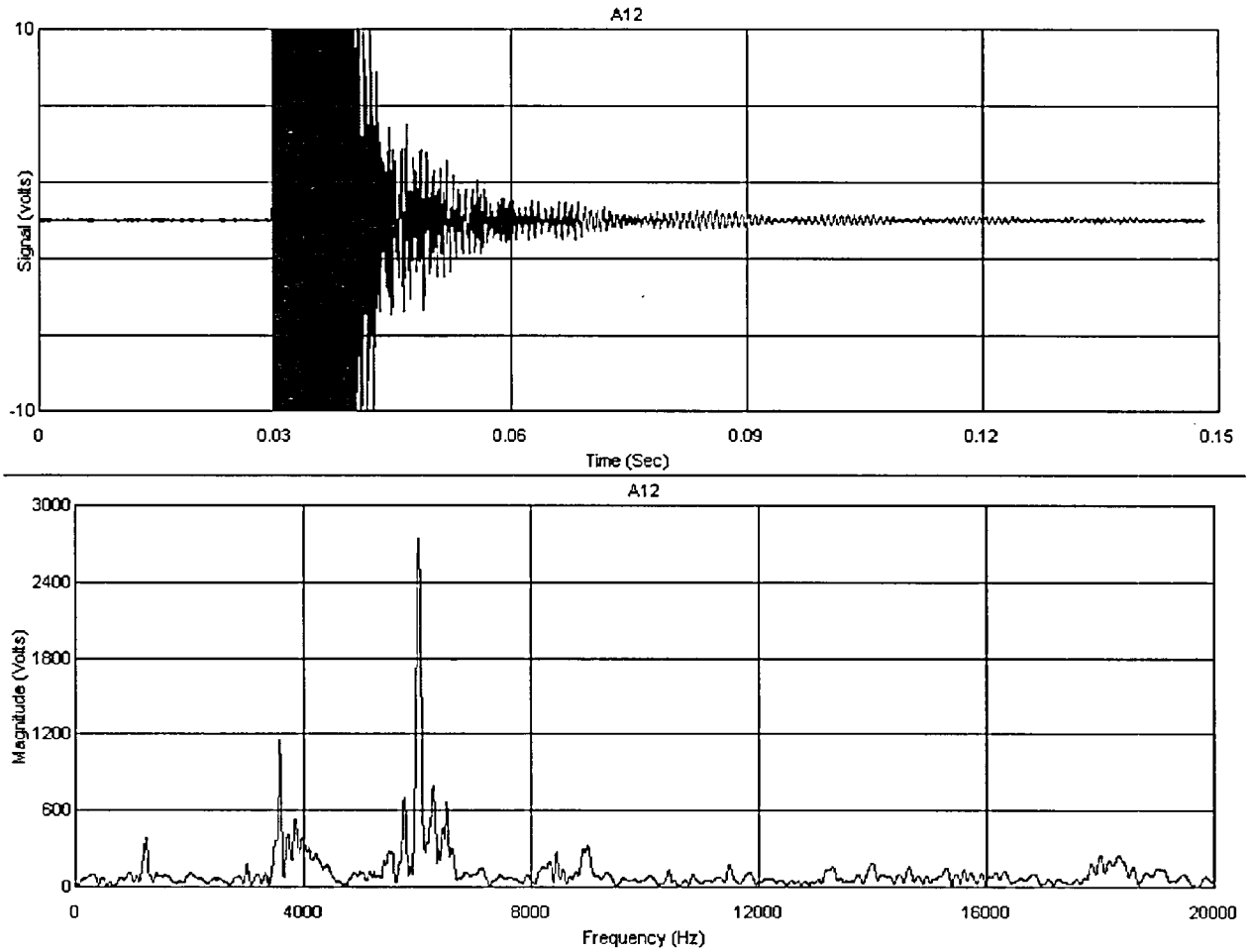

Figure 6: Time and Frequency Domain Plots of a "Tendon Ping"

Detection of Wire Breaks during SFMT

No wire break events were detected during the LST. The first wire break occurred at 10:39:47 Nov 14, during the SFMT. Wire breaks are expected to have at least as much energy as a Schmidt hammer impact, and are expected to show preferential propagation of acoustic energy along the tendon. However, as the concrete of the vessel became increasingly cracked, it became a poorer medium for the transmission of the sound. As a consequence, only the magnitude and frequency content of the output of sensors near each event could be used to assess whether or not a given event was likely the result of a wire break. Fifty-eight events were detected that matched these criteria. Three of these events detected double wire breaks, and Six events detected multiple wire breaks, excluding the final rupture of the vessel.

Most of the wire breaks were located near 20 deg. Azimuth at elevations between 3m and 9 m. The graph below plots an asterisk at the position of the source of each wire break.

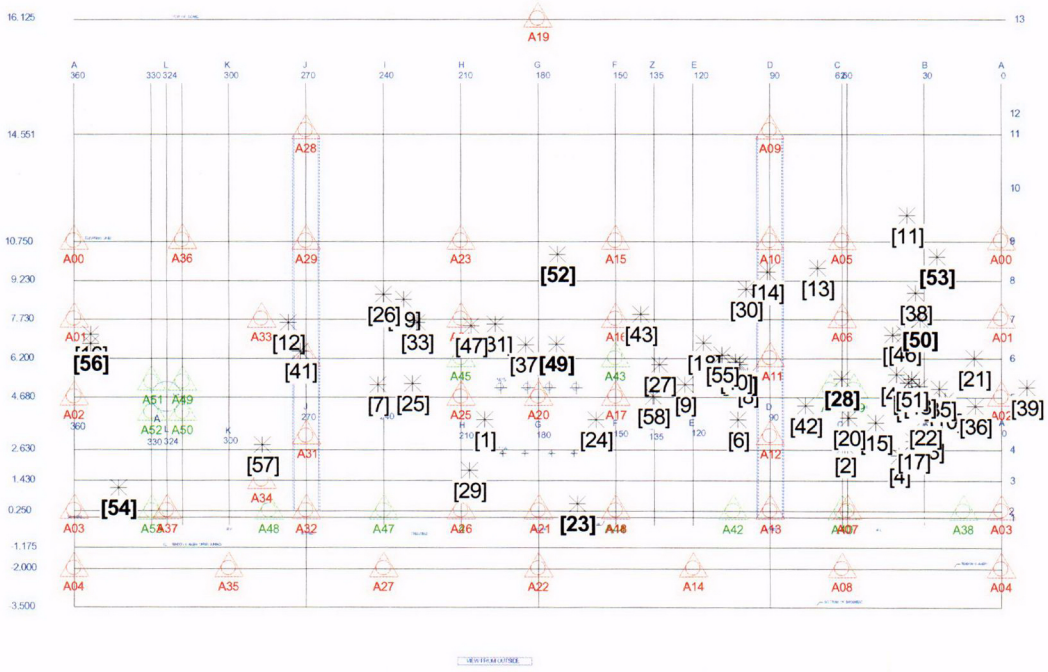

Scale: 2.05 m / cm

0 2m 20m

Figure 7: Flattened elevation view (from outside) of location of wire breaks during SFMT

C129

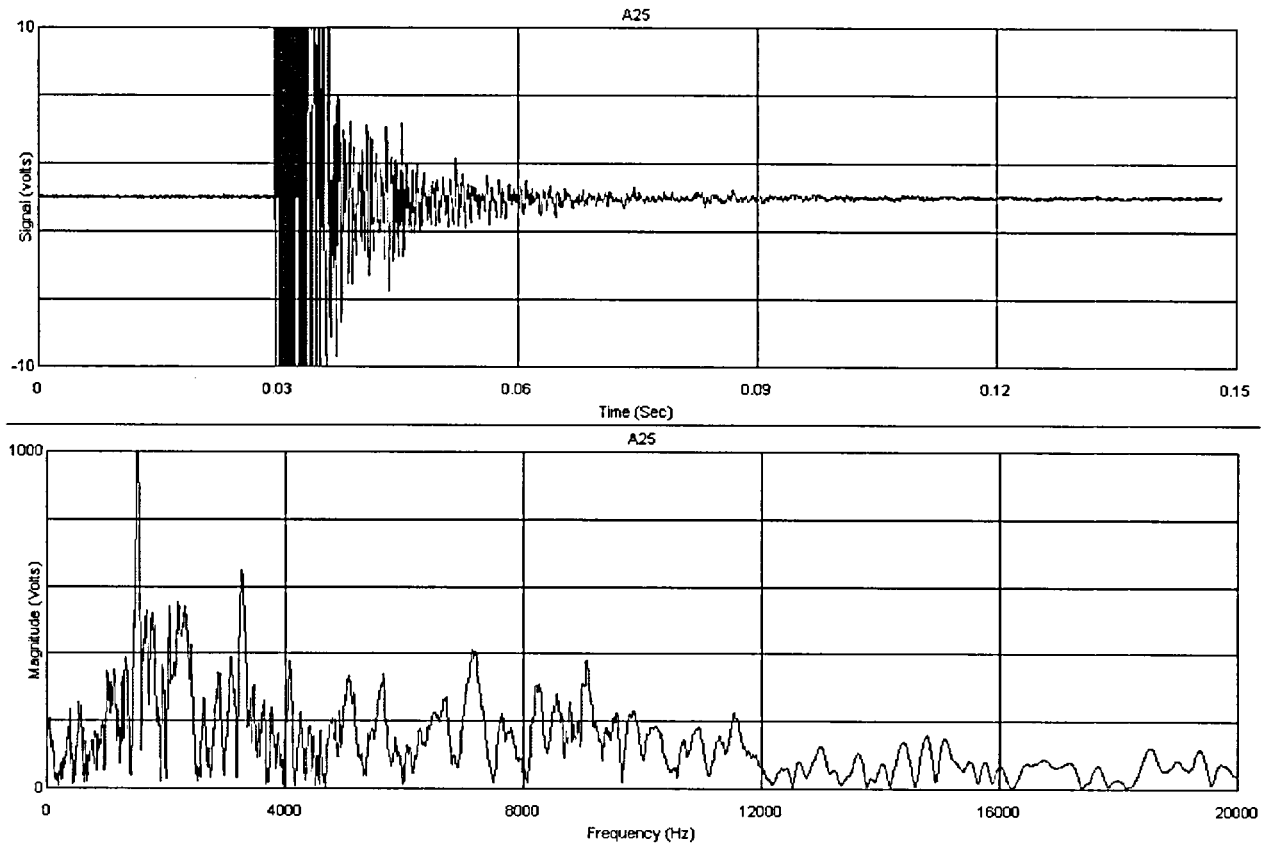

Figure 8: Time Domain and Frequency domain plots of a typical wire break recorded by a nearby sensor

Detection of Events in Basemat during SFMT

During the later stages of the SFMT, events started occurring that originated in the basemat of the PCCV, but which did not have all of the characteristics expected of wire breaks. Sixty-Five events of this type occurredbetween 10:43:37 and at 10:46:03. The graph below shows the locations of these events.

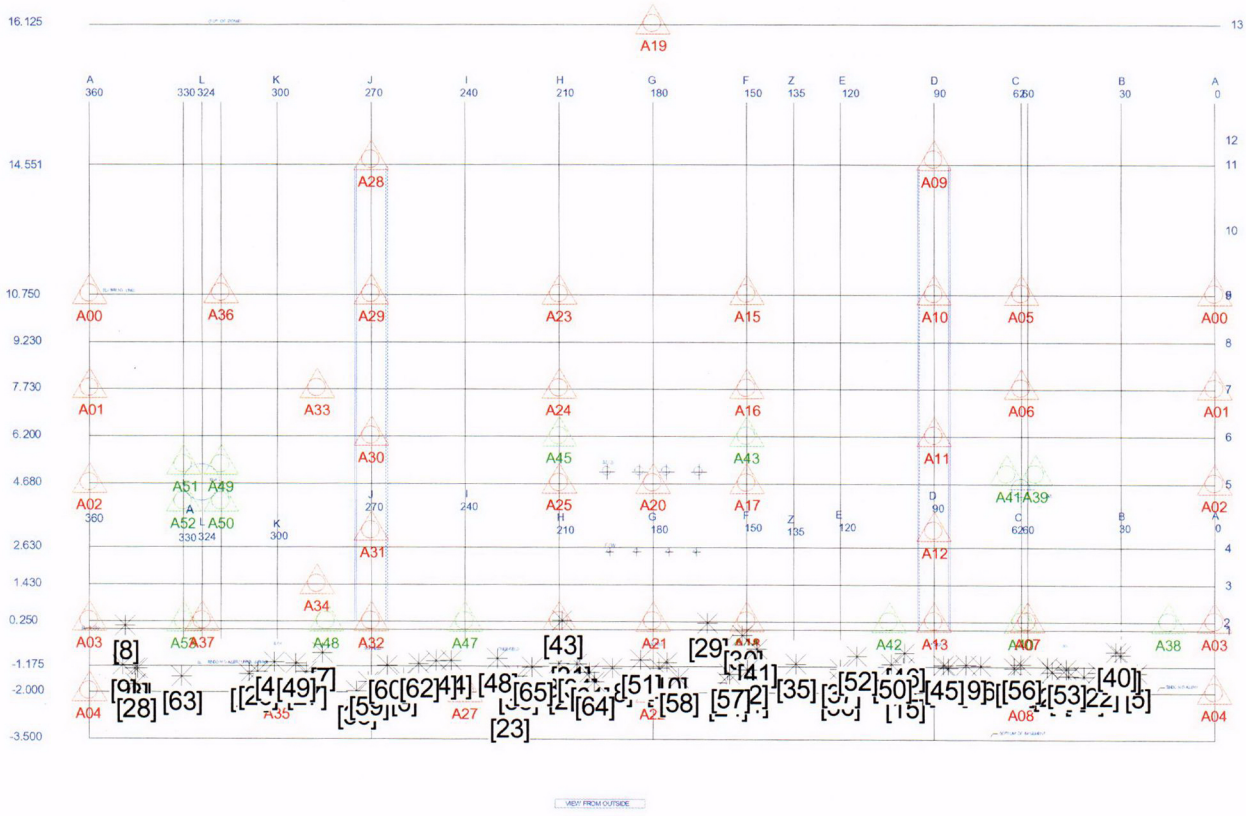

Scale: 2.05 m / cm

0 2m 20m

Figure 9: Location of Events in Basemat during SFMT

C130

Detection of Average Energies of Wire Breaks

As the SFMT progressed, successive wire breaks were detected at increasing pressures. An estimate of the relative energy released by these breaks is made below. Note that the last event is the rupture of the vessel.

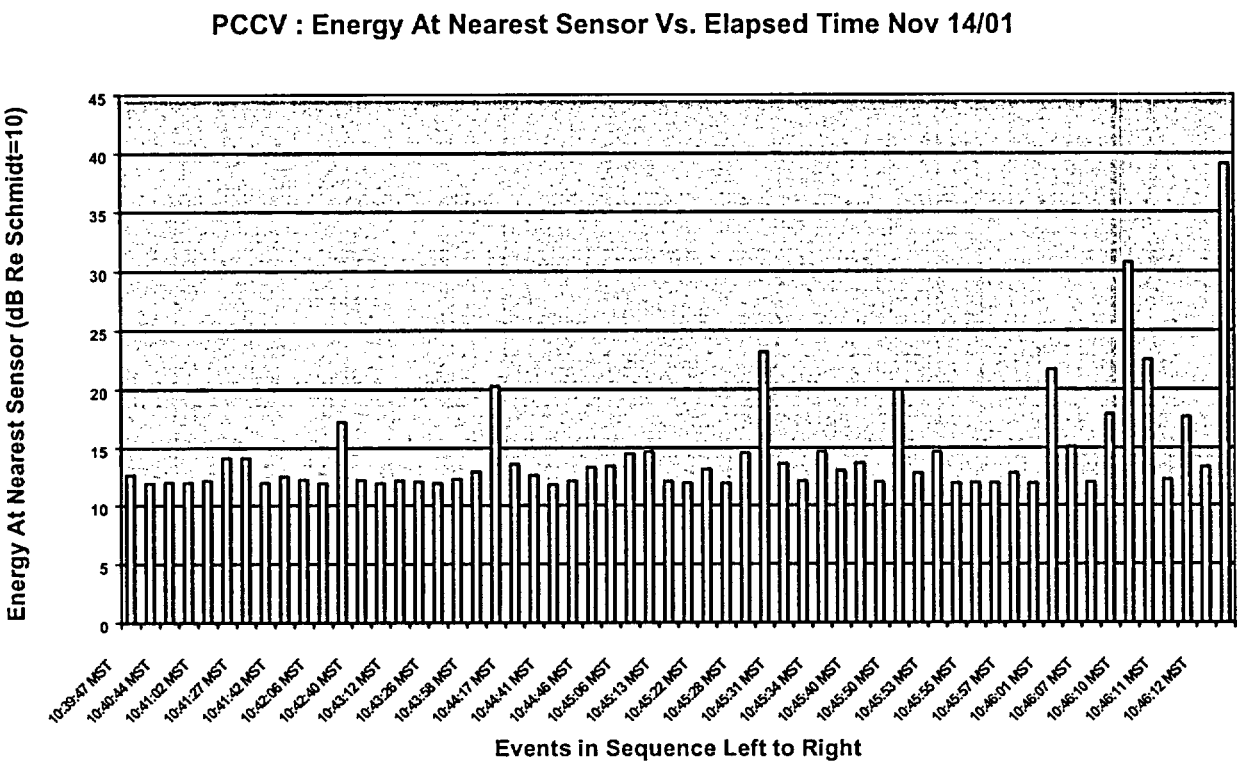

Figure 10 Energy vs Time of wire breaks in SMFT

Detection of Cracking

Throughout the SIT, LST and SFMT, events were detected that had properties consistent with concrete cracking. Most of these events occurred during the LST. Many thousands of these events were heard. Events sufficiently large to be detected at >5dB were located. During the SIT, there were 20 events located, and during the LST, there were 264 events located. Typical cracking behaviour has a time domain graph with multiple events, and a frequency domain that has anomalies from 6 KHz to 12 KHz.

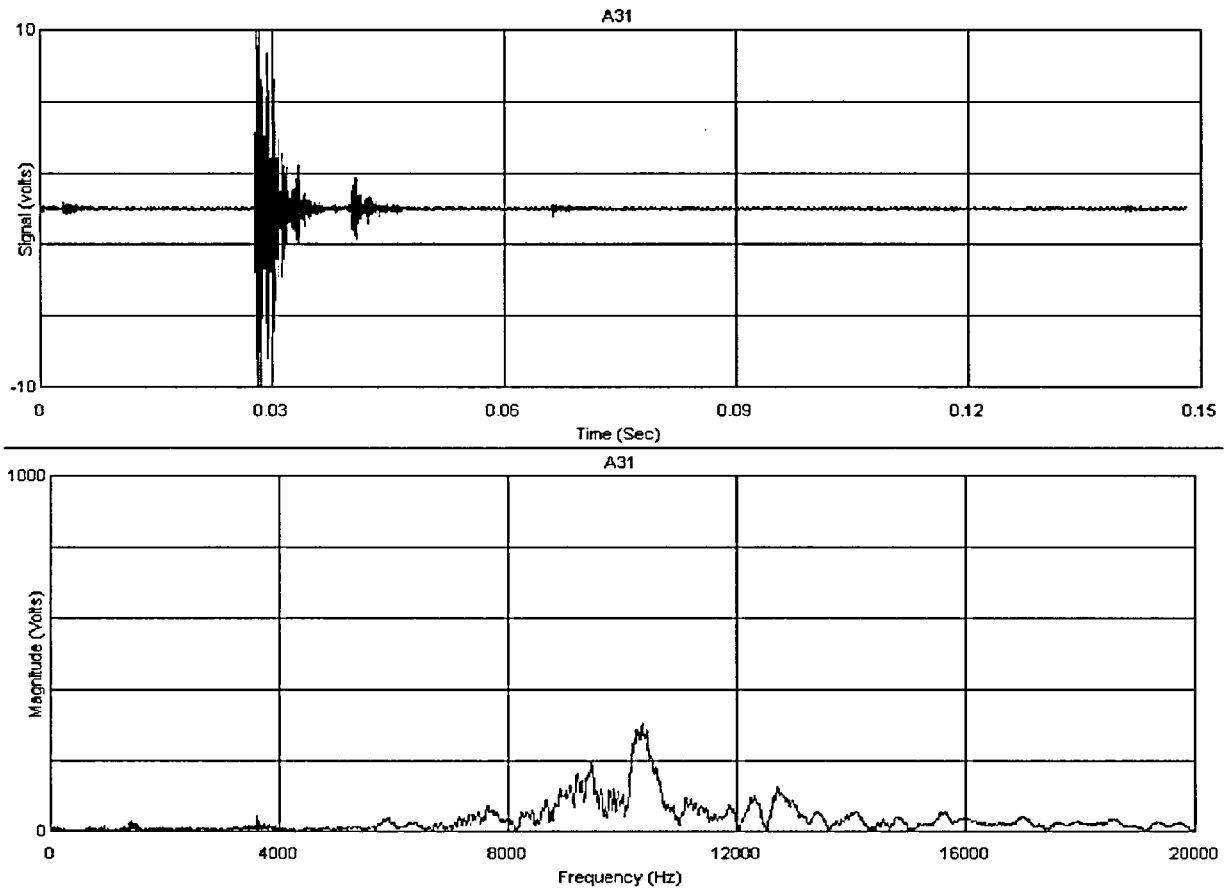

Figure 11 Typical Concrete Cracking Event Large Enough to Locate

Tendon Pings During SFMT

Most of the tendon pings detected during the SFMT occurred in the buttresses with a few originating from the basemat area.

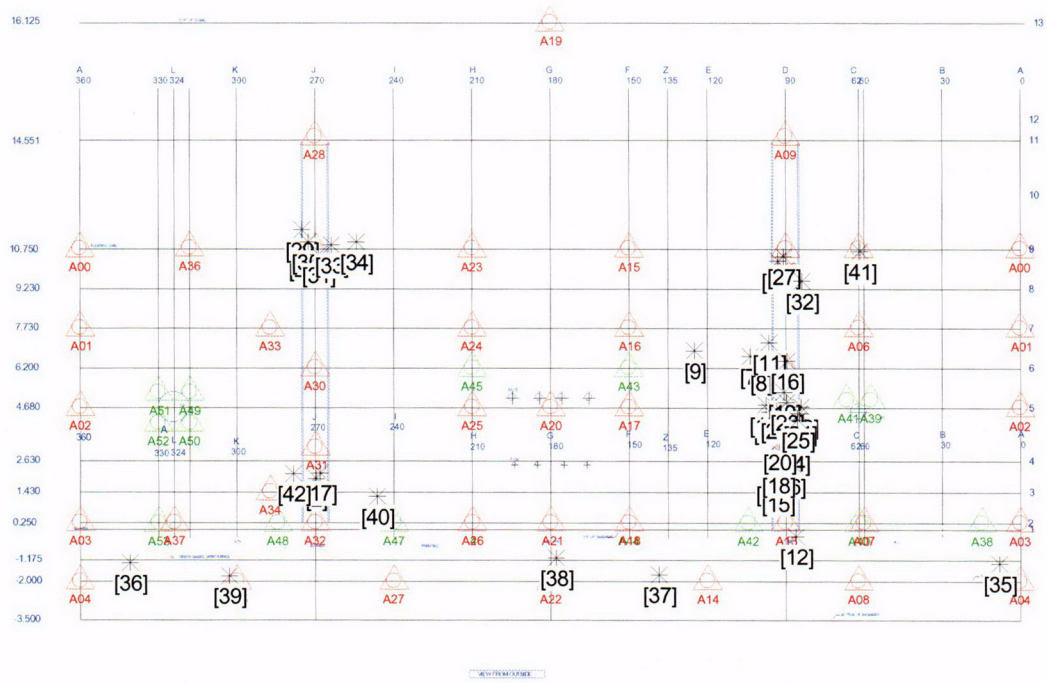

Scale: 2.05 m / cm

0 2m 20m

Figure 12: Tendon Pings During SFMT

C131

Summary of Acoustic Monitoring on PCCV

Background

The PCCV vessel was designed to test the failure modes and prediction strategies developed to model the behavior of the vessel as containment pressures exceed the design pressures.

Acoustic monitoring was represented as being able to detect several useful types of information. These included:

1. Failure of Post-Tensioning Strand Wires
2. Concrete Cracking

Although not originally planned, it was hoped that leak development would also be detected.
Throughout the prestressing phase, and the three testing phases, the monitoring system was continuously active. Fifty Four sensors were applied to the vessel, forty eight externally, and sixteen on the liner internally to the vessel.

Summary of Results

Acoustic monitoring of the vessel detected no wire breaks during the prestressing phase, but detected the development of several large cracks during and after the prestressing phase completion. The largest of these were confirmed by visual examination of the external surface of the vessel before pressurization.

During the LST, 136 large events emanating from the buttresses were detected and identified as "tendon pings" meaning a readjustment of position of the tendon near the anchorage, but these were not wire or tendon failures.

A total of 489 cracking events were detected and mapped on the attached drawings. Some views of these data are available with the visual mapping of the cracks overlaying the plots.

Ten events originating near the tendon gallery indicate concrete crushing in that area.

No tendon failures were detected.

One leak was detected at 2.4 Pd near the equipment hatch. Other leaks became apparent as the pressures increased.

Real time audio of the acoustic sensors was made available to the participants in the LST.

Development of Leaks

Tear in the liner allow nitrogen to flow. This process generates acoustic noise that is detectable by nearby sensors. The graphics below are Fourier Transforms of events detected by the sensors mounted internally on the liner. Figure 1 shows the response before any tearing is suspected. Notice that the output of all of the sensors is very low and displays no anomalies.

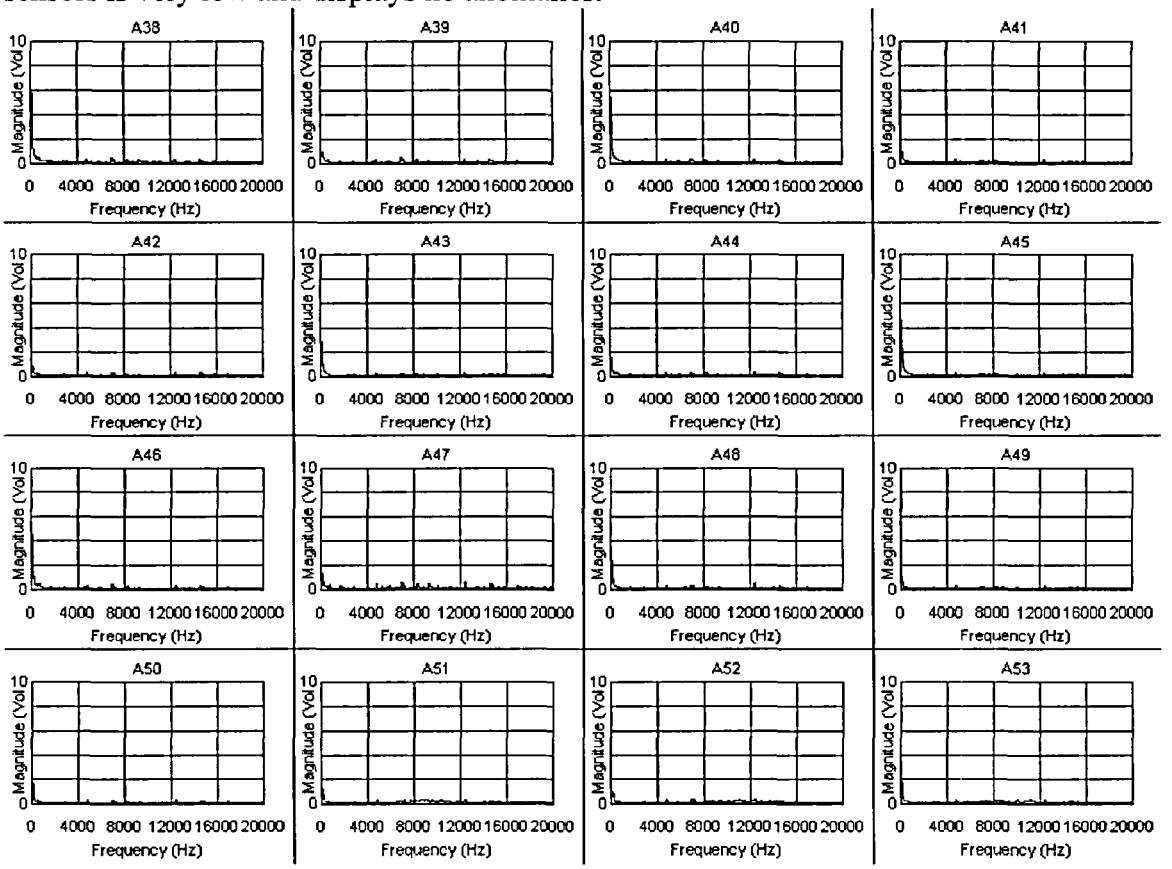

FIG. 1 FFT of internal sensors before liner tearing
Time: 09:27:52 Wed Sept 27, 2000

Figure 2 below shows the development of a suspected tear in the liner near the equipment hatch. Notice that sensors A50, A51, and A52 all show a broadband white noise centered around 8 KHz.

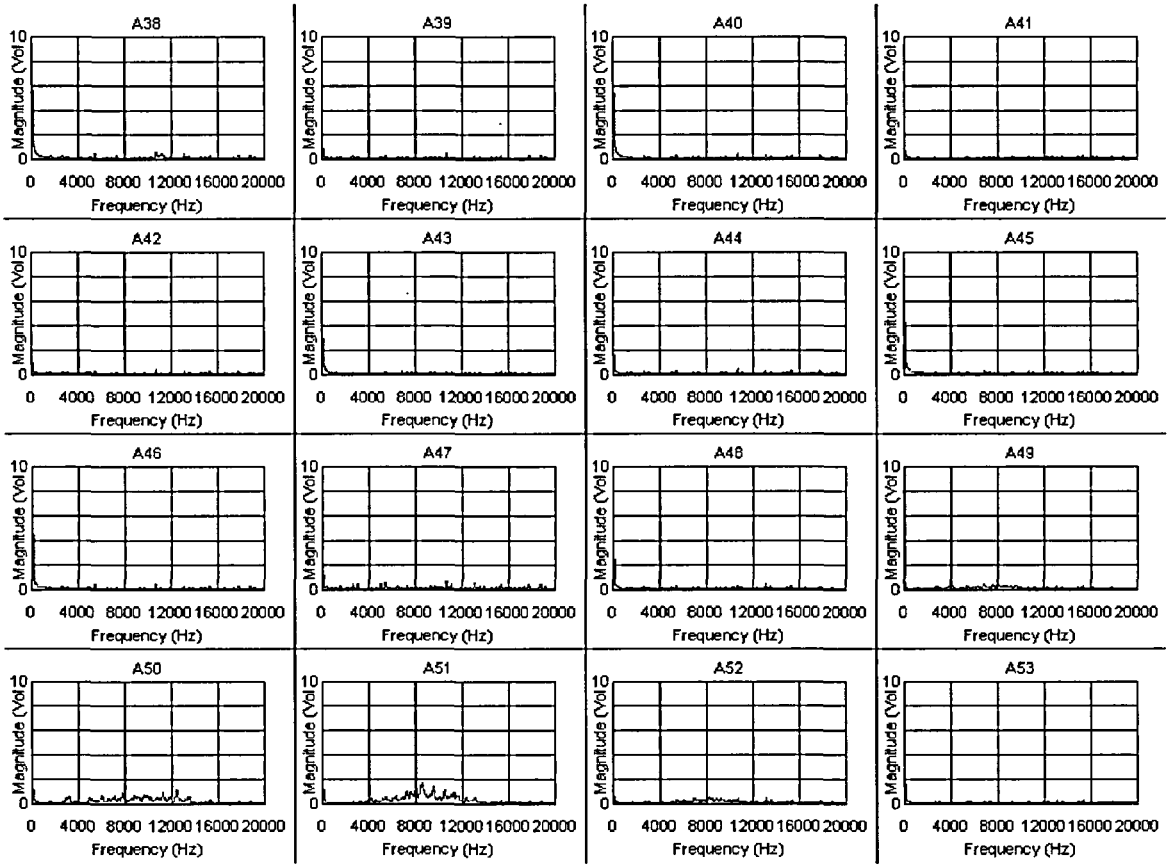

Figure 2. FFT of internal sensors showing noise from liner tear near equipment hatch
Time: 11:18:21 Wed Sept 27, 2000

Figure 3 below shows anomalies that have developed in several places on the liner. Notice that the amplitude of the noise has increased sharply in A50, 51, and 52, indicating that the tears in that area are increasing in size and flow. These anomalies were also detectable on the external sensors.

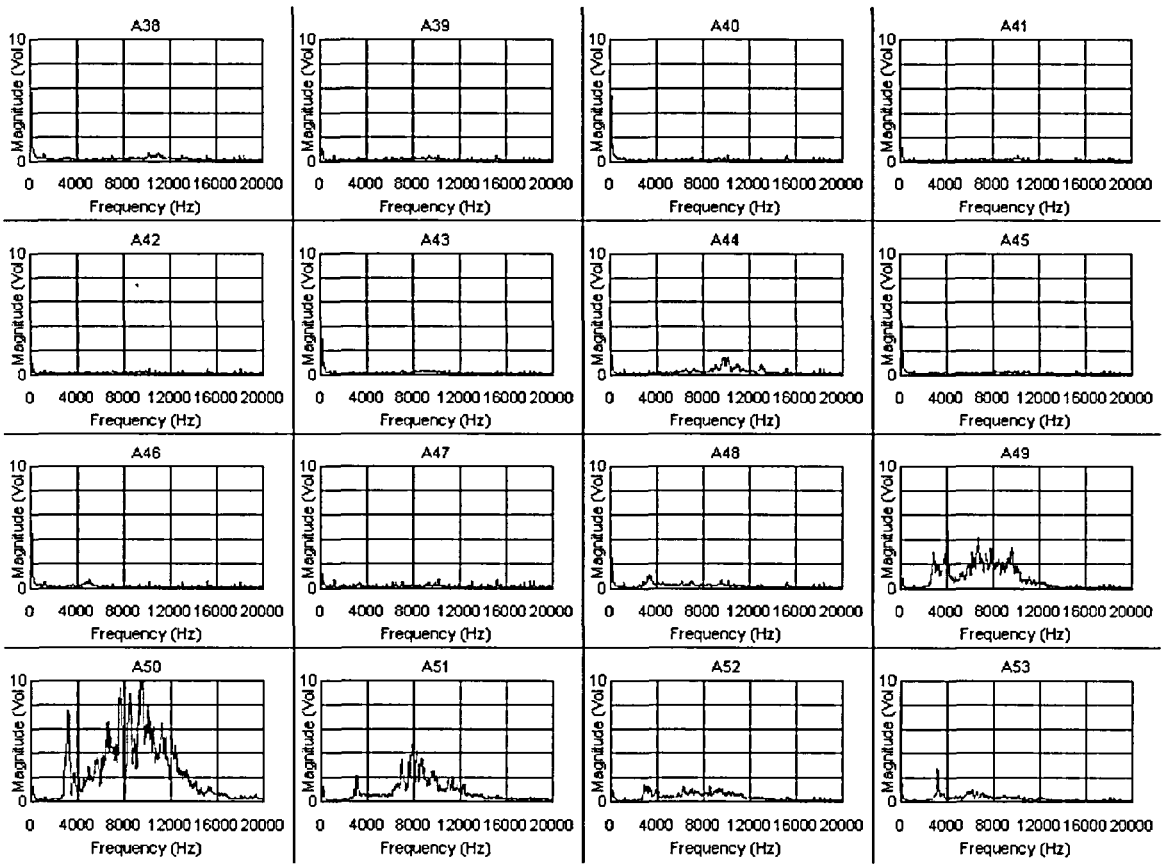

Figure 3. FFT of Internal Sensors showing well developed flow noise from suspected tearing of the liner.
Time 12:12:44 Wed Sept 27, 2000

Figure 4 below also shows increased flow noise in many areas of the liner.

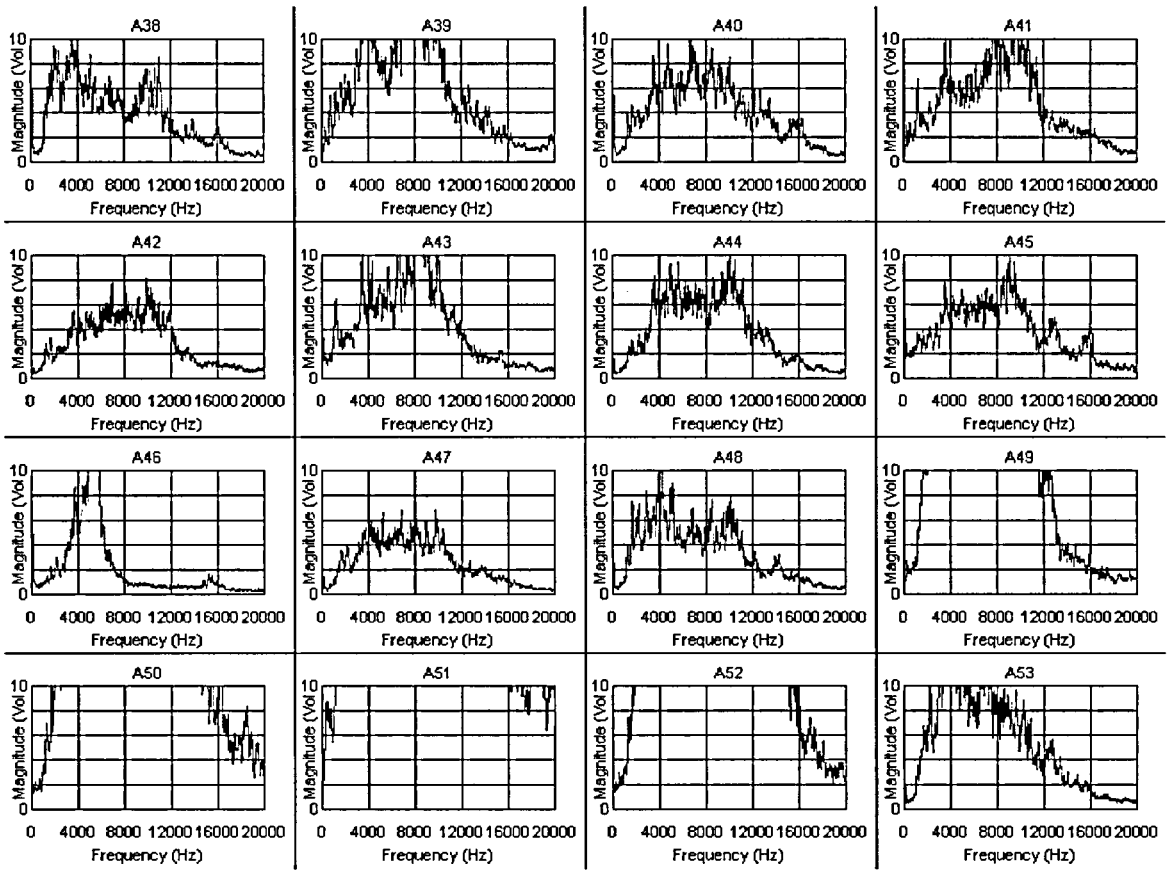

Figure 4. FFT of internal sensors with increased flow
noise from many suspected liner tears
Time: 15:45:49 Wed Sept 27, 2000

Development of concrete cracking

Concrete cracking was detected throughout the construction and testing of the PCCV. Large cracking sounds were located on the elevation view of the vessel. For this summary, only three figures are shown.. Figure 4 shows the position of cracks during the LST. Other views of cracks are available in the attached reports.

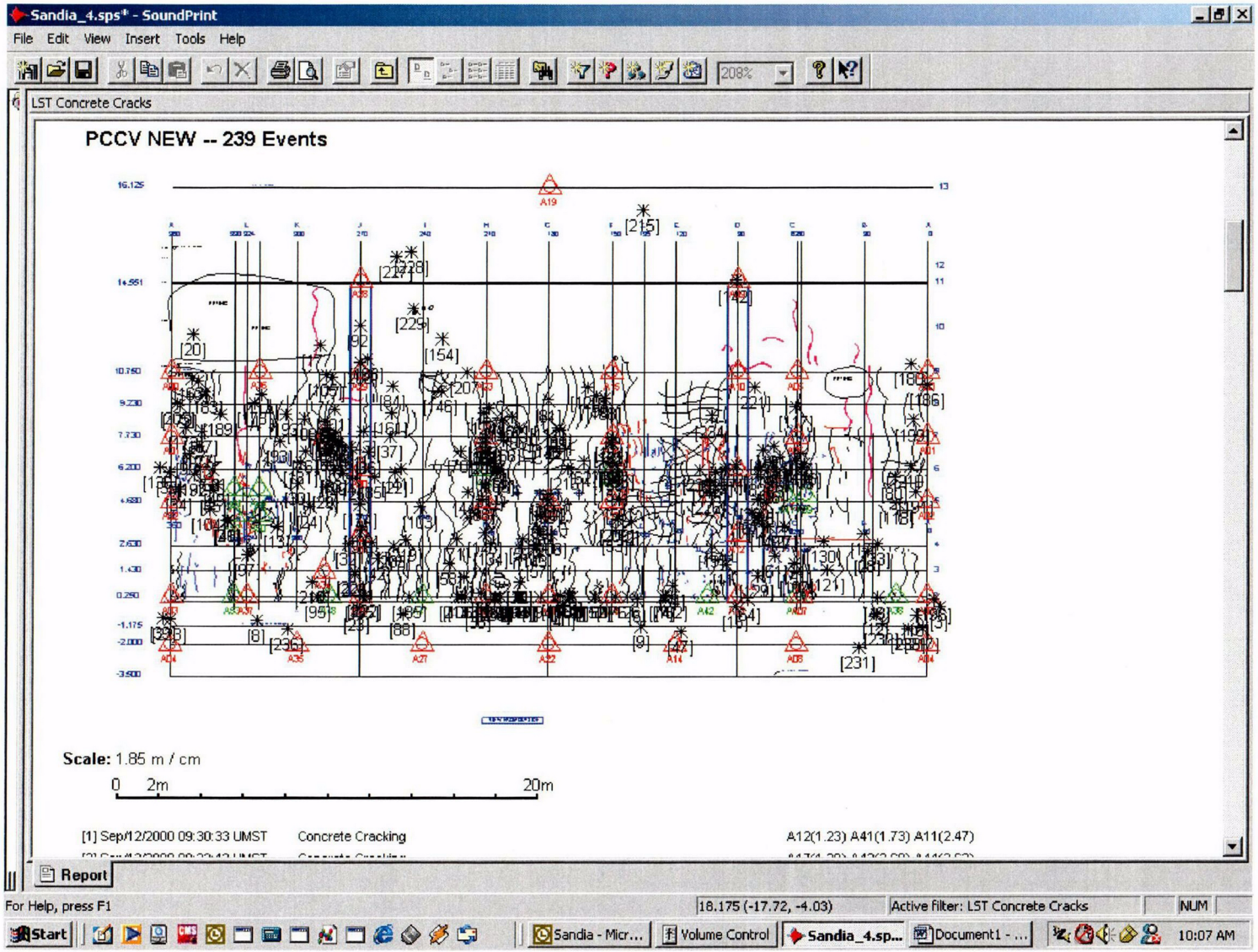

Figure 4 Position of cracking during LST overlain onto map of visual cracking

Events identified as concrete cracking have a sharp time domain signature and a FFT signature with anomalies from 8 KHz to about 12 KHz in the frequency domain. Figure 5 below shows a typical event from cracking of the concrete. The top chart is the time domain representation of the event, while the bollom chart is the frequency domain representation of the same event on the same sensor.

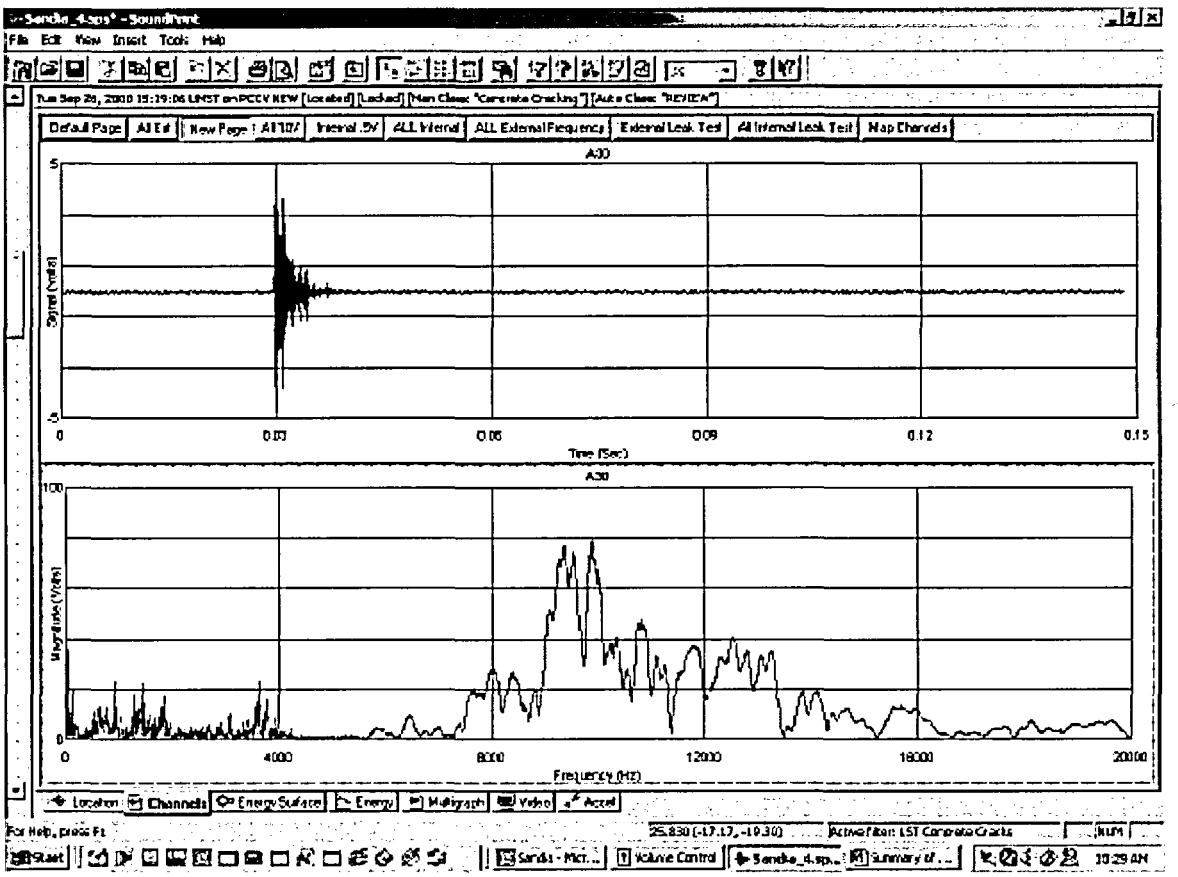

Figure 5 Typical event resulting from concrete cracking during LST

The locations of the "tendon pings" that may have resulted from load distribution is shown below in figure 6.

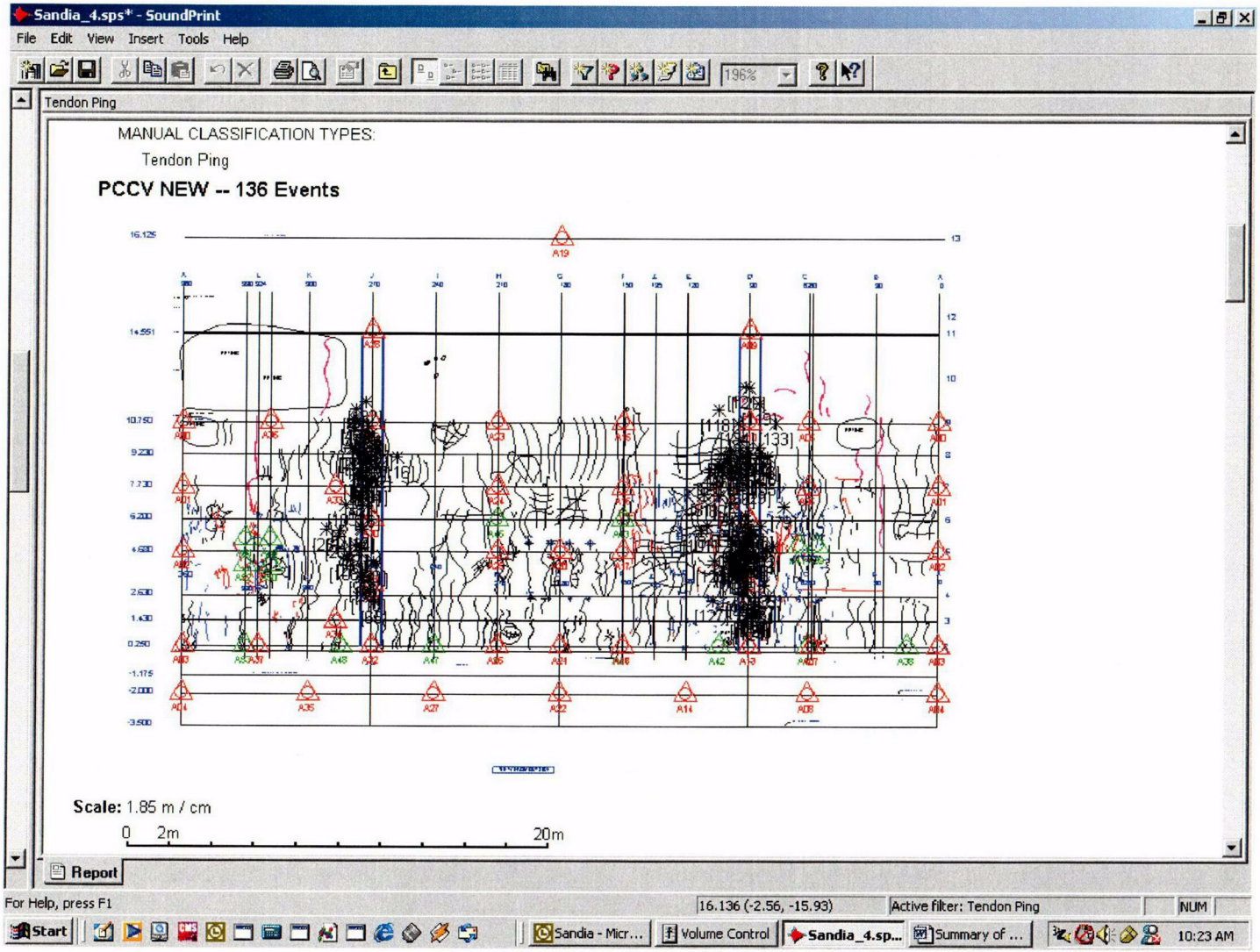

Figure 6 Locations of events identified as tendon pings during the LST

Figure 7 below shows the time and frequency domain plots of a typical tendon ping event.

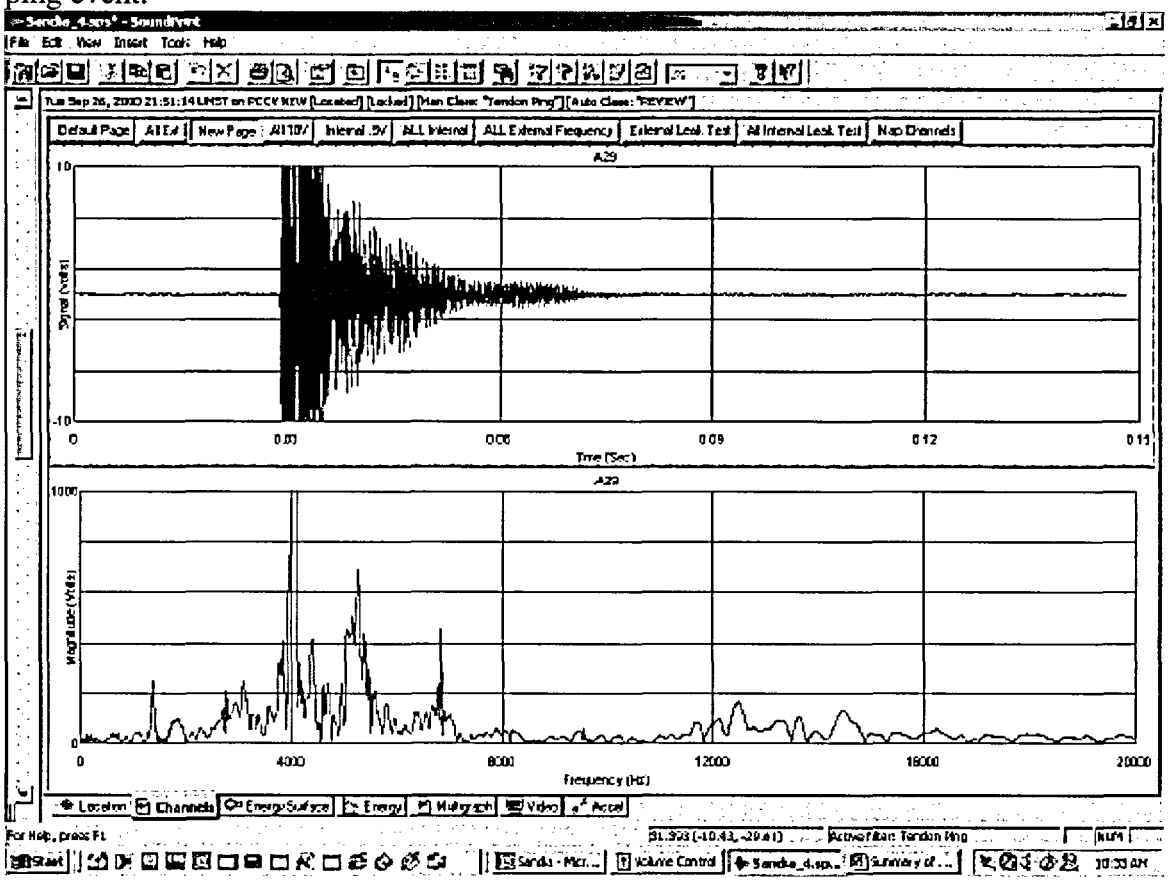

Figure 7 showing Time domain and FFT of a typical tendon ping event.

Conclusion

Acoustic monitoring of the PCCV was able to detect and identify all of the features intended, and some supplementary information was also reported.

- No tendon failures occurred during the construction, the SIT or the LST
- Cracking was widespread and easily detected and mapped
- Other tendon behavior was tracked and reported (tendon pings)
- Localized crushing of the concrete was detected
- Leaks were detected and reported at levels of about 1 mass percent per day

Acoustic monitoring can provide global information about the behavior of a PCCV with widely distributed surface mounted sensors.

SANDIA PCCV

ALBUQUERQUE, NM

SOUNDPRINT® ACOUSTIC MONITORING PROGRAM

REPORT

REPORTING PERIOD: MARCH 13 TO SEPTEMBER 27, 2000

DISCLAIMER

The information provided in this report is not intended to constitute an engineering report and should not be construed as such. The client is advised to retain qualified engineering expertise to interpret the data contained in this report. The information contained in this report is provided "as is" without warranty of any kind, either express or implied. Pure Technologies Ltd. is not liable for any lost profits, lost savings or other incidental, special or consequential damage arising out of the use of the monitoring system or the information contained in this report. Please refer to the terms and conditions attached to Pure's SoundPrint® System Purchase Agreement and Pure's Technical Support Agreement for further details.

® Registered Trademark, property of Pure Technologies Ltd.

TABLE OF CONTENTS

1.0 EXECUTIVE SUMMARY

The following is a summary of relevant activity recorded by the SoundPrint® monitoring system. The summary includes information for both the latest monitoring period and for the entire monitoring period from the start-up date up to and including the most recent monitoring period.

	Period 03/13/2000– 09/27/2000
Operating Efficiency	88.4%
ALL Cracks	489

Comments

Recommendations

There are no new recommendations at this time.

Prepared by:

Peter Paulson
President & CEO

REPORT PRESENTATION

A computerized drawing of the slab with the sensor layout is included on the following page and contains the following symbols:

Sensor Symbol with individual sensor name beneath

Symbolizes an event location. Event details are listed on the page following the drawing.

A list describing event details is provided for each drawing and lists the event number, shown on the computerized drawing, followed by the date, time, event classification and co-ordinates (in meters) to the origin of the events using the three closes sensors.

Event Report For Sandia PCCV

Albuquerque, NM

System Uptime 175 Days (88.4%)

ALL CRACKS

Period: 03/13/2000 to **09/27/2000**

Matched Events: 489

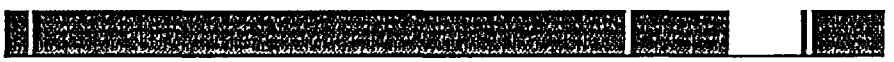

PCCV NEW -- 489 EVENTS

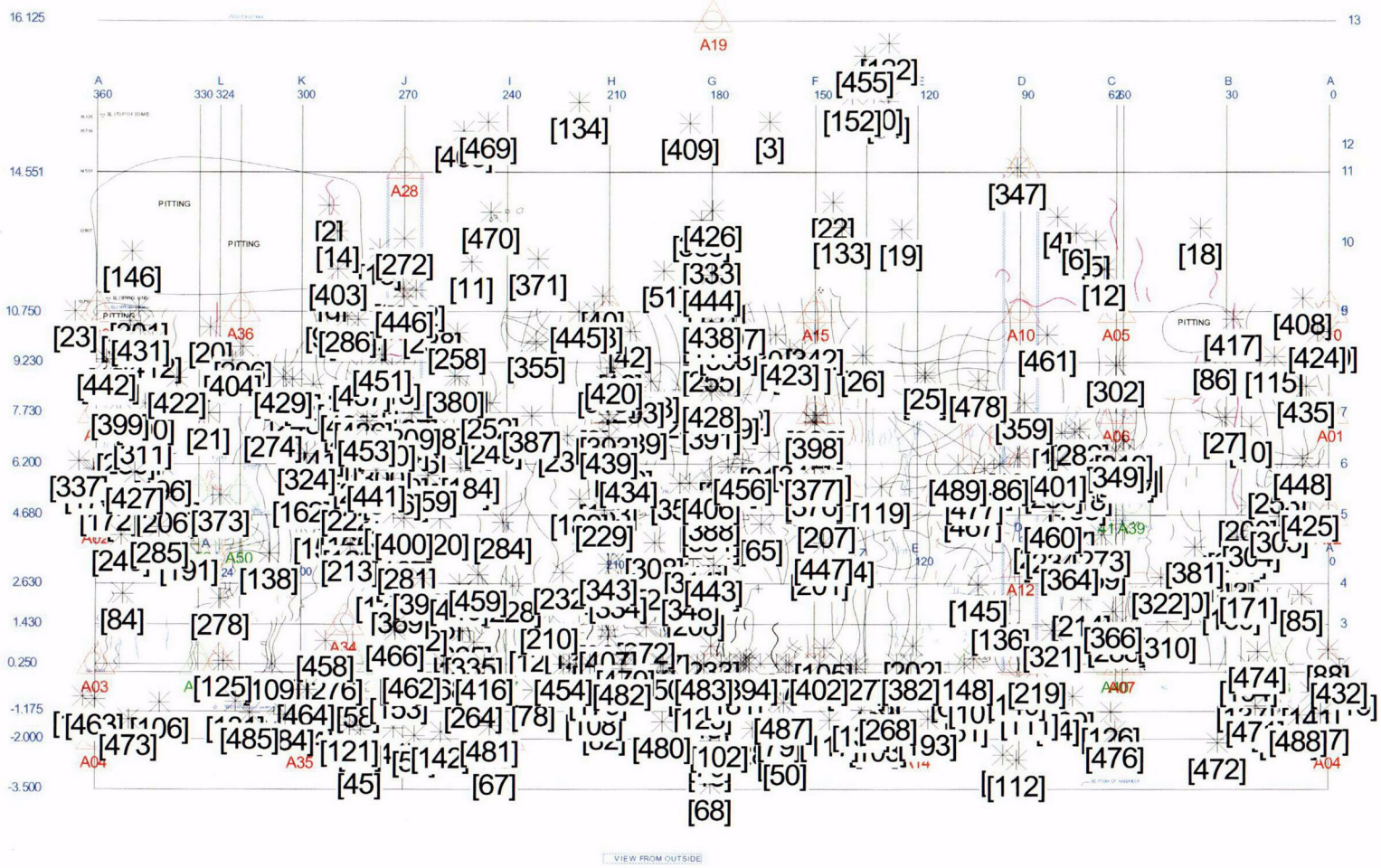

Scale: 1.95 m / cm

0 2m 20m

C134

Events

No.	Date/Time	Classification	Location (m)
[1]	Mar/13/2000 23:25:01 UMST	Possible Cracking Sound	A48(0.90)A34(1.30) A32(2.33)
[2]	Mar/18/2000 07:37:50 UMST	Circumferential Event	A28(2.46) A29(3.86) A36(4.07)
[3]	Mar/20/2000 10:04:33 UMST	Circumferential Event	A19(3.44) A15(5.81) A23(7.33)
[4]	Mar/20/2000 11:20:19 UMST	Circumferential Event	A09(1.82) A10(3.03) A05(3.31)
[5]	Mar/21/2000 14:42:51 UMST	Circumferential Event	A05(2.21) A10(3.05) A09(3.08)
[6]	Mar/25/2000 12:35:37 UMST	Possible Cracking Sound	A09(2.54)A05(2.62) A10(2.85)
[7]	Apr/04/2000 13:42:13 UMST	Possible Cracking Sound	A36(1.52) A33(3.56) A49(4.00)
[8]	Apr/04/2000 14:07:13 UMST	Possible Cracking Sound	A30(2.40) A24(3.84) A33(3.90)
[9]	Apr/06/2000 07:07:36 UMST	Possible Cracking Sound	A29(2.18) A36(2.75) A33(3.67)
[10]	Apr/06/2000 08:42:23 UMST	Circumferential Event	A01(2.30) A02(3.49) A06(3.92)
[11]	Apr/06/2000 09:37:58 UMST	Circumferential Event	A29(2.45) A28(3.42) A23(4.28)
[12]	Apr/06/2000 09:51:18 UMST	Circumferential Event	A05(1.32) A10(2.74) A09(3.88)
[13]	Apr/06/2000 09:51:59 UMST	Possible Cracking Sound	A29(2.01)A28(2.52) 36(4.46)
[14]	Apr/06/2000 12:51:40 UMST	Circumferential Event	A28(2.72) A29(3.09) A36(3.69)
[15]	Apr/12/2000 08:25:11 UMST	Circumferential Event	A00(1.30) A01(1.83) A36(3.98)
[16]	Apr/12/2000 11:31:41 UMST	Circumferential Event	A23(1.45) A24(1.64) A45(3.15)
[17]	Apr/12/2000 11:45:43 UMST	Circumferential Event	A16(3.37) A10(3.40) A15(3.76)
[18]	Apr/13/2000 09:30:02 UMST	Possible Cracking Sound	A05(3.49) A00(4.49) A09(5.52)
[19]	Apr/14/2000 12:46:01 UMST	Possible Cracking Sound	A15(3.51) A09(3.91) A10(4.24)
[20]	Apr/19/2000 15:18:44 UMST	Circumferential Event	A36(1.00) A00(3.33) A01(4.18)
[21]	Apr/19/2000 15:26:04 UMST	Possible Cracking Sound	A51(2.46) A49(2.61) A36(3.21)
[22]	Apr/20/2000 06:43:28 UMST	Possible Cracking Sound	A15(3.30) A09(5.55) A16(6.30)
[23]	Apr/21/2000 10:17:03 UMST	Possible Cracking Sound	A00(0.62) A01(3.10) A36(4.79)
[24]	Apr/24/2000 07:47:13 UMST	Possible Cracking Sound	A02(1.21) A01(3.13) A39(4.51)
[25]	May/02/2000 16:50:19 UMST	Circumferential Event	A10(3.30) A16(3.43) A15(3.69)
[26]	May/02/2000 16:50:29 UMST	Circumferential Event	A15(1.90) A16(2.22) A43(3.54)
[27]	Jul/18/2000 08:31:27 UMST	Possible Cracking Sound	A01(3.02) A06(3.15) A39(3.76)
[28]	Jul/18/2000 08:31:35 UMST	Possible Cracking Sound	A22(1.26) A21(2.28) A44(2.61)
[29]	Jul/18/2000 08:31:45 UMST	Possible Cracking Sound	A40(1.57) A07(1.73) A08(1.78)
[30]	Jul/18/2000 08:31:47 UMST	Possible Cracking Sound	Not Located
[31]	Jul/18/2000 08:32:09 UMST	Possible Cracking Sound	Not Located
[32]	Jul/18/2000 08:32:10 UMST	Possible Cracking Sound	A22(2.00) A18(2.47) A44(2.47)
[33]	Jul/18/2000 08:32:23 UMST	Possible Cracking Sound	Not Located
[34]	Jul/18/2000 08:32:44 UMST	Possible Cracking Sound	A22(0.28) A21(2.53) A46(3.91)
[35]	Jul/18/2000 08:32:50 UMST	Possible Cracking Sound	Not Located
[36]	Jul/18/2000 08:32:50 UMST	Possible Cracking Sound	Not Located
[37]	Jul/18/2000 08:32:53 UMST	Possible Cracking Sound	Not Located
[38]	Jul/18/2000 08:33:01 UMST	Possible Cracking Sound	A35(1.16) A48(1.78) A34(2.54)
[39]	Jul/18/2000 08:33:05 UMST	Possible Cracking Sound	A14(1.89) A18(2.03) A44(2.03)
[40]	Jul/18/2000 08:33:07 UMST	Possible Cracking Sound	A23(0.51) A24(3.50) A45(5.03)
[41]	Jul/18/2000 08:33:10 UMST	Possible Cracking Sound	A32(1.93) A48(2.24) A35(2.74)
[42]	Jul/18/2000 08:33:13 UMST	Possible Cracking Sound	A23(0.84) A24(2.51) A45(4.01)
[43]	Jul/18/2000 08:33:15 UMST	Possible Cracking Sound	A22(0.32) A21(2.58) A46(3.93)

[44]	Jul/18/2000 08:33:16 UMST	Possible Cracking Sound	Not Located
[45]	Jul/18/2000 08:33:32 UMST	Possible Cracking Sound	A35(1.82) A48(2.82) A32(3.08)
[46]	Jul/18/2000 08:33:38 UMST	Possible Cracking Sound	Not Located
[47]	Jul/18/2000 08:33:44 UMST	Possible Cracking Sound	Not Located
[48]	Jul/18/2000 08:33:45 UMST	Possible Cracking Sound	A22(1.11) A21(1.15) A26(3.11)
[49]	Jul/18/2000 08:34:27 UMST	Possible Cracking Sound	Not Located
[50]	Jul/18/2000 08:34:34 UMST	Possible Cracking Sound	A22(2.19) A44(2.67) A18(2.67)
[51]	Jul/18/2000 08:34:35 UMST	Possible Cracking Sound	A23(2.00) A24(4.52) A15(4.55)
[52]	Jul/18/2000 08:34:57 UMST	Possible Cracking Sound	Not Located
[53]	Jul/18/2000 08:35:10 UMST	Possible Cracking Sound	A32(2.17) A27(2.65) A48(2.78)
[54]	Jul/18/2000 08:35:11 UMST	Possible Cracking Sound	A13(1.65) A08(1.95) A40(2.05)
[55]	Jul/18/2000 08:35:32 UMST	Possible Cracking Sound	Not Located
[56]	Jul/18/2000 08:36:09 UMST	Possible Cracking Sound	Not Located
[57]	Jul/18/2000 08:36:15 UMST	Possible Cracking Sound	Not Located
[58]	Jul/18/2000 08:37:02 UMST	Possible Cracking Sound	A48(0.84) A32(1.53) A34(2.05)
[59]	Jul/18/2000 08:37:06 UMST	Possible Cracking Sound	Not Located
[60]	Jul/18/2000 08:37:19 UMST	Possible Cracking Sound	Not Located
[61]	Jul/18/2000 08:37:20 UMST	Possible Cracking Sound	A42(1.25) A14(1.77) A13(1.97)
[62]	Jul/18/2000 08:37:23 UMST	Possible Cracking Sound	Not Located
[63]	Jul/18/2000 08:37:31 UMST	Possible Cracking Sound	Not Located
[64]	Jul/18/2000 08:37:48 UMST	Possible Cracking Sound	A42(0.70) A13(1.99) A14(2.04)
[65]	Jul/18/2000 08:38:32 UMST	Possible Cracking Sound	A20(1.47) A17(1.56) A43(2.36)
[66]	Jul/18/2000 08:39:36 UMST	Possible Cracking Sound	Not Located
[67]	Jul/18/2000 08:39:36 UMST	Possible Cracking Sound	A27(0.66) A47(2.85) A32(3.89)
[68]	Jul/18/2000 08:39:42 UMST	Possible Cracking Sound	A22(1.34) A21(3.60) A46(4.67)
[69]	Jul/18/2000 08:40:00 UMST	Possible Cracking Sound	A35(1.78) A48(1.99) A32(2.33)
[70]	Jul/18/2000 08:40:01 UMST	Possible Cracking Sound	A22(0.04) A21(2.30) A46(3.76)
[71]	Jul/18/2000 08:40:22 UMST	Possible Cracking Sound	A44(1.46) A18(1.46) A21(2.25)
[72]	Jul/18/2000 08:40:25 UMST	Possible Cracking Sound	A35(1.18) A48(1.88) A34(2.58)
[73]	Jul/18/2000 08:40:25 UMST	Possible Cracking Sound	A35(1.24) A37(2.06) A53(2.54)
[74]	Jul/18/2000 08:40:50 UMST	Possible Cracking Sound	A14(2.56) A13(2.76) A42(2.88)
[75]	Jul/18/2000 08:41:39 UMST	Possible Cracking Sound	A21(0.07) A22(2.33) A26(2.98)
[76]	Jul/18/2000 08:42:23 UMST	Possible Cracking Sound	Not Located
[77]	Jul/18/2000 08:42:37 UMST	Possible Cracking Sound	A42(0.18) A13(1.33) A14(2.92)
[78]	Jul/18/2000 08:43:10 UMST	Possible Cracking Sound	A47(1.12) A27(1.69) A26(2.31)
[79]	Jul/18/2000 08:43:13 UMST	Possible Cracking Sound	A18(1.95) A44(1.95) A22(2.08)
[80]	Jul/18/2000 08:43:23 UMST	Possible Cracking Sound	A15(2.14) A16(3.70) A23(3.82)
[81]	Jul/18/2000 08:43:24 UMST	Possible Cracking Sound	Not Located
[82]	Jul/18/2000 08:43:32 UMST	Possible Cracking Sound	A46(1.49) A26(1.49) A27(2.98)
[83]	Jul/18/2000 08:43:33 UMST	Possible Cracking Sound	A14(0.91) A42(2.62) A44(2.86)
[84]	Jul/18/2000 08:43:38 UMST	Possible Cracking Sound	A03(2.23) A02(2.47) A52(2.81)
[85]	Jul/18/2000 08:43:40 UMST	Possible Cracking Sound	A38(2.17) A03(2.21) A02(2.49)
[86]	Jul/18/2000 09:36:32 UMST	Possible Cracking Sound	A05(3.11) A06(3.37) A00(3.53)
[87]	Jul/18/2000 09:46:29 UMST	Possible Cracking Sound	A31(1.06) A32(1.93) A34(2.17)
[88]	Jul/18/2000 09:46:50 UMST	Possible Cracking Sound	A03(0.43) A38(1.52) A04(2.68)
[89]	Jul/18/2000 09:47:46 UMST	Possible Cracking Sound	A44(1.07) A18(1.07) A21(1.91)

[90]	Jul/18/2000 09:47:47 UMST	Possible Cracking Sound	A42(1.67) A14(2.25) A44(2.87)
[91]	Jul/18/2000 09:47:48 UMST	Possible Cracking Sound	A09(4.32) A19(5.64) A15(6.61)
[92]	Jul/18/2000 09:48:04 UMST	Possible Cracking Sound	A29(2.24) A36(2.53) A33(3.06)
[93]	Jul/18/2000 09:48:09 UMST	Possible Cracking Sound	A13(0.93) A42(1.93) A40(2.65)
[94]	Jul/18/2000 09:48:11 UMST	Possible Cracking Sound	A21(1.44) A44(1.54) A18(1.54)
[95]	Jul/18/2000 09:48:20 UMST	Possible Cracking Sound	A18(0.04) A44(0.04) A21(3.02)
[96]	Jul/18/2000 09:48:35 UMST	Possible Cracking Sound	A14(1.19) A18(2.64) A44(2.64)
[97]	Jul/18/2000 09:49:02 UMST	Possible Cracking Sound	Not Located
[98]	Jul/18/2000 09:49:20 UMST	Possible Cracking Sound	A21(0.68) A22(2.02) A26(2.41)
[99]	Jul/18/2000 09:49:21 UMST	Possible Cracking Sound	Not Located
[100]	Jul/18/2000 09:49:30 UMST	Possible Cracking Sound	A04(1.31) A38(1.65) A03(1.99)
[101]	Jul/18/2000 09:49:35 UMST	Possible Cracking Sound	A35(1.18) A37(2.17) A48(2.50)
[102]	Jul/18/2000 09:49:36 UMST	Possible Cracking Sound	A22(0.36) A21(2.01) A44(3.38)
[103]	Jul/18/2000 09:50:01 UMST	Possible Cracking Sound	A14(1.18) A18(2.62) A44(2.62)
[104]	Jul/18/2000 09:51:48 UMST	Possible Cracking Sound	A35(0.76) A48(2.09) A37(2.91)
[105]	Jul/18/2000 09:52:28 UMST	Possible Cracking Sound	A44(0.56) A18(0.56) A21(3.31)
[106]	Jul/18/2000 09:52:54 UMST	Possible Cracking Sound	A53(1.60) A37(2.05) A04(2.18)
[107]	Jul/18/2000 09:53:04 UMST	Possible Cracking Sound	A42(0.73) A13(1.39) A14(2.36)
[108]	Jul/18/2000 09:54:10 UMST	Possible Cracking Sound	A26(1.12) A46(1.12) A47(2.79)
[109]	Jul/18/2000 09:55:48 UMST	Possible Cracking Sound	A37(1.56) A53(2.14) A48(2.38)
[110]	Jul/18/2000 09:56:11 UMST	Possible Cracking Sound	A38(1.39) A04(1.63) A03(1.96)
[111]	Jul/18/2000 09:56:41 UMST	Possible Cracking Sound	A13(1.08) A42(2.02) A40(2.68)
[112]	Jul/18/2000 09:56:49 UMST	Possible Cracking Sound	A13(2.88) A08(2.93) A14(2.97)
[113]	Sep/12/2000 09:30:33 UMST	Concrete Cracking	A12(1.23) A41(1.73) A11(2.47)
[114]	Sep/12/2000 09:33:43 UMST	Concrete Cracking	A17(1.29) A43(2.60) A44(3.62)
[115]	Sep/12/2000 09:48:50 UMST	Concrete Cracking	A00(2.08) A01(2.31) A05(4.77)
[116]	Sep/12/2000 12:21:44 UMST	Concrete Cracking	A03(0.76) A04(1.89) A38(2.12)
[117]	Sep/12/2000 12:22:09 UMST	Possible Cracking Sound	A44(1.74) A18(1.74) A14(2.58)
[118]	Sep/12/2000 12:22:52 UMST	Possible Cracking Sound	Not Located
[119]	Sep/12/2000 12:23:53 UMST	Possible Cracking Sound	A43(2.06) A17(2.12) A16(2.94)
[120]	Sep/12/2000 12:24:10 UMST	Possible Cracking Sound	A09(4.81) A19(5.15) A15(6.72)
[121]	Sep/12/2000 12:24:48 UMST	Possible Cracking Sound	A35(1.50) A48(1.84) A32(2.40)
[122]	Sep/12/2000 12:25:23 UMST	Possible Cracking Sound	A19(5.16) A09(5.33) A15(8.28)
[123]	Sep/12/2000 12:26:53 UMST	Possible Cracking Sound	A21(0.89) A22(1.40) A26(2.90)
[124]	Sep/12/2000 12:28:49 UMST	Possible Cracking Sound	A47(1.27) A26(2.20) A46(2.20)
[125]	Sep/12/2000 12:31:04 UMST	Possible Cracking Sound	A37(0.16) A53(0.72) A35(3.25)
[126]	Sep/12/2000 12:31:55 UMST	Possible Cracking Sound	A08(0.82) A40(1.45) A07(1.48)
[127]	Sep/12/2000 13:22:51 UMST	Concrete Cracking	A26(1.37) A46(1.37) A47(2.18)
[128]	Sep/12/2000 13:27:45 UMST	Concrete Cracking	A26(0.26) A46(0.26) A47(2.77)
[129]	Sep/12/2000 13:53:08 UMST	Concrete Cracking	A44(1.25) A18(1.25) A14(2.73)
[130]	Sep/13/2000 13:06:27 UMST	Concrete Cracking	A42(2.01) A14(2.31) A44(2.53)
[131]	Sep/13/2000 14:27:30 UMST	Concrete Cracking	A37(1.22) A53(1.55) A35(2.20)
[132]	Sep/14/2000 15:57:41 UMST	Concrete Cracking	A14(1.81) A44(1.96) A18(1.96)
[133]	Sep/15/2000 06:45:19 UMST	Small Event on Apex Area	A15(2.64) A09(5.49) A16(5.59)
[134]	Sep/26/2000 13:54:31 UMST	Concrete Cracking	A19(4.57) A28(5.43) A23(6.30)
[135]	Sep/26/2000 13:55:42 UMST	Concrete Cracking	A21(1.05) A44(1.96) A18(1.96)

[136]	Sep/26/2000 14:25:54 UMST	Concrete Cracking	A12(1.51) A13(1.59) A42(1.73)
[137]	Sep/26/2000 14:27:18 UMST	Concrete Cracking	A38(1.22) A03(2.52) A04(2.80)
[138]	Sep/26/2000 14:27:20 UMST	Concrete Cracking	A50(1.01) A49(1.93) A52(2.12)
[139]	Sep/26/2000 14:30:04 UMST	Concrete Cracking	A45(0.62) A24(1.63) A25(1.66)
[140]	Sep/26/2000 14:30:22 UMST	Concrete Cracking	A13(0.45) A42(1.44) A40(2.88)
[141]	Sep/26/2000 14:30:32 UMST	Concrete Cracking	A03(0.99) A38(1.28) A04(1.49)
[142]	Sep/26/2000 14:31:58 UMST	Concrete Cracking	A27(1.89) A32(2.31) A47(2.77)
[143]	Sep/26/2000 14:47:36 UMST	Concrete Cracking	A39(3.27) A38(3.29) A02(3.35)
[144]	Sep/26/2000 14:50:18 UMST	Concrete Cracking	A21(1.51) A26(1.79) A46(1.79)
[145]	Sep/26/2000 14:50:47 UMST	Concrete Cracking	A12(1.32) A42(2.36) A13(2.64)
[146]	Sep/26/2000 14:54:19 UMST	Concrete Cracking	A00(2.07) A36(3.61) A01(4.93)
[147]	Sep/26/2000 15:16:32 UMST	Concrete Cracking	A52(0.43) A51(1.50) A50(1.54)
[148]	Sep/26/2000 15:18:38 UMST	Concrete Cracking	A42(0.17) A13(1.59) A14(2.64)
[149]	Sep/26/2000 15:18:51 UMST	Concrete Cracking	A31(1.67) A30(2.40) A34(2.78)
[150]	Sep/26/2000 15:19:06 UMST	Concrete Cracking	A30(1.65) A31(3.36) A33(3.75)
[151]	Sep/26/2000 15:19:19 UMST	Concrete Cracking	A15(2.92) A23(3.19) A16(4.66)
[152]	Sep/26/2000 15:20:32 UMST	Concrete Cracking	A19(4.61) A09(5.36) A15(6.56)
[153]	Sep/26/2000 15:20:55 UMST	Concrete Cracking	A32(0.57) A48(1.42) A34(2.36)
[154]	Sep/26/2000 15:21:38 UMST	Concrete Cracking	A02(1.24) A51(1.82) A52(2.08)
[155]	Sep/26/2000 15:21:47 UMST	Concrete Cracking	A50(2.45) A49(2.56) A31(2.69)
[156]	Sep/26/2000 15:21:50 UMST	Concrete Cracking	A33(1.02) A30(1.59) A49(3.59)
[157]	Sep/26/2000 15:21:51 UMST	Concrete Cracking	A41(1.03) A39(1.92) A12(2.01)
[158]	Sep/26/2000 15:21:59 UMST	Concrete Cracking	A41(0.91) A39(1.69) A11(1.77)
[159]	Sep/26/2000 15:22:18 UMST	Concrete Cracking	A41(1.44) A39(1.75) A12(2.28)
[160]	Sep/26/2000 15:22:27 UMST	Concrete Cracking	A38(2.50) A03(3.51) A02(3.65)
[161]	Sep/26/2000 15:22:45 UMST	Concrete Cracking	A30(1.85) A33(2.38) A31(2.75)
[162]	Sep/26/2000 15:22:54 UMST	Concrete Cracking	A49(1.82) A50(2.31) A33(2.53)
[163]	Sep/26/2000 15:23:02 UMST	Concrete Cracking	A45(0.74) A25(0.78) A24(2.27)
[164]	Sep/26/2000 15:23:03 UMST	Concrete Cracking	A51(1.64) A02(2.14) A01(2.25)
[165]	Sep/26/2000 15:23:21 UMST	Concrete Cracking	A31(2.09) A30(2.31) A34(3.10)
[166]	Sep/26/2000 15:23:23 UMST	Concrete Cracking	A30(0.74) A33(1.61) A31(3.41)
[167]	Sep/26/2000 15:23:40 UMST	Concrete Cracking	A31(0.62) A30(2.43) A34(2.90)
[168]	Sep/26/2000 15:23:58 UMST	Concrete Cracking	A31(1.77) A30(2.59) A34(2.67)
[169]	Sep/26/2000 15:24:00 UMST	Concrete Cracking	A30(0.66) A33(1.63) A31(3.51)
[170]	Sep/26/2000 15:24:01 UMST	Concrete Cracking	A31(0.69) A34(1.74) A32(2.51)
[171]	Sep/26/2000 15:24:02 UMST	Concrete Cracking	A38(2.59) A02(3.05) A03(3.37)
[172]	Sep/26/2000 15:24:06 UMST	Concrete Cracking	A02(0.71) A01(2.48) A51(2.60)
[173]	Sep/26/2000 15:24:08 UMST	Concrete Cracking	A02(1.38) A01(1.68) A51(3.15)
[174]	Sep/26/2000 15:24:09 UMST	Concrete Cracking	A01(1.31) A02(2.45) A51(2.55)
[175]	Sep/26/2000 15:24:41 UMST	Concrete Cracking	A02(1.26) A01(1.79) A51(3.12)
[176]	Sep/26/2000 15:25:22 UMST	Concrete Cracking	A30(0.87) A33(2.23) A29(3.79)
[177]	Sep/26/2000 15:25:24 UMST	Concrete Cracking	A30(2.11) A33(3.16) A29(3.35)
[178]	Sep/26/2000 15:25:29 UMST	Concrete Cracking	A33(1.15) A29(2.36) A30(2.59)
[179]	Sep/26/2000 15:25:32 UMST	Concrete Cracking	A26(0.54) A46(0.54) A47(2.73)
[180]	Sep/26/2000 15:25:33 UMST	Concrete Cracking	A03(1.04) A04(1.32) A53(3.49)
[181]	Sep/26/2000 15:25:37 UMST	Concrete Cracking	A21(0.80) A22(1.94) A18(2.35)

[182]	Sep/26/2000 15:25:38 UMST	Concrete Cracking	A33(0.95) A30(2.38) A29(2.59)
[183]	Sep/26/2000 15:25:41 UMST	Concrete Cracking	A20(1.14) A45(2.42) A25(2.54)
[184]	Sep/26/2000 15:25:53 UMST	Concrete Cracking	A30(1.94) A31(3.66) A33(3.95)
[185]	Sep/26/2000 15:25:59 UMST	Concrete Cracking	A06(1.32) A11(1.86) A41(2.31)
[186]	Sep/26/2000 15:26:00 UMST	Concrete Cracking	A31(1.39) A32(2.00) A34(2.64)
[187]	Sep/26/2000 15:26:01 UMST	Concrete Cracking	A30(1.79) A33(1.87) A29(2.77)
[188]	Sep/26/2000 15:26:33 UMST	Concrete Cracking	A30(1.76) A33(2.60) A29(3.15)
[189]	Sep/26/2000 15:27:21 UMST	Concrete Cracking	A25(0.98) A45(1.35) A24(2.71)
[190]	Sep/26/2000 15:27:22 UMST	Concrete Cracking	A11(1.52) A06(1.69) A41(2.42)
[191]	Sep/26/2000 15:27:43 UMST	Concrete Cracking	A52(0.40) A50(1.49) A51(1.50)
[192]	Sep/26/2000 15:28:18 UMST	Concrete Cracking	A16(2.19) A43(2.97) A15(3.26)
[193]	Sep/26/2000 15:28:58 UMST	Concrete Cracking	A14(0.69) A42(2.05) A13(3.12)
[194]	Sep/26/2000 15:29:51 UMST	Concrete Cracking	A38(0.84) A03(2.31) A04(3.19)
[195]	Sep/26/2000 15:32:46 UMST	Concrete Cracking	A51(0.84) A52(1.63) A49(2.02)
[196]	Sep/26/2000 15:33:46 UMST	Concrete Cracking	A51(1.37) A52(2.32) A49(2.41)
[197]	Sep/26/2000 15:35:01 UMST	Concrete Cracking	A31(0.19) A34(2.59) A30(2.87)
[198]	Sep/26/2000 15:37:31 UMST	Concrete Cracking	A11(0.20) A41(2.77) A06(3.15)
[199]	Sep/26/2000 15:39:04 UMST	Concrete Cracking	A02(2.91) A39(3.08) A38(3.92)
[200]	Sep/26/2000 15:43:25 UMST	Concrete Cracking	A02(2.38) A39(3.35) A01(3.62)
[201]	Sep/26/2000 15:52:30 UMST	Concrete Cracking	A17(1.31) A43(2.83) A18(3.13)
[202]	Sep/26/2000 16:12:23 UMST	Concrete Cracking	A42(1.75) A14(2.79) A44(2.92)
[203]	Sep/26/2000 16:48:11 UMST	Concrete Cracking	A02(2.73) A39(3.20) A38(3.96)
[204]	Sep/26/2000 19:40:55 UMST	Concrete Cracking	A30(1.04) A33(1.67) A29(3.51)
[205]	Sep/26/2000 19:44:44 UMST	Concrete Cracking	A30(1.15) A33(1.68) A31(3.21)
[206]	Sep/26/2000 19:56:32 UMST	Concrete Cracking	A51(0.96) A52(1.48) A02(2.09)
[207]	Sep/26/2000 19:56:33 UMST	Concrete Cracking	A17(0.37) A43(1.46) A16(2.96)
[208]	Sep/26/2000 19:56:57 UMST	Concrete Cracking	A21(1.97) A20(2.55) A46(3.19)
[209]	Sep/26/2000 19:57:02 UMST	Concrete Cracking	A30(1.52) A33(1.94) A29(3.05)
[210]	Sep/26/2000 19:57:03 UMST	Concrete Cracking	A47(1.98) A26(2.30) A46(2.30)
[211]	Sep/26/2000 19:57:05 UMST	Concrete Cracking	A20(2.14) A25(2.47) A21(2.95)
[212]	Sep/26/2000 19:57:09 UMST	Concrete Cracking	A26(0.72) A46(0.72) A21(2.26)
[213]	Sep/26/2000 19:57:11 UMST	Concrete Cracking	A31(1.66) A34(2.35) A30(2.87)
[214]	Sep/26/2000 19:57:19 UMST	Concrete Cracking	A12(2.05) A40(2.15) A07(2.25)
[215]	Sep/26/2000 19:57:30 UMST	Concrete Cracking	A30(0.49) A31(2.57) A33(2.58)
[216]	Sep/26/2000 19:57:32 UMST	Concrete Cracking	A26(0.53) A46(0.53) A21(2.46)
[217]	Sep/26/2000 19:57:37 UMST	Concrete Cracking	A43(1.36) A16(1.76) A17(2.29)
[218]	Sep/26/2000 19:57:45 UMST	Concrete Cracking	A41(1.04) A39(1.68) A11(1.86)
[219]	Sep/26/2000 19:57:50 UMST	Concrete Cracking	A13(0.52) A42(1.95) A40(2.27)
[220]	Sep/26/2000 19:57:55 UMST	Concrete Cracking	A31(1.77) A30(1.95) A34(4.19)
[221]	Sep/26/2000 19:58:08 UMST	Concrete Cracking	A33(0.67) A30(1.72) A49(3.78)
[222]	Sep/26/2000 19:58:09 UMST	Concrete Cracking	A30(1.80) A33(2.45) A31(2.64)
[223]	Sep/26/2000 19:58:15 UMST	Concrete Cracking	A30(0.55) A33(1.75) A31(3.42)
[224]	Sep/26/2000 19:58:20 UMST	Concrete Cracking	A24(1.64) A45(2.50) A23(3.07)
[225]	Sep/26/2000 19:58:31 UMST	Concrete Cracking	A12(1.22) A41(1.85) A11(2.13)
[226]	Sep/26/2000 19:58:40 UMST	Concrete Cracking	A26(0.63) A46(0.63) A21(2.35)
[227]	Sep/26/2000 19:59:04 UMST	Concrete Cracking	A24(2.24) A45(3.08) A23(3.15)

[228]	Sep/26/2000 19:59:07 UMST	Concrete Cracking	A47(2.33) A31(3.22) A25(3.50)
[229]	Sep/26/2000 19:59:13 UMST	Concrete Cracking	A25(0.19) A45(1.38) A24(2.91)
[230]	Sep/26/2000 19:59:25 UMST	Concrete Cracking	A33(0.33) A30(1.98) A29(3.60)
[231]	Sep/26/2000 19:59:26 UMST	Concrete Cracking	A24(1.39) A45(1.48) A25(2.67)
[232]	Sep/26/2000 19:59:27 UMST	Concrete Cracking	A25(2.18) A46(3.03) A26(3.03)
[233]	Sep/26/2000 19:59:39 UMST	Concrete Cracking	A21(0.53) A22(2.78) A26(3.03)
[234]	Sep/26/2000 20:00:00 UMST	Concrete Cracking	A12(1.35) A41(1.61) A11(2.40)
[235]	Sep/26/2000 20:00:04 UMST	Concrete Cracking	A30(0.21) A33(2.10) A31(3.14)
[236]	Sep/26/2000 20:00:15 UMST	Concrete Cracking	A06(1.23) A41(1.83) A11(2.08)
[237]	Sep/26/2000 20:00:16 UMST	Concrete Cracking	A29(2.51) A30(3.08) A33(3.51)
[238]	Sep/26/2000 20:00:18 UMST	Concrete Cracking	A29(0.83) A33(3.81) A30(4.46)
[239]	Sep/26/2000 20:00:20 UMST	Concrete Cracking	A42(2.13) A14(2.32) A44(2.41)
[240]	Sep/26/2000 20:00:25 UMST	Concrete Cracking	A30(2.82) A24(3.39) A45(3.53)
[241]	Sep/26/2000 20:00:27 UMST	Concrete Cracking	A33(1.10) A30(2.73) A49(2.83)
[242]	Sep/26/2000 20:00:27 UMST	Concrete Cracking	A45(0.50) A24(1.34) A25(1.83)
[243]	Sep/26/2000 20:00:46 UMST	Concrete Cracking	A20(1.46) A21(2.97) A25(3.31)
[244]	Sep/26/2000 20:01:11 UMST	Concrete Cracking	A29(1.36) A33(2.82) A36(3.45)
[245]	Sep/26/2000 20:01:19 UMST	Concrete Cracking	A21(0.87) A44(2.11) A18(2.11)
[246]	Sep/26/2000 20:01:20 UMST	Concrete Cracking	A43(0.32) A16(1.21) A17(1.84)
[247]	Sep/26/2000 20:01:31 UMST	Concrete Cracking	A46(0.45) A26(0.45) A21(2.53)
[248]	Sep/26/2000 20:01:33 UMST	Concrete Cracking	A33(1.43) A36(3.12) A49(3.35)
[249]	Sep/26/2000 20:02:17 UMST	Concrete Cracking	A02(0.95) A52(2.25) A51(2.54)
[250]	Sep/26/2000 20:02:29 UMST	Concrete Cracking	A30(0.14) A33(2.17) A31(3.09)
[251]	Sep/26/2000 20:02:41 UMST	Concrete Cracking	A06(1.24) A39(1.62) A41(1.89)
[252]	Sep/26/2000 20:02:45 UMST	Concrete Cracking	A30(3.10) A24(3.48) A29(3.70)
[253]	Sep/26/2000 20:03:01 UMST	Concrete Cracking	A02(1.88) A01(2.44) A39(4.29)
[254]	Sep/26/2000 20:03:35 UMST	Concrete Cracking	A24(2.30) A45(2.94) A20(3.45)
[255]	Sep/26/2000 20:03:36 UMST	Concrete Cracking	A23(3.26) A15(3.26) A24(3.44)
[256]	Sep/26/2000 20:03:43 UMST	Concrete Cracking	A11(1.02) A41(1.66) A39(2.46)
[257]	Sep/26/2000 20:06:01 UMST	Concrete Cracking	A30(1.21) A33(1.71) A31(3.18)
[258]	Sep/26/2000 20:08:46 UMST	Concrete Cracking	A29(1.67) A33(4.04) A30(4.21)
[259]	Sep/26/2000 20:09:33 UMST	Concrete Cracking	A30(0.78) A31(2.80) A33(3.06)
[260]	Sep/26/2000 20:11:46 UMST	Concrete Cracking	A39(2.57) A07(3.10) A41(3.17)
[261]	Sep/26/2000 20:36:14 UMST	Concrete Cracking	A20(1.63) A21(2.80) A25(3.39)
[262]	Sep/26/2000 20:36:38 UMST	Concrete Cracking	A24(0.32) A45(1.24) A25(2.76)
[263]	Sep/26/2000 20:36:47 UMST	Concrete Cracking	A06(1.66) A11(1.67) A41(1.69)
[264]	Sep/26/2000 20:37:09 UMST	Concrete Cracking	A47(1.24) A27(1.70) A32(2.22)
[265]	Sep/26/2000 20:37:13 UMST	Concrete Cracking	A47(1.59) A32(1.98) A31(2.59)
[266]	Sep/26/2000 20:37:14 UMST	Concrete Cracking	A26(0.59) A46(0.59) A47(2.40)
[267]	Sep/26/2000 20:37:17 UMST	Concrete Cracking	A21(1.64) A26(1.69) A46(1.69)
[268]	Sep/26/2000 20:37:25 UMST	Concrete Cracking	A14(1.34) A18(2.47) A44(2.47)
[269]	Sep/26/2000 20:37:39 UMST	Concrete Cracking	A16(2.54) A43(3.17) A24(3.49)
[270]	Sep/26/2000 20:37:52 UMST	Concrete Cracking	A20(0.76) A25(2.71) A17(3.41)
[271]	Sep/26/2000 20:38:00 UMST	Concrete Cracking	A33(0.27) A30(2.25) A29(3.23)
[272]	Sep/26/2000 20:38:04 UMST	Concrete Cracking	A28(2.12) A29(2.18) A36(5.23)
[273]	Sep/26/2000 20:38:27 UMST	Concrete Cracking	A41(0.90) A39(1.25) A12(2.55)

[274]	Sep/26/2000 20:38:28 UMST	Concrete Cracking	A33(2.12) A49(2.41) A51(3.08)
[275]	Sep/26/2000 20:38:44 UMST	Concrete Cracking	A21(1.34) A46(1.64) A26(1.64)
[276]	Sep/26/2000 20:38:57 UMST	Concrete Cracking	A48(0.57) A34(1.22) A32(2.00)
[277]	Sep/26/2000 20:39:01 UMST	Concrete Cracking	A20(0.01) A25(2.98) A17(2.99)
[278]	Sep/26/2000 20:39:13 UMST	Concrete Cracking	A37(1.94) A50(1.98) A52(2.00)
[279]	Sep/26/2000 20:39:21 UMST	Concrete Cracking	A16(2.47) A43(3.07) A20(3.41)
[280]	Sep/26/2000 20:39:24 UMST	Concrete Cracking	A01(1.16) A02(2.44) A51(2.71)
[281]	Sep/26/2000 20:39:28 UMST	Concrete Cracking	A31(0.40) A30(2.66) A34(2.78)
[282]	Sep/26/2000 20:39:42 UMST	Concrete Cracking	A06(1.16) A11(2.03) A41(2.35)
[283]	Sep/26/2000 20:39:45 UMST	Concrete Cracking	A24(1.53) A23(2.41) A45(2.75)
[284]	Sep/26/2000 20:39:48 UMST	Concrete Cracking	A25(3.09) A31(3.17) A30(3.37)
[285]	Sep/26/2000 20:39:50 UMST	Concrete Cracking	A52(1.16) A51(1.48) A02(1.88)
[286]	Sep/26/2000 20:39:54 UMST	Concrete Cracking	A29(1.65) A33(2.89) A36(3.13)
[287]	Sep/26/2000 20:40:20 UMST	Concrete Cracking	A46(1.14) A26(1.14) A47(1.85)
[288]	Sep/26/2000 20:40:29 UMST	Concrete Cracking	A40(1.15) A07(1.16) A13(3.05)
[289]	Sep/26/2000 20:40:31 UMST	Concrete Cracking	A33(1.25) A36(3.07) A29(3.42)
[290]	Sep/26/2000 20:40:32 UMST	Concrete Cracking	A33(0.24) A30(2.16) A29(3.31)
[291]	Sep/26/2000 20:40:33 UMST	Concrete Cracking	A20(0.14) A25(2.90) A17(3.07)
[292]	Sep/26/2000 20:40:47 UMST	Concrete Cracking	A24(3.05) A16(3.13) A23(3.69)
[293]	Sep/26/2000 20:41:04 UMST	Concrete Cracking	A24(1.08) A23(2.37) A45(2.42)
[294]	Sep/26/2000 20:41:10 UMST	Concrete Cracking	A20(0.23) A25(2.99) A17(3.00)
[295]	Sep/26/2000 20:41:12 UMST	Concrete Cracking	A30(1.11) A33(1.19) A31(3.84)
[296]	Sep/26/2000 20:41:16 UMST	Concrete Cracking	A36(1.08) A33(3.58) A00(4.37)
[297]	Sep/26/2000 20:41:21 UMST	Concrete Cracking	A23(2.98) A15(2.99) A24(4.24)
[298]	Sep/26/2000 20:41:27 UMST	Concrete Cracking	A39(1.34) A06(1.45) A41(1.51)
[299]	Sep/26/2000 20:41:28 UMST	Concrete Cracking	A06(1.32) A39(1.48) A41(1.70)
[300]	Sep/26/2000 20:41:36 UMST	Concrete Cracking	A30(0.71) A33(1.62) A31(3.44)
[301]	Sep/26/2000 20:41:37 UMST	Concrete Cracking	A00(1.23) A36(2.96) A01(3.36)
[302]	Sep/26/2000 20:41:39 UMST	Concrete Cracking	A06(1.41) A05(1.61) A10(3.20)
[303]	Sep/26/2000 20:41:53 UMST	Concrete Cracking	A33(1.03) A29(2.47) A30(2.84)
[304]	Sep/26/2000 20:41:55 UMST	Concrete Cracking	A02(2.29) A39(3.55) A38(4.05)
[305]	Sep/26/2000 20:41:57 UMST	Concrete Cracking	A02(1.44) A01(3.41) A39(4.28)
[306]	Sep/26/2000 20:42:03 UMST	Concrete Cracking	A21(1.38) A26(1.60) A46(1.60)
[307]	Sep/26/2000 20:42:19 UMST	Concrete Cracking	A26(0.66) A46(0.66) A21(2.32)
[308]	Sep/26/2000 20:42:20 UMST	Concrete Cracking	A25(1.57) A20(1.85) A45(2.70)
[309]	Sep/26/2000 20:42:28 UMST	Concrete Cracking	A15(1.33) A16(2.59) A43(4.03)
[310]	Sep/26/2000 20:42:29 UMST	Concrete Cracking	A07(1.80) A40(1.95) A38(3.44)
[311]	Sep/26/2000 20:42:33 UMST	Concrete Cracking	A01(1.43) A51(2.58) A02(2.91)
[312]	Sep/26/2000 20:42:49 UMST	Concrete Cracking	A21(1.39) A26(1.59) A46(1.59)
[313]	Sep/26/2000 20:42:50 UMST	Concrete Cracking	A29(0.69) A28(3.61) A33(4.07)
[314]	Sep/26/2000 20:42:51 UMST	Concrete Cracking	A20(1.35) A25(2.76) A21(3.23)
[315]	Sep/26/2000 20:42:53 UMST	Concrete Cracking	A24(1.08) A23(1.94) A45(2.61)
[316]	Sep/26/2000 20:42:57 UMST	Concrete Cracking	A30(0.54) A33(2.40) A31(2.64)
[317]	Sep/26/2000 20:43:00 UMST	Concrete Cracking	A18(0.78) A44(0.78) A14(3.15)
[318]	Sep/26/2000 20:43:02 UMST	Concrete Cracking	A29(1.73) A33(1.90) A30(2.87)
[319]	Sep/26/2000 20:43:21 UMST	Concrete Cracking	A06(0.83) A39(1.96) A41(2.06)

[320]	Sep/26/2000 20:43:30 UMST	Concrete Cracking	A43(0.34) A16(1.19) A17(1.86)
[321]	Sep/26/2000 20:43:38 UMST	Concrete Cracking	A13(1.37) A40(2.09) A12(2.13)
[322]	Sep/26/2000 20:44:11 UMST	Concrete Cracking	A39(2.32) A41(2.79) A07(2.81)
[323]	Sep/26/2000 20:55:32 UMST	Concrete Cracking	A30(1.49) A31(1.61) A33(3.31)
[324]	Sep/26/2000 20:59:54 UMST	Concrete Cracking	A33(1.65) A49(2.30) A30(2.85)
[325]	Sep/26/2000 21:17:59 UMST	Concrete Cracking	A46(0.46) A26(0.46) A47(2.81)
[326]	Sep/26/2000 21:18:32 UMST	Concrete Cracking	A21(1.46) A26(1.53) A46(1.53)
[327]	Sep/26/2000 21:18:34 UMST	Concrete Cracking	A44(1.22) A18(1.22) A14(2.86)
[328]	Sep/26/2000 21:18:38 UMST	Concrete Cracking	A21(0.95) A44(2.03) A18(2.03)
[329]	Sep/26/2000 21:18:46 UMST	Concrete Cracking	A21(1.42) A26(1.56) A46(1.56)
[330]	Sep/26/2000 21:18:49 UMST	Concrete Cracking	A46(1.01) A26(1.01) A47(3.14)
[331]	Sep/26/2000 21:18:51 UMST	Concrete Cracking	A20(0.01) A25(2.98) A17(2.99)
[332]	Sep/26/2000 21:18:52 UMST	Concrete Cracking	A26(0.94) A46(0.94) A47(2.04)
[333]	Sep/26/2000 21:18:55 UMST	Concrete Cracking	A23(3.54) A15(3.55) A24(5.77)
[334]	Sep/26/2000 21:18:59 UMST	Concrete Cracking	A25(2.00) A26(2.47) A46(2.47)
[335]	Sep/26/2000 21:19:01 UMST	Concrete Cracking	A47(1.13) A32(2.16) A27(3.05)
[336]	Sep/26/2000 21:19:06 UMST	Concrete Cracking	A32(0.16) A48(1.59) A34(2.22)
[337]	Sep/26/2000 21:19:06 UMST	Concrete Cracking	A01(1.53) A02(1.68) A51(3.62)
[338]	Sep/26/2000 21:19:12 UMST	Concrete Cracking	A21(1.26) A46(1.72) A26(1.72)
[339]	Sep/26/2000 21:19:15 UMST	Concrete Cracking	A20(1.52) A43(2.49) A17(2.88)
[340]	Sep/26/2000 21:19:17 UMST	Concrete Cracking	A21(1.00) A44(1.98) A18(1.98)
[341]	Sep/26/2000 21:19:18 UMST	Concrete Cracking	A24(2.98) A16(2.99) A20(3.05)
[342]	Sep/26/2000 21:19:19 UMST	Concrete Cracking	A15(0.65) A16(2.37) A43(3.90)
[343]	Sep/26/2000 21:19:22 UMST	Concrete Cracking	A25(1.46) A46(2.97) A26(2.97)
[344]	Sep/26/2000 21:19:35 UMST	Concrete Cracking	A23(2.98) A15(2.99) A24(4.24)
[345]	Sep/26/2000 21:19:38 UMST	Concrete Cracking	A43(0.56) A16(1.18) A17(1.97)
[346]	Sep/26/2000 21:19:39 UMST	Concrete Cracking	A26(1.49) A46(1.49) A21(1.50)
[347]	Sep/26/2000 21:19:42 UMST	Concrete Cracking	A09(0.09) A10(4.29) A05(5.16)
[348]	Sep/26/2000 21:19:50 UMST	Concrete Cracking	A20(2.13) A21(2.46) A25(3.14)
[349]	Sep/26/2000 21:19:52 UMST	Concrete Cracking	A06(1.14) A41(1.67) A39(1.67)
[350]	Sep/26/2000 21:19:54 UMST	Concrete Cracking	A20(1.04) A45(3.02) A43(3.03)
[351]	Sep/26/2000 21:19:57 UMST	Concrete Cracking	A24(0.68) A45(0.85) A25(2.37)
[352]	Sep/26/2000 21:20:17 UMST	Concrete Cracking	A23(2.99) A15(3.02) A24(3.99)
[353]	Sep/26/2000 21:20:37 UMST	Concrete Cracking	A20(1.31) A45(2.15) A25(2.27)
[354]	Sep/26/2000 21:20:42 UMST	Concrete Cracking	A43(0.53) A17(0.99) A16(2.06)
[355]	Sep/26/2000 21:20:47 UMST	Concrete Cracking	A23(2.31) A24(3.01) A29(3.94)
[356]	Sep/26/2000 21:20:51 UMST	Concrete Cracking	A21(1.38) A26(1.60) A46(1.60)
[357]	Sep/26/2000 21:20:56 UMST	Concrete Cracking	A24(2.98) A16(2.99) A20(3.05)
[358]	Sep/26/2000 21:21:00 UMST	Concrete Cracking	A15(2.58) A16(3.44) A23(3.53)
[359]	Sep/26/2000 21:21:03 UMST	Concrete Cracking	A11(1.83) A06(2.68) A10(2.72)
[360]	Sep/26/2000 21:21:07 UMST	Concrete Cracking	A24(2.98) A16(2.99) A20(3.05)
[361]	Sep/26/2000 21:21:09 UMST	Concrete Cracking	A21(0.30) A22(2.27) A44(2.68)
[362]	Sep/26/2000 21:21:12 UMST	Concrete Cracking	A31(1.50) A32(1.53) A34(2.18)
[363]	Sep/26/2000 21:21:14 UMST	Concrete Cracking	A23(3.82) A15(4.28) A19(5.94)
[364]	Sep/26/2000 21:21:15 UMST	Concrete Cracking	A12(1.50) A41(1.69) A39(2.30)
[365]	Sep/26/2000 21:21:24 UMST	Concrete Cracking	A21(0.54) A22(2.37) A44(2.44)

[366]	Sep/26/2000 21:21:29 UMST	Concrete Cracking	A40(1.56) A07(1.58) A12(3.02)
[367]	Sep/26/2000 21:21:32 UMST	Concrete Cracking	A18(0.80) A44(0.80) A21(2.18)
[368]	Sep/26/2000 21:21:38 UMST	Concrete Cracking	A32(1.19) A47(1.79) A48(2.62)
[369]	Sep/26/2000 21:21:43 UMST	Concrete Cracking	A31(0.91) A34(1.82) A32(2.00)
[370]	Sep/26/2000 21:21:51 UMST	Concrete Cracking	A16(0.26) A43(1.27) A17(2.79)
[371]	Sep/26/2000 21:21:55 UMST	Concrete Cracking	A23(2.61) A29(4.20) A28(4.74)
[372]	Sep/26/2000 21:21:57 UMST	Concrete Cracking	A26(1.55) A46(1.55) A21(2.18)
[373]	Sep/26/2000 21:21:59 UMST	Concrete Cracking	A49(0.56) A51(0.63) A50(1.31)
[374]	Sep/26/2000 21:22:00 UMST	Concrete Cracking	A43(0.28) A16(1.41) A17(1.68)
[375]	Sep/26/2000 21:22:05 UMST	Concrete Cracking	A24(0.30) A45(1.23) A25(2.75)
[376]	Sep/26/2000 21:22:07 UMST	Concrete Cracking	A43(0.48) A17(1.04) A16(2.01)
[377]	Sep/26/2000 21:22:08 UMST	Concrete Cracking	A43(0.01) A17(1.52) A16(1.52)
[378]	Sep/26/2000 21:22:11 UMST	Concrete Cracking	A24(0.06) A45(1.47) A25(2.99)
[379]	Sep/26/2000 21:22:19 UMST	Concrete Cracking	A18(0.72) A44(0.72) A21(2.26)
[380]	Sep/26/2000 21:22:25 UMST	Concrete Cracking	A29(2.43) A30(3.01) A33(3.37)
[381]	Sep/26/2000 21:22:32 UMST	Concrete Cracking	A39(2.22) A41(3.02) A02(3.99)
[382]	Sep/26/2000 21:22:38 UMST	Concrete Cracking	A42(1.73) A14(2.26) A44(2.81)
[383]	Sep/26/2000 21:22:43 UMST	Concrete Cracking	A23(0.44) A24(3.05) A45(4.57)
[384]	Sep/26/2000 21:22:46 UMST	Concrete Cracking	A00(1.01) A01(2.91) A36(3.22)
[385]	Sep/26/2000 21:22:51 UMST	Concrete Cracking	A33(1.84) A36(2.55) A49(3.78)
[386]	Sep/26/2000 21:22:52 UMST	Concrete Cracking	A16(0.08) A43(1.46) A17(2.98)
[387]	Sep/26/2000 21:22:53 UMST	Concrete Cracking	A24(2.25) A45(2.67) A25(3.71)
[388]	Sep/26/2000 21:22:55 UMST	Concrete Cracking	A20(0.32) A25(2.99) A17(3.01)
[389]	Sep/26/2000 21:23:06 UMST	Concrete Cracking	A24(0.86) A45(1.63) A25(3.03)
[390]	Sep/26/2000 21:23:08 UMST	Concrete Cracking	A01(1.45) A00(3.10) A51(3.14)
[391]	Sep/26/2000 21:23:11 UMST	Concrete Cracking	A24(2.98) A16(2.99) A20(3.05)
[392]	Sep/26/2000 21:23:27 UMST	Concrete Cracking	A29(0.73) A28(3.67) A33(4.20)
[393]	Sep/26/2000 21:23:32 UMST	Concrete Cracking	A24(0.27) A45(1.26) A25(2.78)
[394]	Sep/26/2000 21:23:36 UMST	Concrete Cracking	A21(1.12) A18(1.86) A44(1.86)
[395]	Sep/26/2000 21:23:38 UMST	Concrete Cracking	A21(1.40) A26(1.59) A46(1.59)
[396]	Sep/26/2000 21:23:43 UMST	Concrete Cracking	A31(0.65) A32(2.61) A34(2.64)
[397]	Sep/26/2000 21:23:45 UMST	Concrete Cracking	A15(2.27) A23(3.70) A16(3.74)
[398]	Sep/26/2000 21:24:34 UMST	Concrete Cracking	A16(0.29) A43(1.24) A17(2.76)
[399]	Sep/26/2000 21:45:39 UMST	Concrete Cracking	A01(0.81) A00(2.71) A02(3.52)
[400]	Sep/26/2000 21:45:40 UMST	Concrete Cracking	A31(1.43) A30(1.62) A33(3.59)
[401]	Sep/26/2000 21:45:54 UMST	Concrete Cracking	A11(1.11) A41(1.81) A06(2.20)
[402]	Sep/26/2000 21:45:55 UMST	Concrete Cracking	A44(0.17) A18(0.17) A21(3.15)
[403]	Sep/26/2000 21:45:59 UMST	Concrete Cracking	A29(2.31) A36(3.10) A28(3.59)
[404]	Sep/26/2000 21:46:00 UMST	Concrete Cracking	A36(1.51) A33(3.64) A49(4.03)
[405]	Sep/26/2000 21:46:17 UMST	Concrete Cracking	A01(1.54) A00(1.59) A36(4.08)
[406]	Sep/26/2000 21:46:23 UMST	Concrete Cracking	A20(0.96) A45(3.03) A43(3.04)
[407]	Sep/26/2000 21:46:51 UMST	Concrete Cracking	A46(0.82) A26(0.82) A47(3.09)
[408]	Sep/26/2000 21:47:11 UMST	Concrete Cracking	A00(0.87) A01(3.51) A05(5.41)
[409]	Sep/26/2000 21:47:15 UMST	Concrete Cracking	A19(3.12) A23(6.08) A15(6.69)
[410]	Sep/26/2000 21:47:56 UMST	Concrete Cracking	A30(1.14) A33(1.32) A29(3.56)
[411]	Sep/26/2000 21:48:15 UMST	Concrete Cracking	A46(0.47) A26(0.47) A21(2.51)

[412]	Sep/26/2000 21:48:21 UMST	Concrete Cracking	A00(1.87) A01(2.66) A36(2.72)
[413]	Sep/26/2000 21:48:22 UMST	Concrete Cracking	A23(2.98) A15(2.99) A24(4.24)
[414]	Sep/26/2000 21:48:23 UMST	Concrete Cracking	A23(2.99) A15(3.00) A24(4.04)
[415]	Sep/26/2000 21:48:24 UMST	Concrete Cracking	A33(0.71) A30(2.79) A29(2.85)
[416]	Sep/26/2000 21:48:32 UMST	Concrete Cracking	A47(0.61) A27(2.33) A32(2.37)
[417]	Sep/26/2000 21:48:40 UMST	Concrete Cracking	A00(2.80) A05(3.38) A01(3.95)
[418]	Sep/26/2000 21:48:55 UMST	Concrete Cracking	A23(2.98) A15(2.99) A24(4.24)
[419]	Sep/26/2000 21:48:59 UMST	Concrete Cracking	A00(0.59) A01(2.43) A02(5.48)
[420]	Sep/26/2000 21:49:03 UMST	Concrete Cracking	A24(1.35) A23(1.68) A45(2.88)
[421]	Sep/26/2000 21:49:06 UMST	Concrete Cracking	A15(1.28) A16(1.83) A43(3.34)
[422]	Sep/26/2000 21:49:33 UMST	Concrete Cracking	A01(2.56) A36(2.72) A00(3.05)
[423]	Sep/26/2000 21:49:34 UMST	Concrete Cracking	A15(1.33) A16(2.04) A43(3.51)
[424]	Sep/26/2000 21:49:38 UMST	Concrete Cracking	A00(0.69) A01(2.45) A02(5.48)
[425]	Sep/26/2000 21:49:52 UMST	Concrete Cracking	A02(0.71) A01(2.65) A03(4.91)
[426]	Sep/26/2000 21:50:19 UMST	Concrete Cracking	A15(4.23) A23(4.26) A19(5.64)
[427]	Sep/26/2000 21:50:20 UMST	Concrete Cracking	A02(1.69) A51(1.98) A01(2.11)
[428]	Sep/26/2000 21:50:22 UMST	Concrete Cracking	A24(3.05) A16(3.06) A45(3.69)
[429]	Sep/26/2000 21:50:32 UMST	Concrete Cracking	A33(2.10) A36(2.35) A49(3.74)
[430]	Sep/26/2000 21:51:07 UMST	Concrete Cracking	A21(0.39) A22(2.29) A26(2.60)
[431]	Sep/26/2000 21:52:40 UMST	Concrete Cracking	A00(1.34) A01(2.90) A36(2.94)
[432]	Sep/26/2000 21:53:16 UMST	Concrete Cracking	A03(0.34) A38(1.80) A04(2.17)
[433]	Sep/26/2000 21:53:27 UMST	Concrete Cracking	A33(0.40) A30(2.48) A29(3.08)
[434]	Sep/26/2000 22:16:26 UMST	Concrete Cracking	A45(0.58) A25(1.57) A24(1.69)
[435]	Sep/26/2000 22:17:08 UMST	Concrete Cracking	A01(1.03) A00(2.33) A02(3.90)
[436]	Sep/26/2000 22:17:15 UMST	Concrete Cracking	A33(0.55) A30(2.07) A29(3.09)
[437]	Sep/26/2000 22:17:38 UMST	Concrete Cracking	A33(1.36) A29(2.14) A30(3.06)
[438]	Sep/26/2000 22:17:46 UMST	Concrete Cracking	A23(2.98) A15(2.99) A24(4.24)
[439]	Sep/26/2000 22:17:49 UMST	Concrete Cracking	A24(0.74) A45(0.79) A25(2.31)
[440]	Sep/26/2000 22:18:01 UMST	Concrete Cracking	A31(1.71) A47(2.74) A32(2.88)
[441]	Sep/26/2000 22:18:21 UMST	Concrete Cracking	A30(0.83) A33(1.95) A31(2.96)
[442]	Sep/26/2000 22:18:36 UMST	Concrete Cracking	A00(1.46) A01(1.61) A36(4.16)
[443]	Sep/26/2000 22:19:09 UMST	Concrete Cracking	A20(1.50) A21(2.94) A17(3.27)
[444]	Sep/26/2000 22:19:24 UMST	Concrete Cracking	A23(3.18) A15(3.19) A24(5.09)
[445]	Sep/26/2000 22:19:27 UMST	Concrete Cracking	A23(0.89) A24(3.15) A45(4.63)
[446]	Sep/26/2000 22:20:24 UMST	Concrete Cracking	A29(0.46) A28(3.84) A33(3.88)
[447]	Sep/26/2000 22:20:29 UMST	Concrete Cracking	A17(0.88) A43(2.37) A20(3.36)
[448]	Sep/26/2000 22:21:12 UMST	Concrete Cracking	A01(1.56) A02(1.86) A00(4.44)
[449]	Sep/26/2000 22:21:36 UMST	Concrete Cracking	A26(0.53) A46(0.53) A47(2.45)
[450]	Sep/26/2000 22:21:57 UMST	Concrete Cracking	A21(1.45) A26(1.53) A46(1.53)
[451]	Sep/26/2000 22:22:36 UMST	Concrete Cracking	A29(1.44) A33(2.04) A30(3.32)
[452]	Sep/26/2000 22:25:01 UMST	Concrete Cracking	A33(0.69) A30(1.67) A29(3.43)
[453]	Sep/26/2000 22:25:09 UMST	Concrete Cracking	A33(0.74) A30(1.58) A29(3.55)
[454]	Sep/26/2000 22:33:24 UMST	Concrete Cracking	A46(1.31) A26(1.31) A47(1.68)
[455]	Sep/26/2000 22:43:32 UMST	Concrete Cracking	A19(4.53) A09(5.63) A15(7.75)
[456]	Sep/27/2000 03:05:13 UMST	Concrete Cracking	A20(1.79) A43(2.07) A16(2.56)
[457]	Sep/27/2000 07:09:31 UMST	Concrete Cracking	A04(0.80) A03(1.50) A38(1.93)

[458]	Sep/27/2000 07:22:25 UMST	Concrete Cracking	A34(0.73) A48(1.08) A32(2.36)
[459]	Sep/27/2000 07:56:41 UMST	Concrete Cracking	A31(2.18) A47(2.77) A32(3.42)
[460]	Sep/27/2000 07:59:36 UMST	Concrete Cracking	A41(1.38) A11(1.70) A12(1.90)
[461]	Sep/27/2000 08:00:09 UMST	Concrete Cracking	A10(1.05) A05(2.11) A06(3.07)
[462]	Sep/27/2000 12:05:41 UMST	Concrete Cracking	A32(0.25) A48(1.68) A34(2.27)
[463]	Sep/27/2000 12:22:49 UMST	Concrete Cracking	A03(1.05) A04(1.20) A53(3.18)
[464]	Sep/27/2000 12:49:41 UMST	Crushing Concrete	A35(1.50) A48(1.58) A34(2.23)
[465]	Sep/27/2000 13:01:32 UMST	Concrete Cracking	A32(1.16) A34(1.46) A48(1.63)
[466]	Sep/27/2000 13:01:32 UMST	Concrete Cracking	A32(1.03) A34(1.49) A48(1.56)
[467]	Sep/27/2000 13:01:56 UMST	Concrete Cracking	A11(1.73) A12(2.39) A41(3.68)
[468]	Sep/27/2000 13:04:28 UMST	Concrete Cracking	A28(2.03) A29(5.65) A23(6.86)
[469]	Sep/27/2000 13:04:29 UMST	Concrete Cracking	A28(2.78) A29(6.15) A23(6.67)
[470]	Sep/27/2000 13:05:35 UMST	Concrete Cracking	A28(2.84) A29(3.89) A23(4.56)
[471]	Sep/27/2000 13:20:04 UMST	Concrete Cracking	A38(1.41) A04(2.34) A03(2.46)
[472]	Sep/27/2000 13:21:07 UMST	Concrete Cracking	A38(2.93) A08(2.96) A04(3.21)
[473]	Sep/27/2000 13:34:56 UMST	Crushing Concrete	A04(1.15) A03(1.92) A53(2.61)
[474]	Sep/27/2000 13:35:58 UMST	Crushing Concrete	A38(0.70) A03(2.09) A04(3.33)
[475]	Sep/27/2000 13:37:28 UMST	Concrete Cracking	A11(1.04) A12(3.10) A41(3.53)
[476]	Sep/27/2000 13:37:46 UMST	Crushing Concrete	A08(0.23) A40(2.02) A07(2.03)
[477]	Sep/27/2000 13:38:01 UMST	Concrete Cracking	A11(1.43) A12(2.82) A41(3.70)
[478]	Sep/27/2000 13:38:03 UMST	Concrete Cracking	A10(2.39) A11(2.77) A06(4.11)
[479]	Sep/27/2000 13:43:18 UMST	Crushing Concrete	A26(0.57) A46(0.57) A21(2.50)
[480]	Sep/27/2000 13:49:57 UMST	Crushing Concrete	A22(1.50) A21(2.24) A46(2.34)
[481]	Sep/27/2000 13:50:01 UMST	Crushing Concrete	A27(0.62) A47(1.90) A32(3.12)
[482]	Sep/27/2000 13:51:37 UMST	Concrete Cracking	A46(0.43) A26(0.43) A21(2.58)
[483]	Sep/27/2000 14:05:10 UMST	Crushing Concrete	A21(0.21) A22(2.26) A26(2.78)
[484]	Sep/27/2000 14:15:21 UMST	Concrete Cracking	A35(0.86) A37(2.46) A48(2.51)
[485]	Sep/27/2000 14:15:22 UMST	Crushing Concrete	A35(1.67) A37(1.72) A53(2.09)
[486]	Sep/27/2000 14:18:42 UMST	Concrete Cracking	A11(0.58) A12(3.11) A41(3.15)
[487]	Sep/27/2000 14:24:44 UMST	Crushing Concrete	A44(1.46) A18(1.46) A22(2.38)
[488]	Sep/27/2000 14:36:18 UMST	Concrete Cracking	A04(1.13) A38(1.64) A03(1.76)
[489]	Sep/27/2000 14:44:02 UMST	Concrete Cracking	A11(1.79) A12(3.54) A43(4.17)

SANDIA PCCV

ALBUQUERQUE, NM

SOUNDPRINT® ACOUSTIC MONITORING PROGRAM

REPORT

REPORTING PERIOD: SEPTEMBER 12 TO SEPTEMBER 27, 2000

DISCLAIMER

The information provided in this report is not intended to constitute an engineering report and should not be construed as such. The client is advised to retain qualified engineering expertise to interpret the data contained in this report. The information contained in this report is provided "as is" without warranty of any kind, either express or implied. Pure Technologies Ltd. is not liable for any lost profits, lost savings or other incidental, special or consequential damage arising out of the use of the monitoring system or the information contained in this report. Please refer to the terms and conditions attached to Pure's SoundPrint® System Purchase Agreement and Pure's Technical Support Agreement for further details.

® Registered Trademark, property of Pure Technologies Ltd.

TABLE OF CONTENTS

1.0 EXECUTIVE SUMMARY

The following is a summary of relevant activity recorded by the SoundPrint® monitoring system. The summary includes information for both the latest monitoring period and for the entire monitoring period from the start-up date up to and including the most recent monitoring period.

	Period 09/12/2000– 09/27/2000
Operating Efficiency	100 %
LST Concrete Cracks	239

Comments

Recommendations

There are no new recommendations at this time.

Prepared by:

Peter Paulson
President & CEO

REPORT PRESENTATION

A computerized drawing of the slab with the sensor layout is included on the following page and contains the following symbols:

Sensor Symbol with individual sensor name beneath

Symbolizes an event location. Event details are listed on the page following the drawing.

A list describing event details is provided for each drawing and lists the event number, shown on the computerized drawing, followed by the date, time, event classification and coordinates (in meters) to the origin of the events using the three closes sensors.

Event Report For Sandia PCCV

Albuquerque, NM

System Uptime 15.9 Days (100%)

LST Concrete Cracks

Period: 09/12/2000 to **09/27/2000**

Matched Events: 239

PCCV NEW -- 239 EVENTS

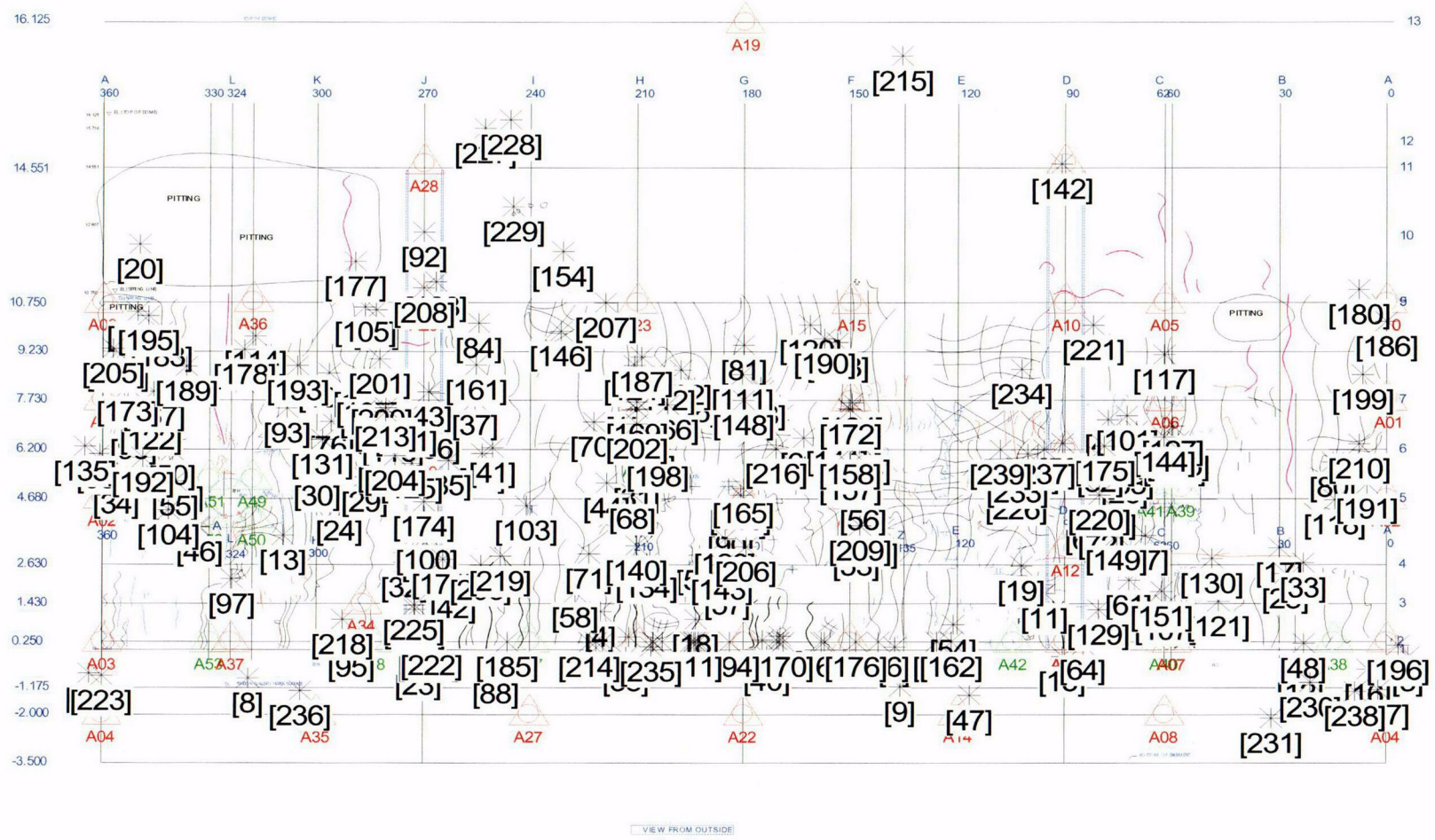

Scale: 1.95 m / cm

0 2m 20m

Events

No.	Date/Time	Classification	Location (m)
[1]	Sep/12/2000 09:30:33 UMST	Concrete Cracking	A12(1.23) A41(1.73) A11(2.47)
[2]	Sep/12/2000 09:33:43 UMST	Concrete Cracking	A17(1.29) A43(2.60) A44(3.62)
[3]	Sep/12/2000 12:21:44 UMST	Concrete Cracking	A03(0.76) A04(1.89) A38(2.12)
[4]	Sep/12/2000 13:22:51 UMST	Concrete Cracking	A26(1.37) A46(1.37) A47(2.18)
[5]	Sep/12/2000 13:27:45 UMST	Concrete Cracking	A26(0.26) A46(0.26) A47(2.77)
[6]	Sep/12/2000 13:53:08 UMST	Concrete Cracking	A44(1.25) A18(1.25) A14(2.73)
[7]	Sep/13/2000 13:06:27 UMST	Concrete Cracking	A42(2.01) A14(2.31) A44(2.53)
[8]	Sep/13/2000 14:27:30 UMST	Concrete Cracking	A37(1.22) A53(1.55) A35(2.20)
[9]	Sep/14/2000 15:57:41 UMST	Concrete Cracking	A14(1.81) A44(1.96) A18(1.96)
[10]	Sep/26/2000 13:55:42 UMST	Concrete Cracking	A21(1.05) A44(1.96) A18(1.96)
[11]	Sep/26/2000 14:25:54 UMST	Concrete Cracking	A12(1.51) A13(1.59) A42(1.73)
[12]	Sep/26/2000 14:27:18 UMST	Concrete Cracking	A38(1.22) A03(2.52) A04(2.80)
[13]	Sep/26/2000 14:27:20 UMST	Concrete Cracking	A50(1.01) A49(1.93) A52(2.12)
[14]	Sep/26/2000 14:30:04 UMST	Concrete Cracking	A45(0.62) A24(1.63) A25(1.66)
[15]	Sep/26/2000 14:30:22 UMST	Concrete Cracking	A13(0.45) A42(1.44) A40(2.88)
[16]	Sep/26/2000 14:30:32 UMST	Concrete Cracking	A03(0.99) A38(1.28) A04(1.49)
[17]	Sep/26/2000 14:47:36 UMST	Concrete Cracking	A39(3.27) A38(3.29) A02(3.35)
[18]	Sep/26/2000 14:50:18 UMST	Concrete Cracking	A21(1.51) A26(1.79) A46(1.79)
[19]	Sep/26/2000 14:50:47 UMST	Concrete Cracking	A12(1.32) A42(2.36) A13(2.64)
[20]	Sep/26/2000 14:54:19 UMST	Concrete Cracking	A00(2.07) A36(3.61) A01(4.93)
[21]	Sep/26/2000 15:16:32 UMST	Concrete Cracking	A52(0.43) A51(1.50) A50(1.54)
[22]	Sep/26/2000 15:19:06 UMST	Concrete Cracking	A30(1.65) A31(3.36) A33(3.75)
[23]	Sep/26/2000 15:20:55 UMST	Concrete Cracking	A32(0.57) A48(1.42) A34(2.36)
[24]	Sep/26/2000 15:21:47 UMST	Concrete Cracking	A50(2.45) A49(2.56) A31(2.69)
[25]	Sep/26/2000 15:21:51 UMST	Concrete Cracking	A41(1.03) A39(1.92) A12(2.01)
[26]	Sep/26/2000 15:21:59 UMST	Concrete Cracking	A41(0.91) A39(1.69) A11(1.77)
[27]	Sep/26/2000 15:22:18 UMST	Concrete Cracking	A41(1.44) A39(1.75) A12(2.28)
[28]	Sep/26/2000 15:22:27 UMST	Concrete Cracking	A38(2.50) A03(3.51) A02(3.65)
[29]	Sep/26/2000 15:22:45 UMST	Concrete Cracking	A30(1.85) A33(2.38) A31(2.75)
[30]	Sep/26/2000 15:22:54 UMST	Concrete Cracking	A49(1.82) A50(2.31) A33(2.53)
[31]	Sep/26/2000 15:23:02 UMST	Concrete Cracking	A45(0.74) A25(0.78) A24(2.27)
[32]	Sep/26/2000 15:24:01 UMST	Concrete Cracking	A31(0.69) A34(1.74) A32(2.51)
[33]	Sep/26/2000 15:24:02 UMST	Concrete Cracking	A38(2.59) A02(3.05) A03(3.37)
[34]	Sep/26/2000 15:24:06 UMST	Concrete Cracking	A02(0.71) A01(2.48) A51(2.60)
[35]	Sep/26/2000 15:24:08 UMST	Concrete Cracking	A02(1.38) A01(1.68) A51(3.15)
[36]	Sep/26/2000 15:25:22 UMST	Concrete Cracking	A30(0.87) A33(2.23) A29(3.79)
[37]	Sep/26/2000 15:25:24 UMST	Concrete Cracking	A30(2.11) A33(3.16) A29(3.35)
[38]	Sep/26/2000 15:25:32 UMST	Concrete Cracking	A26(0.54) A46(0.54) A47(2.73)
[39]	Sep/26/2000 15:25:33 UMST	Concrete Cracking	A03(1.04) A04(1.32) A53(3.49)
[40]	Sep/26/2000 15:25:37 UMST	Concrete Cracking	A21(0.80) A22(1.94) A18(2.35)
[41]	Sep/26/2000 15:25:53 UMST	Concrete Cracking	A30(1.94) A31(3.66) A33(3.95)
[42]	Sep/26/2000 15:26:00 UMST	Concrete Cracking	A31(1.39) A32(2.00) A34(2.64)
[43]	Sep/26/2000 15:26:01 UMST	Concrete Cracking	A30(1.79) A33(1.87) A29(2.77)

[44]	Sep/26/2000 15:27:21 UMST	Concrete Cracking	A25(0.98) A45(1.35) A24(2.71)
[45]	Sep/26/2000 15:27:22 UMST	Concrete Cracking	A11(1.52) A06(1.69) A41(2.42)
[46]	Sep/26/2000 15:27:43 UMST	Concrete Cracking	A52(0.40) A50(1.49) A51(1.50)
[47]	Sep/26/2000 15:28:58 UMST	Concrete Cracking	A14(0.69) A42(2.05) A13(3.12)
[48]	Sep/26/2000 15:29:51 UMST	Concrete Cracking	A38(0.84) A03(2.31) A04(3.19)
[49]	Sep/26/2000 15:32:46 UMST	Concrete Cracking	A51(0.84) A52(1.63) A49(2.02)
[50]	Sep/26/2000 15:33:46 UMST	Concrete Cracking	A51(1.37) A52(2.32) A49(2.41)
[51]	Sep/26/2000 15:35:01 UMST	Concrete Cracking	A31(0.19) A34(2.59) A30(2.87)
[52]	Sep/26/2000 15:37:31 UMST	Concrete Cracking	A11(0.20) A41(2.77) A06(3.15)
[53]	Sep/26/2000 15:52:30 UMST	Concrete Cracking	A17(1.31) A43(2.83) A18(3.13)
[54]	Sep/26/2000 16:12:23 UMST	Concrete Cracking	A42(1.75) A14(2.79) A44(2.92)
[55]	Sep/26/2000 19:56:32 UMST	Concrete Cracking	A51(0.96) A52(1.48) A02(2.09)
[56]	Sep/26/2000 19:56:33 UMST	Concrete Cracking	A17(0.37) A43(1.46) A16(2.96)
[57]	Sep/26/2000 19:56:57 UMST	Concrete Cracking	A21(1.97) A20(2.55) A46(3.19)
[58]	Sep/26/2000 19:57:03 UMST	Concrete Cracking	A47(1.98) A26(2.30) A46(2.30)
[59]	Sep/26/2000 19:57:05 UMST	Concrete Cracking	A20(2.14) A25(2.47) A21(2.95)
[60]	Sep/26/2000 19:57:09 UMST	Concrete Cracking	A26(0.72) A46(0.72) A21(2.26)
[61]	Sep/26/2000 19:57:19 UMST	Concrete Cracking	A12(2.05) A40(2.15) A07(2.25)
[62]	Sep/26/2000 19:57:37 UMST	Concrete Cracking	A43(1.36) A16(1.76) A17(2.29)
[63]	Sep/26/2000 19:57:45 UMST	Concrete Cracking	A41(1.04) A39(1.68) A11(1.86)
[64]	Sep/26/2000 19:57:50 UMST	Concrete Cracking	A13(0.52) A42(1.95) A40(2.27)
[65]	Sep/26/2000 19:58:08 UMST	Concrete Cracking	A33(0.67) A30(1.72) A49(3.78)
[66]	Sep/26/2000 19:58:20 UMST	Concrete Cracking	A24(1.64) A45(2.50) A23(3.07)
[67]	Sep/26/2000 19:58:31 UMST	Concrete Cracking	A12(1.22) A41(1.85) A11(2.13)
[68]	Sep/26/2000 19:59:13 UMST	Concrete Cracking	A25(0.19) A45(1.38) A24(2.91)
[69]	Sep/26/2000 19:59:25 UMST	Concrete Cracking	A33(0.33) A30(1.98) A29(3.60)
[70]	Sep/26/2000 19:59:26 UMST	Concrete Cracking	A24(1.39) A45(1.48) A25(2.67)
[71]	Sep/26/2000 19:59:27 UMST	Concrete Cracking	A25(2.18) A46(3.03) A26(3.03)
[72]	Sep/26/2000 20:00:00 UMST	Concrete Cracking	A12(1.35) A41(1.61) A11(2.40)
[73]	Sep/26/2000 20:00:15 UMST	Concrete Cracking	A06(1.23) A41(1.83) A11(2.08)
[74]	Sep/26/2000 20:00:20 UMST	Concrete Cracking	A42(2.13) A14(2.32) A44(2.41)
[75]	Sep/26/2000 20:00:27 UMST	Concrete Cracking	A45(0.50) A24(1.34) A25(1.83)
[76]	Sep/26/2000 20:00:27 UMST	Concrete Cracking	A33(1.10) A30(2.73) A49(2.83)
[77]	Sep/26/2000 20:01:11 UMST	Concrete Cracking	A29(1.36) A33(2.82) A36(3.45)
[78]	Sep/26/2000 20:01:20 UMST	Concrete Cracking	A43(0.32) A16(1.21) A17(1.84)
[79]	Sep/26/2000 20:01:31 UMST	Concrete Cracking	A46(0.45) A26(0.45) A21(2.53)
[80]	Sep/26/2000 20:03:01 UMST	Concrete Cracking	A02(1.88) A01(2.44) A39(4.29)
[81]	Sep/26/2000 20:03:36 UMST	Concrete Cracking	A23(3.26) A15(3.26) A24(3.44)
[82]	Sep/26/2000 20:03:43 UMST	Concrete Cracking	A11(1.02) A41(1.66) A39(2.46)
[83]	Sep/26/2000 20:06:01 UMST	Concrete Cracking	A30(1.21) A33(1.71) A31(3.18)
[84]	Sep/26/2000 20:08:46 UMST	Concrete Cracking	A29(1.67) A33(4.04) A30(4.21)
[85]	Sep/26/2000 20:09:33 UMST	Concrete Cracking	A30(0.78) A31(2.80) A33(3.06)
[86]	Sep/26/2000 20:36:38 UMST	Concrete Cracking	A24(0.32) A45(1.24) A25(2.76)
[87]	Sep/26/2000 20:36:47 UMST	Concrete Cracking	A06(1.66) A11(1.67) A41(1.69)
[88]	Sep/26/2000 20:37:09 UMST	Concrete Cracking	A47(1.24) A27(1.70) A32(2.22)
[89]	Sep/26/2000 20:37:39 UMST	Concrete Cracking	A16(2.54) A43(3.17) A24(3.49)

[90]	Sep/26/2000 20:37:52 UMST	Concrete Cracking	A20(0.76) A25(2.71) A17(3.41)
[91]	Sep/26/2000 20:38:00 UMST	Concrete Cracking	A33(0.27) A30(2.25) A29(3.23)
[92]	Sep/26/2000 20:38:04 UMST	Concrete Cracking	A28(2.12) A29(2.18) A36(5.23)
[93]	Sep/26/2000 20:38:28 UMST	Concrete Cracking	A33(2.12) A49(2.41) A51(3.08)
[94]	Sep/26/2000 20:38:44 UMST	Concrete Cracking	A21(1.34) A46(1.64) A26(1.64)
[95]	Sep/26/2000 20:38:57 UMST	Concrete Cracking	A48(0.57) A34(1.22) A32(2.00)
[96]	Sep/26/2000 20:39:01 UMST	Concrete Cracking	A20(0.01) A25(2.98) A17(2.99)
[97]	Sep/26/2000 20:39:13 UMST	Concrete Cracking	A37(1.94) A50(1.98) A52(2.00)
[98]	Sep/26/2000 20:39:21 UMST	Concrete Cracking	A16(2.47) A43(3.07) A20(3.41)
[99]	Sep/26/2000 20:39:24 UMST	Concrete Cracking	A01(1.16) A02(2.44) A51(2.71)
[100]	Sep/26/2000 20:39:28 UMST	Concrete Cracking	A31(0.40) A30(2.66) A34(2.78)
[101]	Sep/26/2000 20:39:42 UMST	Concrete Cracking	A06(1.16) A11(2.03) A41(2.35)
[102]	Sep/26/2000 20:39:45 UMST	Concrete Cracking	A24(1.53) A23(2.41) A45(2.75)
[103]	Sep/26/2000 20:39:48 UMST	Concrete Cracking	A25(3.09) A31(3.17) A30(3.37)
[104]	Sep/26/2000 20:39:50 UMST	Concrete Cracking	A52(1.16) A51(1.48) A02(1.88)
[105]	Sep/26/2000 20:39:54 UMST	Concrete Cracking	A29(1.65) A33(2.89) A36(3.13)
[106]	Sep/26/2000 20:40:20 UMST	Concrete Cracking	A46(1.14) A26(1.14) A47(1.85)
[107]	Sep/26/2000 20:40:29 UMST	Concrete Cracking	A40(1.15) A07(1.16) A13(3.05)
[108]	Sep/26/2000 20:40:31 UMST	Concrete Cracking	A33(1.25) A36(3.07) A29(3.42)
[109]	Sep/26/2000 20:40:32 UMST	Concrete Cracking	A33(0.24) A30(2.16) A29(3.31)
[110]	Sep/26/2000 20:40:33 UMST	Concrete Cracking	A20(0.14) A25(2.90) A17(3.07)
[111]	Sep/26/2000 20:40:47 UMST	Concrete Cracking	A24(3.05) A16(3.13) A23(3.69)
[112]	Sep/26/2000 20:41:04 UMST	Concrete Cracking	A24(1.08) A23(2.37) A45(2.42)
[113]	Sep/26/2000 20:41:12 UMST	Concrete Cracking	A30(1.11) A33(1.19) A31(3.84)
[114]	Sep/26/2000 20:41:16 UMST	Concrete Cracking	A36(1.08) A33(3.58) A00(4.37)
[115]	Sep/26/2000 20:41:27 UMST	Concrete Cracking	A39(1.34) A06(1.45) A41(1.51)
[116]	Sep/26/2000 20:41:28 UMST	Concrete Cracking	A06(1.32) A39(1.48) A41(1.70)
[117]	Sep/26/2000 20:41:39 UMST	Concrete Cracking	A06(1.41) A05(1.61) A10(3.20)
[118]	Sep/26/2000 20:41:57 UMST	Concrete Cracking	A02(1.44) A01(3.41) A39(4.28)
[119]	Sep/26/2000 20:42:03 UMST	Concrete Cracking	A21(1.38) A26(1.60) A46(1.60)
[120]	Sep/26/2000 20:42:28 UMST	Concrete Cracking	A15(1.33) A16(2.59) A43(4.03)
[121]	Sep/26/2000 20:42:29 UMST	Concrete Cracking	A07(1.80) A40(1.95) A38(3.44)
[122]	Sep/26/2000 20:42:33 UMST	Concrete Cracking	A01(1.43) A51(2.58) A02(2.91)
[123]	Sep/26/2000 20:42:51 UMST	Concrete Cracking	A20(1.35) A25(2.76) A21(3.23)
[124]	Sep/26/2000 20:42:53 UMST	Concrete Cracking	A24(1.08) A23(1.94) A45(2.61)
[125]	Sep/26/2000 20:42:57 UMST	Concrete Cracking	A30(0.54) A33(2.40) A31(2.64)
[126]	Sep/26/2000 20:43:00 UMST	Concrete Cracking	A18(0.78) A44(0.78) A14(3.15)
[127]	Sep/26/2000 20:43:21 UMST	Concrete Cracking	A06(0.83) A39(1.96) A41(2.06)
[128]	Sep/26/2000 20:43:30 UMST	Concrete Cracking	A43(0.34) A16(1.19) A17(1.86)
[129]	Sep/26/2000 20:43:38 UMST	Concrete Cracking	A13(1.37) A40(2.09) A12(2.13)
[130]	Sep/26/2000 20:44:11 UMST	Concrete Cracking	A39(2.32) A41(2.79) A07(2.81)
[131]	Sep/26/2000 20:59:54 UMST	Concrete Cracking	A33(1.65) A49(2.30) A30(2.85)
[132]	Sep/26/2000 21:18:38 UMST	Concrete Cracking	A21(0.95) A44(2.03) A18(2.03)
[133]	Sep/26/2000 21:18:52 UMST	Concrete Cracking	A26(0.94) A46(0.94) A47(2.04)
[134]	Sep/26/2000 21:18:59 UMST	Concrete Cracking	A25(2.00) A26(2.47) A46(2.47)
[135]	Sep/26/2000 21:19:06 UMST	Concrete Cracking	A01(1.53) A02(1.68) A51(3.62)

[136]	Sep/26/2000 21:19:06 UMST	Concrete Cracking	A32(0.16) A48(1.59) A34(2.22)
[137]	Sep/26/2000 21:19:12 UMST	Concrete Cracking	A21(1.26) A46(1.72) A26(1.72)
[138]	Sep/26/2000 21:19:17 UMST	Concrete Cracking	A21(1.00) A44(1.98) A18(1.98)
[139]	Sep/26/2000 21:19:18 UMST	Concrete Cracking	A24(2.98) A16(2.99) A20(3.05)
[140]	Sep/26/2000 21:19:22 UMST	Concrete Cracking	A25(1.46) A46(2.97) A26(2.97)
[141]	Sep/26/2000 21:19:38 UMST	Concrete Cracking	A43(0.56) A16(1.18) A17(1.97)
[142]	Sep/26/2000 21:19:42 UMST	Concrete Cracking	A09(0.09) A10(4.29) A05(5.16)
[143]	Sep/26/2000 21:19:50 UMST	Concrete Cracking	A20(2.13) A21(2.46) A25(3.14)
[144]	Sep/26/2000 21:19:52 UMST	Concrete Cracking	A06(1.14) A41(1.67) A39(1.67)
[145]	Sep/26/2000 21:19:57 UMST	Concrete Cracking	A24(0.68) A45(0.85) A25(2.37)
[146]	Sep/26/2000 21:20:47 UMST	Concrete Cracking	A23(2.31) A24(3.01) A29(3.94)
[147]	Sep/26/2000 21:20:51 UMST	Concrete Cracking	A21(1.38) A26(1.60) A46(1.60)
[148]	Sep/26/2000 21:21:07 UMST	Concrete Cracking	A24(2.98) A16(2.99) A20(3.05)
[149]	Sep/26/2000 21:21:15 UMST	Concrete Cracking	A12(1.50) A41(1.69) A39(2.30)
[150]	Sep/26/2000 21:21:24 UMST	Concrete Cracking	A21(0.54) A22(2.37) A44(2.44)
[151]	Sep/26/2000 21:21:29 UMST	Concrete Cracking	A40(1.56) A07(1.58) A12(3.02)
[152]	Sep/26/2000 21:21:32 UMST	Concrete Cracking	A18(0.80) A44(0.80) A21(2.18)
[153]	Sep/26/2000 21:21:51 UMST	Concrete Cracking	A16(0.26) A43(1.27) A17(2.79)
[154]	Sep/26/2000 21:21:55 UMST	Concrete Cracking	A23(2.61) A29(4.20) A28(4.74)
[155]	Sep/26/2000 21:22:00 UMST	Concrete Cracking	A43(0.28) A16(1.41) A17(1.68)
[156]	Sep/26/2000 21:22:05 UMST	Concrete Cracking	A24(0.30) A45(1.23) A25(2.75)
[157]	Sep/26/2000 21:22:07 UMST	Concrete Cracking	A43(0.48) A17(1.04) A16(2.01)
[158]	Sep/26/2000 21:22:08 UMST	Concrete Cracking	A43(0.01) A17(1.52) A16(1.52)
[159]	Sep/26/2000 21:22:11 UMST	Concrete Cracking	A24(0.06) A45(1.47) A25(2.99)
[160]	Sep/26/2000 21:22:19 UMST	Concrete Cracking	A18(0.72) A44(0.72) A21(2.26)
[161]	Sep/26/2000 21:22:25 UMST	Concrete Cracking	A29(2.43) A30(3.01) A33(3.37)
[162]	Sep/26/2000 21:22:38 UMST	Concrete Cracking	A42(1.73) A14(2.26) A44(2.81)
[163]	Sep/26/2000 21:22:46 UMST	Concrete Cracking	A00(1.01) A01(2.91) A36(3.22)
[164]	Sep/26/2000 21:22:52 UMST	Concrete Cracking	A16(0.08) A43(1.46) A17(2.98)
[165]	Sep/26/2000 21:22:55 UMST	Concrete Cracking	A20(0.32) A25(2.99) A17(3.01)
[166]	Sep/26/2000 21:23:06 UMST	Concrete Cracking	A24(0.86) A45(1.63) A25(3.03)
[167]	Sep/26/2000 21:23:08 UMST	Concrete Cracking	A01(1.45) A00(3.10) A51(3.14)
[168]	Sep/26/2000 21:23:27 UMST	Concrete Cracking	A29(0.73) A28(3.67) A33(4.20)
[169]	Sep/26/2000 21:23:32 UMST	Concrete Cracking	A24(0.27) A45(1.26) A25(2.78)
[170]	Sep/26/2000 21:23:36 UMST	Concrete Cracking	A21(1.12) A18(1.86) A44(1.86)
[171]	Sep/26/2000 21:23:43 UMST	Concrete Cracking	A31(0.65) A32(2.61) A34(2.64)
[172]	Sep/26/2000 21:24:34 UMST	Concrete Cracking	A16(0.29) A43(1.24) A17(2.76)
[173]	Sep/26/2000 21:45:39 UMST	Concrete Cracking	A01(0.81) A00(2.71) A02(3.52)
[174]	Sep/26/2000 21:45:40 UMST	Concrete Cracking	A31(1.43) A30(1.62) A33(3.59)
[175]	Sep/26/2000 21:45:54 UMST	Concrete Cracking	A11(1.11) A41(1.81) A06(2.20)
[176]	Sep/26/2000 21:45:55 UMST	Concrete Cracking	A44(0.17) A18(0.17) A21(3.15)
[177]	Sep/26/2000 21:45:59 UMST	Concrete Cracking	A29(2.31) A36(3.10) A28(3.59)
[178]	Sep/26/2000 21:46:00 UMST	Concrete Cracking	A36(1.51) A33(3.64) A49(4.03)
[179]	Sep/26/2000 21:46:17 UMST	Concrete Cracking	A01(1.54) A00(1.59) A36(4.08)
[180]	Sep/26/2000 21:47:11 UMST	Concrete Cracking	A00(0.87) A01(3.51) A05(5.41)
[181]	Sep/26/2000 21:47:56 UMST	Concrete Cracking	A30(1.14) A33(1.32) A29(3.56)

[182]	Sep/26/2000 21:48:15 UMST	Concrete Cracking	A46(0.47) A26(0.47) A21(2.51)
[183]	Sep/26/2000 21:48:21 UMST	Concrete Cracking	A00(1.87) A01(2.66) A36(2.72)
[184]	Sep/26/2000 21:48:24 UMST	Concrete Cracking	A33(0.71) A30(2.79) A29(2.85)
[185]	Sep/26/2000 21:48:32 UMST	Concrete Cracking	A47(0.61) A27(2.33) A32(2.37)
[186]	Sep/26/2000 21:48:59 UMST	Concrete Cracking	A00(0.59) A01(2.43) A02(5.48)
[187]	Sep/26/2000 21:49:03 UMST	Concrete Cracking	A24(1.35) A23(1.68) A45(2.88)
[188]	Sep/26/2000 21:49:06 UMST	Concrete Cracking	A15(1.28) A16(1.83) A43(3.34)
[189]	Sep/26/2000 21:49:33 UMST	Concrete Cracking	A01(2.56) A36(2.72) A00(3.05)
[190]	Sep/26/2000 21:49:34 UMST	Concrete Cracking	A15(1.33) A16(2.04) A43(3.51)
[191]	Sep/26/2000 21:49:52 UMST	Concrete Cracking	A02(0.71) A01(2.65) A03(4.91)
[192]	Sep/26/2000 21:50:20 UMST	Concrete Cracking	A02(1.69) A51(1.98) A01(2.11)
[193]	Sep/26/2000 21:50:32 UMST	Concrete Cracking	A33(2.10) A36(2.35) A49(3.74)
[194]	Sep/26/2000 21:51:07 UMST	Concrete Cracking	A21(0.39) A22(2.29) A26(2.60)
[195]	Sep/26/2000 21:52:40 UMST	Concrete Cracking	A00(1.34) A01(2.90) A36(2.94)
[196]	Sep/26/2000 21:53:16 UMST	Concrete Cracking	A03(0.34) A38(1.80) A04(2.17)
[197]	Sep/26/2000 21:53:27 UMST	Concrete Cracking	A33(0.40) A30(2.48) A29(3.08)
[198]	Sep/26/2000 22:16:26 UMST	Concrete Cracking	A45(0.58) A25(1.57) A24(1.69)
[199]	Sep/26/2000 22:17:08 UMST	Concrete Cracking	A01(1.03) A00(2.33) A02(3.90)
[200]	Sep/26/2000 22:17:15 UMST	Concrete Cracking	A33(0.55) A30(2.07) A29(3.09)
[201]	Sep/26/2000 22:17:38 UMST	Concrete Cracking	A33(1.36) A29(2.14) A30(3.06)
[202]	Sep/26/2000 22:17:49 UMST	Concrete Cracking	A24(0.74) A45(0.79) A25(2.31)
[203]	Sep/26/2000 22:18:01 UMST	Concrete Cracking	A31(1.71) A47(2.74) A32(2.88)
[204]	Sep/26/2000 22:18:21 UMST	Concrete Cracking	A30(0.83) A33(1.95) A31(2.96)
[205]	Sep/26/2000 22:18:36 UMST	Concrete Cracking	A00(1.46) A01(1.61) A36(4.16)
[206]	Sep/26/2000 22:19:09 UMST	Concrete Cracking	A20(1.50) A21(2.94) A17(3.27)
[207]	Sep/26/2000 22:19:27 UMST	Concrete Cracking	A23(0.89) A24(3.15) A45(4.63)
[208]	Sep/26/2000 22:20:24 UMST	Concrete Cracking	A29(0.46) A28(3.84) A33(3.88)
[209]	Sep/26/2000 22:20:29 UMST	Concrete Cracking	A17(0.88) A43(2.37) A20(3.36)
[210]	Sep/26/2000 22:21:12 UMST	Concrete Cracking	A01(1.56) A02(1.86) A00(4.44)
[211]	Sep/26/2000 22:21:57 UMST	Concrete Cracking	A21(1.45) A26(1.53) A46(1.53)
[212]	Sep/26/2000 22:25:01 UMST	Concrete Cracking	A33(0.69) A30(1.67) A29(3.43)
[213]	Sep/26/2000 22:25:09 UMST	Concrete Cracking	A33(0.74) A30(1.58) A29(3.55)
[214]	Sep/26/2000 22:33:24 UMST	Concrete Cracking	A46(1.31) A26(1.31) A47(1.68)
[215]	Sep/26/2000 22:43:32 UMST	Concrete Cracking	A19(4.53) A09(5.63) A15(7.75)
[216]	Sep/27/2000 03:05:13 UMST	Concrete Cracking	A20(1.79) A43(2.07) A16(2.56)
[217]	Sep/27/2000 07:09:31 UMST	Concrete Cracking	A04(0.80) A03(1.50) A38(1.93)
[218]	Sep/27/2000 07:22:25 UMST	Concrete Cracking	A34(0.73) A48(1.08) A32(2.36)
[219]	Sep/27/2000 07:56:41 UMST	Concrete Cracking	A31(2.18) A47(2.77) A32(3.42)
[220]	Sep/27/2000 07:59:36 UMST	Concrete Cracking	A41(1.38) A11(1.70) A12(1.90)
[221]	Sep/27/2000 08:00:09 UMST	Concrete Cracking	A10(1.05) A05(2.11) A06(3.07)
[222]	Sep/27/2000 12:05:41 UMST	Concrete Cracking	A32(0.25) A48(1.68) A34(2.27)
[223]	Sep/27/2000 12:22:49 UMST	Concrete Cracking	A03(1.05) A04(1.20) A53(3.18)
[224]	Sep/27/2000 13:01:32 UMST	Concrete Cracking	A32(1.03) A34(1.49) A48(1.56)
[225]	Sep/27/2000 13:01:32 UMST	Concrete Cracking	A32(1.16) A34(1.46) A48(1.63)
[226]	Sep/27/2000 13:01:56 UMST	Concrete Cracking	A11(1.73) A12(2.39) A41(3.68)

[227]	Sep/27/2000 13:04:28 UMST	Concrete Cracking	A28(2.03) A29(5.65) A23(6.86)
[228]	Sep/27/2000 13:04:29 UMST	Concrete Cracking	A28(2.78) A29(6.15) A23(6.67)
[229]	Sep/27/2000 13:05:35 UMST	Concrete Cracking	A28(2.84) A29(3.89) A23(4.56)
[230]	Sep/27/2000 13:20:04 UMST	Concrete Cracking	A38(1.41) A04(2.34) A03(2.46)
[231]	Sep/27/2000 13:21:07 UMST	Concrete Cracking	A38(2.93) A08(2.96) A04(3.21)
[232]	Sep/27/2000 13:37:28 UMST	Concrete Cracking	A11(1.04) A12(3.10) A41(3.53)
[233]	Sep/27/2000 13:38:01 UMST	Concrete Cracking	A11(1.43) A12(2.82) A41(3.70)
[234]	Sep/27/2000 13:38:03 UMST	Concrete Cracking	A10(2.39) A11(2.77) A06(4.11)
[235]	Sep/27/2000 13:51:37 UMST	Concrete Cracking	A46(0.43) A26(0.43) A21(2.58)
[236]	Sep/27/2000 14:15:21 UMST	Concrete Cracking	A35(0.86) A37(2.46) A48(2.51)
[237]	Sep/27/2000 14:18:42 UMST	Concrete Cracking	A11(0.58) A12(3.11) A41(3.15)
[238]	Sep/27/2000 14:36:18 UMST	Concrete Cracking	A04(1.13) A38(1.64) A03(1.76)
[239]	Sep/27/2000 14:44:02 UMST	Concrete Cracking	A11(1.79) A12(3.54) A43(4.17)

SANDIA PCCV

ALBUQUERQUE, NM

SOUNDPRINT® ACOUSTIC MONITORING PROGRAM

REPORT

REPORTING PERIOD: SEPTEMBER 27 TO SEPTEMBER 27, 2000

DISCLAIMER

The information provided in this report is not intended to constitute an engineering report and should not be construed as such. The client is advised to retain qualified engineering expertise to interpret the data contained in this report. The information contained in this report is provided "as is" without warranty of any kind, either express or implied. Pure Technologies Ltd. is not liable for any lost profits, lost savings or other incidental, special or consequential damage arising out of the use of the monitoring system or the information contained in this report. Please refer to the terms and conditions attached to Pure's SoundPrint® System Purchase Agreement and Pure's Technical Support Agreement for further details.

TABLE OF CONTENTS

1.0 EXECUTIVE SUMMARY

The following is a summary of relevant activity recorded by the SoundPrint® monitoring system. The summary includes information for both the latest monitoring period and for the entire monitoring period from the start-up date up to and including the most recent monitoring period.

	Period 09/27/2000– 09/27/2000
Operating Efficiency	100.0%
Concrete Crushing	10

Comments

Recommendations

There are no new recommendations at this time.

Prepared by:

Peter Paulson
President & CEO

REPORT PRESENTATION

A computerized drawing of the slab with the sensor layout is included on the following page and contains the following symbols:


ECZ1A14

Sensor Symbol with individual sensor name beneath


[1]

Symbolizes an event location. Event details are listed on the page following the drawing.

A list describing event details is provided for each drawing and lists the event number, shown on the computerized drawing, followed by the date, time, event classification and coordinates (in meters) to the origin of the events using the three closes sensors.

Event Report For Sandia PCCV

Albuquerque, NM

System Uptime 0.1 Days (100.0%)

Concrete Crushing

Period: 09/27/2000 to **09/27/2000**

Matched Events: 10

PCCV NEW -- 10 EVENTS

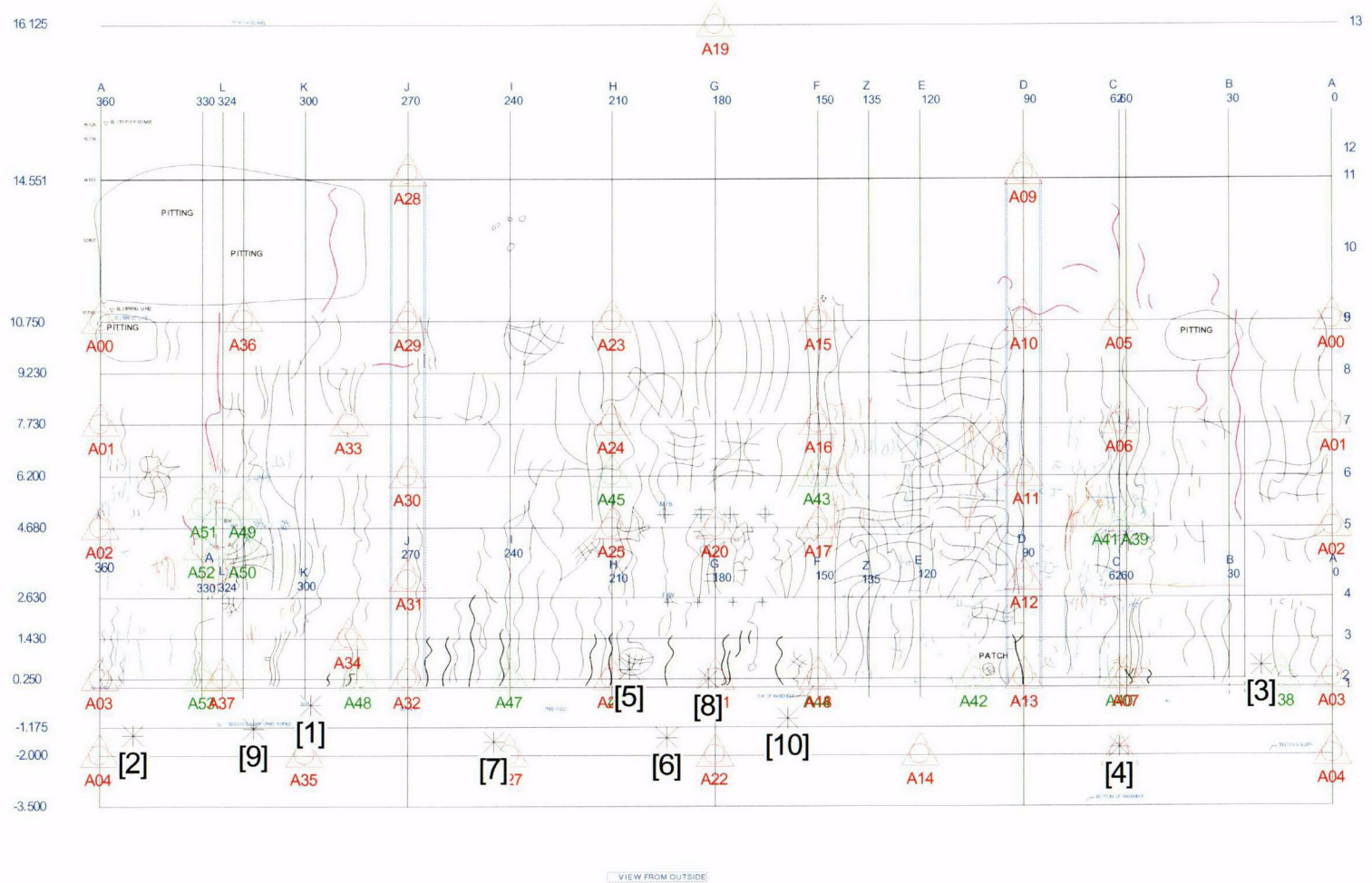

Scale: 1.95 m / cm

0 2m 20m

C136

Events

No.	Date/Time	Classification	Location (m)
[1]	Sep/27/2000 12:49:41 UMST	Crushing Concrete	A35(1.50) A48(1.58) A34(2.23)
[2]	Sep/27/2000 13:34:56 UMST	Crushing Concrete	A04(1.15) A03(1.92) A53(2.61)
[3]	Sep/27/2000 13:35:58 UMST	Crushing Concrete	A38(0.70) A03(2.09) A04(3.33)
[4]	Sep/27/2000 13:37:46 UMST	Crushing Concrete	A08(0.23) A40(2.02) A07(2.03)
[5]	Sep/27/2000 13:43:18 UMST	Crushing Concrete	A26(0.57) A46(0.57) A21(2.50)
[6]	Sep/27/2000 13:49:57 UMST	Crushing Concrete	A22(1.50) A21(2.24) A46(2.34)
[7]	Sep/27/2000 13:50:01 UMST	Crushing Concrete	A27(0.62) A47(1.90) A32(3.12)
[8]	Sep/27/2000 14:05:10 UMST	Crushing Concrete	A21(0.21) A22(2.26) A26(2.78)
[9]	Sep/27/2000 14:15:22 UMST	Crushing Concrete	A35(1.67) A37(1.72) A53(2.09)
[10]	Sep/27/2000 14:24:44 UMST	Crushing Concrete	A44(1.46) A18(1.46) A22(2.38)

SANDIA PCCV

ALBUQUERQUE, NM

SOUNDPRINT® ACOUSTIC MONITORING PROGRAM

REPORT

REPORTING PERIOD: SEPTEMBER 26 TO SEPTEMBER 27, 2000

TABLE OF CONTENTS

1.0 EXECUTIVE SUMMARY

The following is a summary of relevant activity recorded by the SoundPrint® monitoring system. The summary includes information for both the latest monitoring period and for the entire monitoring period from the start-up date up to and including the most recent monitoring period.

	Period 09/26/2000– 09/27/2000
Operating Efficiency	100.0%
Tendon Pings	136

Comments

Recommendations

There are no new recommendations at this time.

Prepared by:

Peter Paulson
President & CEO

REPORT PRESENTATION

A computerized drawing of the slab with the sensor layout is included on the following page and contains the following symbols:


ECZ1A14

Sensor Symbol with individual sensor name beneath


[1]

Symbolizes an event location. Event details are listed on the page following the drawing.

A list describing event details is provided for each drawing and lists the event number, shown on the computerized drawing, followed by the date, time, event classification and co-ordinates (in meters) to the origin of the events using the three closes sensors.

Event Report For Sandia PCCV

Albuquerque, NM

System Uptime 1.9 Days (100.0%)

Tendon Pings

Period: 09/26/2000 to **09/27/2000**

Matched Events: 136

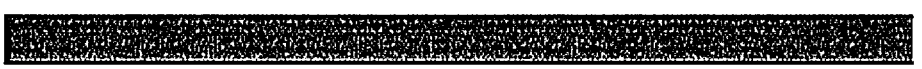

9/26/2000 9/28/2000

PCCV NEW -- 136 EVENTS

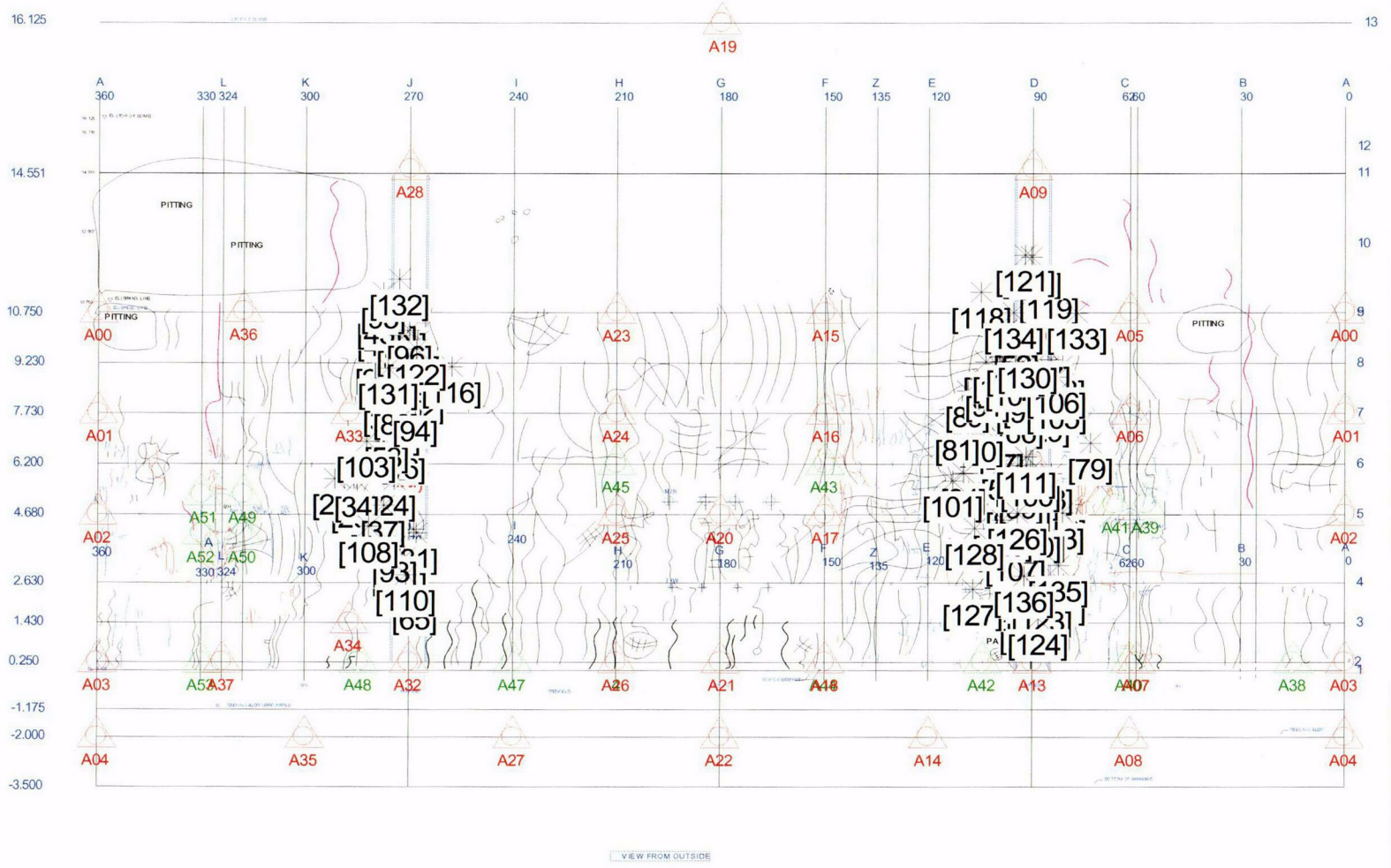

Scale: 1.95 m / cm

0 2m 20m

C137

Events

No.	Date/Time	Classification	Location (m)
[1]	Sep/26/2000 20:43:28 UMST	Tendon Ping	A12(1.58) A11(2.00) A41(3.30)
[2]	Sep/26/2000 20:43:36 UMST	Tendon Ping	A41(1.20) A11(1.66) A39(2.11)
[3]	Sep/26/2000 20:43:40 UMST	Tendon Ping	A30(1.63) A31(1.64) A33(3.24)
[4]	Sep/26/2000 20:43:42 UMST	Tendon Ping	A30(1.34) A31(1.88) A33(3.02)
[5]	Sep/26/2000 20:44:18 UMST	Tendon Ping	A11(1.41) A12(1.70) A41(2.64)
[6]	Sep/26/2000 20:44:37 UMST	Tendon Ping	A11(1.28) A12(1.79) A41(2.15)
[7]	Sep/26/2000 20:45:16 UMST	Tendon Ping	A11(1.55) A41(1.56) A12(1.87)
[8]	Sep/26/2000 21:26:04 UMST	Tendon Ping	A33(1.26) A30(1.26) A29(3.44)
[9]	Sep/26/2000 21:26:07 UMST	Tendon Ping	A33(1.26) A30(2.13) A29(2.56)
[10]	Sep/26/2000 21:28:00 UMST	Tendon Ping	A11(0.73) A41(2.24) A12(2.34)
[11]	Sep/26/2000 21:28:36 UMST	Tendon Ping	A29(1.49) A33(2.00) A30(3.26)
[12]	Sep/26/2000 21:28:39 UMST	Tendon Ping	A29(1.72) A33(2.09) A30(2.83)
[13]	Sep/26/2000 21:51:11 UMST	Tendon Ping	A29(0.82) A33(3.26) A36(3.96)
[14]	Sep/26/2000 21:51:14 UMST	Tendon Ping	A29(0.53) A33(3.01) A30(4.02)
[15]	Sep/26/2000 21:51:59 UMST	Tendon Ping	A30(0.59) A33(2.30) A31(2.69)
[16]	Sep/26/2000 21:52:10 UMST	Tendon Ping	A30(0.65) A33(1.80) A31(3.68)
[17]	Sep/26/2000 21:52:18 UMST	Tendon Ping	A33(1.86) A29(1.92) A30(2.65)
[18]	Sep/26/2000 21:52:20 UMST	Tendon Ping	A31(0.51) A34(2.42) A30(2.77)
[19]	Sep/26/2000 21:52:41 UMST	Tendon Ping	A29(0.23) A33(3.26) A30(4.40)
[20]	Sep/26/2000 21:52:43 UMST	Tendon Ping	A29(1.47) A33(2.01) A30(3.43)
[21]	Sep/26/2000 21:52:43 UMST	Tendon Ping	A10(1.58) A11(3.02) A06(3.44)
[22]	Sep/26/2000 21:52:46 UMST	Tendon Ping	A29(1.54) A33(1.96) A30(3.44)
[23]	Sep/26/2000 21:52:53 UMST	Tendon Ping	A29(0.43) A33(3.33) A28(4.27)
[24]	Sep/26/2000 21:53:08 UMST	Tendon Ping	A30(0.65) A33(2.39) A31(2.59)
[25]	Sep/26/2000 21:53:11 UMST	Tendon Ping	A30(1.79) A33(2.38) A31(2.71)
[26]	Sep/26/2000 21:53:11 UMST	Tendon Ping	A33(2.03) A30(2.18) A49(2.68)
[27]	Sep/26/2000 21:53:28 UMST	Tendon Ping	A31(1.71) A30(1.98) A34(3.16)
[28]	Sep/26/2000 21:53:30 UMST	Tendon Ping	A11(0.61) A41(2.02) A12(2.81)
[29]	Sep/26/2000 21:53:39 UMST	Tendon Ping	A11(1.81) A06(2.37) A10(2.82)
[30]	Sep/26/2000 21:54:16 UMST	Tendon Ping	A31(1.09) A30(1.97) A34(3.36)
[31]	Sep/26/2000 21:54:18 UMST	Tendon Ping	A31(0.99) A30(2.09) A34(3.30)
[32]	Sep/26/2000 21:55:21 UMST	Tendon Ping	A33(1.15) A30(2.16) A29(2.59)
[33]	Sep/26/2000 21:55:36 UMST	Tendon Ping	A41(1.49) A11(1.71) A12(1.80)
[34]	Sep/26/2000 22:22:46 UMST	Tendon Ping	A30(1.59) A33(2.06) A31(2.94)
[35]	Sep/26/2000 22:23:22 UMST	Tendon Ping	A12(0.53) A13(2.47) A42(2.71)
[36]	Sep/26/2000 22:23:36 UMST	Tendon Ping	A29(1.25) A33(2.59) A30(3.32)
[37]	Sep/26/2000 22:23:36 UMST	Tendon Ping	A30(1.45) A31(1.94) A33(2.95)
[38]	Sep/26/2000 22:23:38 UMST	Tendon Ping	A29(1.02) A33(2.47) A30(3.62)
[39]	Sep/26/2000 22:23:42 UMST	Tendon Ping	A12(1.18) A11(2.00) A41(2.86)
[40]	Sep/26/2000 22:23:49 UMST	Tendon Ping	A12(1.40) A11(2.20) A41(3.34)
[41]	Sep/26/2000 22:23:50 UMST	Tendon Ping	A33(1.40) A30(1.53) A29(3.07)
[42]	Sep/26/2000 22:24:08 UMST	Tendon Ping	A29(0.89) A33(2.92) A36(3.92)
[43]	Sep/26/2000 22:24:09 UMST	Tendon Ping	A10(1.50) A05(2.66) A06(2.78)

[44]	Sep/26/2000 22:24:10 UMST	Tendon Ping	A10(1.68) A06(2.73) A05(2.86)
[45]	Sep/26/2000 22:24:12 UMST	Tendon Ping	A29(0.88) A33(3.26) A36(3.90)
[46]	Sep/26/2000 22:24:28 UMST	Tendon Ping	A10(2.45) A11(2.92) A06(4.32)
[47]	Sep/26/2000 22:24:29 UMST	Tendon Ping	A11(1.17) A06(3.74) A41(3.77)
[48]	Sep/26/2000 22:24:42 UMST	Tendon Ping	A11(1.04) A12(2.02) A41(2.21)
[49]	Sep/26/2000 22:24:42 UMST	Tendon Ping	A11(1.30) A12(2.04) A41(3.00)
[50]	Sep/26/2000 22:24:58 UMST	Tendon Ping	A33(1.56) A30(1.76) A29(2.80)
[51]	Sep/26/2000 22:24:59 UMST	Tendon Ping	A33(1.64) A29(2.25) A30(2.33)
[52]	Sep/26/2000 22:25:02 UMST	Tendon Ping	A10(0.94) A05(3.36) A11(3.77)
[53]	Sep/26/2000 22:25:03 UMST	Tendon Ping	A30(1.16) A33(1.21) A29(3.64)
[54]	Sep/26/2000 22:25:06 UMST	Tendon Ping	A12(1.38) A11(1.67) A41(2.33)
[55]	Sep/26/2000 22:25:08 UMST	Tendon Ping	A12(1.48) A11(1.58) A41(2.50)
[56]	Sep/26/2000 22:25:08 UMST	Tendon Ping	A12(1.34) A11(1.72) A41(2.30)
[57]	Sep/26/2000 22:25:11 UMST	Tendon Ping	A10(1.61) A11(3.35) A05(3.92)
[58]	Sep/26/2000 22:25:44 UMST	Tendon Ping	A11(0.83) A12(3.16) A41(3.38)
[59]	Sep/26/2000 22:26:01 UMST	Tendon Ping	A12(1.38) A11(1.73) A41(2.07)
[60]	Sep/26/2000 22:26:08 UMST	Tendon Ping	A12(1.35) A11(1.73) A41(2.19)
[61]	Sep/26/2000 22:26:34 UMST	Tendon Ping	A29(0.89) A33(2.91) A30(3.70)
[62]	Sep/26/2000 22:27:04 UMST	Tendon Ping	A11(0.42) A41(2.98) A12(3.03)
[63]	Sep/26/2000 22:30:11 UMST	Tendon Ping	A12(1.23) A13(1.70) A42(2.34)
[64]	Sep/26/2000 22:30:12 UMST	Tendon Ping	A12(1.32) A13(1.74) A42(2.54)
[65]	Sep/27/2000 07:57:00 UMST	Tendon Ping	A31(0.86) A32(2.07) A34(2.08)
[66]	Sep/27/2000 07:57:06 UMST	Tendon Ping	A11(1.74) A10(2.86) A06(3.12)
[67]	Sep/27/2000 07:57:22 UMST	Tendon Ping	A11(1.15) A12(1.97) A41(2.64)
[68]	Sep/27/2000 07:57:23 UMST	Tendon Ping	A11(0.99) A12(2.11) A41(2.57)
[69]	Sep/27/2000 07:57:33 UMST	Tendon Ping	A12(1.34) A11(1.95) A41(3.00)
[70]	Sep/27/2000 07:57:45 UMST	Tendon Ping	A11(0.46) A41(2.34) A12(2.61)
[71]	Sep/27/2000 07:57:49 UMST	Tendon Ping	A12(0.12) A13(2.81) A41(3.08)
[72]	Sep/27/2000 07:57:54 UMST	Tendon Ping	A10(2.00) A11(3.35) A05(4.38)
[73]	Sep/27/2000 07:57:55 UMST	Tendon Ping	A10(2.26) A11(2.37) A06(3.30)
[74]	Sep/27/2000 07:57:56 UMST	Tendon Ping	A10(1.47) A11(3.08) A05(3.24)
[75]	Sep/27/2000 07:57:58 UMST	Tendon Ping	A12(1.06) A11(2.29) A41(3.12)
[76]	Sep/27/2000 07:58:02 UMST	Tendon Ping	A12(0.94) A11(2.60) A41(3.33)
[77]	Sep/27/2000 07:58:03 UMST	Tendon Ping	A12(1.05) A13(2.52) A41(2.78)
[78]	Sep/27/2000 07:58:12 UMST	Tendon Ping	A10(1.78) A06(2.42) A05(2.48)
[79]	Sep/27/2000 07:58:16 UMST	Tendon Ping	A06(1.44) A11(1.78) A41(1.97)
[80]	Sep/27/2000 07:58:18 UMST	Tendon Ping	A11(1.87) A10(3.70) A06(4.27)
[81]	Sep/27/2000 07:58:18 UMST	Tendon Ping	A11(2.46) A16(3.83) A10(3.98)
[82]	Sep/27/2000 07:58:19 UMST	Tendon Ping	A29(2.14) A33(2.27) A30(2.46)
[83]	Sep/27/2000 07:58:20 UMST	Tendon Ping	A11(0.78) A12(2.27) A41(2.46)
[84]	Sep/27/2000 07:58:21 UMST	Tendon Ping	A11(1.99) A12(3.40) A43(4.00)
[85]	Sep/27/2000 07:58:22 UMST	Tendon Ping	A11(1.20) A12(2.17) A41(3.01)
[86]	Sep/27/2000 07:58:23 UMST	Tendon Ping	A29(0.76) A33(2.72) A30(3.87)
[87]	Sep/27/2000 07:58:30 UMST	Tendon Ping	A11(2.19) A10(2.42) A06(3.24)
[88]	Sep/27/2000 07:58:31 UMST	Tendon Ping	A33(1.39) A30(2.00) A29(2.62)
[89]	Sep/27/2000 07:58:33 UMST	Tendon Ping	A11(2.88) A10(2.99) A16(4.16)

[90]	Sep/27/2000 07:58:34 UMST	Tendon Ping	A10(2.23) A11(2.34) A06(3.08)
[91]	Sep/27/2000 07:58:34 UMST	Tendon Ping	A10(2.41) A11(2.82) A06(4.19)
[92]	Sep/27/2000 07:58:35 UMST	Tendon Ping	A31(0.26) A34(2.51) A30(2.82)
[93]	Sep/27/2000 07:58:36 UMST	Tendon Ping	A31(0.70) A30(2.51) A34(2.64)
[94]	Sep/27/2000 07:58:37 UMST	Tendon Ping	A30(1.77) A33(1.89) A29(2.79)
[95]	Sep/27/2000 07:58:37 UMST	Tendon Ping	A29(0.96) A33(3.74) A28(3.77)
[96]	Sep/27/2000 07:58:38 UMST	Tendon Ping	A29(0.54) A33(3.01) A30(4.01)
[97]	Sep/27/2000 07:58:39 UMST	Tendon Ping	A10(1.24) A05(2.62) A06(3.00)
[98]	Sep/27/2000 07:58:40 UMST	Tendon Ping	A10(1.87) A11(3.08) A06(3.99)
[99]	Sep/27/2000 07:58:41 UMST	Tendon Ping	A11(0.64) A12(2.52) A41(2.72)
[100]	Sep/27/2000 07:58:43 UMST	Tendon Ping	A11(0.19) A41(2.59) A12(2.86)
[101]	Sep/27/2000 07:58:53 UMST	Tendon Ping	A11(2.34) A12(3.42) A43(3.72)
[102]	Sep/27/2000 07:58:55 UMST	Tendon Ping	A10(1.71) A11(3.20) A05(3.94)
[103]	Sep/27/2000 07:58:55 UMST	Tendon Ping	A33(0.99) A30(1.40) A49(3.89)
[104]	Sep/27/2000 07:58:57 UMST	Tendon Ping	A10(1.78) A11(2.89) A06(3.54)
[105]	Sep/27/2000 07:58:59 UMST	Tendon Ping	A06(2.19) A11(2.26) A10(2.49)
[106]	Sep/27/2000 07:59:00 UMST	Tendon Ping	A10(2.05) A06(2.37) A11(2.70)
[107]	Sep/27/2000 07:59:01 UMST	Tendon Ping	A12(0.78) A11(2.47) A41(3.05)
[108]	Sep/27/2000 07:59:02 UMST	Tendon Ping	A31(1.64) A30(2.21) A34(2.94)
[109]	Sep/27/2000 07:59:03 UMST	Tendon Ping	A29(1.63) A33(2.16) A30(2.92)
[110]	Sep/27/2000 08:00:05 UMST	Tendon Ping	A31(0.30) A34(2.17) A32(2.62)
[111]	Sep/27/2000 08:00:20 UMST	Tendon Ping	A11(0.29) A41(2.89) A06(3.24)
[112]	Sep/27/2000 08:00:47 UMST	Tendon Ping	A12(1.12) A13(1.81) A42(2.43)
[113]	Sep/27/2000 08:00:48 UMST	Tendon Ping	A12(1.43) A13(1.48) A42(2.01)
[114]	Sep/27/2000 08:01:26 UMST	Tendon Ping	A12(1.28) A13(1.63) A42(2.26)
[115]	Sep/27/2000 08:01:28 UMST	Tendon Ping	A12(1.32) A13(1.63) A42(2.34)
[116]	Sep/27/2000 08:01:38 UMST	Tendon Ping	A29(2.03) A30(3.16) A33(3.24)
[117]	Sep/27/2000 08:01:53 UMST	Tendon Ping	A12(0.69) A13(2.33) A42(2.91)
[118]	Sep/27/2000 08:02:46 UMST	Tendon Ping	A10(1.60) A09(3.96) A05(4.31)
[119]	Sep/27/2000 08:02:53 UMST	Tendon Ping	A10(1.02) A05(2.49) A09(3.42)
[120]	Sep/27/2000 08:04:32 UMST	Tendon Ping	A10(1.67) A09(2.63) A05(3.27)
[121]	Sep/27/2000 08:18:33 UMST	Tendon Ping	A10(1.74) A09(2.58) A05(3.46)
[122]	Sep/27/2000 12:39:29 UMST	Tendon Ping	A29(1.12) A33(2.71) A30(3.45)
[123]	Sep/27/2000 12:43:06 UMST	Tendon Ping	A12(0.95) A13(2.01) A42(2.63)
[124]	Sep/27/2000 12:43:37 UMST	Tendon Ping	A13(1.32) A12(1.60) A42(2.07)
[125]	Sep/27/2000 13:00:14 UMST	Tendon Ping	A12(1.61) A11(1.89) A41(3.21)
[126]	Sep/27/2000 13:00:17 UMST	Tendon Ping	A11(1.54) A12(1.63) A41(2.76)
[127]	Sep/27/2000 13:04:22 UMST	Tendon Ping	A12(1.84) A42(2.21) A13(2.77)
[128]	Sep/27/2000 13:17:59 UMST	Tendon Ping	A12(1.99) A11(2.54) A42(4.02)
[129]	Sep/27/2000 13:58:55 UMST	Tendon Ping	A10(1.35) A11(3.32) A05(3.50)
[130]	Sep/27/2000 13:58:56 UMST	Tendon Ping	A10(1.19) A05(3.15) A11(3.37)
[131]	Sep/27/2000 14:16:51 UMST	Tendon Ping	A33(1.74) A29(1.79) A30(2.94)
[132]	Sep/27/2000 14:18:45 UMST	Tendon Ping	A29(1.04) A28(3.32) A33(4.26)
[133]	Sep/27/2000 14:19:08 UMST	Tendon Ping	A10(1.26) A05(1.52) A06(3.38)
[134]	Sep/27/2000 14:19:09 UMST	Tendon Ping	A10(0.54) A05(3.33) A09(4.33)

[135]	Sep/27/2000 14:45:59 UMST	Tendon Ping	A12(0.75) A41(2.42) A13(3.00)
[136]	Sep/27/2000 14:46:00 UMST	Tendon Ping	A12(0.39) A13(2.59) A42(2.85)

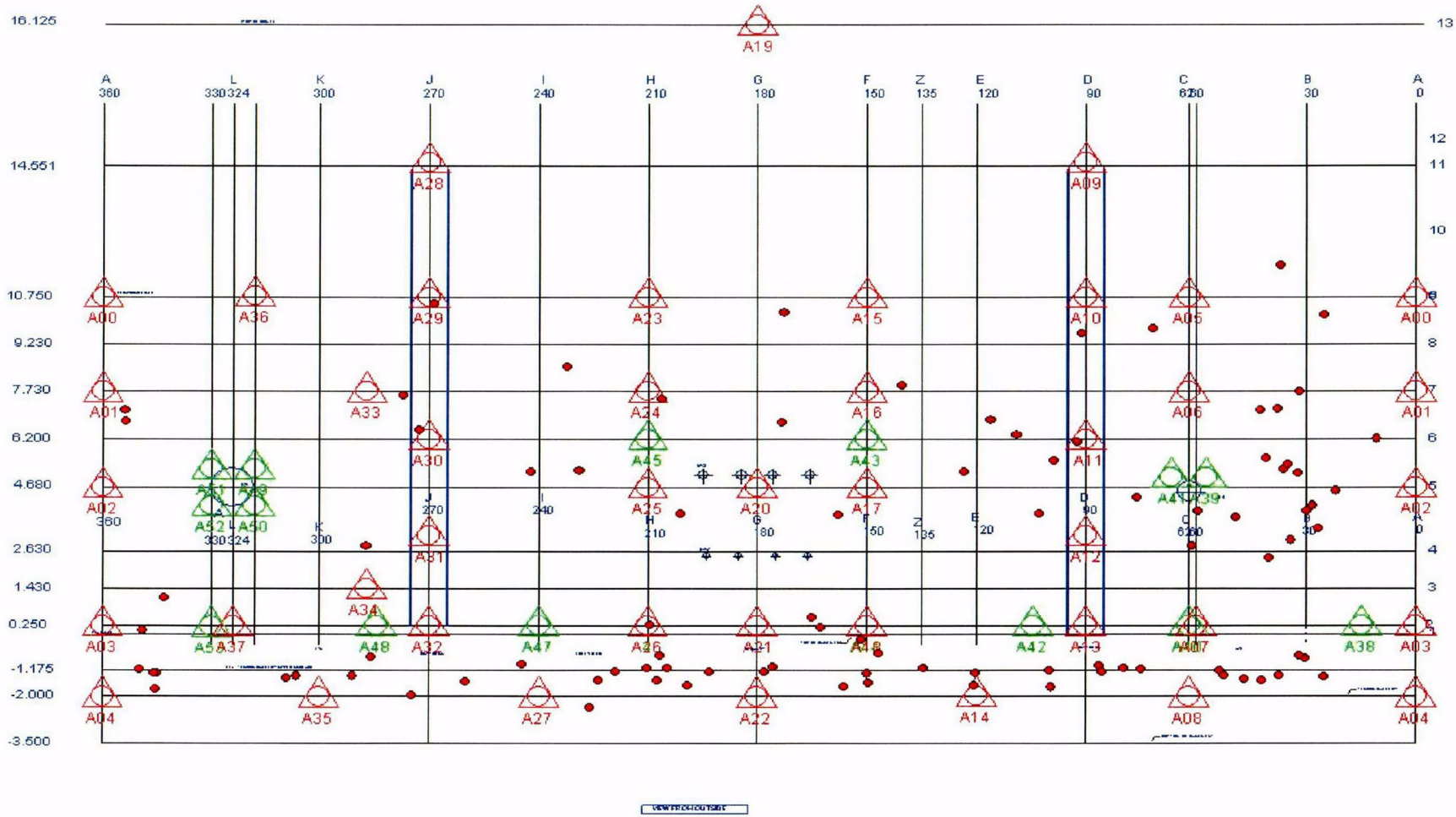

All 92 wire breaks before failure during test Nov. 14, 2001
(Many contain multiple wire failures at one location)

C138

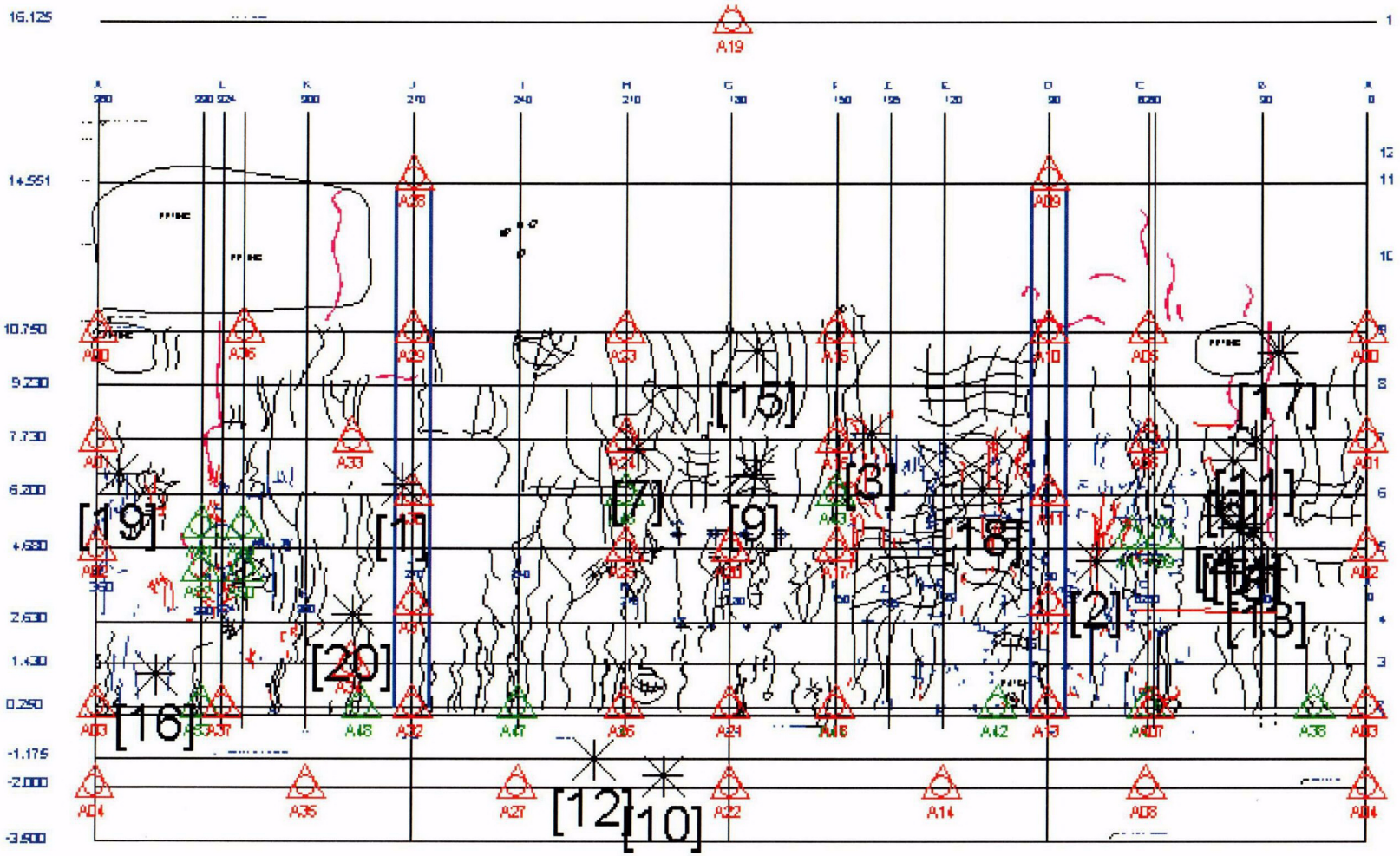

Wire breaks during the period of 10:45 AM to 10:47 AM
End at 10:46:12 (197 psi to 200 psi)

K-76

C138A

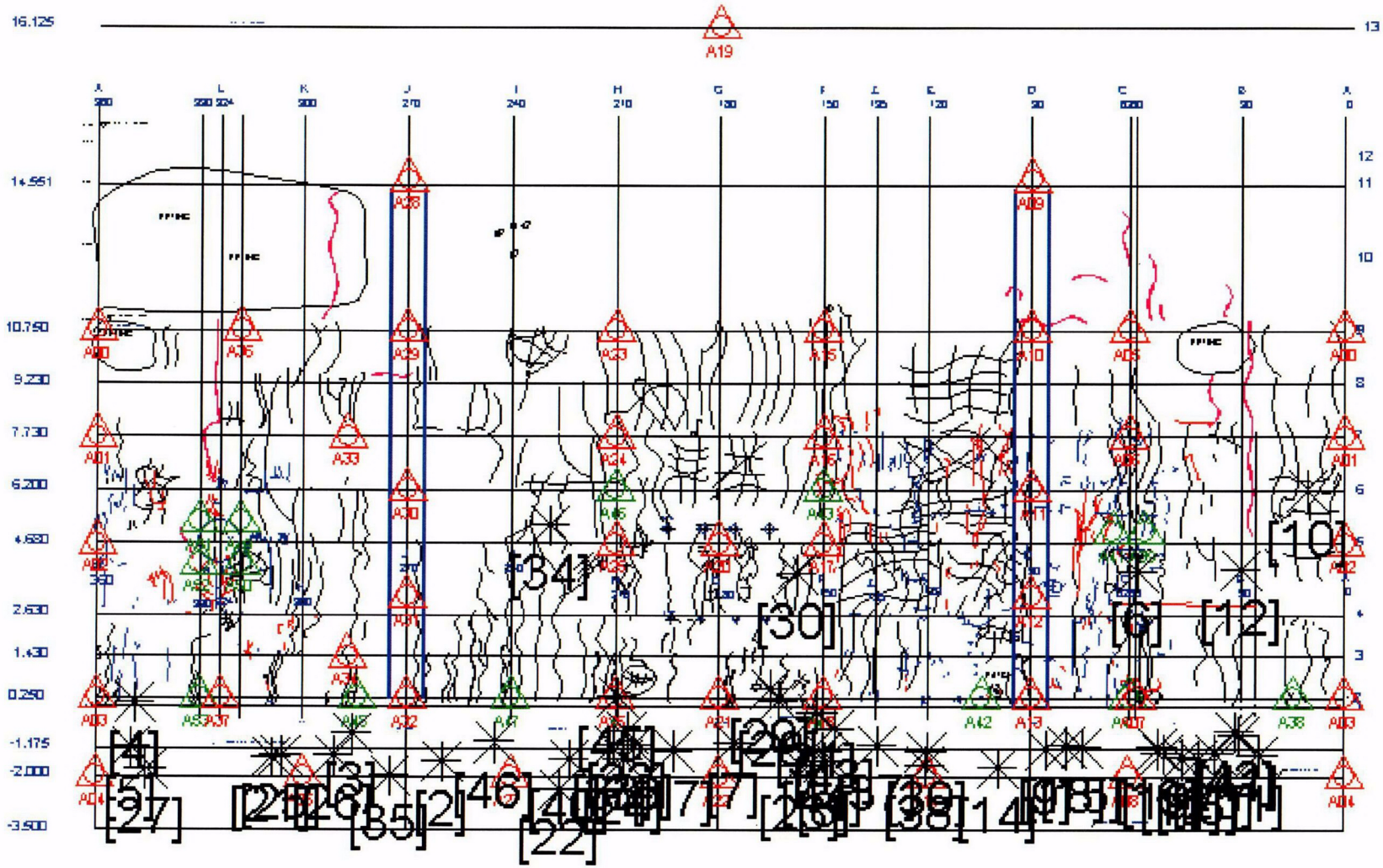

Wire breaks during the minute of 10:44 AM to 10:45 AM
193 psi to 193 psi

K-77

C139

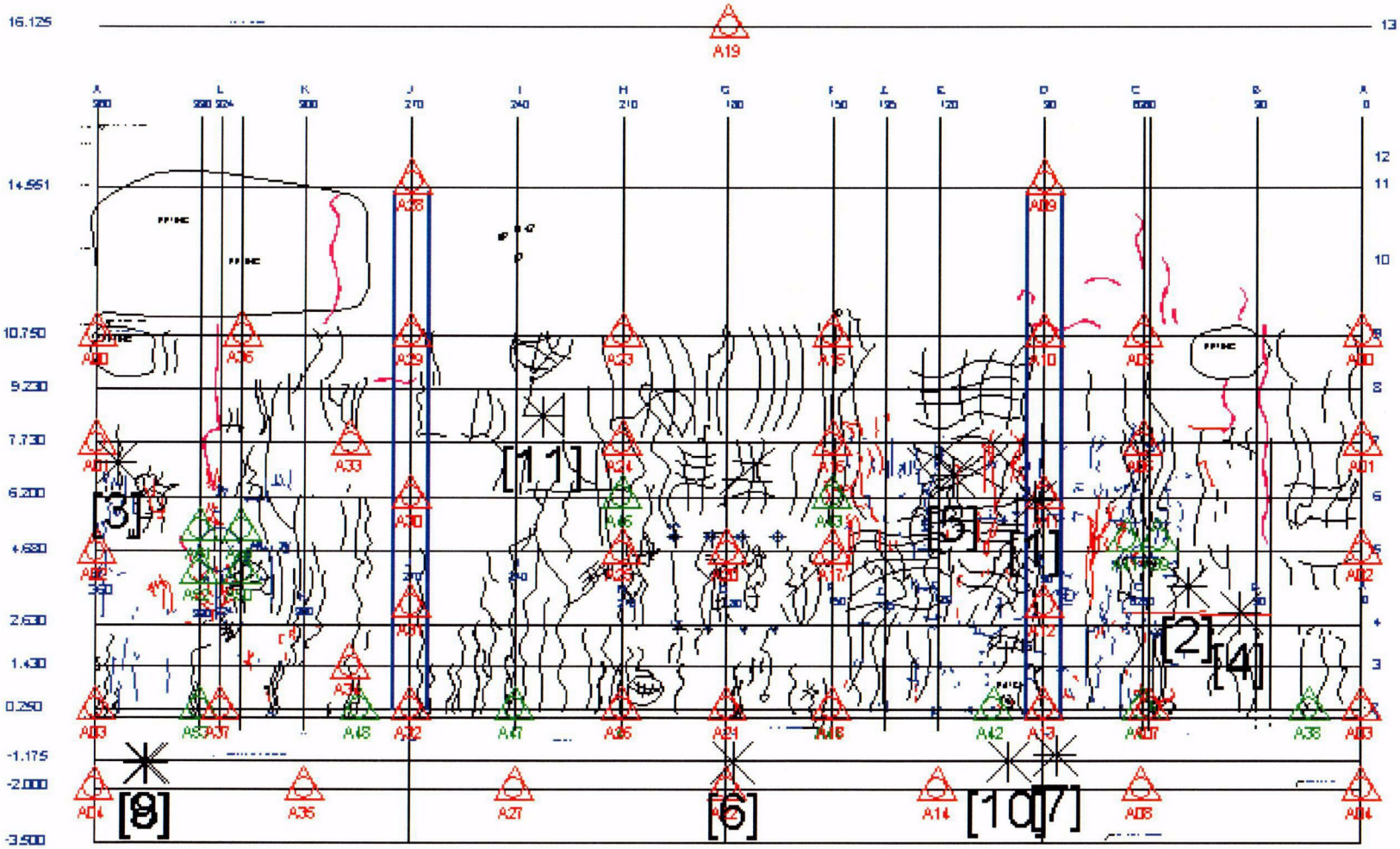

Wire breaks during the minute of 10:43 AM to 10:44 AM
192 PSI to 193 PSI

C140

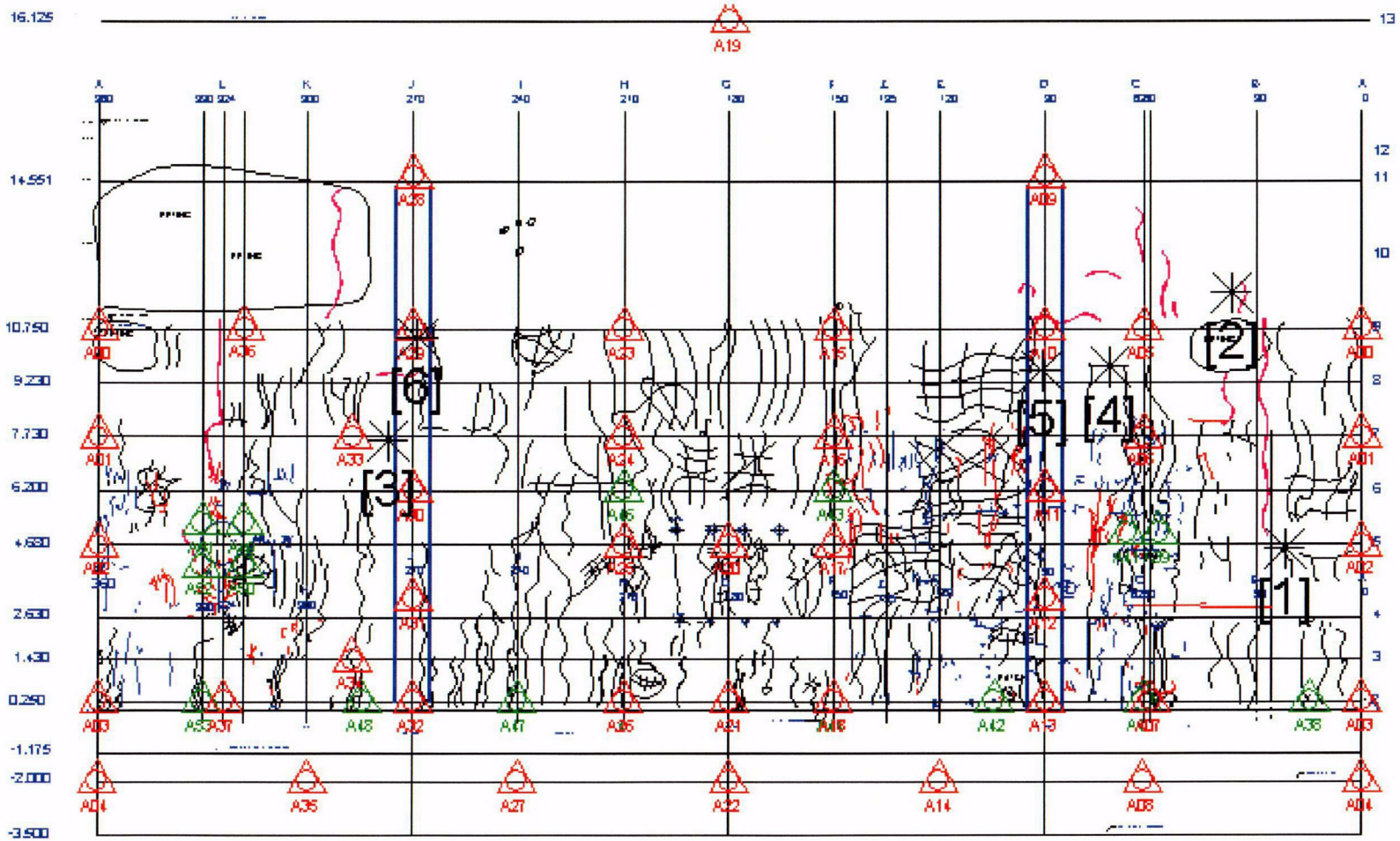

Wire breaks during the minute of 10:42 AM to 10:43 AM
188 PSI to 192 PSI

C141

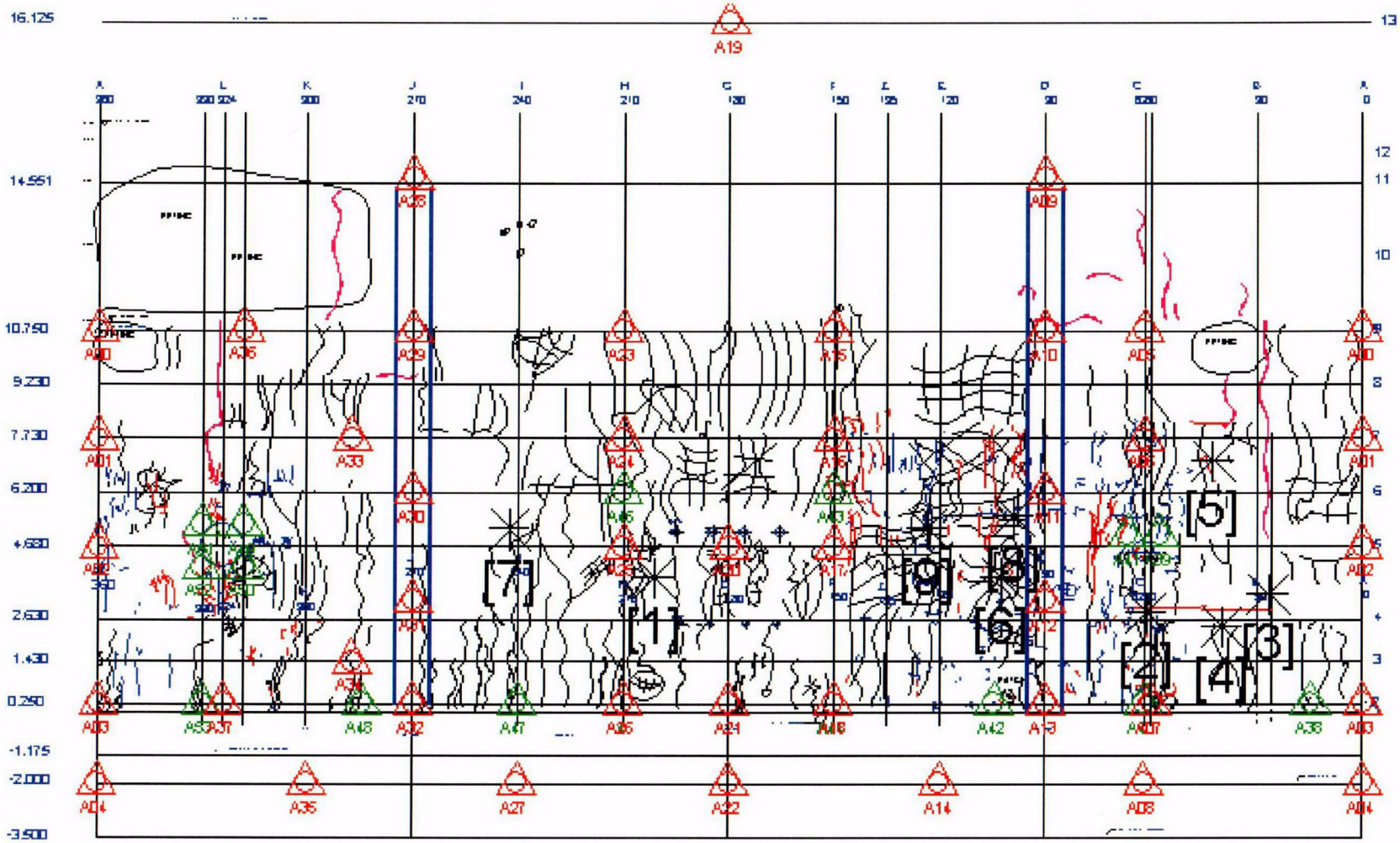

K-80

Wire breaks during the period 10:39 AM to 10:42 AM (First Breaks)
Approximately 188 PSI

C142

Appendix L: Metallurgical Analysis of PCCV Liner Tears

Metallurgical Analysis of PCCV Liner Tears

K. H. Eckelmeyer, J. A. VanDenAvyle, A. C. Kilgo, and L. D. Lambert

Executive Summary:
Substantial amounts of grinding done in association with repair welding were observed in conjunction with nearly all of the 26 liner tears. This grinding produced localized thin areas adjacent to a number of the repair welds. Thinning permitted localized plastic deformation culminating in tearing to occur in the more severely ground regions prior to the onset of general plasticity in the bulk of the liner. This appears to have contributed strongly to the observed liner tearing.

Geometric features may also have contributed to formation of some of the tears. Acoustic data suggested that initial tearing occurred in the equipment hatch transition region, despite grinding being less severe here than in some other areas where tearing did not occur until later. Back-up bar irregularities associated with repair welding (missing segments, various sized segments, etc.) may also have contributed to several tears, but appear to have been primarily responsible for only tear #16. Discontinuities in horizontal stiffeners may also have exacerbated strain localization and contributed to the formation of some tears.

While the ¼-scale liner material met most of the mechanical property specifications for full thickness plate, the ratio of yield to ultimate tensile strength was unusually high for hot rolled steel plate, making the model liner particularly sensitive to local variations in thickness. The necessity of rolling the liner plate to ~ 25% of usual thickness may have increased tensile and particularly yield strength, making it more prone to localized plastic deformation and tearing than typical full-thickness liner material.

Portions of the heat affected zones adjacent to the welds were slightly softer than the base metal, possibly because relatively low temperature finish rolling left a small amount of warm work in the base metal. The amount of softening, however, was not sufficient to cause complete plastic strain localization and tearing, as appeared to have occurred in the liner. Consistent with this, tensile tests on welded samples gave similar strengths, but lower elongations, to those of unwelded material. Also consistent with this, lesser but varied degrees of localized plastic deformation were observed adjacent to some liner welds where little or no grinding and/or repair welding had been done, and where tearing had not occurred. In the more severe cases, the onset of necking, which culminates in tearing, may have occurred. Tear #12 may represent a tear that formed in the absence of prior grinding.

There was no indication that deficiencies in the liner material or welds contributed to tearing, other than as described above. The only exception to this was tear #1, which occurred at a lack-of-fusion defect in the region of a repair weld.

Background:

An instrumented quarter-scale model of a nuclear reactor containment structure was constructed and pressure tested to characterize its mechanical response. The design pressure for this structure was 0.39MPa, and analytical predictions were that failure would occur between 2 and 4 times this design pressure. During pressure testing of this structure leaks were detected beginning at 2.5 times design pressure. At 3.3 times design pressure the leak rate exceeded pressurization capacity and the test was terminated prior to structural failure. Approximately 0.4% global hoop strain occurred in the structure. Post-test examination revealed that 26 tears had formed in the interior steel liner, and that these tears were responsible for the leaks.

The locations of these tears are shown in Figure 1. Seven of the tears were associated with structural features, such as feedwater penetrations and the equipment hatch transition boundary. Acoustic signals suggested that the earliest tearing occurred in the equipment hatch area. The remaining nineteen tears occurred in "free-field" areas distant from any gross structural transitions.

A metallurgical study has been conducted to characterize these tears. This report summarizes the findings and conclusions of this study.

Macro Examination of Liner Interior and Exterior:

Initial macroscopic inspection of liner tear regions consisted of visual inspection of the inside surface, inspection of photographs of the outside surface (taken prior to concrete placement), and ultrasonic measurement of liner thickness. (Note that throughout this report the descriptors "inside", "interior", and "front side" are used to indicate the surface of the liner facing the inside of the structure, while "outside", "exterior" and "back side" are used to indicate the liner surface facing the concrete.) Following initial inspection, sections surrounding many of the tears were cut out and removed. This permitted more detailed observation of features such as back-up bars. A number of macroscopic characteristics were found to be common to nearly all of the tears:

- Tears were oriented perpendicular to the circumference of the cylindrical structure, i.e., vertically. This indicated that they formed primarily due to circumferential (hoop) stresses. The only exceptions were tears along the feedwater penetrations – these initiated at the 3 and 9 o'clock positions (vertically), then extended along the semicircular transition boundary.
- Tears occurred in conjunction with vertical field welds. Typically the tears formed parallel to the welds, less than a few millimeters into the plate from the fusion zone boundaries. No cases of failure in the primary fusion zone were observed, except for a few cases where separate tears developed on opposite sides of the weld, then linked together through the fusion zone. Several tears occurred somewhat farther from the vertical field welds, but never more than 3 centimeters.
- Tears occurred in regions in which repair welding and associated grinding (pre-repair and/or post-repair) had been done.

- Substantial localized plastic deformation occurred in the regions of the tears. This suggested that the tears formed by ductile rupture following localized plastic strain, rather than by brittle fracture at abnormally low strain.
- Liner thinning was detected in the vicinities of the tears and the nearby areas where grinding had been done in conjunction with repair welding. It was not apparent, however, whether this thinning was associated with grinding that took place prior to testing of the structure, with plastic deformation which occurred during testing of the structure, or with both.

Summaries of macroscopic observations on the "free-field" and "feature-associated" tears and their surroundings are given in Tables 1 and 2, respectively. The descriptions of "apparent extent of repair welding" and "apparent extent of grinding" are qualitative descriptors based on visual observation only. These were used primarily to aid in the selection of a range of tear samples for more detailed quantitative characterization, which will be described in a later section. Photographs taken during construction helped correlate liner outside features (stiffeners, anchors, weld back-up bars, etc.) with the locations of the tears. Photographs comparing the front side (interior) and back side (exterior prior to concrete placement) features in the vicinities of a number of tears are shown in Figures 2 to 18.

Examination of Table 1 shows no indication that the "free-field" tears occurred preferentially in the proximity of anchors or horizontal welds and the associated stiffeners. Some of these tears, however, may have been exacerbated by abnormalities such as discontinuities in stiffeners and/or back-up bars. This will be discussed in greater detail in a subsequent section.

A number of features were observed in the field welds of the model that would not be characteristic or allowed in full-scale liners. In many cases these were inevitable consequences of the difficulties involved in fabricating a ¼-scale model. For example, it was clear that fit-up and distortion had been difficult issues during the liner erection and welding process. As a result, there were areas where adjacent plates appeared to be misaligned by more than one-quarter the plate thickness (Ref. 1).

Irregularities were also observed in the back-up bars. It is important to note, however, that while permitted by ASME Code (Ref. 2), MHI does not typically use back-up bars in fabrication of full-sized liners; they were used here because of difficulties associated with fabricating a ¼-scale model. The irregularities observed included use of varying sizes of back-up bar (ranging from 3 mm thick x 13 mm wide to 6 mm thick x 25 mm wide), areas in which segments of back-up bar were removed and not replaced during repair welding, and the absence of welds between adjacent sections of back-up bar. All of these provide discontinuities that could facilitate strain localization, and would not be allowed in full scale liners (Ref. 2). Subsequent investigation did not suggest that such back-up bar irregularities in the *vertical* welds were primarily responsible for any tears. A missing back-up bar segment in a *horizontal* field weld appeared to be primarily responsible for tear # 16, as will be described in more detail in later sections.

Substantial amounts of grinding were also commonly observed in the vicinities of repair welds. Extensive repair welding had been done, presumably in areas where radiographic examination revealed evidence of porosity in the fusion zones. While the intent of this grinding had been to remove the defected fusion zone volumes, grinding frequently extended out into the adjacent plates, often by one to two centimeters. Heat tinting from subsequent welding confirmed that some of this grinding had been done *prior to* repair welding. However, the absence of heat tinting in other areas indicated that additional grinding had also been done *following* repair welding, apparently for cosmetic purposes. Visual observation indicated that severe grinding had been done in a number of areas, suggesting that grinding depth might have exceeded the 12.5% undercut allowed in full scale liners (Ref. 3), thus promoting plastic strain localization. (This was confirmed by subsequent measurements, as will be described in a later section.)

Thickness measurements were made in the vicinities of many of the tears using an ultrasonic technique. The probe used had a lateral spatial resolution of 2 to 3 mm. Thickness measurements were made alongside and parallel to many of the tears (typically ~4 to 6 mm from the tear), and in some cases both ahead of the tears and at greater lateral distances from the tears. Repeated trials showed these measurements to be reproducible within ~0.05 mm (~3% of initial thickness).

Substantial thinning was detected in the vicinities of most of the tears, as shown in Figures 19 to 36. This thinning was typically confined to ~20 mm on either side of the weld; the nominal thickness of ~1.8 mm was generally found at greater distances from the welds. Adjacent to many of the tears, however, thickness reductions of 25% or greater were frequently observed in one or more measurements. In the most extreme case (tear #17) a thickness reduction of 63% was detected adjacent to the tear. Unfortunately, there was no way to distinguish how much of the measured thinning was caused by grinding (prior to pressurization of the structure) and how much was caused by localized plastic deformation (during pressurization of the structure). Distinguishing the magnitudes of these two contributions to thinning required metallographic cross-sectioning and examination of the torn areas, as will be described in a later section.

Liner buckling was also observed in numerous areas, both areas where tearing occurred and in areas without tears. It was apparent that this compressive buckling occurred during unloading in regions where localized plastic deformation had occurred in tension during testing of the structure. In many cases this buckling occurred adjacent to the welds, indicating that plastic deformation had been locally concentrated there.

The degree of buckling varied with location. The largest amounts of buckling were generally observed in the vicinities of the tears, including along the welds where tearing occurred at higher or lower levels. Relatively large amounts of buckling were also observed in welds associated with structural discontinuities, including the edges of the buttresses. In free-field areas, the degree of buckling seemed relatively high between the equipment hatch transition and the air lock. This may indicate that global strains were higher in this area for some reason. This is also consistent with the observation that a disproportionate number of tears occurred in this region. Considerably less buckling was

observed near the top of the liner, consistent with lower overall stresses expected in this area.

In summary, the most provocative macroscopic observations were that nearly all tears occurred following localized plastic deformation adjacent to weld repairs where grinding may have resulted in localized liner thinning. Some, but not nearly all, of the tears occurred in areas where structural transitions or irregularities in back-up bars may have intensified stress and/or strain localization. Buckling indicated that localized plastic deformation also occurred near some welds where tearing was not observed.

Material and Properties:

The liner material was specified to be SGV 410 per JIS G 3118 (Ref. 4). This is a plain carbon structural steel plate containing 0.21% carbon (maximum), 0.85% to 1.20% manganese, 0.15% to 0.30% silicon, 0.035% phosphorus (maximum), and 0.040% sulfur (maximum). Carbon and manganese are the primary strengtheners in this material, and phosphorus and sulfur are limited to promote weldability. (Excessive P and S promote hot cracking in the weld fusion zones. No evidence of this was observed in the liner welds.) The specified mechanical properties for SGV 410 are:

- Yield Strength: 225 MPa (33 ksi) (minimum)
- Ultimate tensile Strength: 410 to 490 MPa (59 to 71 ksi)
- Elongation: 21% minimum (in 50 mm gauge length of 25 mm wide sample).

SGV 410 plate is not commercially produced in thicknesses below 6.4 mm. MHI was able to obtain 1.8 mm thick material for the liner via a special order. While this material was as close as could be obtained to full scale SGV 410, it is possible that rolling the material to less than 30% of its normal minimum thickness could result in some alteration of mechanical properties, potentially making the model liner material less than perfectly characteristic of full-scale liners.

MHI material qualification tests showed the following average tensile properties (average of six samples, 3 from each orientation; no significant orientation differences were observed):

- Yield Strength: 383 MPa (55 ksi)
- Ultimate Tensile Strength: 498 MPa (72 ksi)
- Elongation: 33%

The observed ultimate tensile strength was slightly higher than the specified upper limit. Otherwise the material conformed to the mechanical properties specified for SGV 410. The yield strength, however, was 70% over the specified minimum, and was quite high for a steel of this composition. Both the high ultimate strength and the high yield strength may have resulted from low finishing temperature, as might be expected when rolling unusually thin material. The 33% elongation to failure dramatically exceeded the ~0.4% global strain at which tearing occurred in the liner.

The ratio of yield strength to ultimate strength provides a measure of the susceptibility of a material to plastic strain localization due to variations in thickness, for example, local thinning resulting from grinding. For the material in question, the yield strength represents 77% of the ultimate tensile strength. This is unusually high for hot rolled plain carbon steel plate, where the YS/UTS ratio is typically in the 0.5 to 0.7 range (Ref. 5). The high YS/UTS ratio of the steel used in the model makes this material unusually susceptible to plastic strain localization and subsequent tearing due to variations in thickness. Based on a simple uniaxial analysis, areas in which grinding resulted in thinning greater than ~23% would exceed the ultimate strength before the yield strength was reached in the surrounding (unthinned) material. This would result in complete localization of plastic deformation culminating in tearing in these thinned regions prior to the onset of general plasticity in the overall structure. Implications based on this simple uniaxial approach may not be quantitatively applicable to the biaxially stressed liner and its geometric complexities. Nonetheless, it appears that the unusually high yield strength of the liner material may have made the liner particularly sensitive to variations in thickness caused by grinding done in conjunction with liner weld repairs.

The microstructures and hardnesses of welded liner material were characterized by Sandia. Samples from two MHI practice weld plates were cross-sectioned, mounted, polished, and etched. Both showed microstructures typical of welded plain carbon structural steel, i.e., a progression from:

- base metal consisting of fine-grained equiaxed ferrite and pearlite (Figure 37), to
- fine-grained heat affected zone (HAZ) consisting of equiaxed ferrite and pearlite (Figure 38), to
- progressively coarser-grained heat affected zone consisting of acicular ferrite and pearlite (Figure 39), to
- fusion zone consisting of course columnar grains (formed during solidification) which have transformed on cooling to mixed ferrite and pearlite (Figure 40).

A second weld pass had been made in one of the practice weld panels. The heating from this second pass altered the microstructure of the initial weld metal. Figure 41 shows that the initial weld metal has been re-austenitized and recrystallized, eliminating the prior-columnar solidification structure, then transformed to a finer-grained assemblage of equiaxed ferrite and pearlite. This characteristic microstructural difference was used to distinguish between original and repair welds in metallographic samples taken from the liner tear areas, as will be discussed in a later section.

Microhardness measurements were made to provide an estimate of strength variations across the weld. Twenty-five Vickers hardness measurements were made using a 100 gram load in each of the following areas: the base metal, the fine-grained portion of the heat affected zone adjacent to the base metal, the intermediate-grained portion near the middle of the heat affected zone, the coarse-grained portion of the heat affected zone adjacent to the fusion zone, the as-solidified fusion zone, and the portion of the fusion zone that had been re-austenitized during subsequent weld passes. The results of these measurements are shown in Table 3. It can be seen that the fine and medium grain-sized

portions of the heat affected zone were slightly softer than the base metal. This may reflect annealing out of residual deformation strengthening left in the ¼-scale liner plate due to low finishing temperature. The coarse-grained portion of the heat affected zone was somewhat harder, presumably due to the higher cooling rates in this area (Ref. 6). The fusion zone was considerably harder than either the base metal or any portion of the heat affected zone.

Conversion of these hardness measurements to ultimate tensile strengths (Ref. 7) indicates that the UTS in the outer portions of the HAZ may be ~5% lower than that of the base metal. This may be sufficient to cause some plastic strain localization in the HAZ, but not the dramatic localization that was observed in conjunction with the liner tears. Based on a simple uniaxial analysis, the UTS in the HAZ would have to be ~23% lower than that of the base metal for complete strain localization to occur, i.e., for the HAZ to reach its ultimate strength before the base metal began to plastically deform.

Tensile tests of welded specimens had been previously conducted by MHI (Ref. 8). These tests included plates that had been welded with different root gaps, plates that had been welded with and without back-up bars, and plates that had been repair welded. No significant property variations were detected with any of these welding parameters. Photographs of these samples indicated that the weld beads and back-up bars had been ground off during tensile sample preparation, leaving uniformly thick gauge sections. Yield and ultimate tensile strengths were statistically equivalent to those of the unwelded material. The most obvious effect of welding was a substantial decrease in elongation (33% for unwelded samples vs. an average of 19% for welded samples). None of the 24 samples failed in the fusion zone. Nearly all of them failed adjacent to (within 6 mm of) the weld, either in the weld heat affected zone or in the nearby base metal. The observed decrease in tensile elongation was, at least in part, due to the fact that the harder fusion zones deformed less than the other portions of the samples. The lateral restraint provided by the harder fusion zones may also have increased deformation resistance in the heat affected zones, further decreasing elongation and masking the slight reductions in UTS expected based on the lower hardnesses found in the outer portions of the heat affected zones.

Three sets of tensile bars were also machined from the MHI practice weld panels and tested at Sandia. These samples were geometrically identical to those tested by MHI, i.e., 25 mm wide x 50 mm gauge length. One set consisted of three unwelded base metal samples. The second set consisted of three welded samples, but with the weld beads and back-up bars left in place (in contrast to the MHI tests where these were ground off). The expectation was that the increased lateral constraint might cause failure adjacent to the welds to occur at lower strains more characteristic of the liner. The third set was similar to the second, but represented regions in which there were significant offsets between the two plates (in excess of the 0.25 x thickness limit allowed by the ASME Boiler and Pressure Vessel Code for full-scale liners (Ref. 1)). These tests were intended to simulate locations in the liner where fit-up difficulties resulted in similarly large offsets, as described previously.

The results of these tests are summarized in Table 4 and compared with previous test results in Table 5. It can be seen that the Sandia results are in general agreement with those of MHI. While slightly higher strengths and slightly lower ductilities were obtained by Sandia for similar conditions, these small differences are not believed to be significant. The lower elongations observed in the welded samples were due, at least in part, to the absence of yielding or plastic deformation in the thicker, harder, and highly constrained fusion zones, as well as the increased resistance to deformation in the adjacent HAZ regions due to the lateral restraint provided by the fusion zones. It was clear, however, that substantial plastic deformation occurred in the base metal, even in samples that failed near the weld. This is consistent with expectations based on the hardness measurements, which suggested that the strength of the HAZ was only ~5% lower than that of the base metal, far less than the ~23% difference that would be required to cause complete plastic strain localization in the HAZ.

The location and nature of failure changed with test condition. One of the well-aligned welded samples failed prematurely along the fusion zone boundary due to a lack-of-fusion defect. The other two failed far from the weld. Apparently the additional lateral restraint provided by the weld bead and back-up bar increased resistance to plastic deformation adjacent to the weld enough that it forced deformation to concentrate far away in the region of reduced lateral restraint.

In the three welded samples where the plates were significantly offset, deformation and subsequent failure occurred adjacent to the weld. Apparently the increased bending stresses associated with the offsets caused deformation to concentrate near the weld, despite the high lateral restraint in this area. The yield strength was slightly lower than in the well-aligned weld samples, but ultimate strength and elongation were not reduced by the weld offset.

Scanning electron microscope characterization of the fracture surfaces showed that all of the samples failed by microvoid coalescence, as is typical of ductile failure following extensive plastic deformation (Figures 42 to 44). There may have been some tendency for the microvoids to be less fully developed in samples with substantial weld offsets (compare Figure 44 with 42 and 43), but not a dramatic one. Even in the sample that failed prematurely due to weld lack-of-fusion defects, the adjacent fracture surface (beyond the defect) exhibited typical microvoid coalescence failure.

Combining the Sandia microhardness data with the MHI and Sandia tensile results, the following conclusions can be reached regarding mechanical behavior of welded tensile samples:

- Under conditions of relatively mild lateral restraint (e.g., the MHI tests where the weld bead and back-up bars were ground off), there is a tendency for deformation, tensile instability, and subsequent fracture to concentrate adjacent to the weld. This is consistent with the slightly lower microhardnesses observed in the weld heat affected zones.

- Under conditions of greater lateral restraint (e.g., the Sandia tests where the weld bead and back-up bars were left on), deformation, tensile instability, and subsequent fracture tend to concentrate distant from the weld away from the region of high lateral restraint.
- Substantial weld offsets result in additional bending stresses that cause deformation and subsequent fracture to again concentrate adjacent to the weld, despite high lateral restraint in this area.
- No cases of dramatic strain localization were observed. In the most extreme cases examined plastic deformation was only mildly concentrated near the weld, i.e., plastic strain localization was far less severe than was observed adjacent to many repaired welds in the liner. Consistent with this, no substantial changes in ultimate strength or overall ductility occurred with variations in lateral constraint or weld alignment.

Applying the combined hardness and tensile information to the liner application suggests that, in situations of uniformly high lateral restraint, such as are characteristic of the liner, plastic deformation would be expected to concentrate slightly, but not severely, in the heat affected zones adjacent to the welds. Tearing would typically occur adjacent to the welds, but only after substantial amounts of plastic deformation had occurred throughout the structure (contrary to the observation that liner tearing occurred following only ~0.4% global strain). The presence of offsets in the welds might cause a modest, but not dramatic, increase in the tendency for strain localization adjacent to the welds.

In summary, the mechanical testing results did not suggest that deficiencies in the properties of either the base metal or weld metal, nor excessive softening in the weld heat affected zones could account for the extensive localized plastic deformation culminating in tearing that appeared to have occurred in the liner.

The Sandia tensile tests also provided an opportunity to determine the effects of geometric and stress state variables on reduction of thickness at the point of fracture. Broken tensile bars corresponding to all three sets of conditions were metallographically mounted, ground, and polished, permitting characterization of deformation-induced reduction in thickness at the failure location (as well as a function of distance from the failure). Micrographs of these cross sections are shown in figures 45 to 48. The sample thicknesses at the points of failure were measured using a calibrated scale internal to the metallograph. These are tabulated in Table 4. The reductions in thickness at the point of failure were found to be remarkably constant, regardless of variations such as proximity to the weld, degree of lateral constraint, or extent of weld offset. The average thickness at the point of fracture was 51% of original thickness, with a standard deviation of only 2.6%. The consistent 49% deformation-induced reduction in thickness proved to be very useful in assessing the amounts of grinding that had been done at the tear locations in the liner, as described in the next section.

Measurements were also made of the amounts of thinning that occurred in the offset welded samples on the opposite sides of the weld from the fracture. While necking occurred only on the sides where failure eventually occurred, the opposite sides were presumably approaching the point of incipient necking and tensile instability. These

samples exhibited an average of 12% maximum reduction in thickness in this region. This is in good agreement with the average observed uniform elongation of 12% to 13% (Table 4). It would be expected, then, that weld regions should plastically thin approximately 12% to 13% prior to the onset of non-uniform deformation. Liner regions that have plastically thinned substantially more than this might reasonably be thought to have begun to neck, hence to be approaching the point at which tearing could occur.

Metallographic Examination of Cross-Sections Through Tears:

Sections surrounding a number of the tears were removed from the liner for more detailed examination. These samples were selected to represent a wide range of the macroscopically observed variations, i.e., tear size, proximity to weld fusion line, proximity to structural features, horizontal welds, and anchors; visually apparent extent of repair welding and associated grinding, and nearby back-up bar geometry. The only unique tears that were not removed were numbers 3, 5-1, and 5-2 around the feedwater penetration. These were deemed too difficult to remove, as well as too difficult to repair in the event of a decision to retest the structure.

Metallographic examination was performed on cross-sections of samples from these regions. The cross-sections were taken near the midpoint of each tear, presumably near where each tear initiated. In cases where grinding was visually apparent near the tear midpoint the cross-sections were taken where the grinding appeared to be most severe. The locations where these cross-sections were taken and the surrounding details are shown in Figures 49 to 63. The samples were mounted, polished, and etched with a combination of 2% nital and Vilella's reagent to reveal the microstructure of the fusion zone, the surrounding heat affected zone, and the base metal.

The fracture surfaces of two samples (#12 and #14-2) were also examined by scanning electron microscopy. These fracture surfaces, shown in Figures 64 and 65, exhibited 100% microvoid coalescence, similar to the ductile fracture surfaces observed on the tensile bars, confirming that liner tearing occurred by ductile fracture in association with localized plastic deformation.

The metallographic results are summarized in Tables 6 and 7. Photographs of selected areas surrounding the tears are also shown in Figures 66-83. However, complete metallographic characterization of the tear regions required observation at various magnifications of regions as far as several centimeters on either side of the tear. It was not practical to include all of this information photographically. Hence, Tables 6 and 7 summarize the most important metallographic observations made surrounding each tear.

All of the welds, with the exception of the weld at tear #1, were found to be sound, and the microstructures of the base metal, heat affected zones, and fusion zones were similar to those seen in the weld test panels, as described previously. Localized plastic deformation was observed in conjunction with all of the tears (except the initiation area of tear #1), similar to what was observed in the tensile samples. Tearing was not found to be associated with any *particular* microconstituent, but occurred in various

microstructural regions, including the recrystallized fusion zones of previous welds, the coarse and fine-grained regions of weld heat affected zones, and the base metal.

Estimates of the amounts of grinding associated with each tear were obtained based on the previously described knowledge that ~ 49% reduction in thickness occurs due to plastic deformation prior to fracture. The method used is illustrated in Figure 84. The liner thickness at each tear location was measured using a calibrated scale internal to the metallograph. This tear thickness was then divided by 0.51 to obtain the local pre-deformation thickness at/near each tear location. This pre-deformation thickness was subtracted from the initial liner thickness to determine the amount of material removed by prior grinding. Finally, the amount of material removed by grinding was divided by initial liner thickness to determine the percentage of grinding-related thickness reduction associated with each tear initiation site. These results are given in Tables 6 and 7. These percentages of original liner thickness removed by grinding are estimated to be accurate to +/- 5% absolute, i.e., 40% grinding implies 35% to 45%.

Two additional methods were used to confirm these estimates in selected cases, as illustrated in Figure 84. The amounts of grinding deduced from these two additional methods are also included in Tables 6 and 7.

First, in a number of samples where tearing occurred very close to the weld fusion line, the liner thickness immediately next to the thick undeformed weld bead provided a reasonable estimate of the original post-grinding thickness at the (nearby) tear site. Grinding reductions obtained by this method are also estimated to be accurate to +/- 5% absolute. Consistent with this, no discrepancies greater than 10% were found between the estimates obtained by this method and the primary method, described in the previous paragraph.

Second, in some samples banding (a manifestation of chemical segregation patterns in the original ingot which have been elongated by the plate rolling process) was continuously or semi-continuously apparent from near the tear location back into the unground base metal. These bands are always parallel to the free surfaces of the rolled plates. Hence, locations where the edges of the cross-sectioned samples were at slight angles to these bands represented regions where the liner surfaces had been tapered by grinding. By following the bands from the tear location back into the unground base metal it was possible to estimate the amount of material that had been ground off of each side of the plate. This method was judged to be less accurate than the previous two methods because of the inherent imprecision in following bands over what was frequently a substantial distance from the tear to the unground portion of the plate. As a result, estimates obtained by this method were judged to be accurate to only +/- 10%. Consistent with this, larger discrepancies were found between the estimates obtained by this method and those obtained by the previous two methods. However, with the exception of tear #9, no discrepancies in excess of 15% were observed.

Examination of Tables 6 and 7 reveals that the estimated amounts of grinding obtained by all three methods are in reasonable agreement. Furthermore, it can be seen that, with the

possible exception of tear #12, at least 25% of the original liner thickness had been ground off in all locations where the tears initiated. This provides a strong indication that liner thinning due to grinding predisposed severely ground areas surrounding repair welds to plastic strain localization and tearing during testing of the model.

Descriptions of Specific Free-Field Tears:

Tear #1: Tear #1 was distinct from all other tears in that it initiated at a weld defect. Tear #1 is described in Tables 1 and 6, and pictured in Figures 2, 19, 49, 66 and 67. At its midpoint (presumably the initiation site), the tear was oriented at 90 degrees to the primary tensile stress and there was no microstructural indication of plastic deformation having preceding fracture (Figure 66). Detailed examination of the fracture profile in the initiation region revealed that the surface was covered with a foreign substance, perhaps residue from the primer paint (too dark to be seen in Figure 66) – this indicated that welding had failed to completely melt and join the adjacent pieces in this area. The microstructure on opposite sides of the tear were distinctly different: recrystallized fusion zone from the original weld on the repair weld side, and unaltered heat affected zone from the original weld on the opposite side. No effort was made to remove the surface residue to permit SEM examination of the underlying surface. It seems clear, however, that this represented a weld defect, likely a lack-of-fusion defect similar to the one seen in one of the welded tensile bars. Assuming that no plastic deformation occurred adjacent to this defect, the measured thickness indicated that 22% of the liner thickness had been ground off in this area.

As a check, an additional cross-section was polished ~2 cm down the tear from the initiation site, at a location removed from the weld defect (the opposite edge of the cross-section sample, shown in Figure 49). This cross-section is shown in Figure 67. The tear appeared quite different in this location: a predominantly 45 degree shear failure accompanied by substantial local plastic deformation. This clearly represents a region where the tear had propagated into sound metal after having been initiated at the nearby weld defect. The amount of grinding estimated from the deformation-reduced thickness at the tear in this location was ~20%, in excellent agreement with the 22% measured in the undeformed area adjacent to the weld defect.

Tears #2-1, 2-2, 2-3: These tears are described in Tables 1 and 6, and pictured in Figures 3, 20, 50, 51, 52, 68, 69 and 70. They occurred along a vertical field weld that had undergone numerous overlapping repairs. The repeated repair welding resulted in a band as wide as 3 cm consisting largely of weld metal, much of which had been re-austenitized and recrystallized from the heat associated with subsequent welds. Extensive grinding was visually apparent over a broad area on either side of the tears (Figures 20, 50, 51 and 52). Immediately adjacent to tear #2-1 a small section of plate remained attached to the massive weld bead (Figure 68), permitting direct measurement of the residual thickness after grinding, as illustrated in Figure 84. Sufficiently continuous banding was apparent in #2-2 and #2-3 to permit grinding reduction to be estimated from the tapering of the ground surface with respect to these bands. In all three cases the amounts of grinding inferred by the three different methods were in reasonable agreement with one another,

thus confirming the validity of the primary method based on reduced thickness at the tear location. Grinding had reduced the thickness by 45% or more in the regions where each of these tears occurred, enough to cause complete plastic strain localization culminating in ductile tearing when the structure was tested.

Another distinguishing characteristic of this weld was the large number of short segments of back-up bar resulting from repetitive repair of this joint (Figures 3, 50 and 51). In addition to being short, three different cross-sections of back-up bar were used. These included sections of 3 mm x 13 mm, 3 mm x 19 mm, and 6 mm x 25 mm. Metallographic and hardness measurements on various portions of back-up bar showed ferrite and pearlite microstructures ranging from R_B 62 to R_B 70. It was not clear whether these back-up bar variations contributed significantly to tearing in this area or others.

Tears #4-1 and 4-3: These tears are described in Tables 1 and 6, and pictured in Figures 4, 21, 53, 54, 71 and 72. The joint along which these tears formed was somewhat unusual in that no back-up bar was present (either the weld had been made with no back-up bar, or the back-up bar was later completely ground off). This joint was otherwise similar to #2, i.e., one where numerous overlapping repairs had been made, resulting in a band as wide as 5 cm consisting largely of weld metal, much of which had been re-austenitized and recrystallized. Other than the unusual number of overlapping repair welds, the metallography revealed no distinguishing features associated with the tears. As with tear #2, grinding had reduced the liner thickness by approximately 45% in the regions where each of these tears occurred, enough to cause complete plastic strain localization and ductile tearing when the structure was tested.

In addition, a parallel repair weld approximately 25 mm in from the primary weld near tear #4-3 clearly represented an area in which the liner had been inadvertently breached as repair-associated grinding was being done, and had itself been repair welded. The appearance of this and other similar areas in which liner "grind-through's" had been repair welded confirmed that grinding done in conjunction with repair welding had, in some areas, removed substantial portions of the adjacent liner, resulting in extensive liner thinning and, in some areas, liner penetration requiring additional repair.

Tear #6-2: This tear was examined as a proxy for four tears, 6-1, 6-2, 11-1, and 11-2, which all occurred along the left-hand side of the same vertical field weld. They are described in Tables 1 and 6, and pictured in Figures 5, 6, 22, 23, 24, 55 and 73. While ultrasonic thickness measurements failed to detect a great deal of thinning adjacent to this tear, far greater thinning was observed below the end of the tear (Figure 23). The metallographic cross-section showed that highly localized grinding had been done on the exterior side adjacent to the edge of the back-up bar. This resulted in a narrow band of thinned material immediately next to the back-up bar, consistent with the ultrasonic measurements. The other distinguishing aspect of these tears was the unusually large number of short back-up bar segments along this weld (Figures 5 and 6). While metallography indicated a single repair weld in sample #6-2, the number of back-up bar segments attests that numerous/repeated repairs had been made at various heights along this joint. It is not clear whether the large number of short back-up bar segments

contributed to tearing. However, approximately 33% of the original liner thickness had been ground off in this region, enough to cause complete plastic strain localization and ductile tearing when the structure was tested.

Tear #8-1: This tear is described in Tables 1 and 6, and pictured in Figures 7, 25, 56 and 78. It represented a tear that occurred in an area where a segment of back-up bar had been left missing during repair welding. This may have exacerbated strain localization in this region, but the estimated 30% grinding reduction of liner thickness observed in this area was, by itself, likely sufficient to cause severe plastic strain localization and subsequent ductile tearing.

Tear #8-2: Tear #8-2 is described in Table 1 and 6, and pictured in Figures 26, 57 and 75. It was unique in that it occurred relatively distant from the weld in an area where macroscopic examination revealed evidence of substantial grinding (Figure 26), but no apparent repair weld. Metallographic examination revealed, however, that at least two repair welds had been made adjacent to the vertical joint, apparently to repair an inadvertent "grind-through" made in association with repairs on the main weld. Following repair of this "grind-through", the weld bead of this repair had been ground off from both front and back sides, leaving no obvious evidence of this defect having been made or repaired. However, this grinding reduced the wall thickness in the repaired "grind-through" area by approximately 60%, resulting in severe localization of plastic deformation culminating in ductile tearing when the structure was tested.

Tear #9: This tear is described in Tables 1 and 6, and pictured in Figures 8, 27, 58 and 76. It represented a typical repair welded joint far from either anchors or horizontal stiffeners. In other respects it was similar to tear #6-2, one where a narrow band of thinning resulted from heavy grinding adjacent to the back-up bar, and where numerous back-up segments indicated a series of repairs at various heights along a vertical field weld. Metallographic examination revealed no unusual microstructural features. While this sample showed the greatest discrepancy in percent grinding estimated by different methods, all methods indicated that sufficient grinding had been done to cause substantial strain localization and ductile tearing when the structure was tested. Approximately 40 to 45% thinning appears to have been done by grinding based on two of the three estimation methods.

Tear #10: This tear is described in Table 1 and pictured in Figures 9 and 28. No metallographic sample was taken in this region because this tear was similar in most respects to #8-1.

Tears #14-1 and 14-2: These tears are described in Table 1 and pictured in Figures 10 and 29. No metallographic samples were taken in this region because these tears were similar in many respects to #8-1. SEM fractography showed that tearing occurred by microvoid coalescence (Figure 65).

Tear #16: This tear is described in Table 1 and pictured in Figures 11 and 30. It formed distant from the vertical field weld in an area where no grinding or repair of this weld were macroscopically apparent. Back-side photographs, however, showed a missing

segment of back-up bar in a *horizontal* field weld, apparently where a repair had been made in *this* weld (Figure 11). This missing segment of horizontal back-up bar reduced the circumferential stiffness in this area, providing for plastic strain localization and tearing. Comparison of front and back-side photographs (Figure 11) indicated that the tear began at the termination of the horizontal back-up bar, then propagated down through the "rat-hole" in the horizontal stiffener, and along the vertical field weld. The cause of this tear was macroscopically apparent, so no metallography was done on it.

Tear #17: This tear is described in Tables 1 and 6, and pictured in Figures 12, 31, 59, 77 and 78. It represented one that occurred along a relatively isolated single repair weld. As was the case with several vertical welds in the vicinity of the feedwater and main steam penetrations, the original weld appeared to have been made without any back-up bar (or the back-up bar was subsequently ground off). Macroscopic observation suggested that the repair had been made by grinding off the weld bead on the back side, then making a repair weld on the front side (the inside of the liner). The metallographic cross section revealed a much more complex sequence of grinding and repair welding. While the specific order of events could not be deduced, it was clear that multiple side-by-side repair welds had been made in this region. Substantial grinding had been done on both the inside and outside of the liner in association with these repairs. The net result was that the portion of the liner adjacent to the final repair weld was thinned more than 70%. Failure occurred in this thinned region due to plastic strain localization culminating in ductile tearing.

Descriptions of Specific Feature-Associated Tears:

Tears #3 and 5-1: These tears are described in Table 2 and pictured in Figures 13 and 14. They occurred along opposite ends of the feedwater penetration transition weld, i.e., in areas that were mirror images of one another. No metallographic samples were taken from these regions because their locations made removal difficult and because repair would be difficult in the event a decision was made to retest the structure. The fact that tear #3 was substantially larger than tear #5-1 may have resulted from more extensive grinding and weld repair on this end of the transition. On the other hand, it could also have been exacerbated by a difference in horizontal stiffener terminations revealed by the back-side photographs. At #3 the horizontal stiffener ends very close to the transition weld (within 1 cm – see Figure 13), creating a very limited length of low stiffness, hence a region of potentially very high strain localization. At #5-1 the horizontal stiffener ends much farther from the transition weld (~10 cm – see Figure 14), thus providing a longer length of low stiffness over which the local strain could distribute, (i.e., lower strain localization).

Tear #5-2: This tear occurred along a vertical weld slightly above #5-1. No metallographic samples were taken for the same reasons mentioned above. However, the back-side photographs (Figures 13 and 14) revealed a significant difference between the region in which tear #5-2 occurred and the corresponding mirror image region at the opposite end of the feedwater penetration transition. At one end there was a vertical weld in the high strain region between the nearest concrete anchor and the stiff feedwater

transition – tear #5-2 formed along this weld. At the opposite end, no vertical weld was present in the corresponding high strain region and no tearing occurred.

Tears #7 and 15: These tears occurred near the lower and upper corners of the equipment hatch transition joint, respectively. They are described in Tables 2 and 7, and pictured in Figures 15, 16, 32, 33, 60, 61, 79, 80 and 81. Acoustic monitoring suggested that initial tearing occurred in the vicinity of this transition joint. While this transition represented a region where complex stresses and high local strains were expected, liner thinning resulting from grinding done in association with repair welding was also substantial in the areas of these tears: 25% to 30% at tear #7 and ~ 50% at tear #15. This thinning undoubtedly exacerbated plastic strain localization and tearing in these areas, however, it is likely that high strains at this transition also contributed to tearing. No unusual microstructural features were observed in the vicinities of these tears.

Tears #12 and 13: These tears also occurred along the equipment hatch transition joint, but near its midpoint, rather than the corners. They are described in Tables 2 and 7, and pictured in Figures 17, 18, 34, 35, 62, 63, 64, 82 and 83. Both formed near horizontal field welds and the associated "rat-hole" discontinuities in horizontal stiffeners, although back-side photographs indicated that patches were welded in between the adjoining stiffener segments, minimizing strain localization in these regions (unless the welds at the ends of these patches failed). Evidence of ~30% thinning from grinding was found at tear #13.

The extent of thinning from grinding was much less clear in the vicinity of tear #12. Little evidence of grinding or weld repair was macroscopically apparent on either the front or back side. Consistent with this, ultrasonic thickness measurements indicated ~22% thinning approximately 5 mm adjacent to this tear (Figure 34), only slightly greater than the amount expected based on cross-sections of the tensile samples (Figures 45 to 48). Consistent with this, metallographic observation of the portion on the side of the tear where the ultrasonic measurements had been made indicated only a small amount of grinding, ~10%.. However, the opposite side (adjacent to the weld fusion zone) showed a different and thinner section at the tear location, suggesting ~27% reduction by grinding. Microstructural observation of the weld failed to unequivocally reveal whether a repair weld had been made in this area. The fusion zone was wider (~8 mm) than most initial welds, suggesting that a repair had been made. But no evidence remained of the previous weld – perhaps the initial fusion zone had been completely ground out prior to repair or the repair weld had completely consumed it – this was observed in several other areas where it was macroscopically apparent that repair welds *had been* made. Tear #12 may be the one most likely to represent a "true structural effect", i.e., to not have resulted from excessive grinding, backing bar abnormalities, or weld defects. However, there is a substantial degree of uncertainty regarding the amount of thinning from grinding in the vicinity of this tear.

Metallographic Examination of Cross-Sections Through Welds Where Substantial Plastic Deformation But No Tearing Occurred:

In addition to the tear regions, metallographic cross-sections were also taken from several regions where there was evidence of substantial localized plastic deformation, but where no tearing had occurred. Samples 18-1 and 18-2 were across a vertical field weld that exhibited substantial buckling and "orange peel" evidence of localized plasticity. This weld was in the region between the equipment hatch transition and the air lock, where the largest amounts of buckling and tearing were observed. It had been initially made and subsequently repaired from the front side (inside of the liner), but no back-up bar had apparently been used in making either the initial or repair weld. 18-2 contained a single isolated repair weld and a modest amount of associated grinding, while 18-1 was a nearby region with no apparent grinding or repair weld. Samples 24-1 and 24-2 represented a region with no apparent grinding or repair welds, but where the highest liner strains were recorded by strain gauges during the test (~7% strain). This weld was near the edge of a buttress, where substantial buckling was observed. 24-2 was taken near the intersection of horizontal and vertical field welds within a "rat-hole" region in a horizontal stiffener. 24-1 was along the same vertical field weld, but above the horizontal weld and stiffener. The locations where these samples were taken and surrounding details are shown in Figures 85 to 88. Metallographic observations made on these samples are shown in Figures 89 to 92 and summarized in Table 8.

Region #18-1 and 18-2: The observations made in these areas are described in Table 8 and pictured in Figures 36, 85, 86, 89 and 90. The cross-section of #18-1 (Figure 89) showed that a modest amount of localized plastic deformation had occurred adjacent to the weld on both sides of the fusion zone. The greatest amount of deformation thinning occurred in the HAZ near the fusion line (13% on one side, 9% on the other side – note that these amounts of thinning are consistent with the ultrasonic thickness measurements, shown in Figure 36). Approximately 5% thinning was uniformly observed over a ~15 mm wide band in the adjacent base metal. Thinning then tapered out gradually to zero over the next ~15 mm. The amount of thinning in the HAZ is in the vicinity of the 12% to 13% required for the onset of necking, as was determined from analysis of the welded tensile samples. However, considerable additional local deformation would be required before tearing would be expected to occur. Consistent with this, no evidence of void formation or shear banding, which would be indicative of incipient failure, was observed.

The cross-section of #18-2 revealed substantially more thinning, 42% on one side of the weld and 31% on the other side (Figure 90). However, it was clear that a substantial, but not quantifiable, amount of this thinning was due to prior grinding, rather than simply to plastic deformation during testing. While considerably higher levels of localized plastic deformation would be expected in these previously ground areas, no evidence of substantial necking or incipient tearing was apparent. This suggests that, while necking may *begin* after only 12% to 13% local thinning, considerably more localized deformation must be accommodated prior to the onset of tearing.

Regions #24-1 and 24-2: These regions are described in Table 8 and pictured in Figures 87, 88, 91 and 92. Sample #24-2 was taken in the "rat-hole" region immediately between the ends of the bridged horizontal stiffeners. This sample was sharply bent, attesting to the complexity of the stresses in this region. The sample exhibited a maximum of at least 20% thickness reduction on one side of the weld and ~14% thickness reduction on the opposite side of the weld (Figure 91). Presumably, the strain gauge in this area recorded only 7% strain because it was not co-located with the point of peak local strain. Thicknesses change rapidly with position in this region, implying much lower strains within several millimeters of the point of maximum thickness reduction.

Significant depressions were present on both inner and outer surfaces at the point of minimum thickness. It is likely that these represented the early stages of necking; this would be expected based on the fact that thinning clearly exceeded the 12% to 13% required for the onset of necking. Precise measurement of maximum reduction was compromised by a very irregular surface and large non-metallic particles at the base of one of these depressions – this may represent a surface defect in the plate. The maximum reductions in thickness were observed in the weld heat affected zones, then tapered out with increasing distance into the base metal. As in regions 18-1 and 18-2, however, there was no evidence of void formation or shear banding, which would be indicative of incipient tearing. This supports the previous contention that considerably more localized deformation must occur following the onset of necking before localized deformation culminates in tearing.

Sample #24-1, taken some distance away from the horizontal stiffeners, exhibited 6% and 5% maximum thickness reduction of opposite sides of the weld. These maximum reductions occurred in the HAZs, and tapered to zero over approximately 10 mm in the adjacent base metal.

The fact that peak strain in #24-2 was several times that in nearby #24-1 may indicate that much more complex stresses and considerably higher local strains can occur in the "rat-hole" regions associated with horizontal stiffeners. While no general tendency was observed for tears to form in these regions, it is possible that in a limited number of cases, the patches that bridged between stiffeners on opposite sides of the vertical field welds failed. This would most likely occur by failure of one of the welds joining the patch to the adjacent stiffeners. Such failures would dramatically decrease stiffness in the "rat-hole" region, thus causing severe strain localization. It may be possible that this is what occurred in the region of #24-2. It may also be possible that this also occurred near tear #12, which was also in a "rat-hole" region. This may help explain why tear #12 occurred in a region where little or no weld repair or grinding had been done. Unfortunately, the "rat-hole" patches and associated welds were buried in the concrete, so this possibility could neither be confirmed nor refuted.

In summary, it is clear that localized plastic deformation also occurred in the heat affected zones adjacent to some welds that had not been repaired or ground, particularly those in regions of high local or global strain. While these amounts of localized plasticity were considerably lower than those associated with tearing, the necking threshold was

likely exceeded in the most severe cases. No evidence of incipient tearing was observed in these areas, however, and it appears that a substantial amount of additional local deformation must occur following the onset of necking before this culminates in tearing.

Conclusions:

- Nearly all of the tears occurred in areas where the liner thickness had been reduced ~25% or more by grinding done in association with repair welding. Extensive localized plastic deformation culminating in ductile tearing occurred in these thinned areas as the structure was being tested. This appears to have been the most prevalent cause of liner failure.
- Geometric features may also have contributed to the formation of some tears. These include structural transitions, such as those at the feedwater penetration and the equipment hatch transition boundaries, discontinuities in horizontal stiffeners, and discontinuities in weld back-up bars. A missing segment in a horizontal back-up bar appears to have been primarily responsible for one tear (#16).
- Only one tear occurred in association with a material or weld defect: a lack-of fusion weld defect was found at the initiation site of tear #1.
- The specially produced quarter-scale liner material exhibited mechanical properties that may have made it particularly prone to plastic strain localization and tearing. While nearly conforming to the specifications for full-thickness material, the quarter-thickness plate exhibited a yield strength much higher than the specified minimum (383 MPa compared with 225 MPa) and an unusually high yield to ultimate strength ratio (0.77). This high YS/UTS ratio is qualitatively consistent with extensive localized plastic strain culminating in ductile tearing occurring in regions where more than ~25% of the liner thickness had been ground off, as was observed near most of the tears.
- Tensile and hardness tests on welded test samples indicated that modest amounts of plastic strain localization should be expected in the weld heat affected zones, but to a much lesser extent than was observed in association with the liner tears. Consistent with this, smaller but significant amounts of localized plastic strain were observed adjacent to some welds that had not been repaired or ground. These strains were sufficient to initiate necking in the most severely strained regions. However, with the possible exception of tear #12, there was no indication that tearing was imminent in regions other than those where repair welding and substantial grinding had been done.

Acknowledgements: Several others contributed to this effort. We appreciate the assistance of Garry Bryant and Carlos Velasquez with metallography, Tom Crenshaw with tensile testing, and Gary Zender with SEM fractography.

References:

1. 1998 ASME Boiler and Pressure Vessel Code, Code for Concrete Reactor Vessels and Containments, Table CC-4523-1, Maximum Allowable Offsets In Final Welded Joints, p. 103.

2. 1998 ASME Boiler and Pressure Vessel Code, Code for Concrete Reactor Vessels and Containments, Section CC-4542, Specifically CC-4542.2, p. 108.
3. 1998 ASME Boiler and Pressure Vessel Code, Code for Concrete Reactor Vessels and Containments, Section CC-4542.5, Specifically CC-4542.2, p. 116.
4. Japanese Industrial Standard JIS G 3118, Carbon Steel Plates for Pressure Vessels for Intermediate and Moderate Temperature Service, 1987.
5. ASM Handbook, 10th Edition, Volume 1, Properties and Selection of Irons, Steels, and High-Performance Alloys, 1990, p. 230.
6. Metals Handbook, 8th Edition, Volume 1, Properties and selection of Metals, 1961, p. 1235.
7. ASM Metals Handbook Desk Edition, 1998, p. 73.
8. Welded Joint Tensile Test Results of PCCV Liner Welding Re-confirmation Test, MH-K9-43.

Tables

Table 1. Macroscopic Descriptions of Free Field Tears

Tear No.	Tear Length (cm)	Distance From Fusion Line (mm) *	Distance From Horizontal Weld (cm) #	Distance From Concrete Anchor (cm) # **	Visually Apparent Extent of Repair Welding ##	Visually Apparent Extent of Grinding ##	Back-up Bar Description In Repair Area
1	4	0	Midway	8 (46)	Single isolated repair	Moderate	Several long patched segments
2-1	8	*	Midway	37 (46)	Extensive & wide	Extensive	Several patches of various sizes
2-2	8	*	Midway	37 (46)	Extensive & wide	Extensive	Many patches of various sizes
2-3	18	*	6	37 (46)	Extensive & wide	Extensive	Long patched segment
4-1	11	* (both sides, crosses final weld)	Midway	Midway (15)	Extensive & wide	Extensive	No back-up bar on original or repair welds
4-2	4	*	Midway	Midway (15)	Extensive & wide	Extensive	No back-up bar on original or repair welds
4-3	14	*	5	Midway (15)	Extensive & wide (Separate repair to side of main weld – repair of "grind-thru"	Extensive	No back-up bar on original or repair welds

6-1	10	2 to 3	0 (Crosses shop weld without back-up bar)	38 (46)	Moderate to Extensive	Moderate to Extensive	Several patches of various sizes
6-2	7	2 to 3	Midway	38 (46)	Extensive	Extensive	Numerous short patched segments
8-1	6	0 to 1	Midway	Midway (46)	Moderate	Moderate	Segment missing in tear region
8-2	4	10	Midway	Midway (46)	None apparent	Extensive	Long (apparently original) segment
9	13	0 to 5	Midway	Midway (46)	Extensive	Extensive	Several patches of various sizes
10	1-1/2	0 to 1	Midway	8 (46)	Extensive	Extensive	Segment missing in tear region
11-1	10	2 to 3	8	38 (46)	Extensive	Extensive	Many patches of various sizes
11-2	6	2 to 3	0 (Begins at shop weld without back-up bar)	38 (46)	Extensive	Extensive	Many patches of various sizes
14-1	8	0 to 3	0 (Begins at field weld w/missing segment of back-up bar)	Midway (46)	Extensive	Extensive	Segments in both vertical & horizontal back-up bars missing in tear region
14-2	13	0 to 3	8	Midway (46)	Extensive	Extensive	Segment missing in tear region

16	8	13 to 25	0 (Crosses field weld w/missing segment of back-up bar)	38 (46)	No repair evident in vertical weld, but repair in horizontal weld	Little or none apparent	Weld repair in horizontal weld left ~4 cm segment of back-up bar missing
17	3	0	Midway	Midway (15)	Single isolated front-side repair to original weld made on back-side	Extensive	No back-up bar on original or repair welds

* Tears #2 and #4 occurred where numerous overlapping repair welds had been made, resulting in a wide band of weld metal.

\# "Midway" implies that tear was distant from horizontal welds and/or anchors, not that centerline of tear was quantitatively equidistant from adjacent features.

** Number in parentheses indicates spacing of anchors in region of tear (in cm)

Qualitative extent of repair welding or grinding based on *visual observation*. Subsequent more detailed examination of metallographic cross-sections showed that these visual estimates were sometimes misleading.

Table 2. Macroscopic Descriptions of Feature-Associated Tears

Tear No.	Tear Description	Apparent Extent of Grinding & Weld Repair *	Structural Features With Potential for Causing Strain Localization
3	>15 cm long tear ~3 mm from fusion line of transition weld of liner to feedwater penetration	Fairly extensive weld repair & grinding in this area	Horizontal stiffener ends very close to transition weld, creating high potential for strain localization in region where tear occurred (compare with less severe mirror image, tear #5-1).
5-1	~4 cm long tear ~6 mm from fusion line of transition weld of liner to feedwater penetration (mirror image of region near tear #3)	Little or no evidence of weld repair or grinding in this area	Similar to, but less severe than situation at tear #3 – horizontal stiffener ends ~10 cm from transition weld, providing a less severe potential for strain localization.
5-2	~8 cm long tear along vertical field weld above tear #5-1	Appears to be front-side repair to original back-side weld in this area (perhaps similar to nearby tear #17)	Vertical field weld between concrete anchor and feedwater transition creates potential for high strain in welded region. No comparable weld is present in the mirror image high strain location, where no tearing occurred.
7	~23 cm long tear along vertical weld near lower corner of equipment hatch transition	Extensive weld repair & grinding in this area	Several horizontal stiffeners end discontinuously in this region, creating high potential for strain localization.
12	~5 cm long tear along vertical weld between liner and equipment hatch transition. Tear crosses horizontal shop weld between "rat-hole" regions in two horizontal stiffeners	Little or no repair welding or grinding apparent in this area	"Rat-hole" region of horizontal stiffeners could cause strain localization if patch-weld failed

13	~9 cm long tear similar to #12, but at near next higher horizontal field weld. Tear midpoint near "rat-hole" region in horizontal stiffener	Extensive grinding and ~10 cm long weld repair in region of tear	"Rat-hole" region of horizontal stiffeners could cause strain localization if patch-weld failed
15	~10 cm long tear along vertical weld near upper corner of equipment hatch transition (similar to #7 at lower corner)	Moderate to extensive grinding and weld repair. Plates appear to have been poorly aligned in this area, creating substantial weld offset.	Two horizontal stiffeners end discontinuously in this area, creating high potential for strain localization.

* *Qualitative* extent of repair welding or grinding based on *visual observation*. Subsequent more detailed examination of metallographic cross-sections showed that these visual estimates were sometimes misleading.

Table 3. Microhardnesses of Zones Surrounding Welds

Zone	Avg. Hardness *	Std. Dev.	UTS (ksi) **	UTS (MPa) **
Base metal	160	6.9	74.5	515
Fine-grained HAZ	151	4.3	71	490
Med-grained HAZ	154	3.4	72	495
Coarse HAZ	164	6.8	76.5	525
Fusion Zone	180	11.4	84	580
Recrystallized fusion zone	173	5.9	80.5	550

* Vickers hardness, 100 gram load

** UTS estimates from Ref. 6. Note that UTS estimates are based on conversion tables for hardness tests made with much heavier loads. As a result, the estimated UTS values should be taken only as approximations; they are useful primarily for comparing the expected *relative* strengths of the various regions, not the *absolute* strengths. For example, the 515 MPa estimated base metal strength is slightly higher than the 498 MPa value measured via tensile tests. The implication regarding the fine and medium grained portions of the HAZ are that their ultimate strengths are expected to be 20 to 25 MPa lower than the base metal. Similarly, the most important implications regarding the ultimate strengths of the virgin and recrystallized fusion zones are that they should be approximately 65 and 35 MPa higher than the base metal, respectively.

Table 4. Results of Tensile Tests Conducted at Sandia

Sample	YS (MPa)	UTS (MPa)	Uniform Elong (%)	Total Elong (%)	Thickness at Fracture (% of original)**
Unwelded					
A1	395	520	15.8	31.3	-
A2	376	512	16.4	30.6	-
A3	418	530	15.7	31.1	48
Welded, No Offset					
B1	409	528	12.2	16.6 *	-
B2	407	497 #	6.2 #	6.6 #	55
B3	403	515	10.6	15.8 *	-
Welded, >25% Offset					
C1	375	520	12.8	16.3	52
C2	350	519	12.7	16.3	50
C3	371	518	12.9	17.2	-

* Failed at or near extensometer knife edge: total elongation reported is artificially low

\# Failed at apparent weld lack-of-fusion defect

** Average thickness at fracture location for all samples was 51% of original thickness; standard deviation was only 2.6% of original thickness regardless of substantial variations in samples and stress conditions (welded vs. unwelded, amount of lateral constraint, degree of weld offset). The 51% value was later used in conjunction with the thickness measured at each of the liner tears to determine the local liner thicknesses prior to tearing, and from this, the local amounts of liner material that had previously been removed by grinding.

Table 5. Summary of Tensile Properties of Material from Practice Weld Panels

Description	Yield Strength (MPa)	Ultimate Strength (MPa)	Uniform Elongation (%)	Total Elongation (%)
JIS Specification	225 (min)	410 to 490	-	21.0 (min)
Unwelded (MHI)	383	498	-	33.0
Welded (MHI)	379	505	-	18.8
Unwelded (SNL)	396	520	16.0	31.0
Welded – Plates Well Aligned (SNL)	406	521	11.5*	>16.0*
Welded – 36% to 70% Weld Offset (SNL)	365	518	12.8	16.6

* One sample failed prematurely at fusion line due to lack-of-fusion defect – 6.2% uniform elongation, 6.6% total elongation. Other two samples failed at extensometer knife edge distant from weld. Properties represent average of these two samples. Total elongation somewhat greater than measured with extensometer as part of necked regions were outside extensometer.

Table 6. Metallographic Descriptions of Free Field Tears

Tear No.	Weld Description	Tear Description	% Grinding Estimated from Thickness At Tear	% Grinding Estimated from Thickness At Weld	% Grinding Estimated From Banding
1	Single repair weld overlapping original weld	Initiated at lack of fusion defect, no evidence of plastic deformation at initiation site. Shear failure with localized deformation in second sample taken beyond weld defect	20%	22%	
2-1	Multiple overlapping repair welds, 16 mm total width	Shear failure with localized deformation in medium to coarse grained HAZ	61%	57%	
2-2	Multiple overlapping repair welds, 29 mm total width	Shear failure with localized deformation in partially recrystallized fusion zone	46%		45%
2-3	Multiple overlapping repair welds, 21 mm total width	Shear failure with localized deformation in fully recrystallized fusion zone	64%		50%
4-1	Multiple overlapping repair welds, 51 mm total width	Shear & tensile or bending failure with localized deformation in region containing both recrystallized and unrecrystallized fusion zone and coarse grained HAZ	46%		
4-3	Two major welds, one ~25 mm from vertical joint – apparently repair of a "grind-thru" in liner wall	Shear failure with localized deformation in coarse-grained HAZ	44%		

6-2	Single repair weld; original weld ground out prior to repair or completely remelted during repair	Shear failure with localized deformation in medium grained HAZ	33%		

8-1	Single repair weld overlapping original weld	Shear & tensile or bending failure with localized deformation in partially recystallized HAZ	30%		
8-2	Several welds, including one ~13 mm from vertical joint – apparently repair of a "grind-thru" in liner wall	Shear failure with localized deformation mostly in recrystallized fusion zone	61%		
9	Single repair weld; original weld ground out prior to repair or completely remelted during repair	Shear failure with localized deformation in medium grained HAZ	42%	44%	27%
17	Multiple welds, one ~15 mm from vertical joint – apparently repair of a "grind-thru" in liner wall	Shear failure with localized deformation through recrystallized fusion zone	74%	82%	

Table 7. Metallographic Descriptions of Feature-Associated Tears

Tear No.	Weld Description	Tear Description	% Grinding Estimated from Thickness At Tear	% Grinding Estimated from Thickness At Weld	% Grinding Estimated From Banding
7	Two or more repair welds overlapping original weld	Shear & tensile or bending failure in medium grained HAZ, likely a combination of tensile & bending stresses	30%		25%
12	Possibility of single repair weld; if so, original weld ground out prior to repair or completely remelted during repair. Definite evidence of grinding on both surfaces, but grinding does not appear deep	Shear failure with localized deformation in base metal	10% to 27%*		10%*
13	Single repair weld; original weld ground out prior to repair or completely remelted during repair	Shear failure with localized deformation in medium to coarse grained HAZ	31%		33%
15	Single repair weld overlapping original weld	Shear failure with localized deformation in coarse grained HAZ	54%		50%

* The smaller estimates were based on examination of liner on opposite side of tear from weld. The larger estimate was based on the portion adjacent to the weld where thickness at the point of tearing was smaller.

Table 8. Metallographic Descriptions of Joints with No Tears

Sample Number	Joint Description	Localized Strain / Thinning
18-1	No repair weld, little or no evidence of grinding	13% maximum reduction in thickness. Minimum thickness in coarse-grained HAZ, gradual increase to full thickness over ~30 mm
18-2	Single repair weld; original weld ground out prior to repair or consumed by repair. Some grinding prior to & following repair welding, but extent of grinding appears less than in most joints with tears	Deformation localized in heat affected zones, but cannot be quantified due to unknown amount of prior grinding
24-1	No repair weld or evidence of grinding	6% maximum reduction in thickness. Minimum thickness in HAZ, gradual increase to full thickness over ~15 mm
24-2	No repair weld, little or no evidence of grinding	~ 20% maximum reduction in thickness. Minimum thickness in HAZ*

* Local depressions were observed on both interior and exterior surfaces in the thinnest region. These may represent early stages of necking. Large non-metallic particles and very irregular surface features in one depression likely represent a surface defect in the plate. The ~20% thickness reduction discounts these embedded particles and very local pits on the one surface, but includes the more general depressions.

Figures

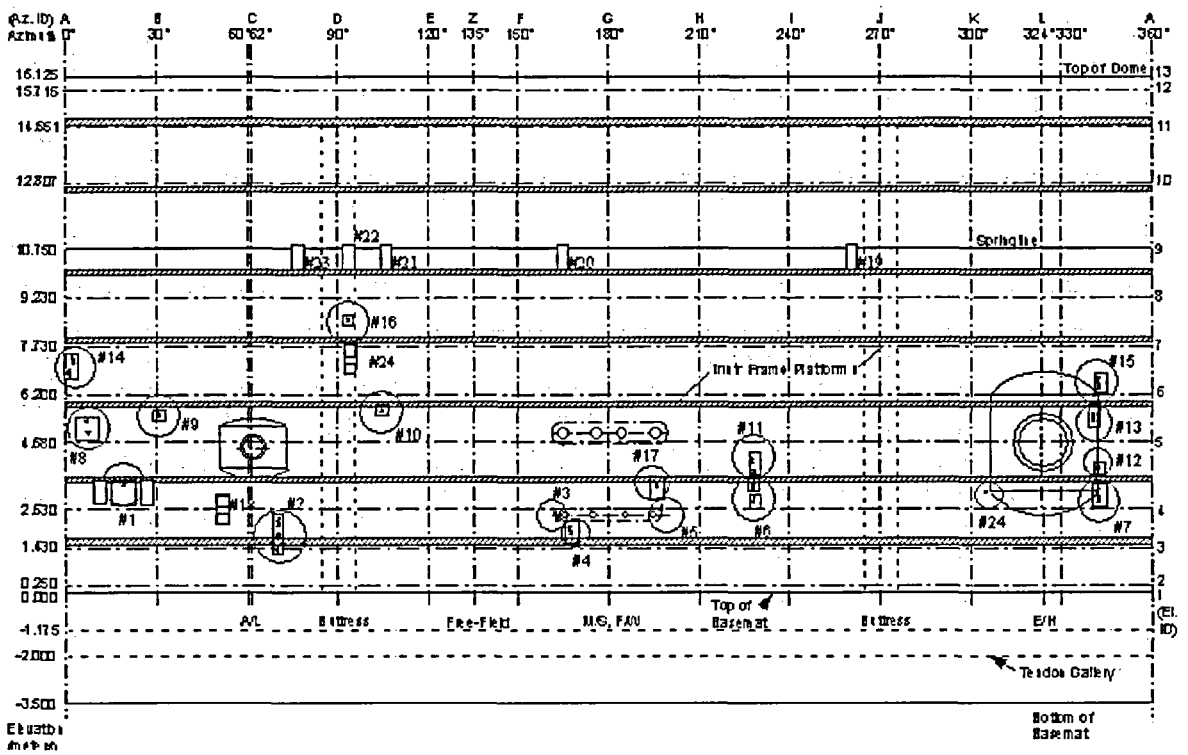

Figure 1. Map showing approximate locations of tears.

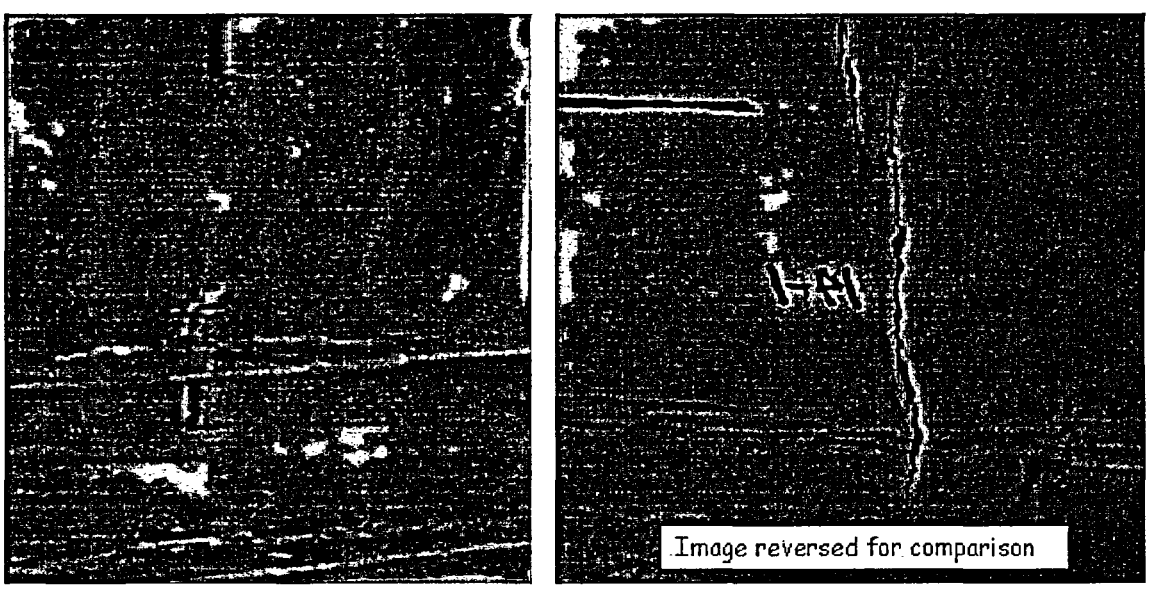

Figure 2. Photographs showing region of tear #1 from outside of liner (left) (prior to concrete placement) and inside of liner (right) (prior to removal of paint). The tear occurred under the wide segment of back-up bar near the top of the left-hand photograph, on the side closest to the anchor.

Figure 3. Photographs showing region of tear #2-3 from outside of liner (left) (prior to concrete placement) and inside of liner (right) (prior to removal of paint).

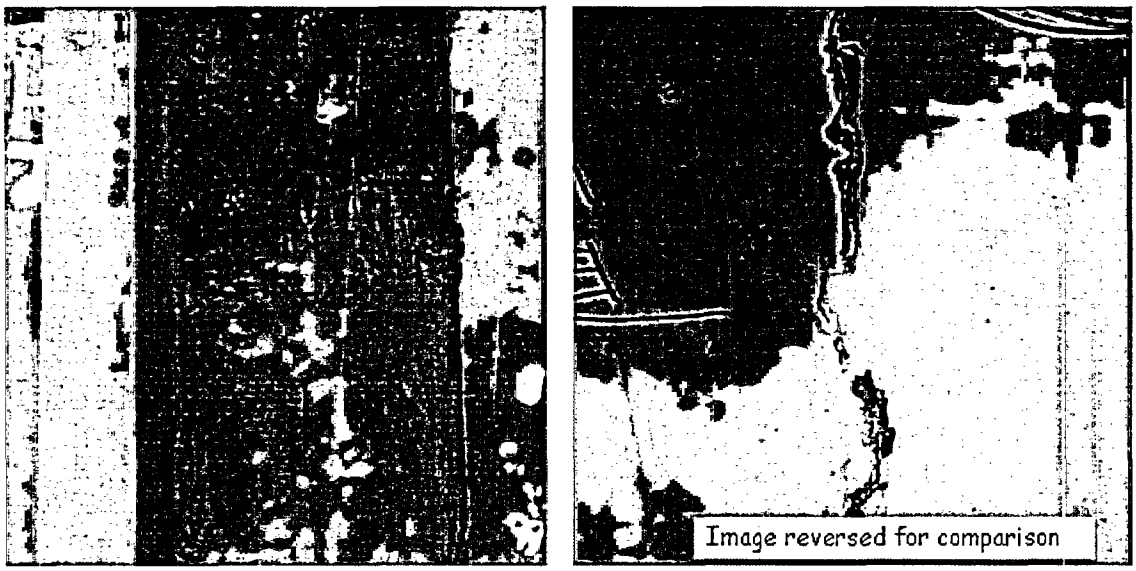

Figure 4. Photographs showing region of tear #4-1 from outside of liner (left) (prior to concrete placement) and inside of liner (right) (prior to removal of paint). Separate tears began of opposite sides of the weld, eventually growing together through the fusion zone.

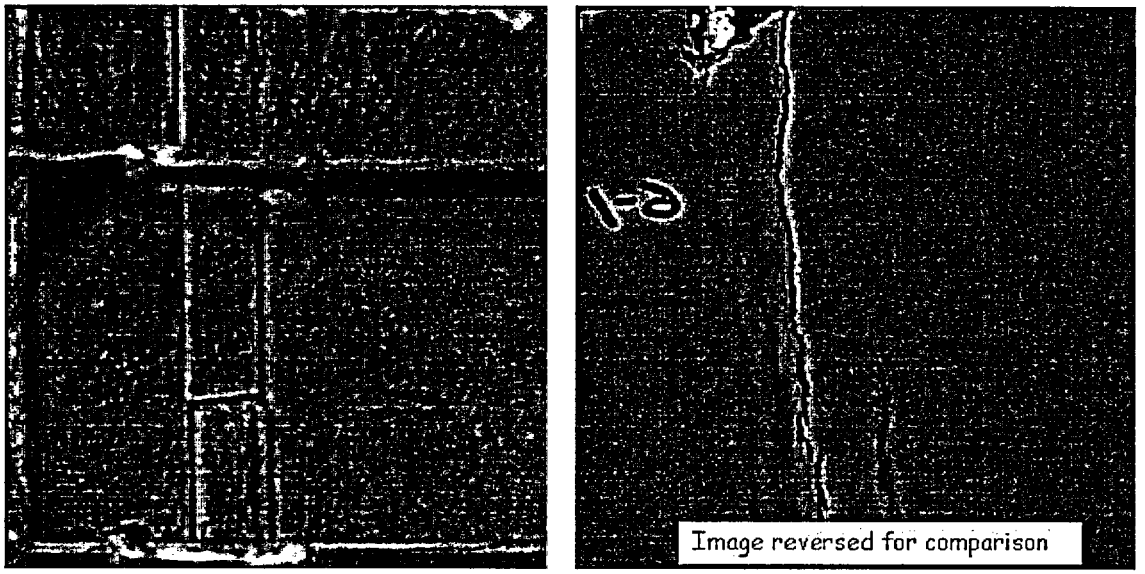

Figure 5. Photographs showing region of tear #6-1 from outside of liner (left) (prior to concrete placement) and inside of liner (right) (prior to removal of paint). Tear #6-2 was along the same vertical weld, but distant from the horizontal weld and associated horizontal stiffeners.

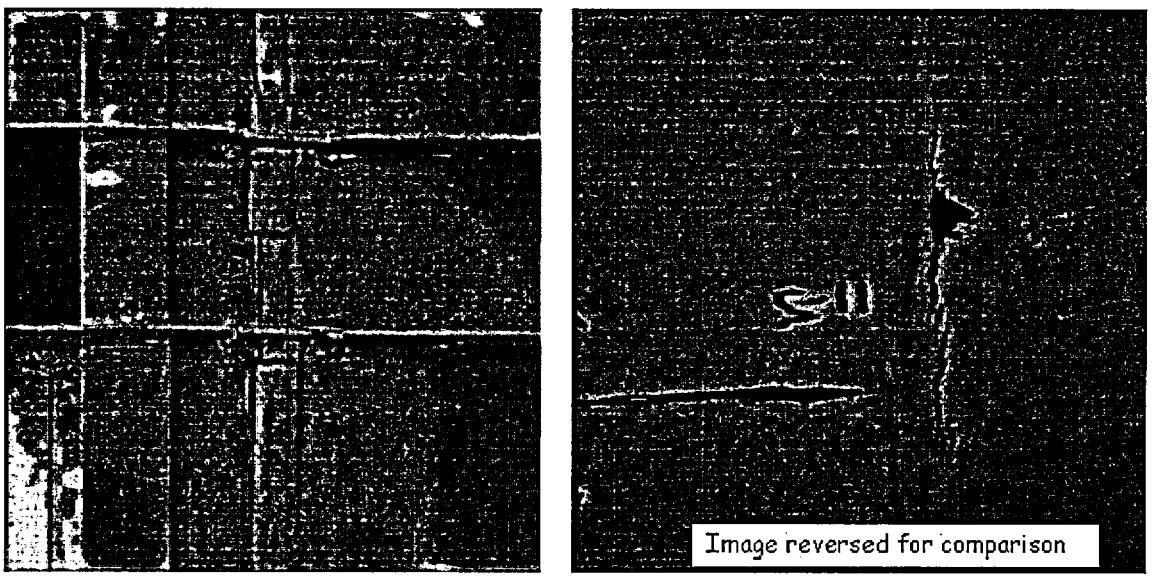

Figure 6. Photographs showing region of tear #11-2 from outside of liner (left) (prior to concrete placement) and inside of liner (right) (prior to removal of paint). Tear #11-1 was along the same vertical weld, but distant from the horizontal weld and associated horizontal stiffeners. Tears #11-1 and 11-2 were along the same vertical weld as tears #6-1 and 6-2.

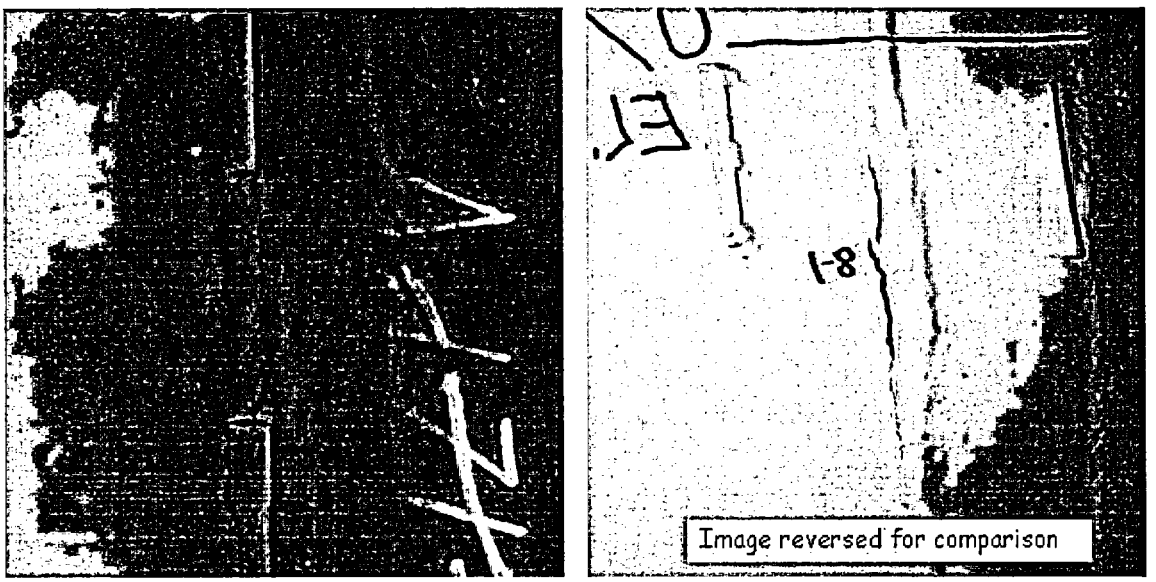

Figure 7. Photographs showing region of tear #8-1 from outside of liner (left) (prior to concrete placement) and inside of liner (right) (prior to removal of paint). Note missing segment of back-up bar in vicinity of repair weld and tear.

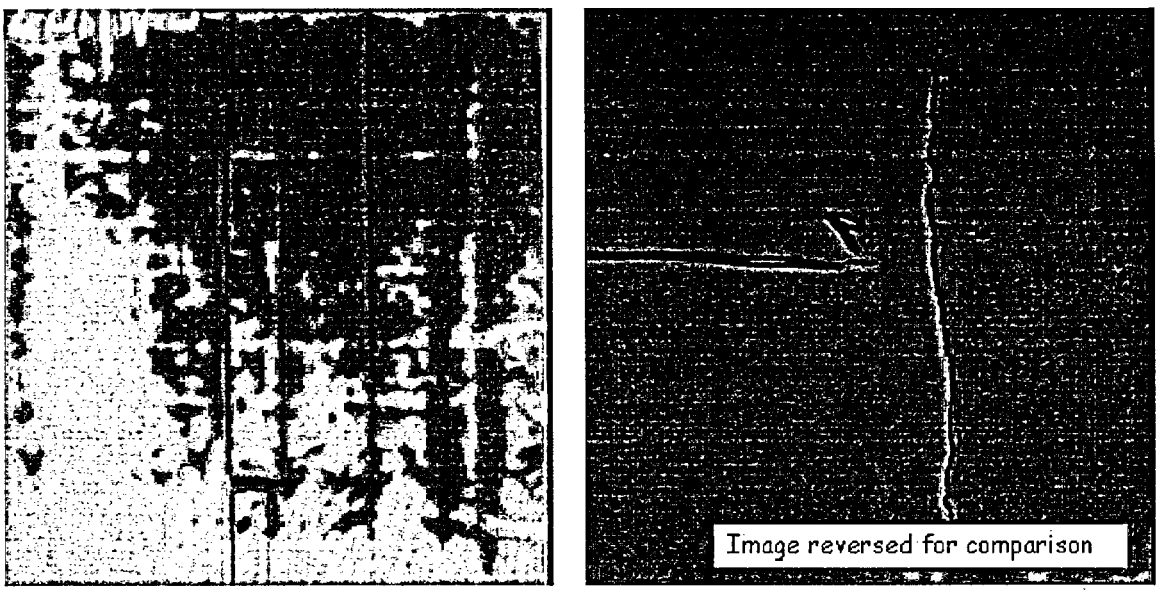

Figure 8. Photographs showing region of tear #9 from outside of liner (left) (prior to concrete placement) and inside of liner (right) (prior to removal of paint).

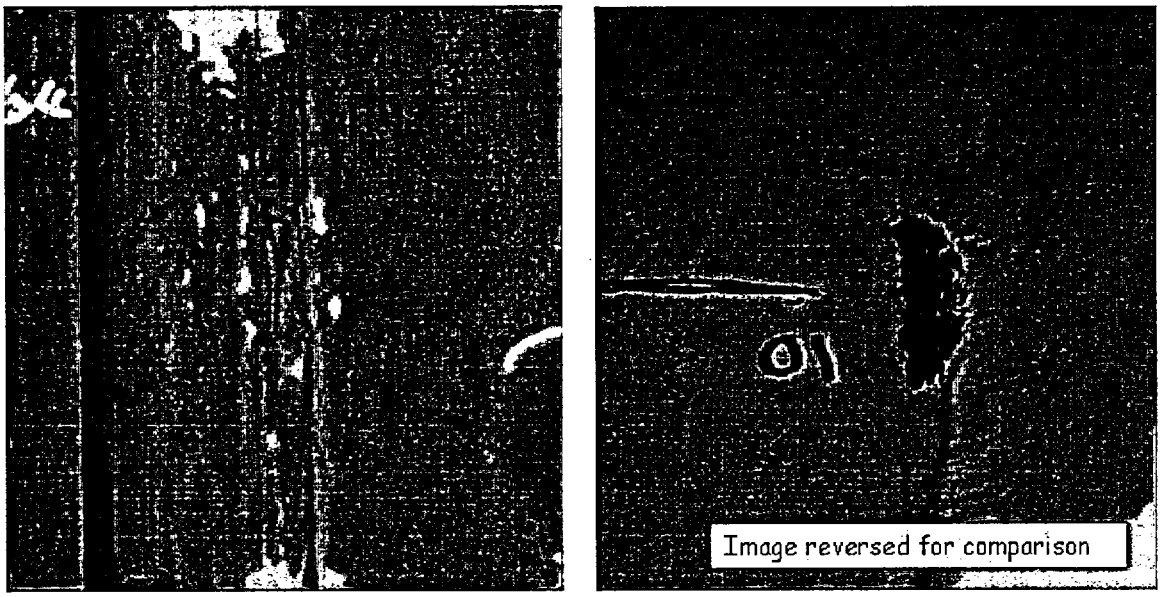

Figure 9. Photographs showing region of tear #10 from outside of liner (left) (prior to concrete placement) and inside of liner (right) (prior to removal of paint). Note missing segment of back-up bar in vicinity of repair weld and tear.

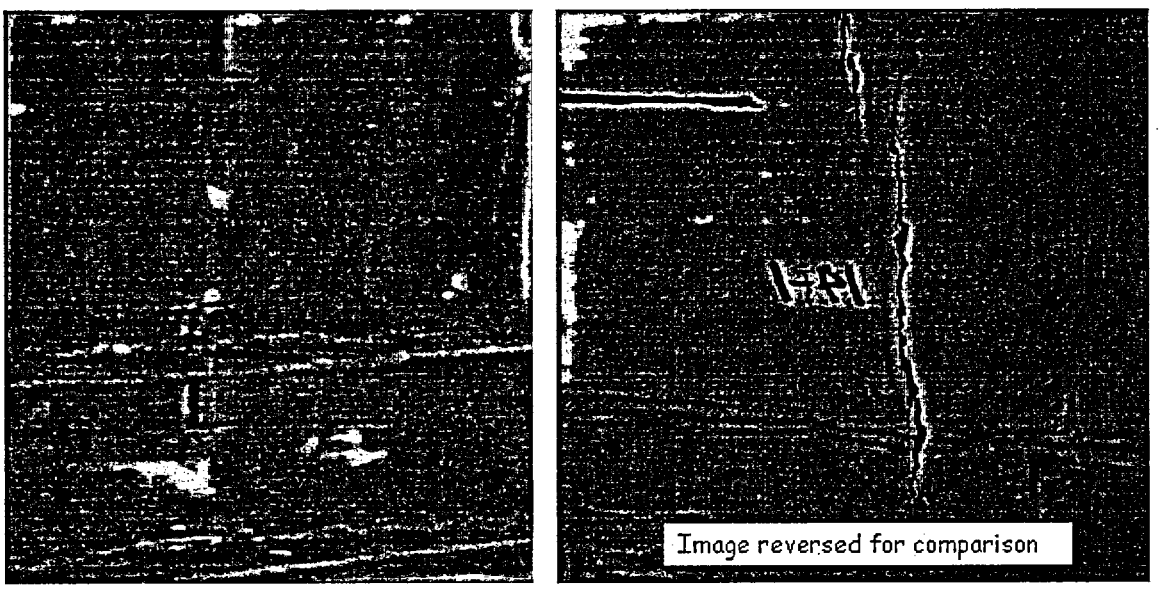

Figure 10. Photographs showing region of tear #14-1 from outside of liner (left) (prior to concrete placement) and inside of liner (right) (prior to removal of paint). Note missing segments of back-up bar in vicinity of repair weld and tear.

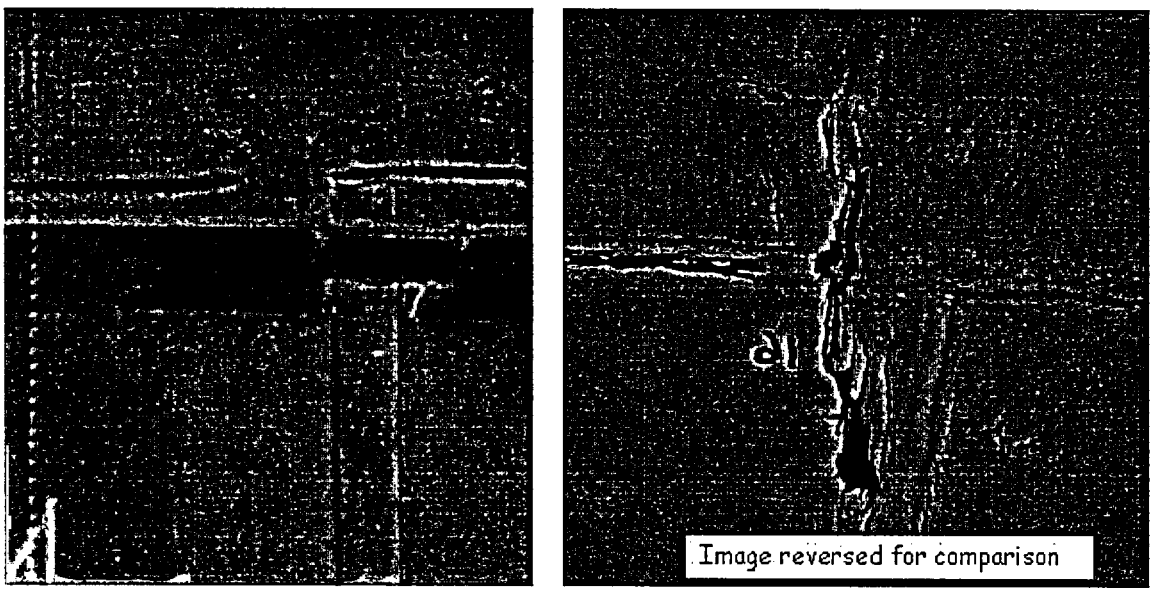

Figure 11. Photographs showing region of tear #16 from outside of liner (left) (prior to concrete placement) and inside of liner (right) (prior to removal of paint). Note missing segment of back-up bar on horizontal weld in vicinity tear.

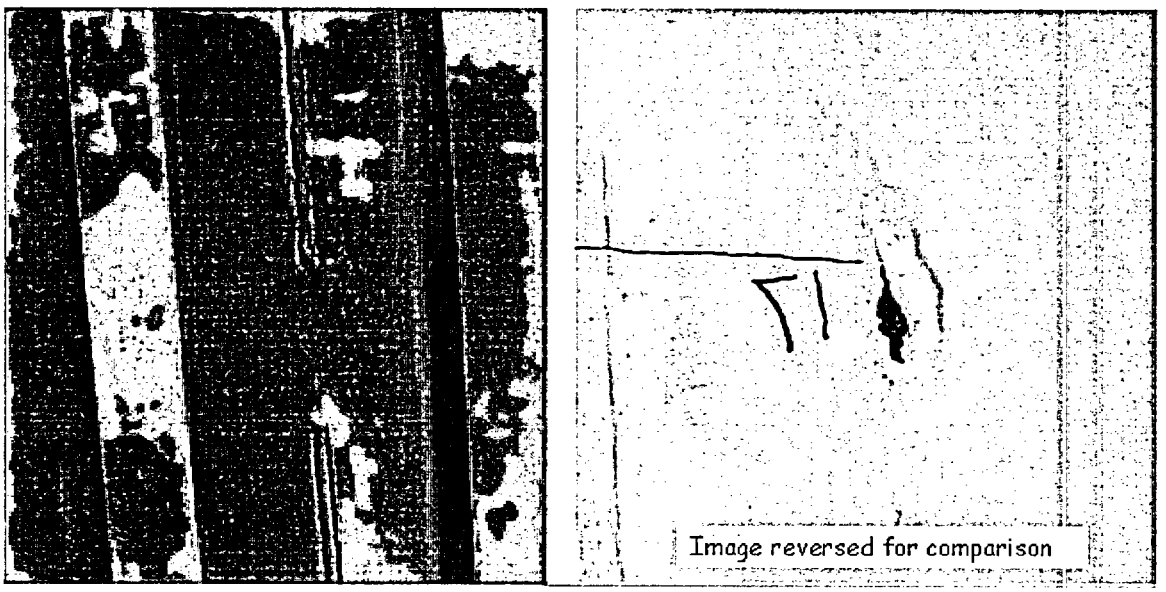

Figure 12. Photographs showing region of tear #17 from outside of liner (left) (prior to concrete placement) and inside of liner (right) (prior to removal of paint). Note how weld bead is ground off on outside surface in vicinity of repair weld (made from inside of liner) and tear.

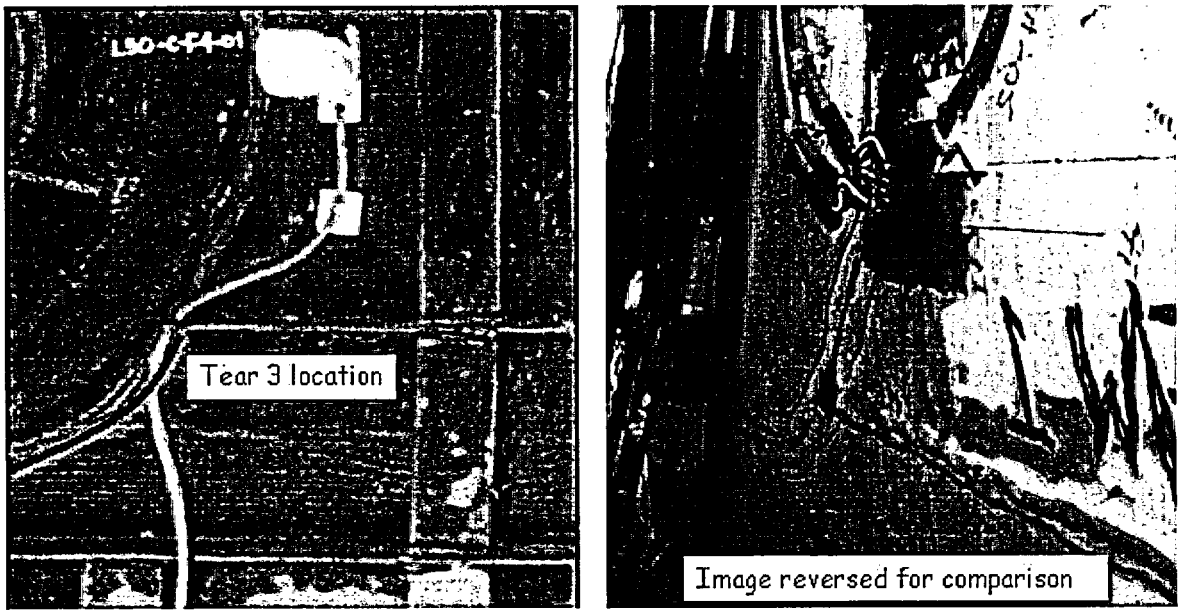

Figure 13. Photographs showing region of tear #3 from outside of liner (left) (prior to concrete placement) and inside of liner (right) (prior to removal of paint).

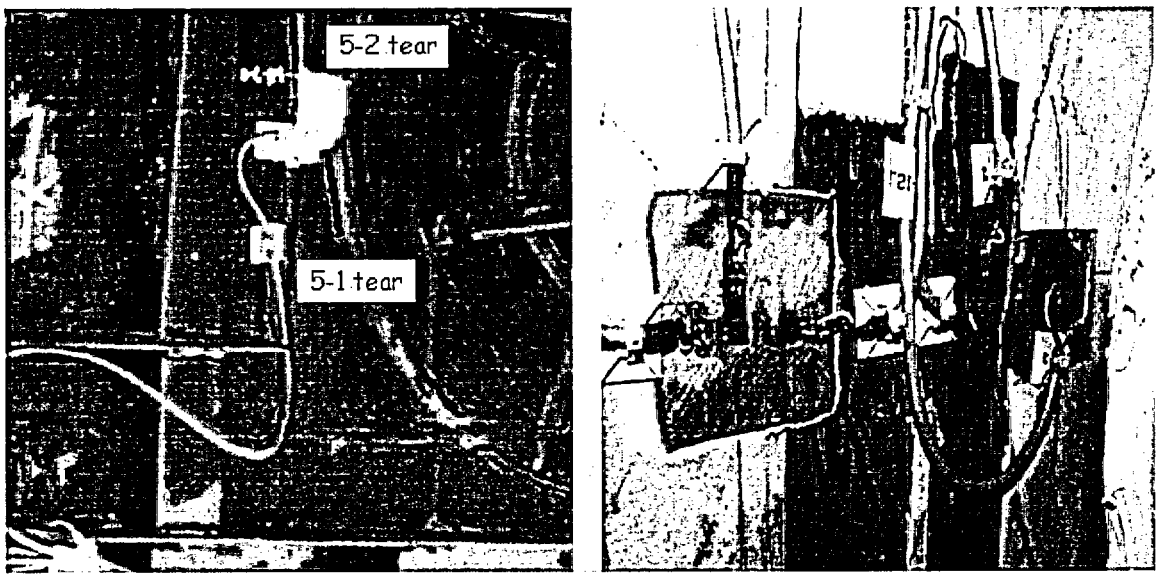

Figure 14. Photographs showing region of tear #5 from outside of liner (left) (prior to concrete placement) and inside of liner (right) (prior to removal of paint).

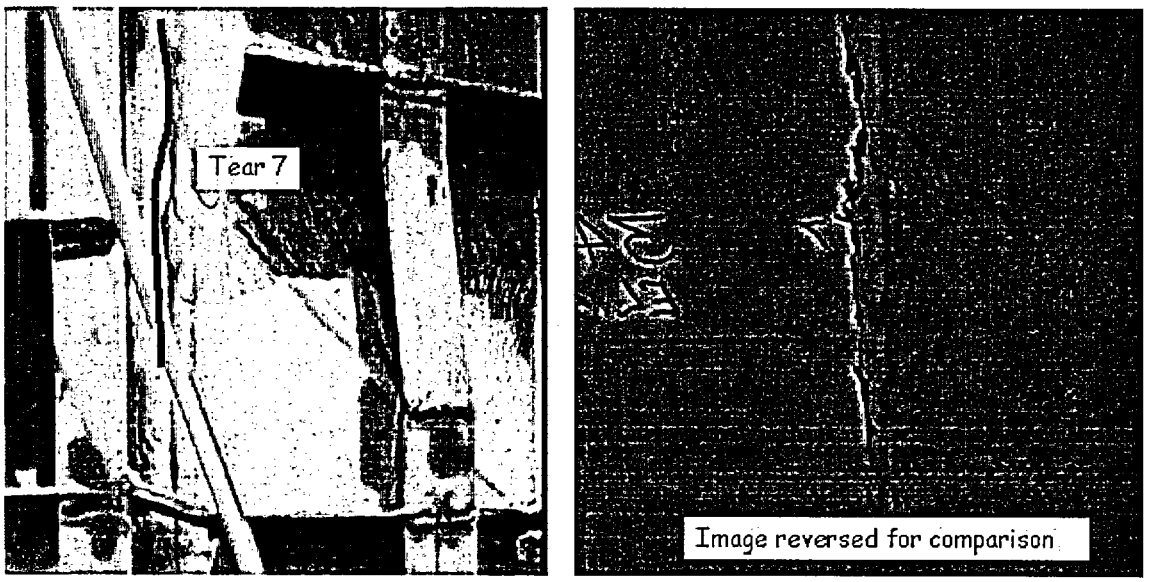

Figure 15. Photographs showing region of tear #7 from outside of liner (left) (prior to concrete placement) and inside of liner (right) (prior to removal of paint).

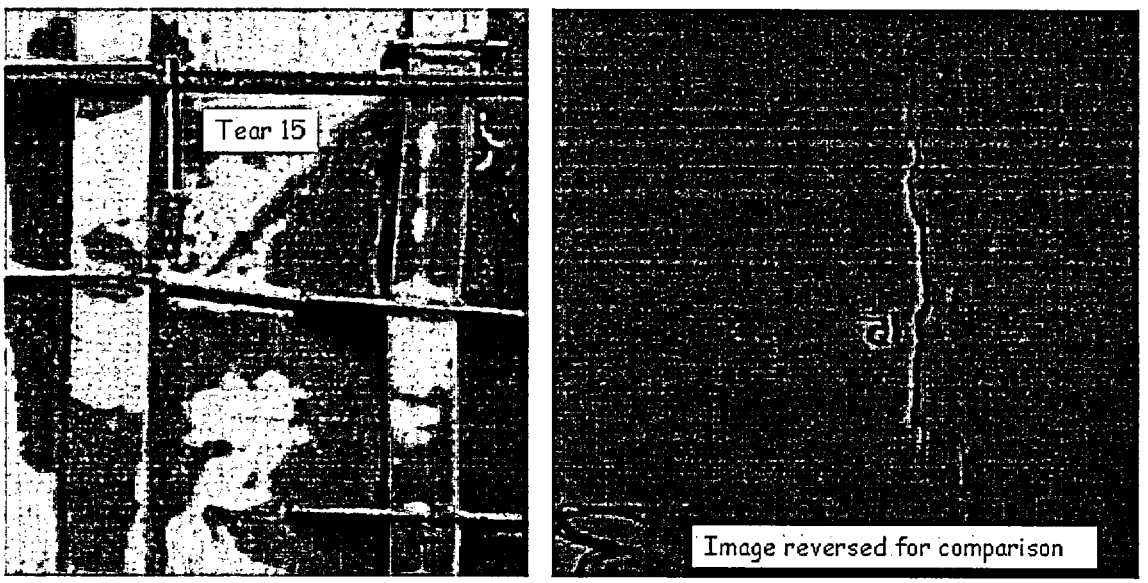

Figure 16. Photographs showing region of tear #15 from outside of liner (left) (prior to concrete placement) and inside of liner (right) (prior to removal of paint).

Figure 17. Photographs showing region of tear #12 from outside of liner (left) (prior to concrete placement) and inside of liner (right) (prior to removal of paint).

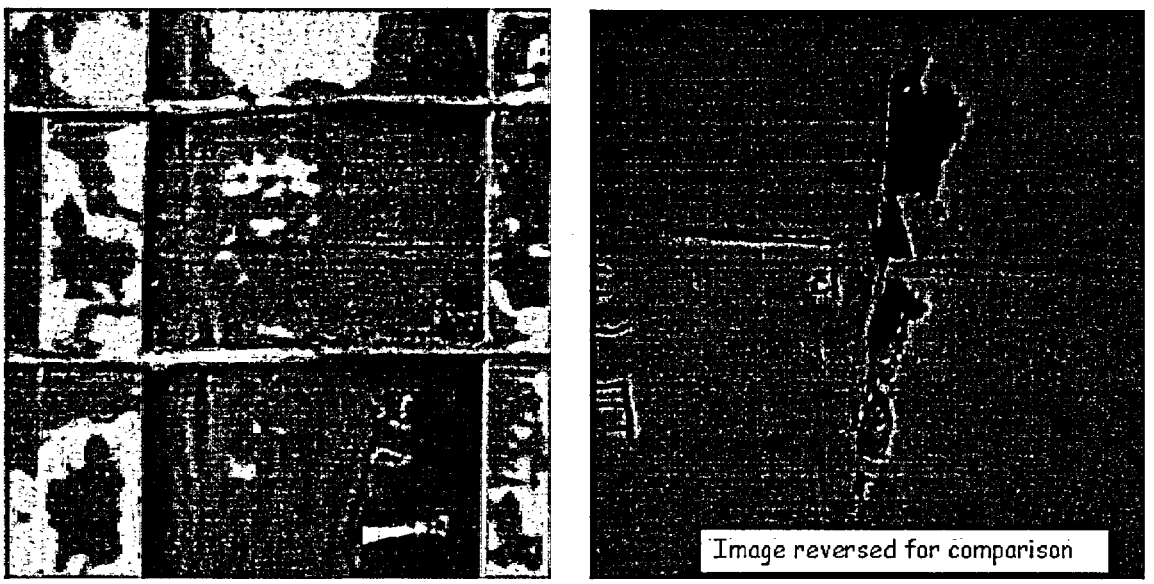

Figure 18. Photographs showing region of tear #13 from outside of liner (left) (prior to concrete placement) and inside of liner (right) (prior to removal of paint).

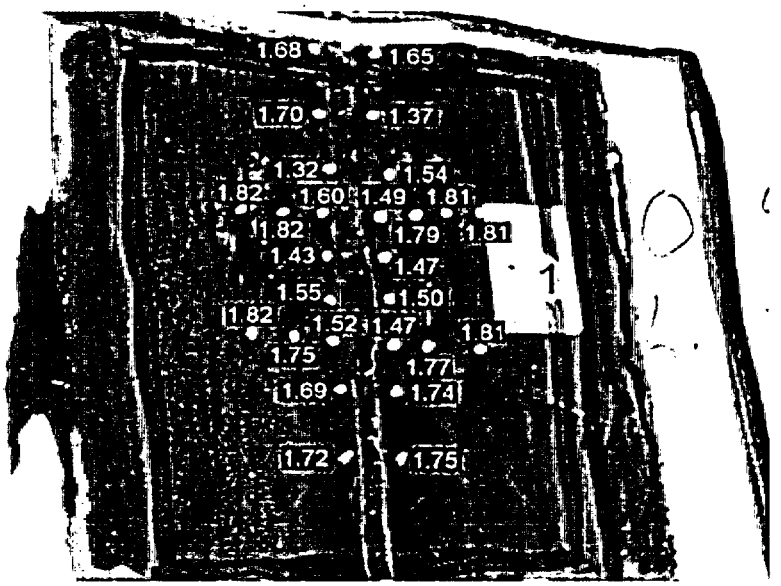

Figure 19. Liner thicknesses (in millimeters) measured ultrasonically in the vicinity of tear #1.

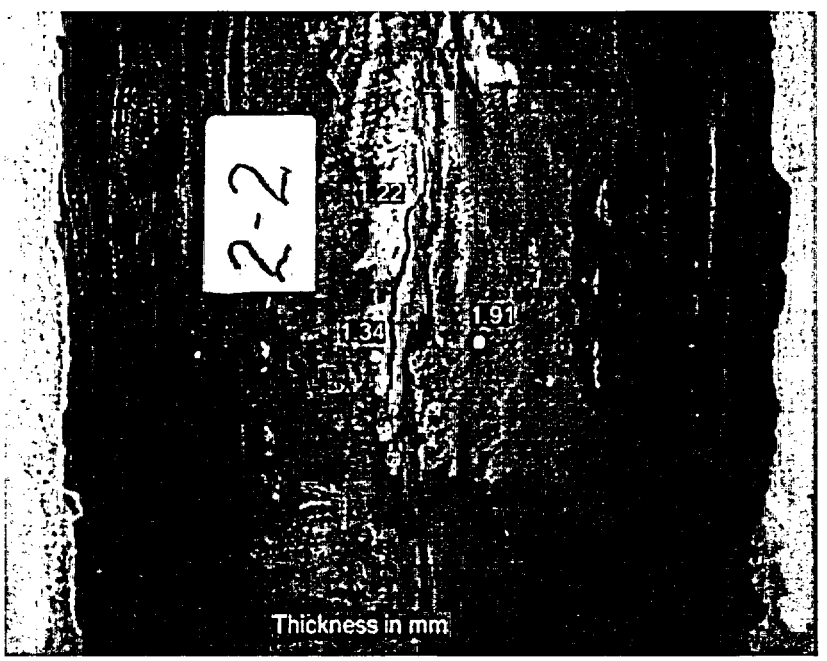

Figure 20. Liner thicknesses (in millimeters) measured ultrasonically in the vicinity of tear #2-2. Note the very wide region of repair welding and grinding. Note also that one measurement is greater than the initial plate thickness due to previous weld repairs.

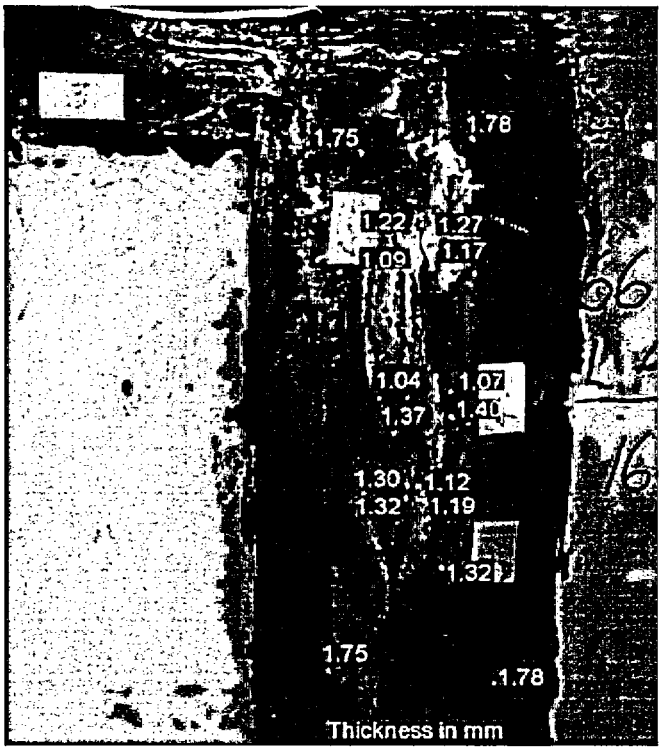

Figure 21. Liner thicknesses (in millimeters) measured ultrasonically in the vicinity of tear #4 (4-1, 4-2, and 4-3).

Figure 22. Liner thicknesses (in millimeters) measured ultrasonically in the vicinity of tear #6-1.

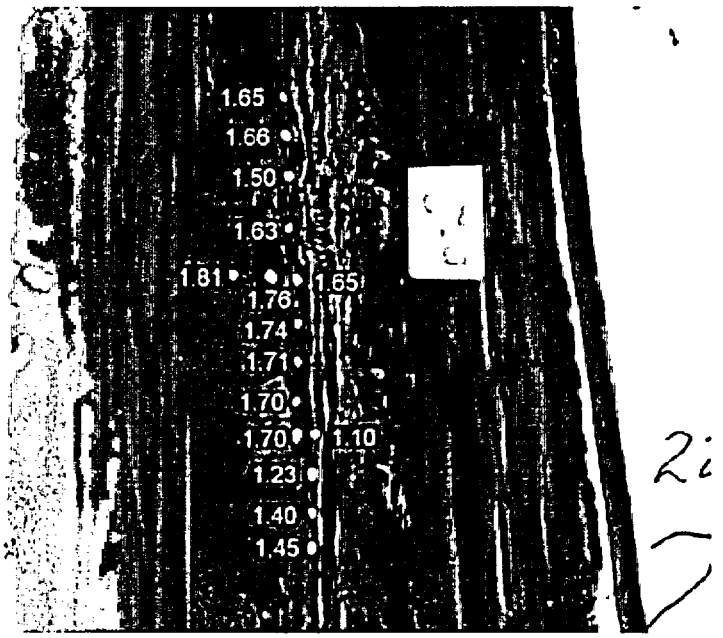

Figure 23. Liner thicknesses (in millimeters) measured ultrasonically in the vicinity of tear #6-2.

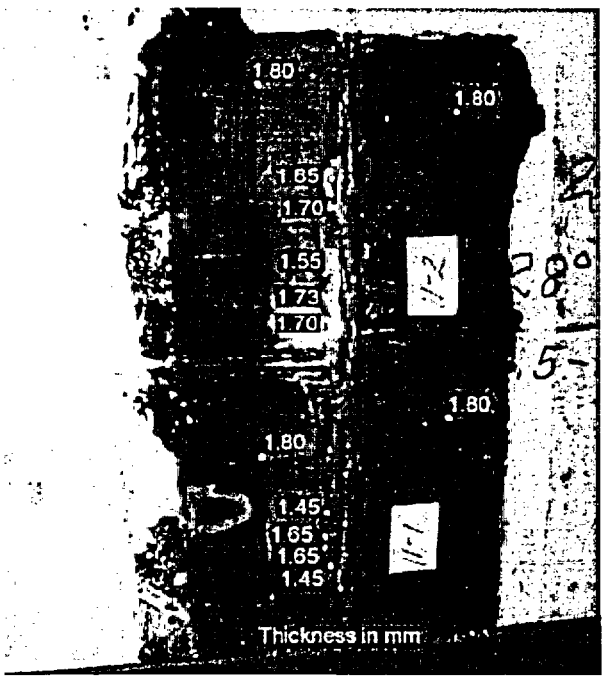

Figure 24. Liner thicknesses (in millimeters) measured ultrasonically in the vicinity of tear #11 (11-1 and 11-2).

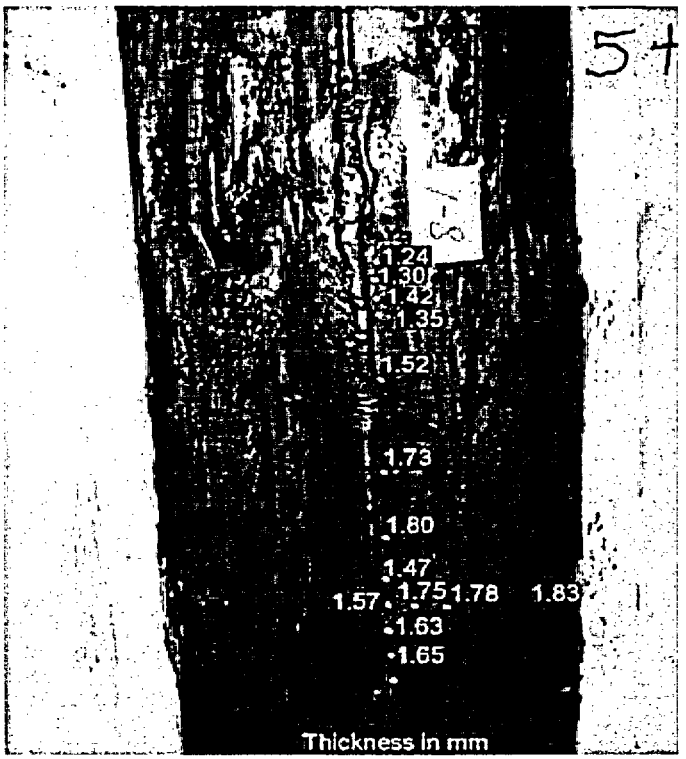

Figure 25. Liner thicknesses (in millimeters) measured ultrasonically in the vicinity of tear #8-1.

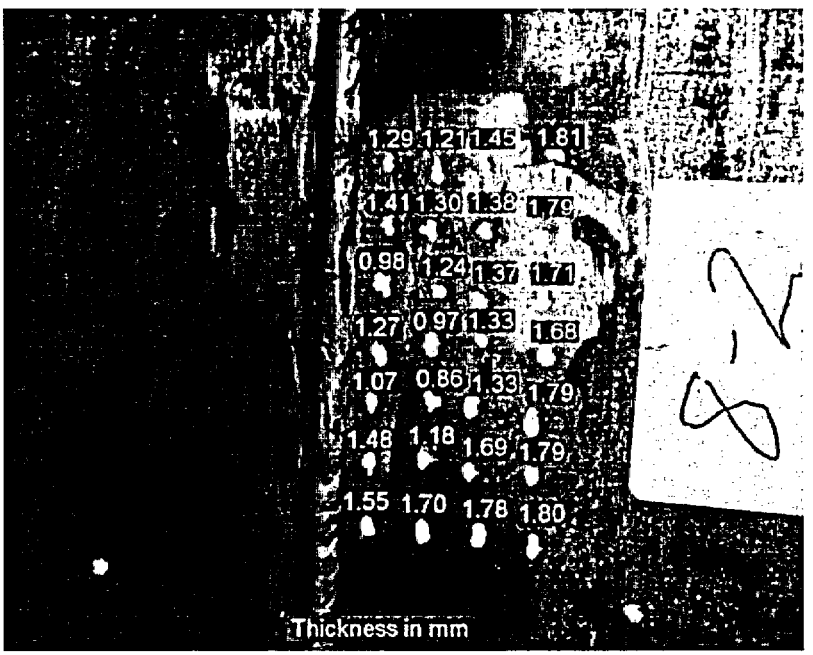

Figure 26. Liner thicknesses (in millimeters) measured ultrasonically in the vicinity of tear #8-2. Note the extensive grinding extending distant from main weld.

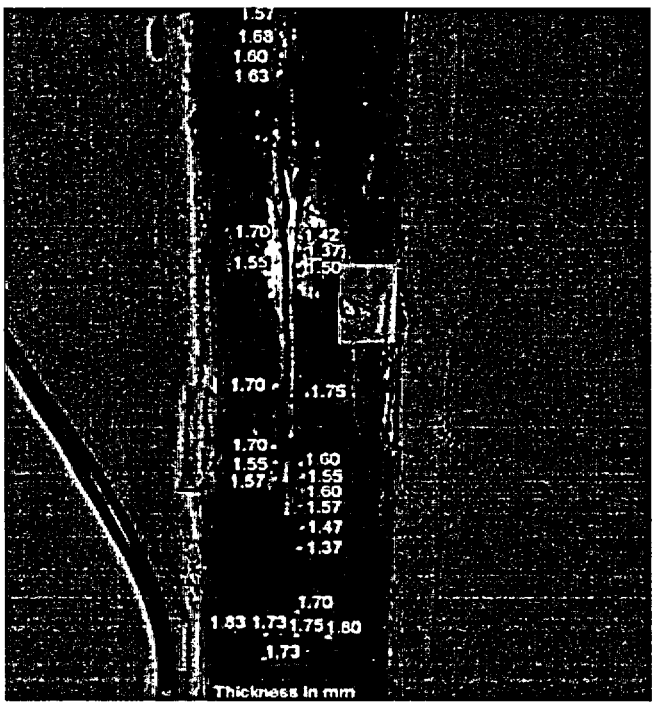

Figure 27. Liner thicknesses (in millimeters) measured ultrasonically in the vicinity of tear #9.

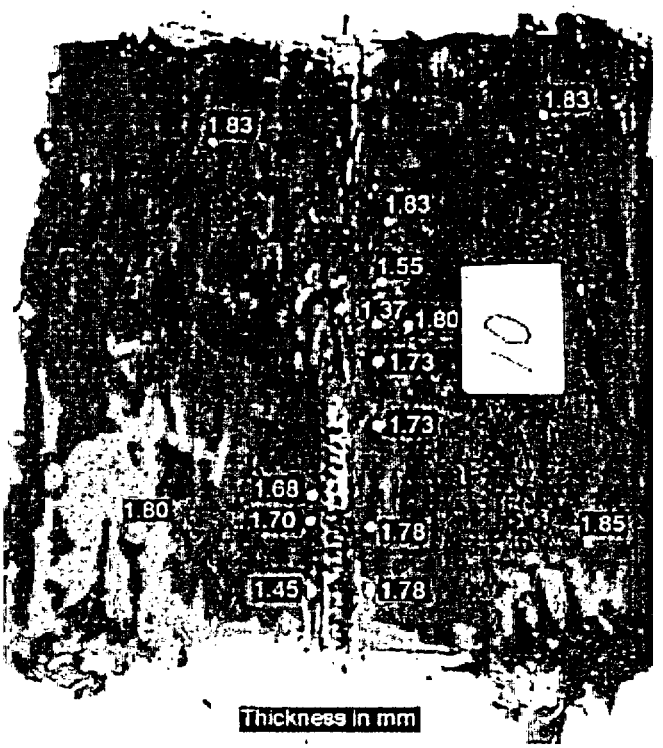

Figure 28. Liner thicknesses (in millimeters) measured ultrasonically in the vicinity of tear #10.

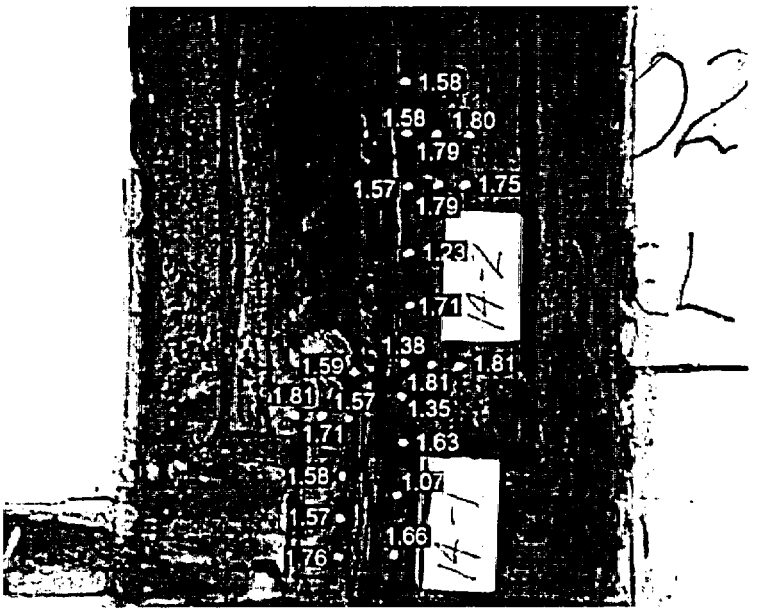

Figure 29. Liner thicknesses (in millimeters) measured ultrasonically in the vicinity of tear #14 (14-1 and 14-2).

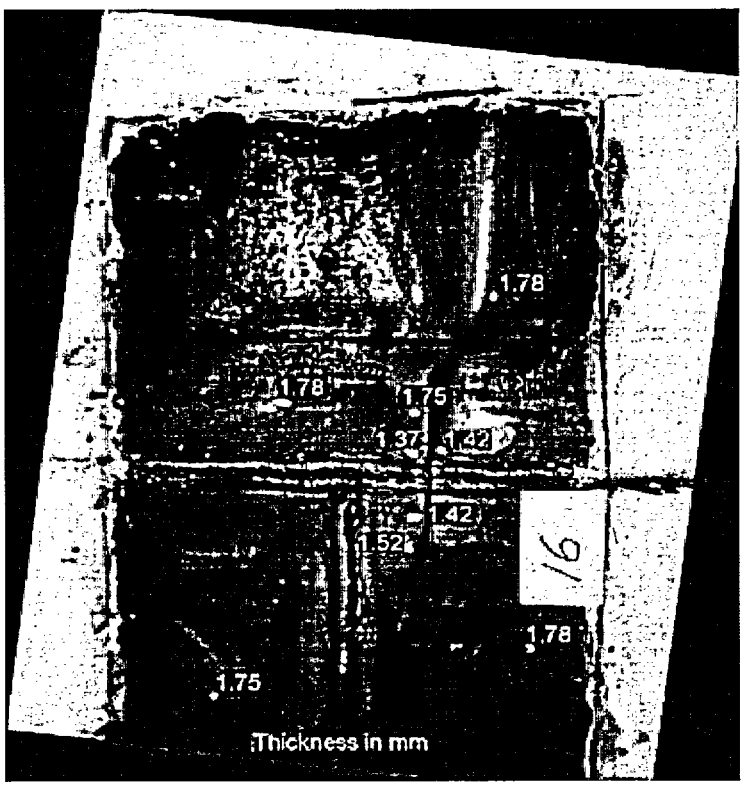

Figure 30. Liner thicknesses (in millimeters) measured ultrasonically in the vicinity of tear #16. Note distance of tear from vertical weld and extensive buckling above tear.

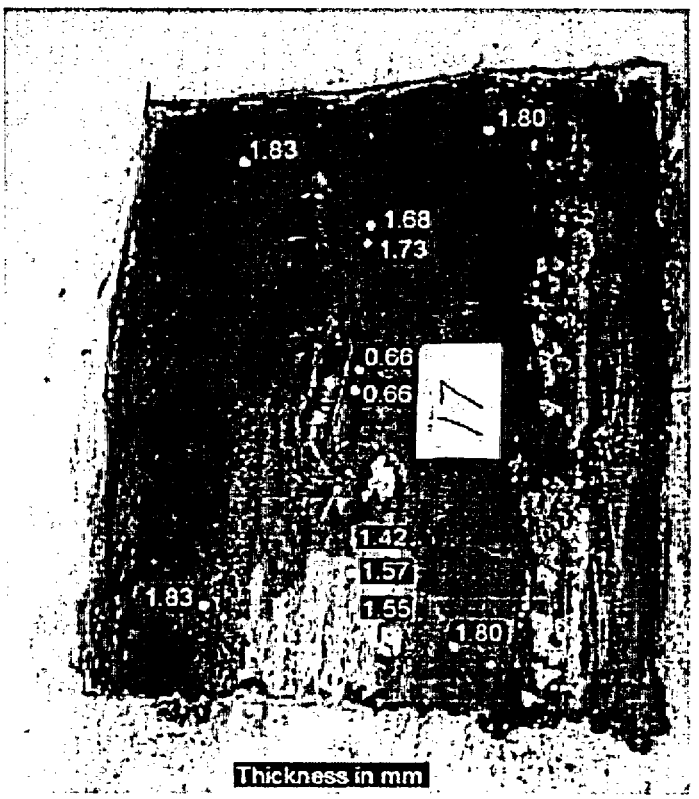

Figure 31. Liner thicknesses (in millimeters) measured ultrasonically in the vicinity of tear #17. Note exceptionally thin areas adjacent to repair weld and tear.

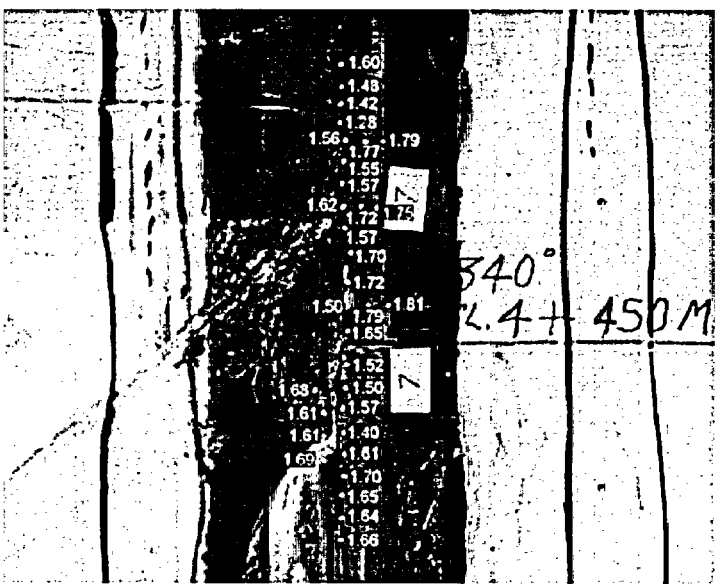

Figure 32. Liner thicknesses (in millimeters) measured ultrasonically in the vicinity of tear #7.

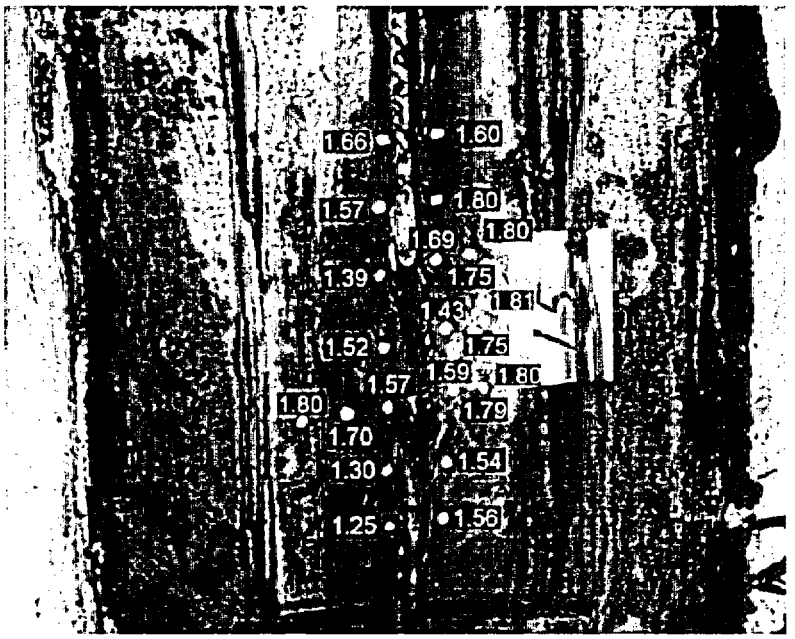

Figure 33. Liner thicknesses (in millimeters) measured ultrasonically in the vicinity of tear #15.

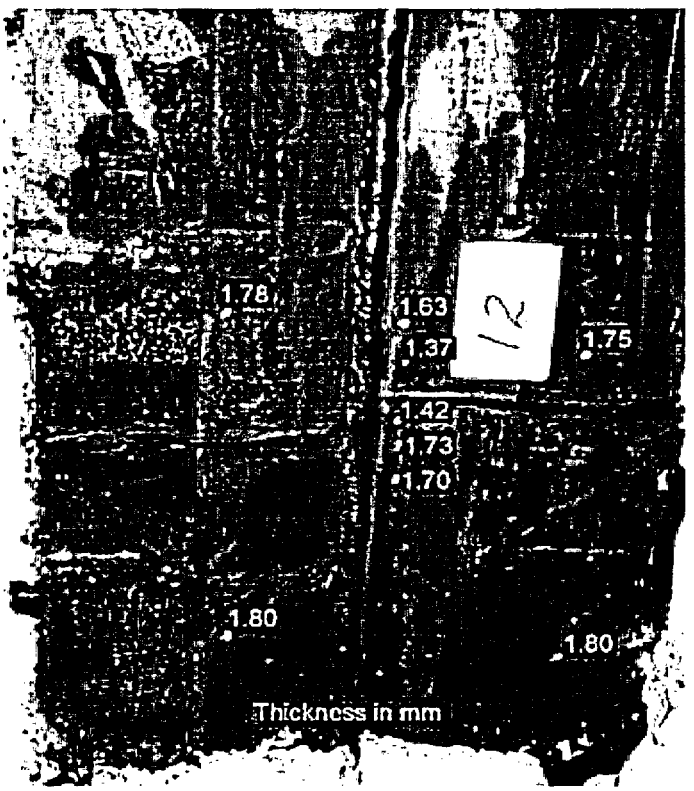

Figure 34. Liner thicknesses (in millimeters) measured ultrasonically in the vicinity of tear #12.

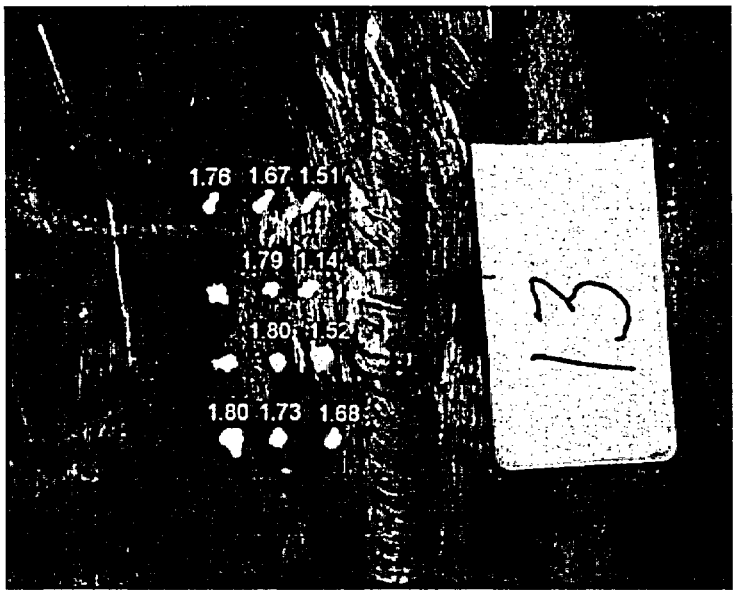

Figure 35. Liner thicknesses (in millimeters) measured ultrasonically in the vicinity of tear #13.

Figure 36. Liner thicknesses (in millimeters) measured ultrasonically in region #18. Buckling and "orange-peel" evidence of substantial plastic deformation, but no tearing, was apparent in this area.

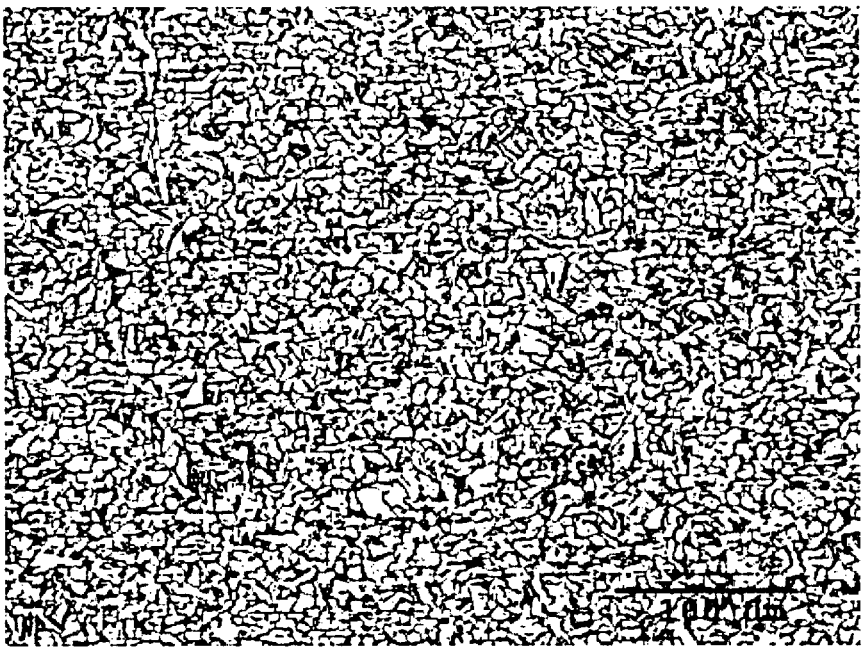

Figure 37. Microstructure of base metal in practice weld panel. Microstructure consists of ferrite (light) and pearlite (dark), typical of hot rolled carbon steel plate. Note the presence of chemical banding parallel to the rolling plane of the plate.

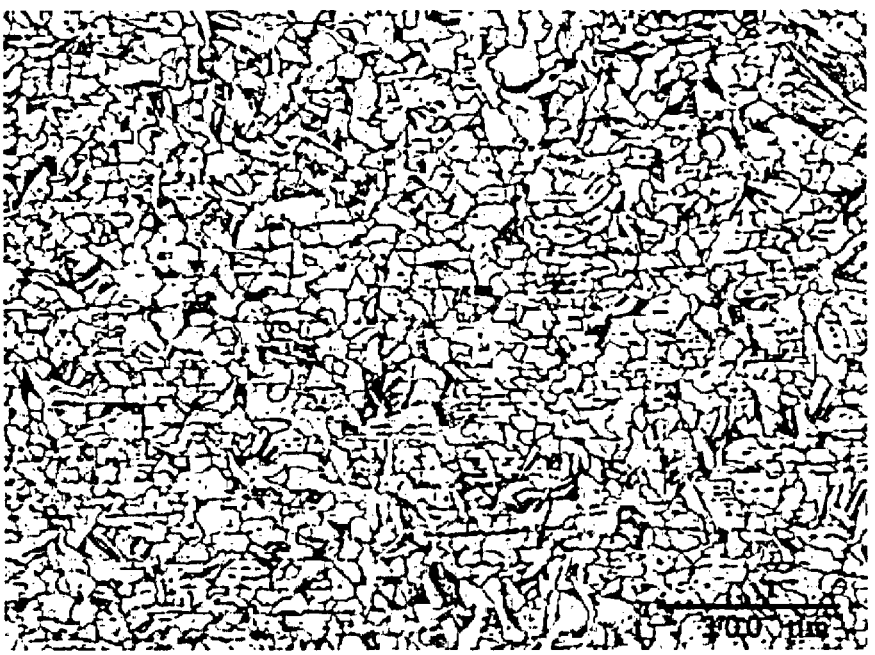

Figure 38. Microstructure of fine-grained portion of heat affected zone (several millimeters from weld) in practice weld panel. Microstructure consists of ferrite (light) and pearlite (dark). Note that the chemical banding persists in this region, indicating that the material, while re-austenitized, had not been heated to a high temperature in the austenite region.

Figure 39. Microstructure of coarse-grained portion of heat affected zone (very close to weld) in practice weld panel. Microstructure consists of acicular ferrite (light) and pearlite (dark), typical of material that had been austenitized at high temperature and cooled fairly rapidly. Note that the chemical banding is no longer present in this region, indicating that the material had been heated to a high temperature in the austenite region.

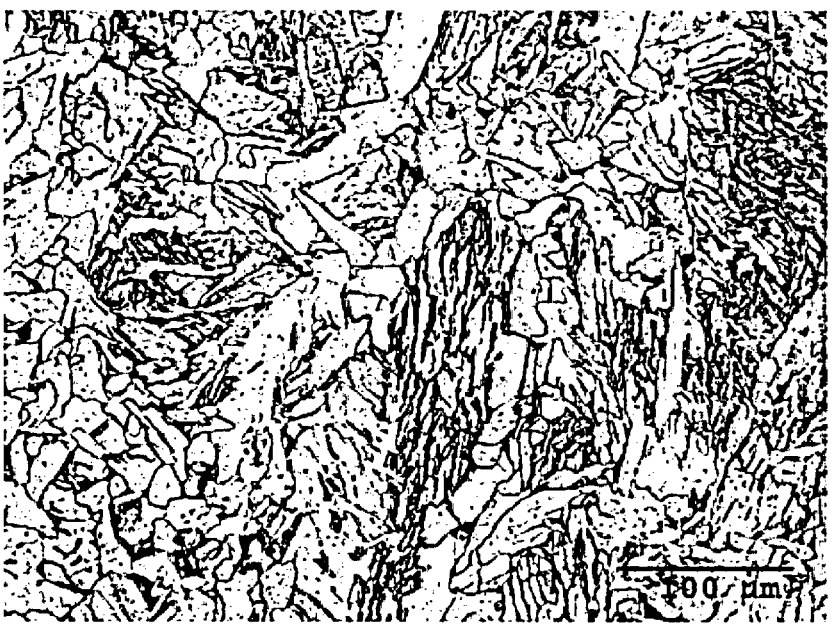

Figure 40. Microstructure of as-solidified fusion zone in practice weld panel. Microstructure consists of columnar prior austenite grains (characteristic of melted and resolidified material) that have transformed on cooling to ferrite and pearlite.

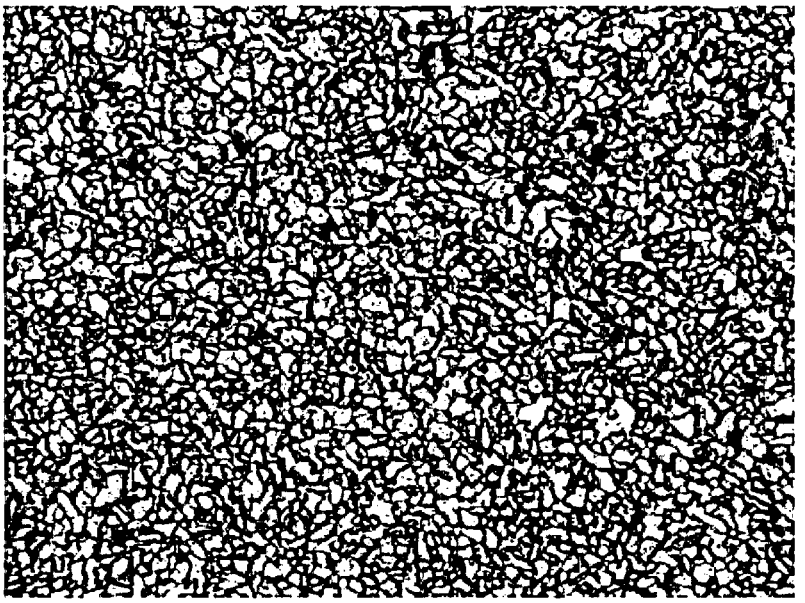

Figure 41. Microstructure of portion of fusion zone that has been re-austenitized during a second weld pass. Note that prior austenite grains have recrystallized, eliminating the columnar appearance, then transformed on cooling to ferrite and pearlite similar in appearance to the fine grained portion of the heat affected zone, but without chemical banding.

Figure 42. Scanning electron micrograph of fracture surface from tensile sample without any weld. Microvoids indicate that failure occurred by ductile rupture, typical of tearing of mild steel plate following extensive plastic deformation.

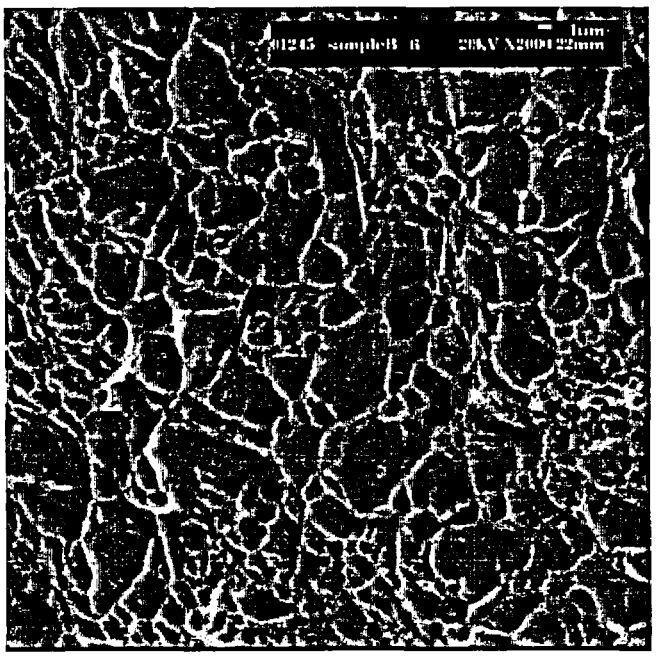

Figure 43. Scanning electron micrograph of fracture surface from welded tensile sample with lack of fusion defect. The location pictured is away from the weld defect, here deformation and fracture occurred in the heat affected zone. Failure here also occurred by ductile rupture.

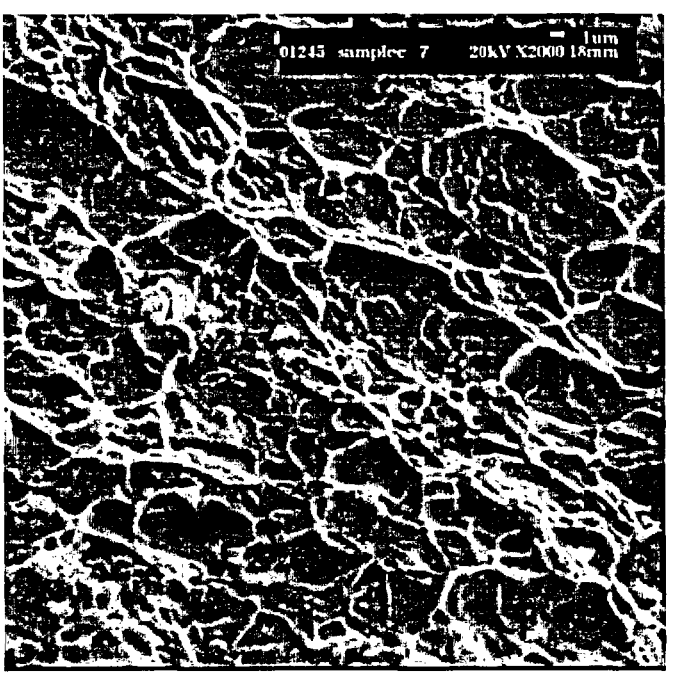

Figure 44. Scanning electron micrograph of fracture surface from welded tensile sample with substantial offset between plates. Failure here also occurred by ductile rupture.

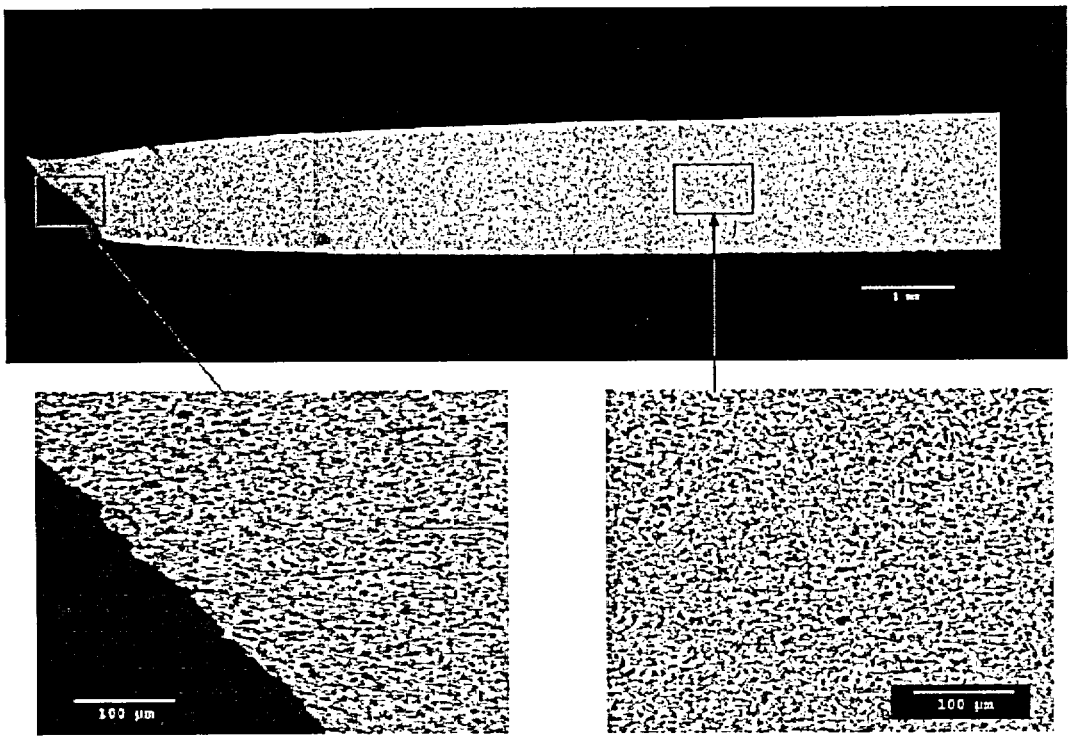

Figure 45. Metallographic cross-section of tensile sample of unwelded base metal (Sample A-3).

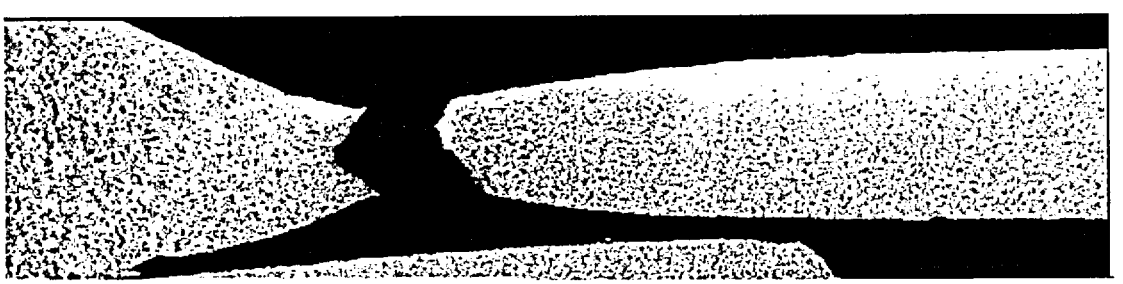

Figure 46. Metallographic cross-section of tensile sample from practice weld panel in area without substantial offset between plates (Sample B-2). This sample broke along the fusion line at an apparent lack of fusion defect. Cross-section is not through defect, but through a sound region adjacent to the defect where ductile tearing occurred.

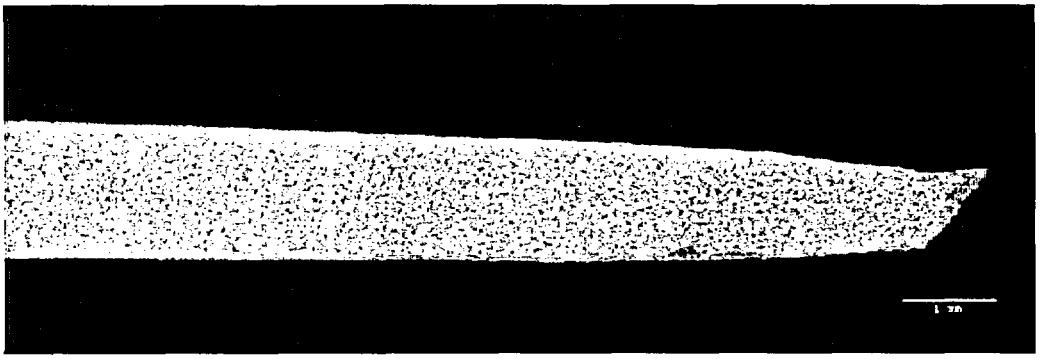

Figure 47. Metallographic cross-section of tensile sample from practice weld panel in area with substantial offset between plates (Sample C-1).

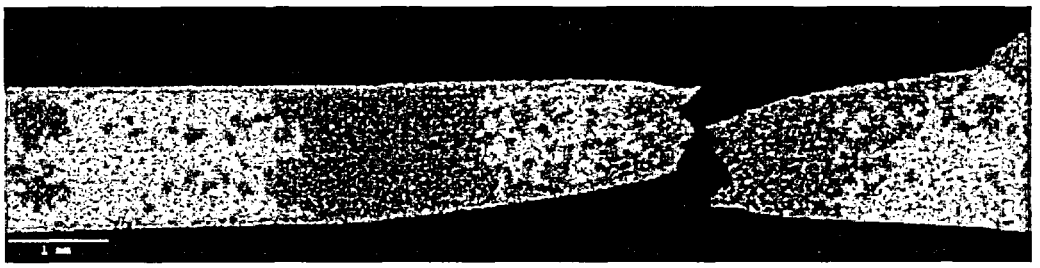

Figure 48. Metallographic cross-section of tensile sample from practice weld panel in area with substantial offset between plates (Sample C-2).

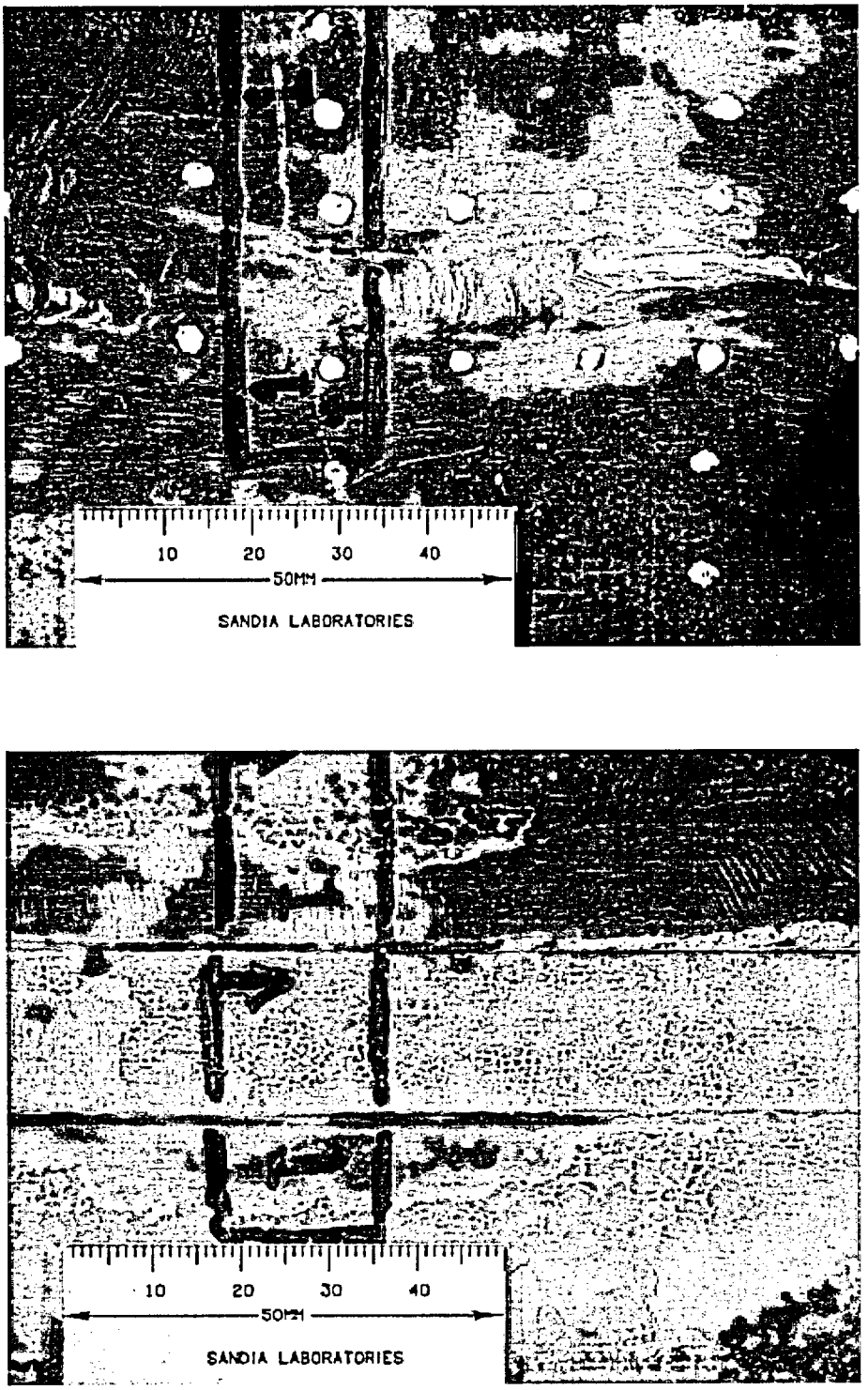

Figure 49. Details of inside (top) and outside (bottom) liner features in region of tear #1 metallographic cross-section (arrows begin at plane of section and indicate view direction).

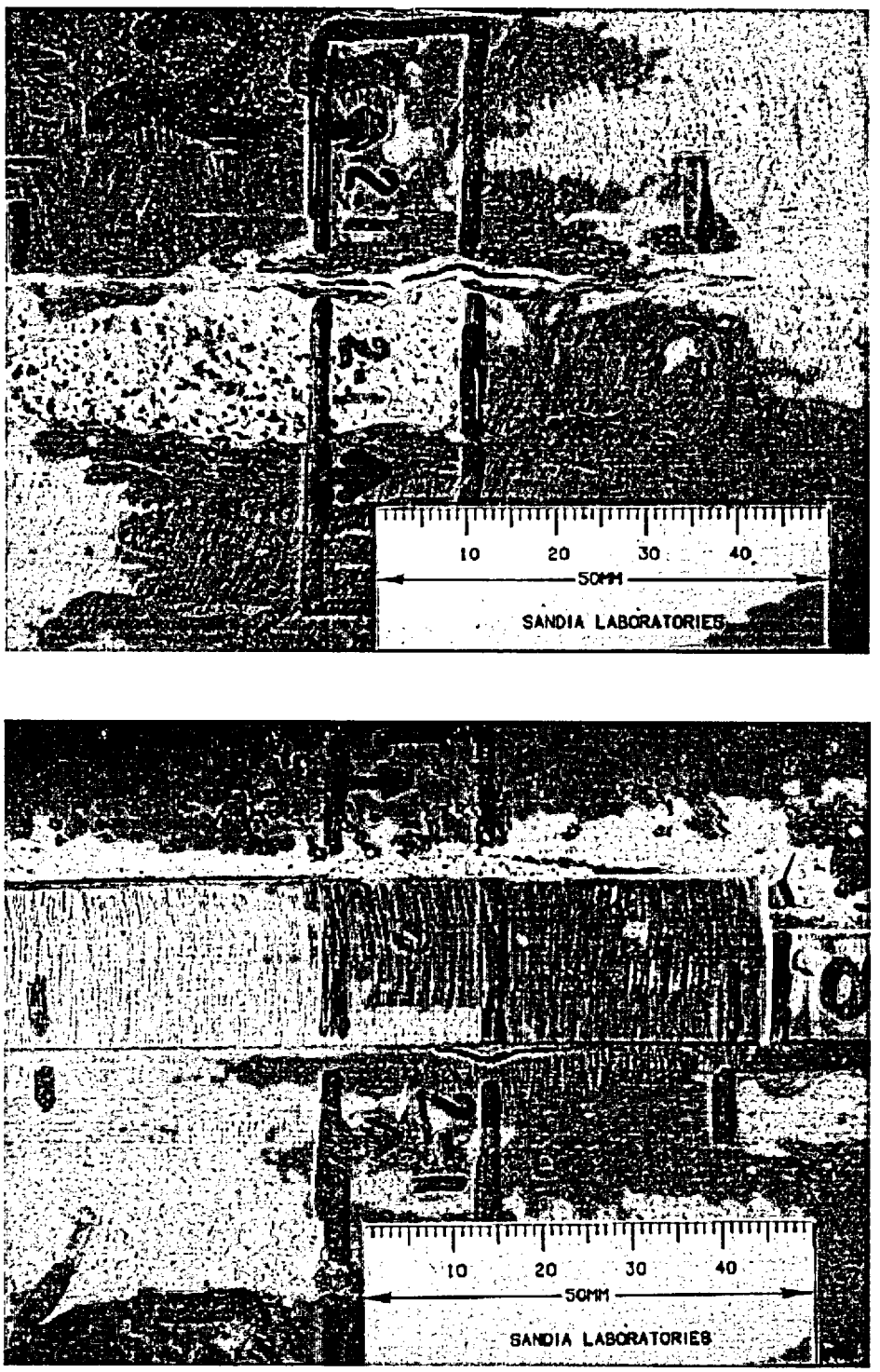

Figure 50. Details of inside (top) and outside (bottom) liner features in region of tear #2-1 metallographic cross-section (arrows begin at plane of section and indicate view direction).

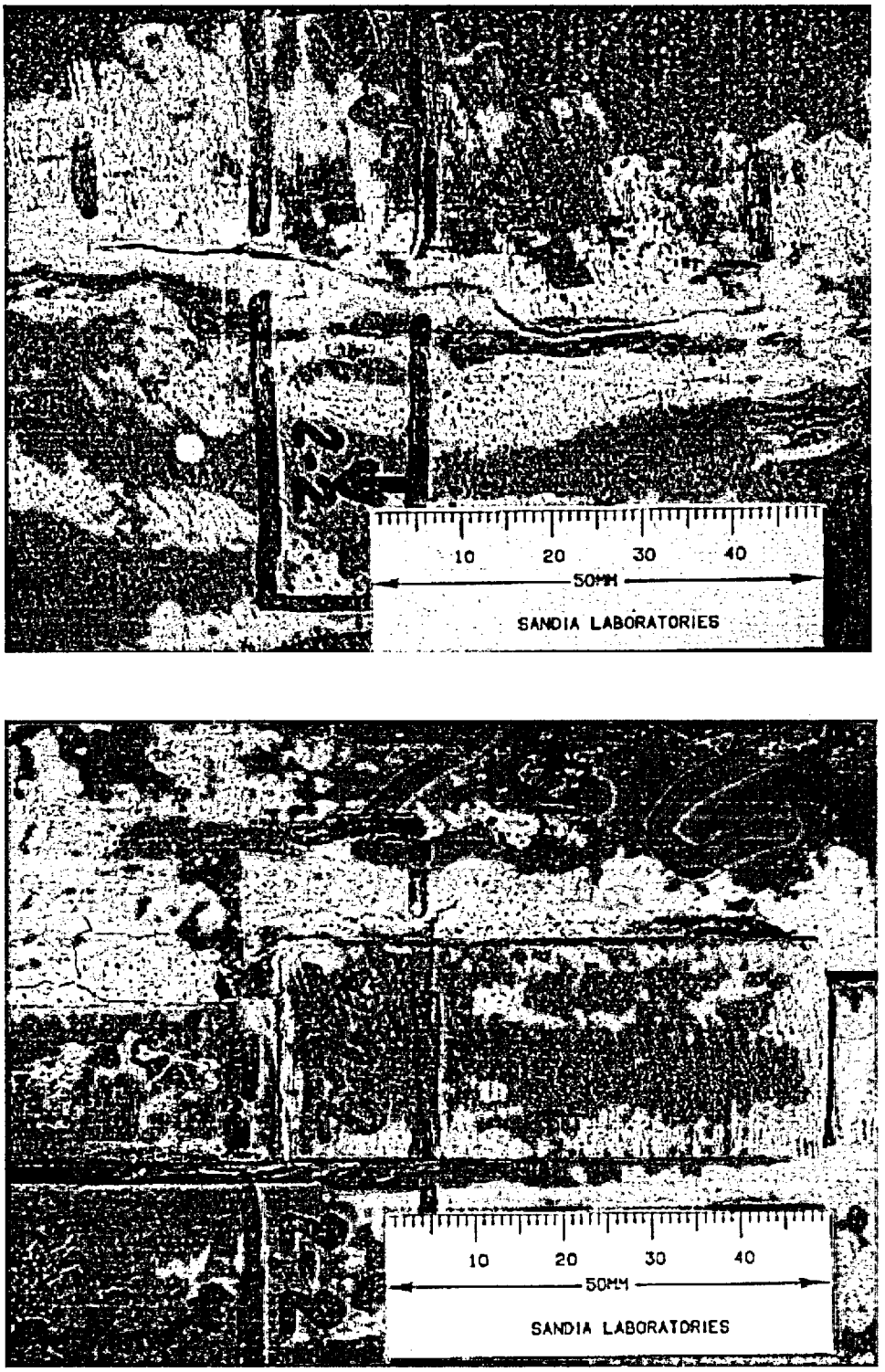

Figure 51. Details of inside (top) and outside (bottom) liner features in region of tear #2-2 metallographic cross-section (arrows begin at plane of section and indicate view direction).

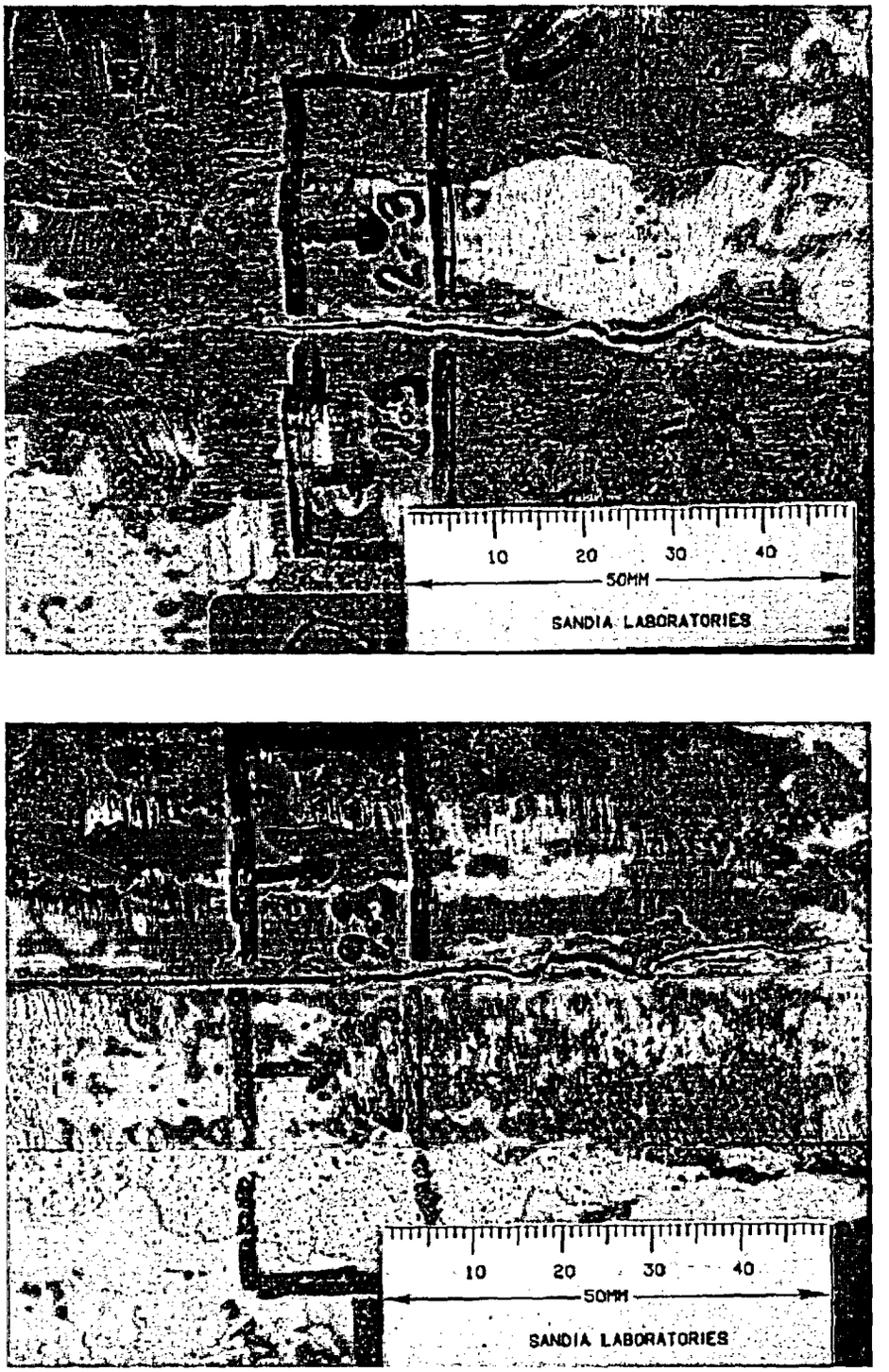

Figure 52. Details of inside (top) and outside (bottom) liner features in region of tear #2-3 metallographic cross-section (arrows begin at plane of section and indicate view direction).

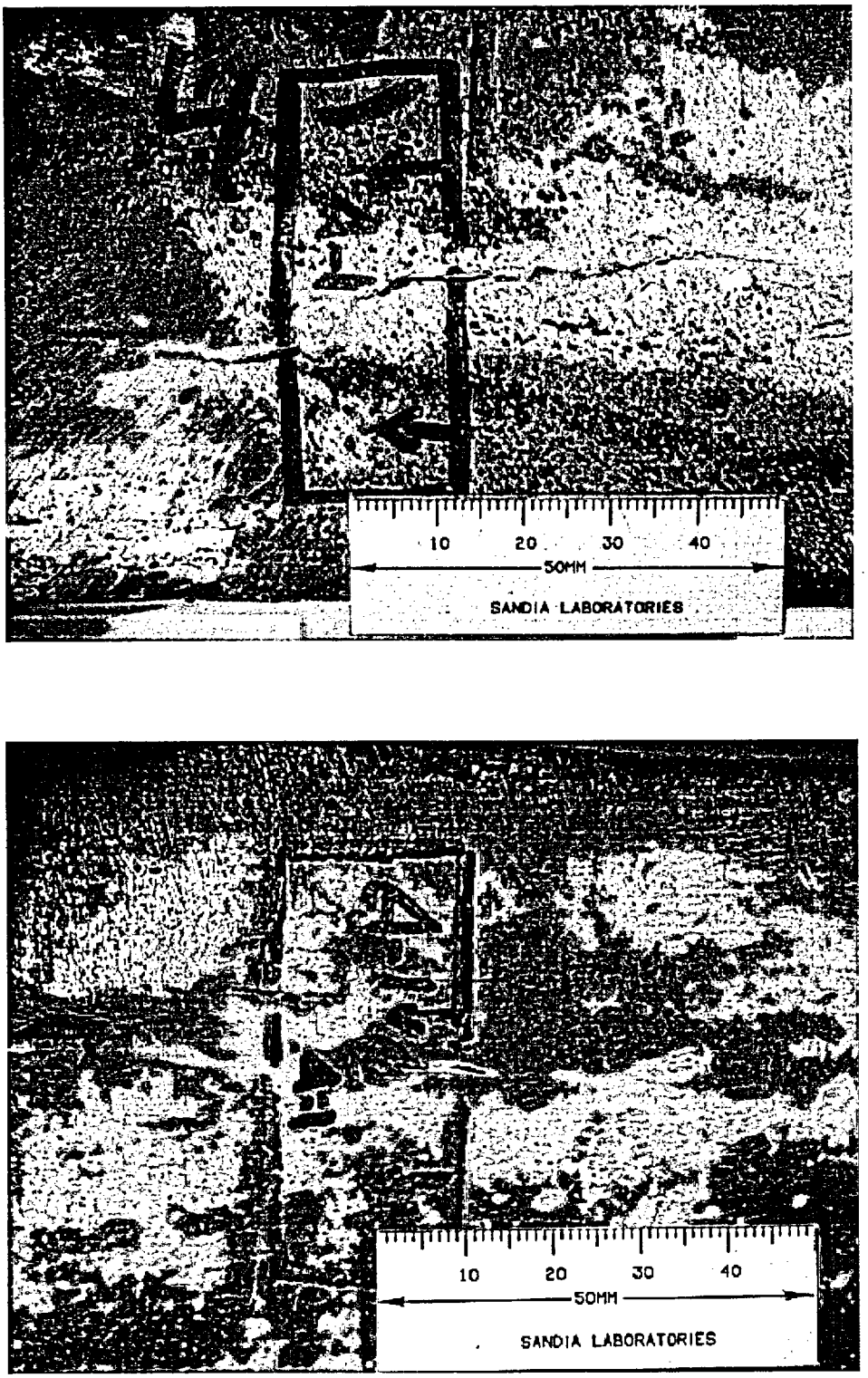

Figure 53. Details of inside (top) and outside (bottom) liner features in region of tear #4-1 metallographic cross-section (arrows begin at plane of section and indicate view direction).

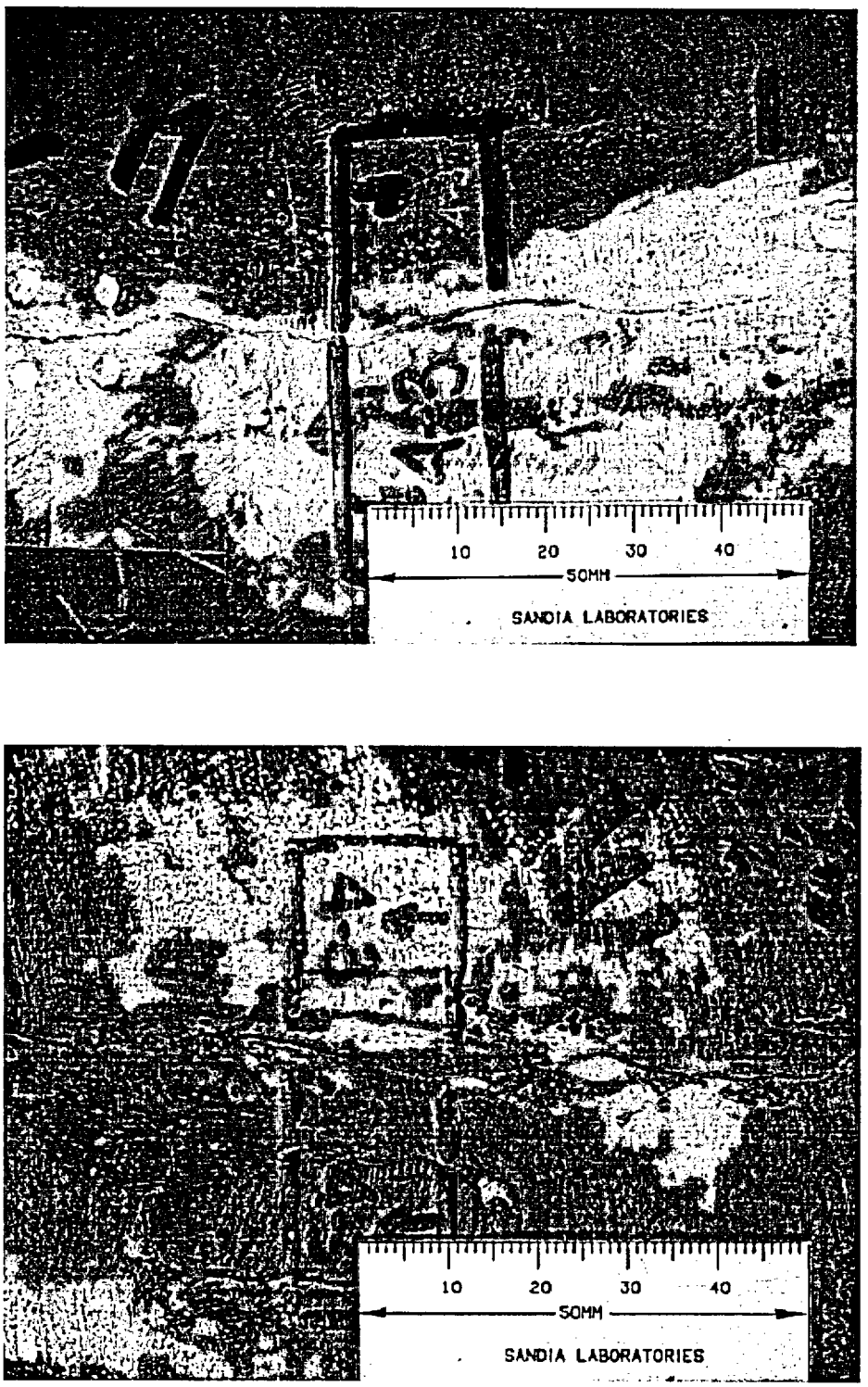

Figure 54. Details of inside (top) and outside (bottom) liner features in region of tear #4-3 metallographic cross-section (arrows begin at plane of section and indicate view direction).

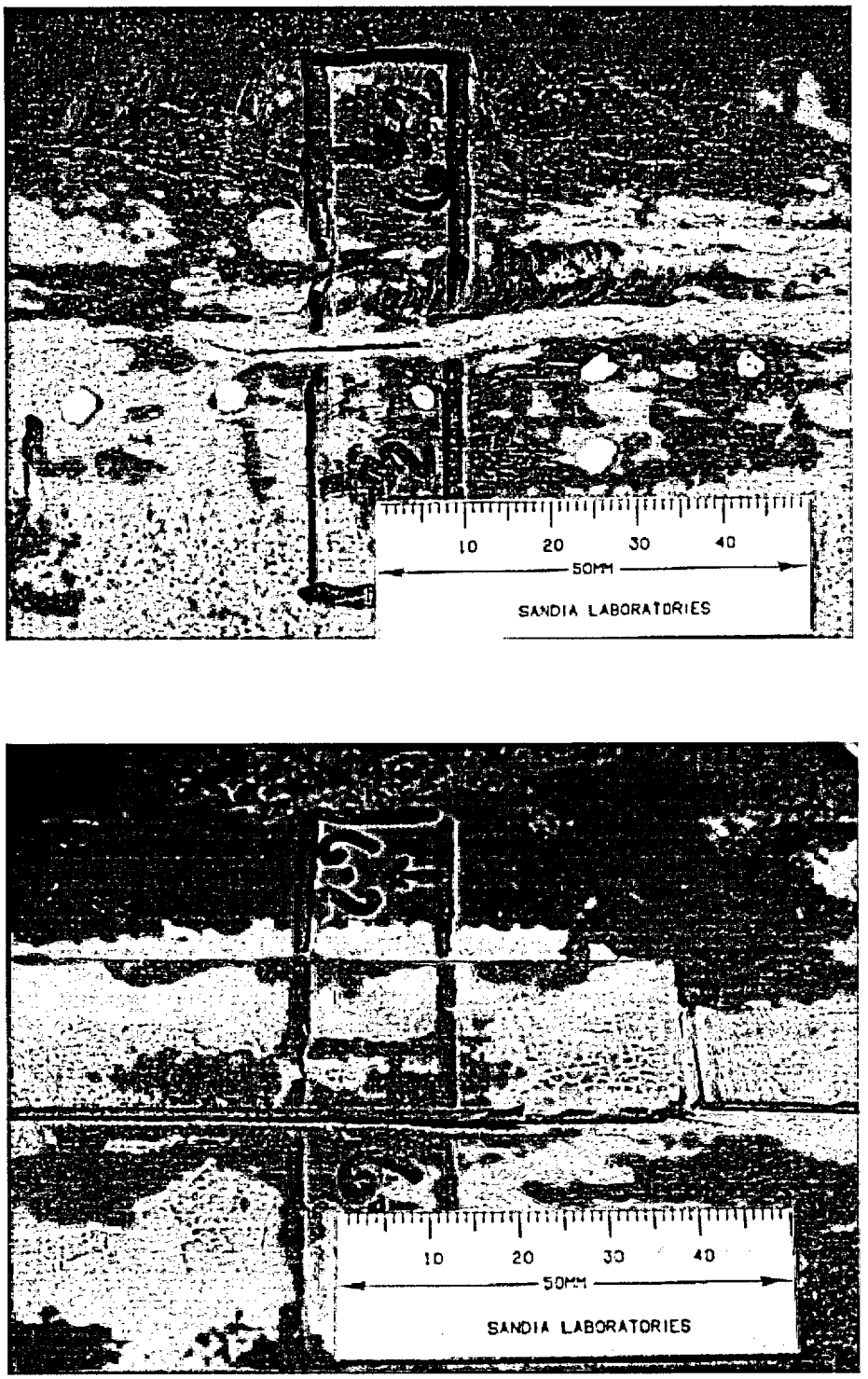

Figure 55. Details of inside (top) and outside (bottom) liner features in region of tear #6-2 metallographic cross-section (arrows begin at plane of section and indicate view direction).

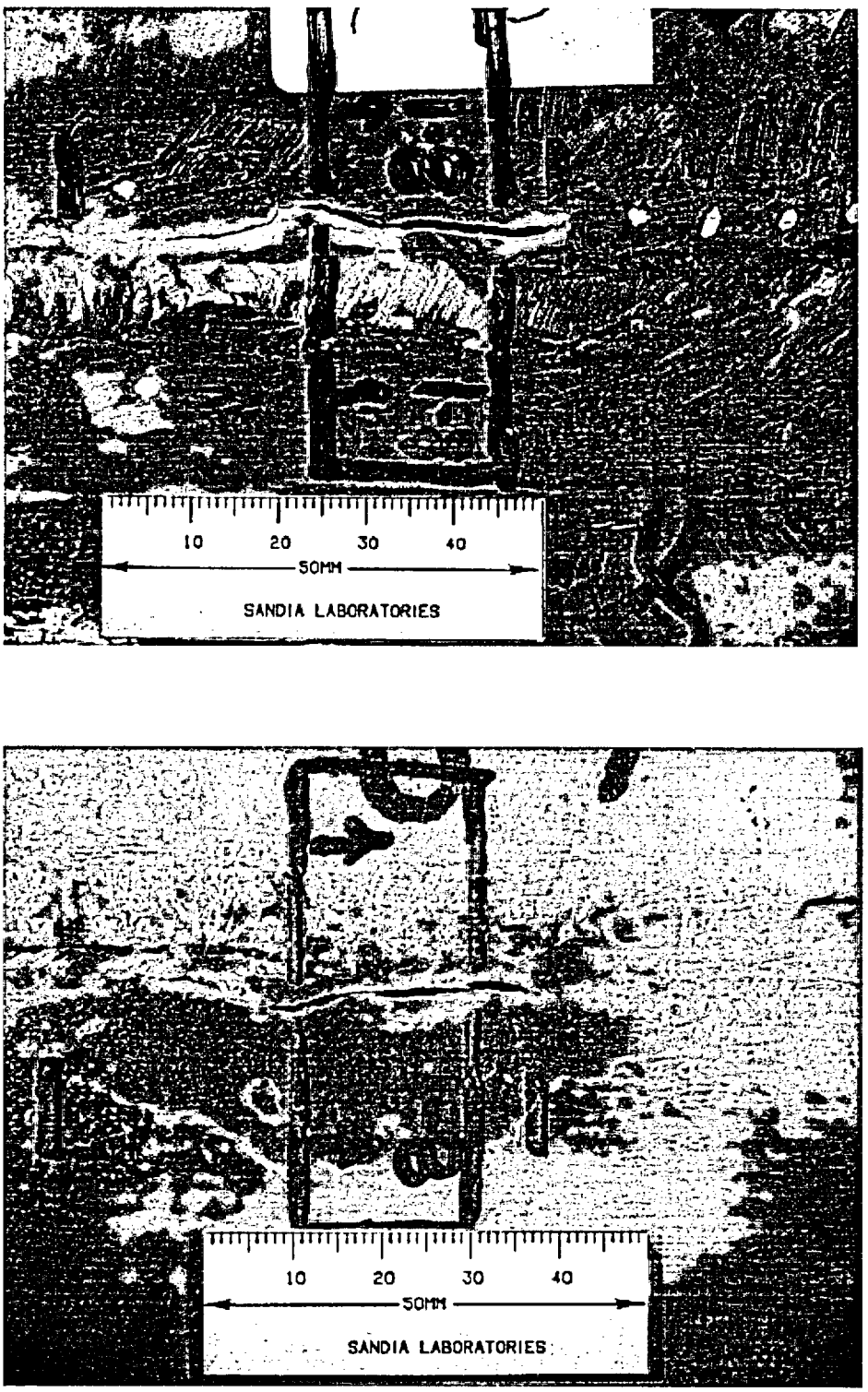

Figure 56. Details of inside (top) and outside (bottom) liner features in region of tear #8-1 metallographic cross-section (arrows begin at plane of section and indicate view direction).

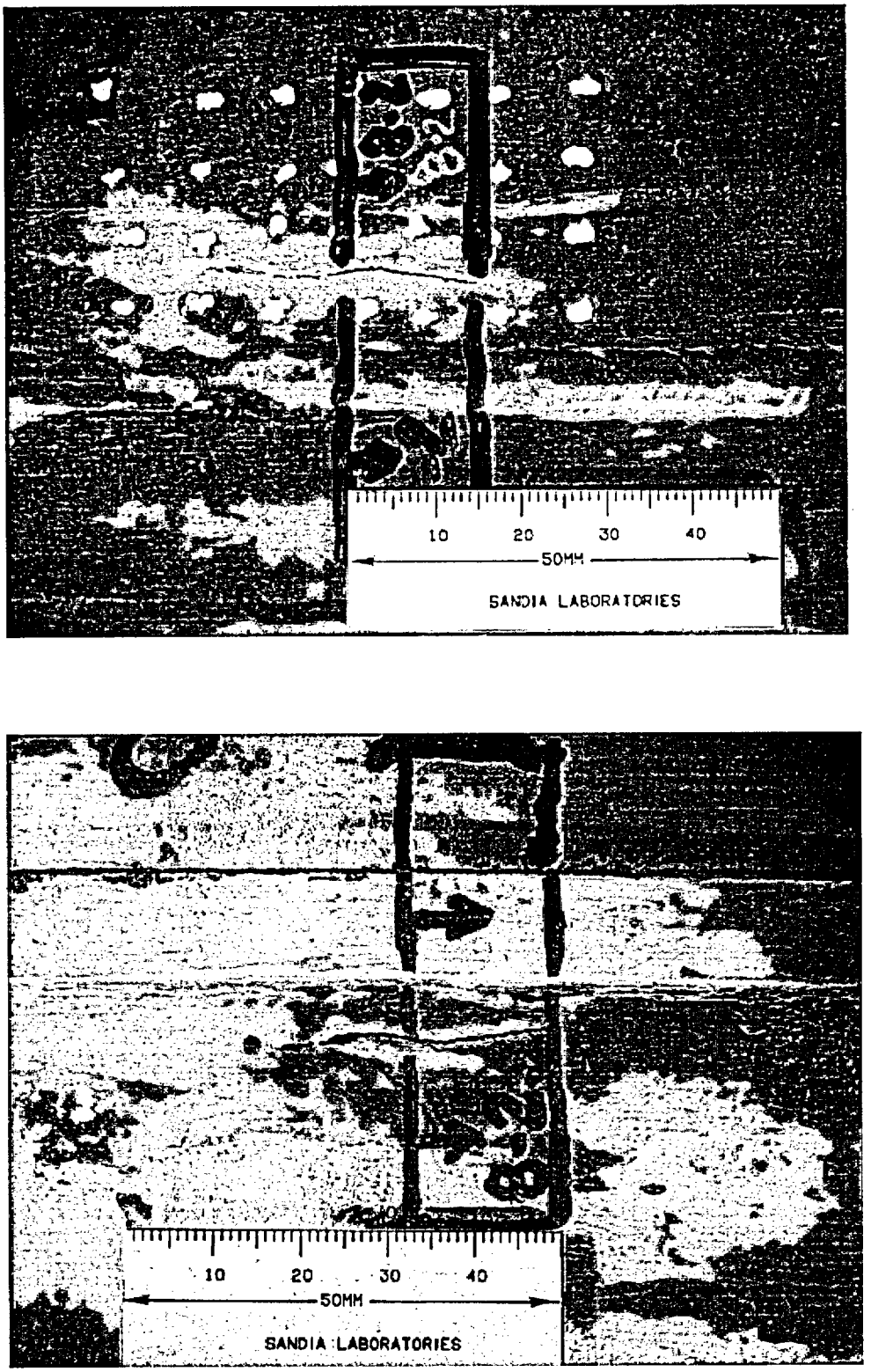

Figure 57. Details of inside (top) and outside (bottom) liner features in region of tear #8-2 metallographic cross-section (arrows begin at plane of section and indicate view direction).

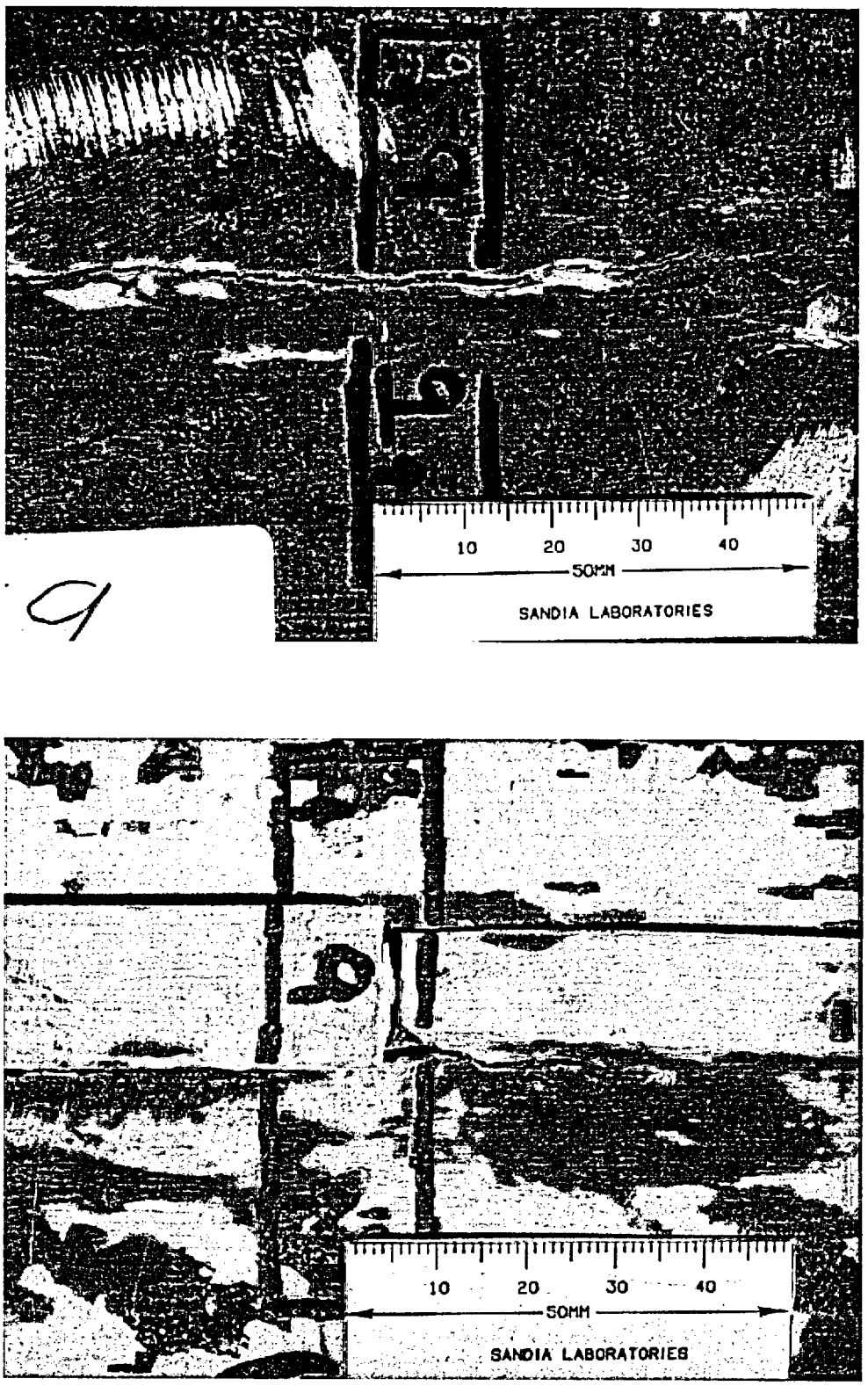

Figure 58. Details of inside (top) and outside (bottom) liner features in region of tear #9 metallographic cross-section (arrows begin at plane of section and indicate view direction).

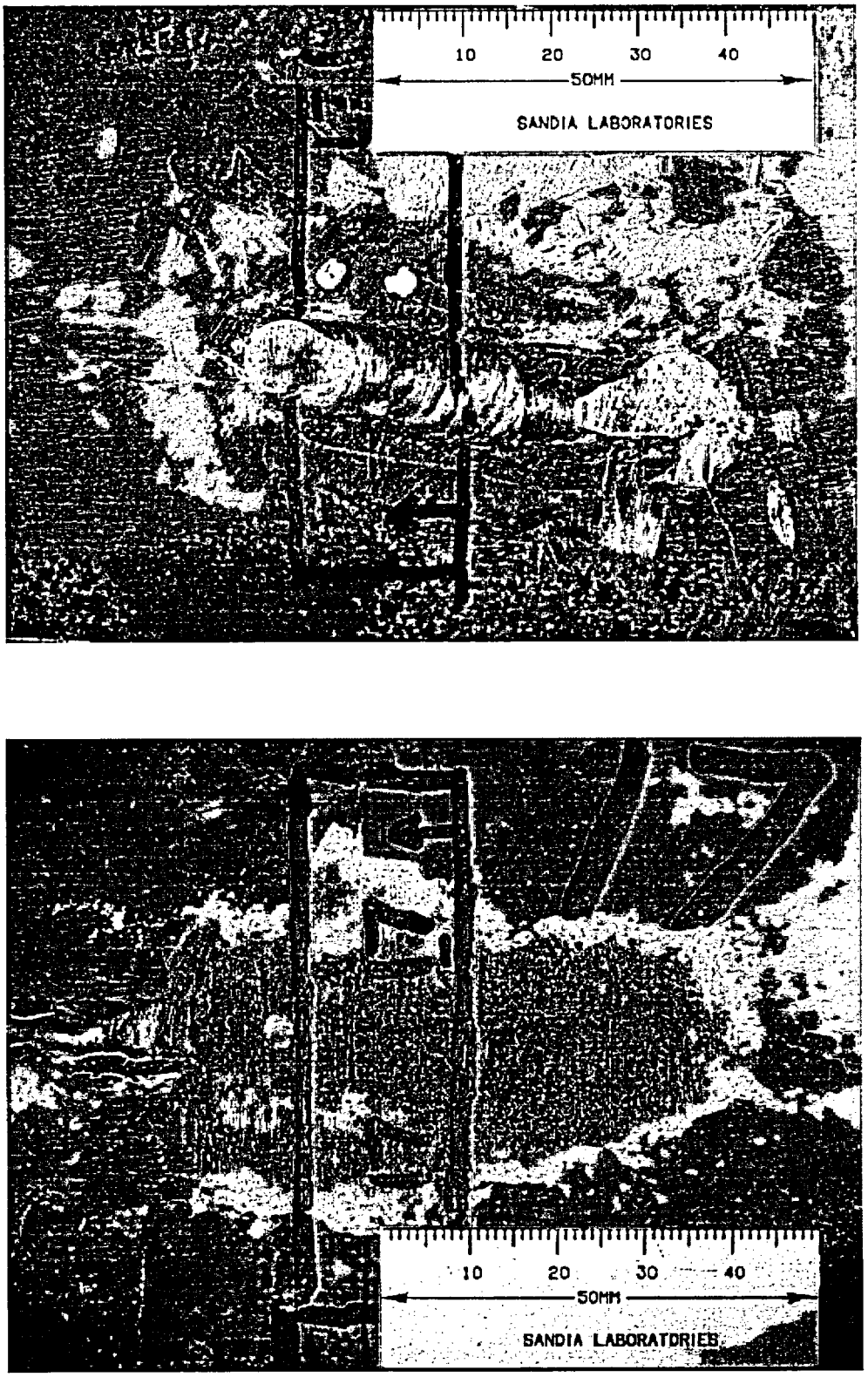

Figure 59. Details of inside (top) and outside (bottom) liner features in region of tear #17 metallographic cross-section (arrows begin at plane of section and indicate view direction).

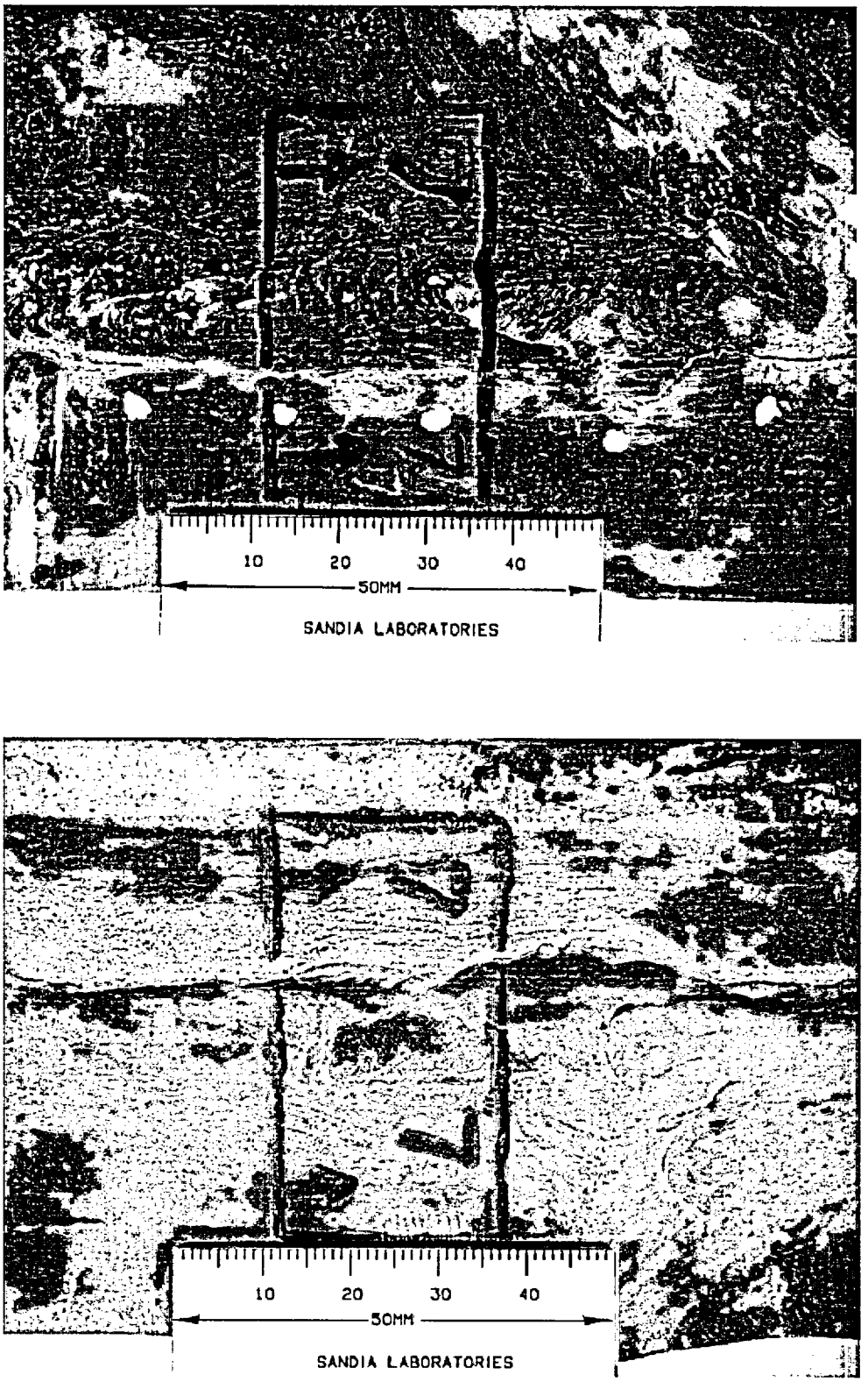

Figure 60. Details of inside (top) and outside (bottom) liner features in region of tear #7 metallographic cross-section (arrows begin at plane of section and indicate view direction).

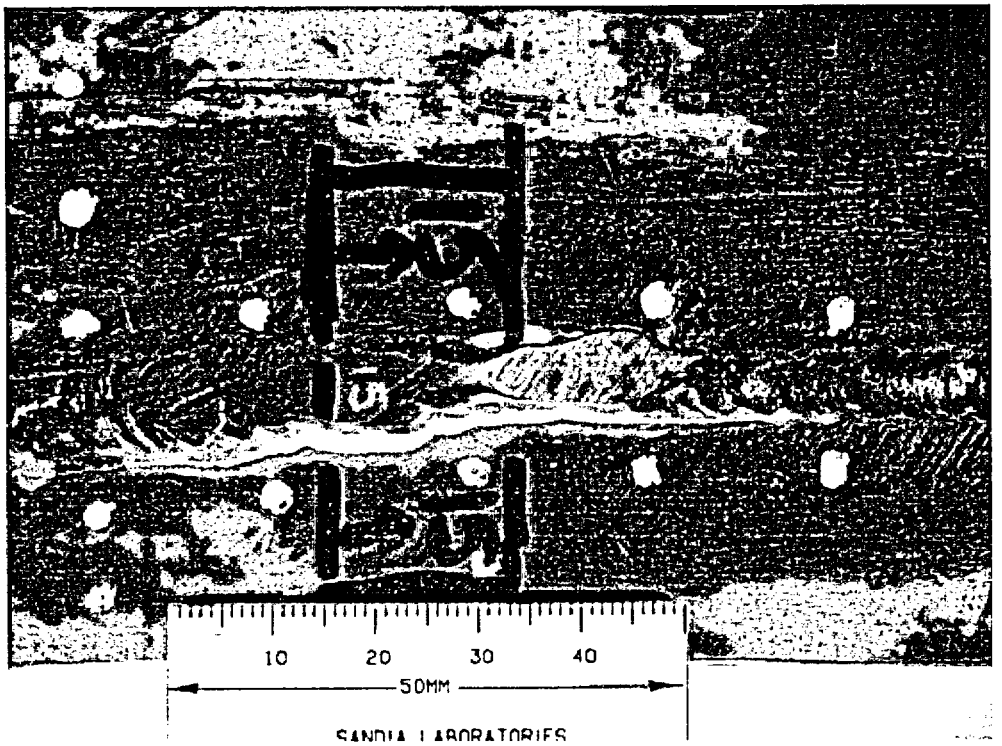

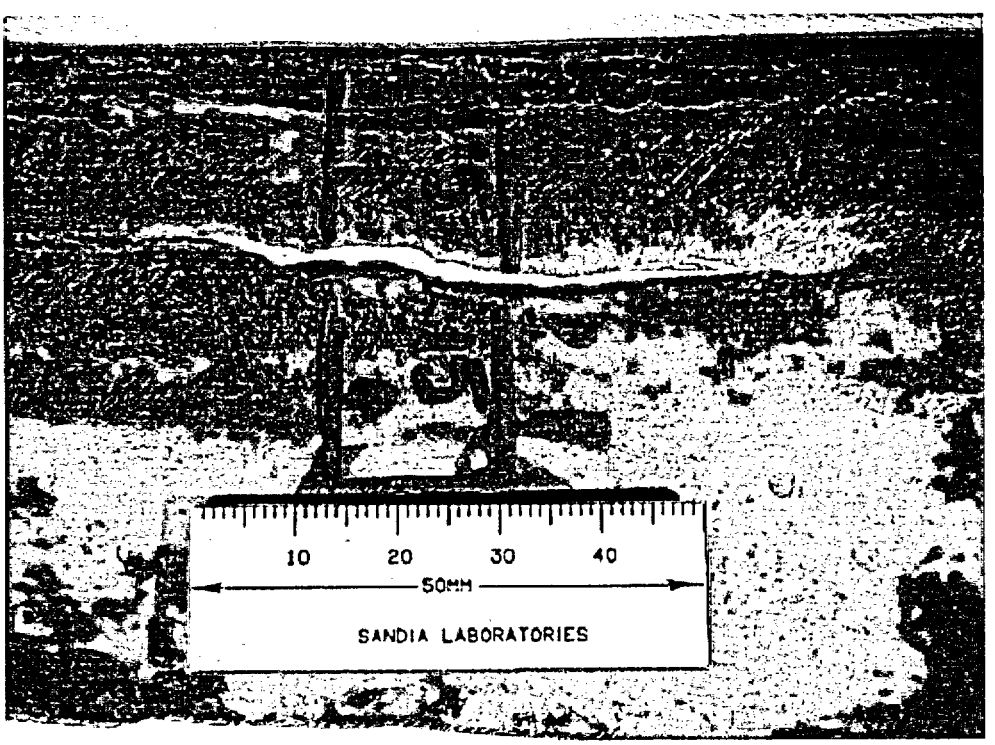

Figure 61. Details of inside (top) and outside (bottom) liner features in region of tear #15 metallographic cross-section (arrows begin at plane of section and indicate view direction).

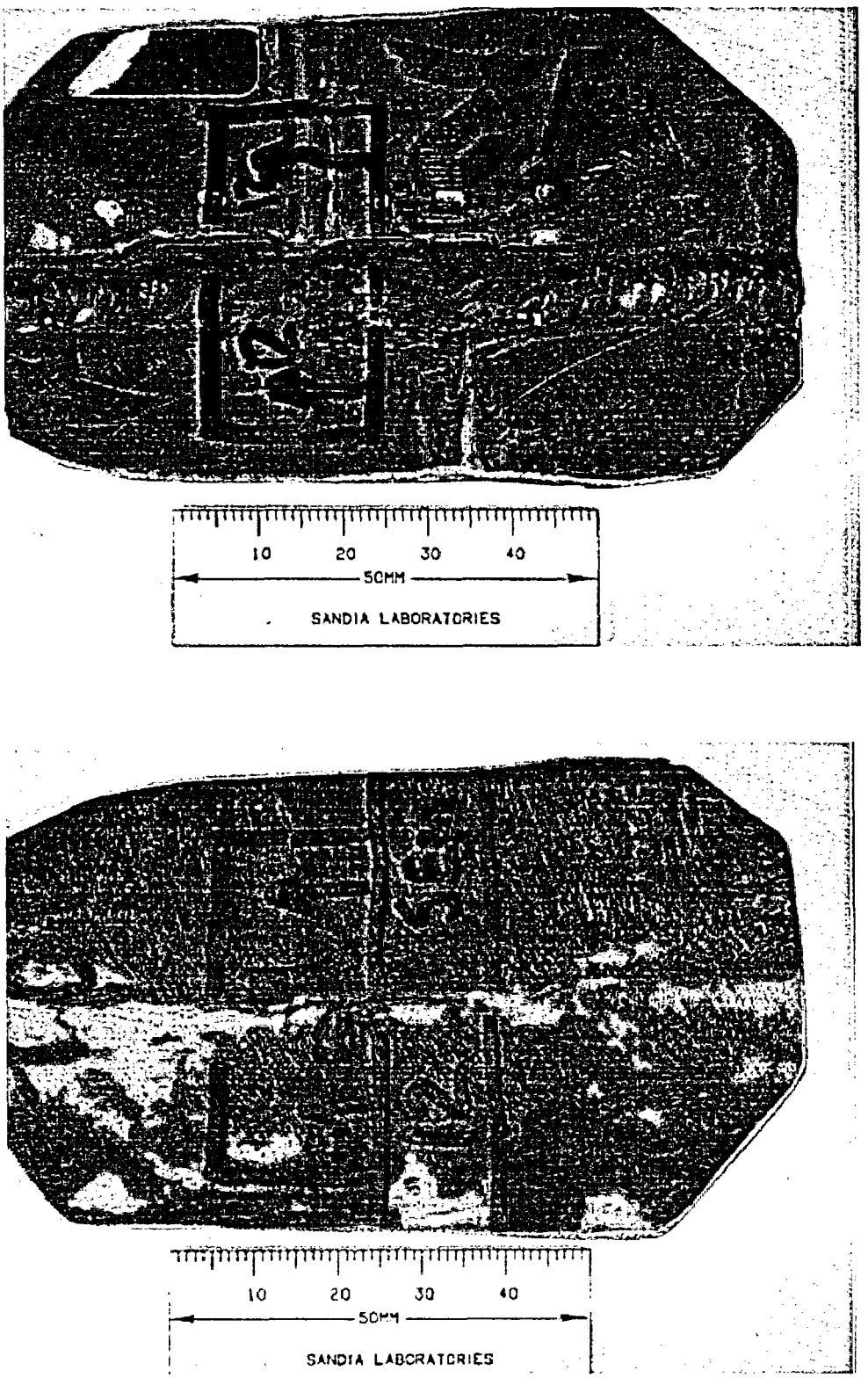

Figure 62. Details of inside (top) and outside (bottom) liner features in region of tear #12 metallographic cross-section (arrows begin at plane of section and indicate view direction). Location of SEM fractographic sample is also shown.

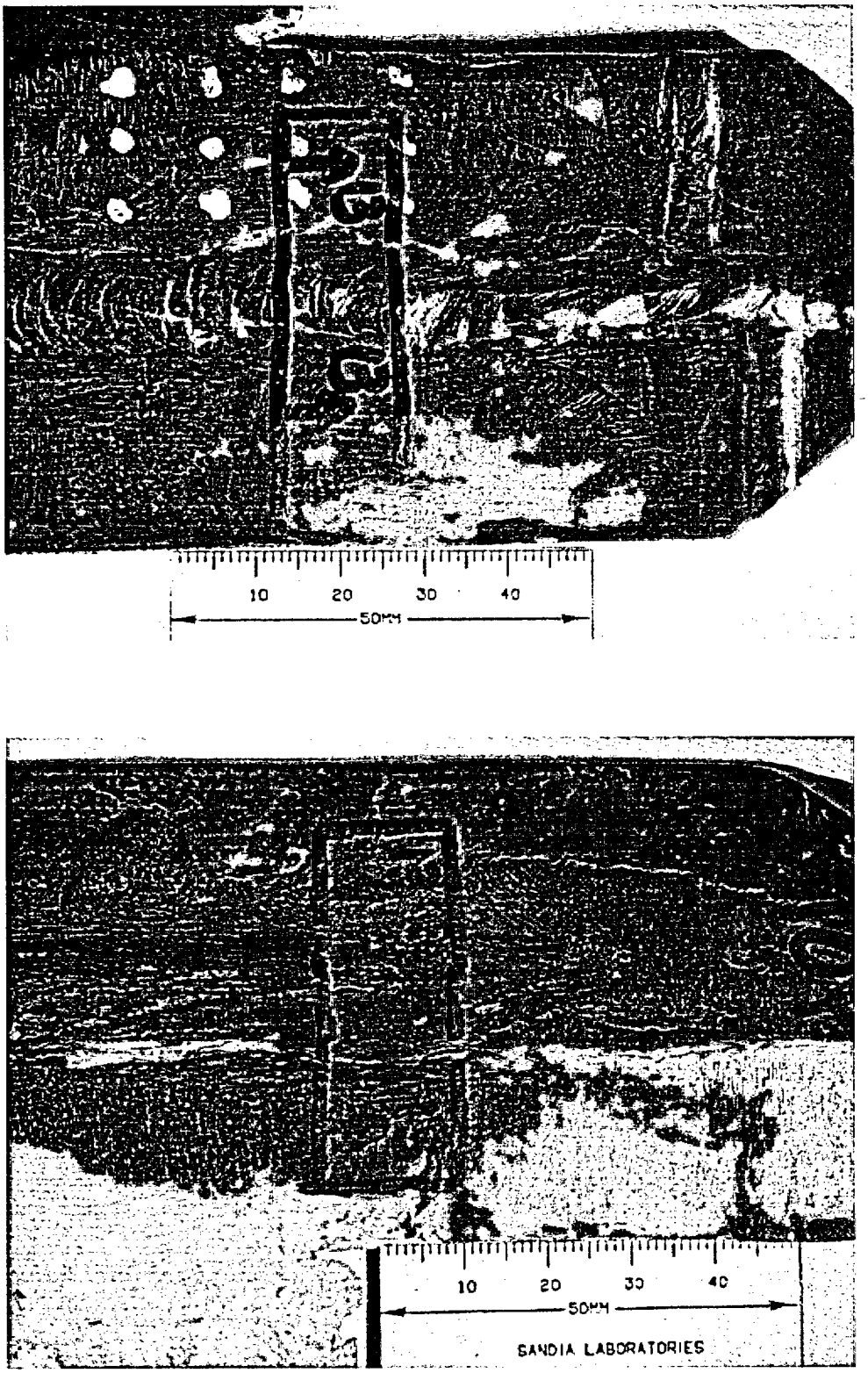

Figure 63. Details of inside (top) and outside (bottom) liner features in region #18-1 metallographic cross-section (arrows begin at plane of section and indicate view direction).

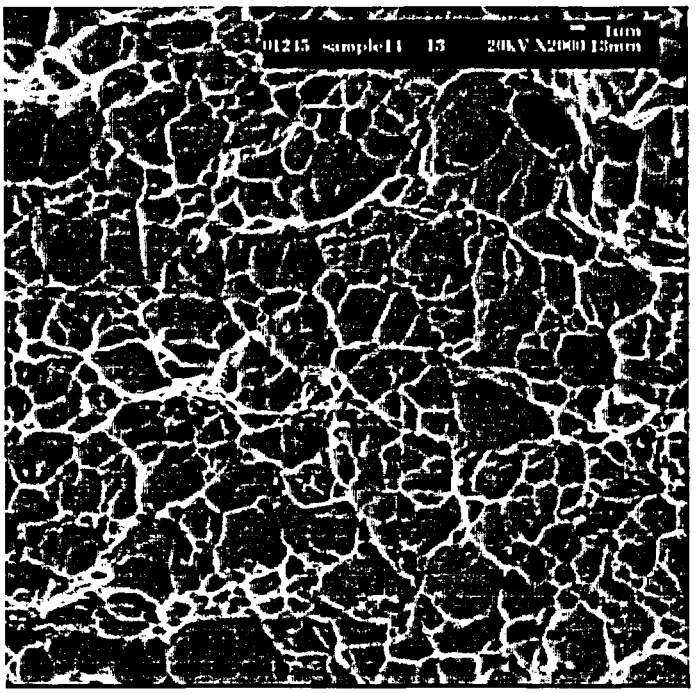

Figure 64. Scanning electron micrograph of fracture surface from tear #14-2. Failure occurred by ductile rupture, as was seen on fracture surfaces from tensile samples shown in Figures 42-44.

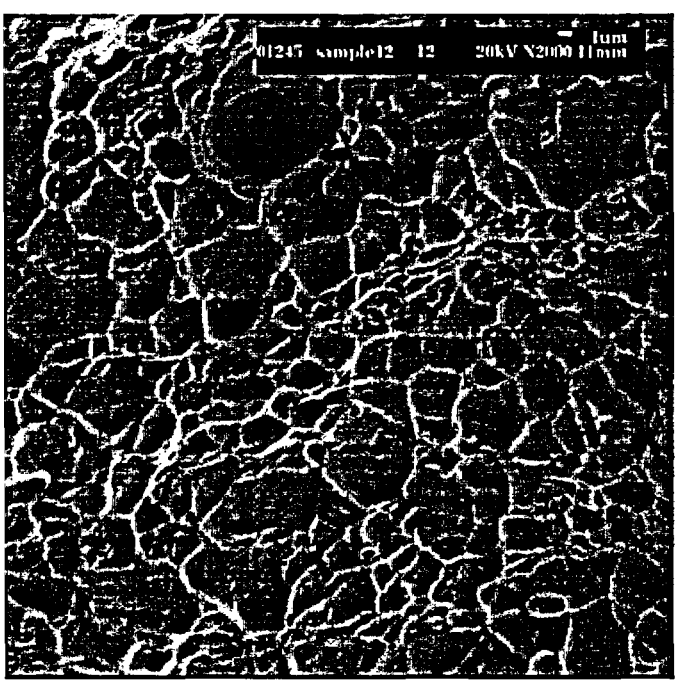

Figure 65. Scanning electron micrograph of fracture surface from tear #12. Failure occurred by ductile rupture, as was seen on fracture surfaces from tensile samples shown in Figures 42-44.

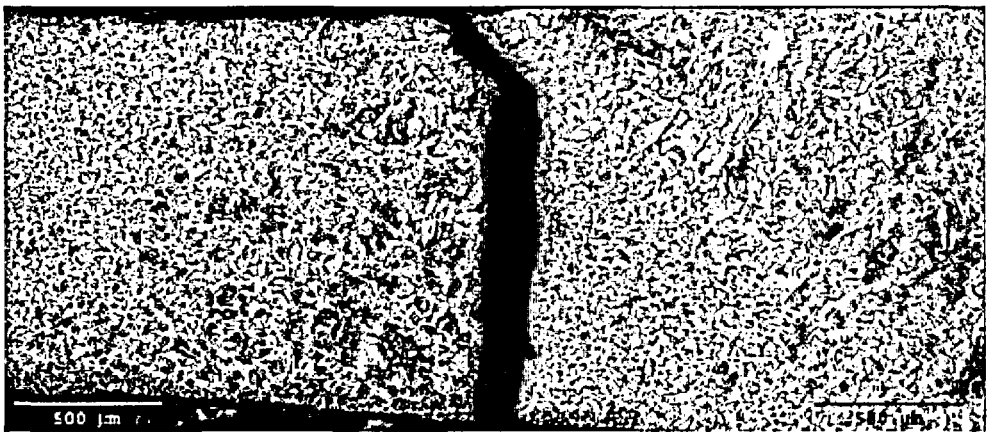

Figure 66. Metallographic cross section of tear #1. This cross section was taken at the location of widest crack opening, corresponding to where the tear apparently initiated. Note that the opening is flat and perpendicular to the liner circumference, and that the microstructure is not continuous across the separation. The "fracture" surfaces were also covered with a layer of foreign material (too dark to be seen here). These features indicate that this area represents a lack of fusion defect, i.e., a region in which the repair weld failed to bridge the gap being welded.

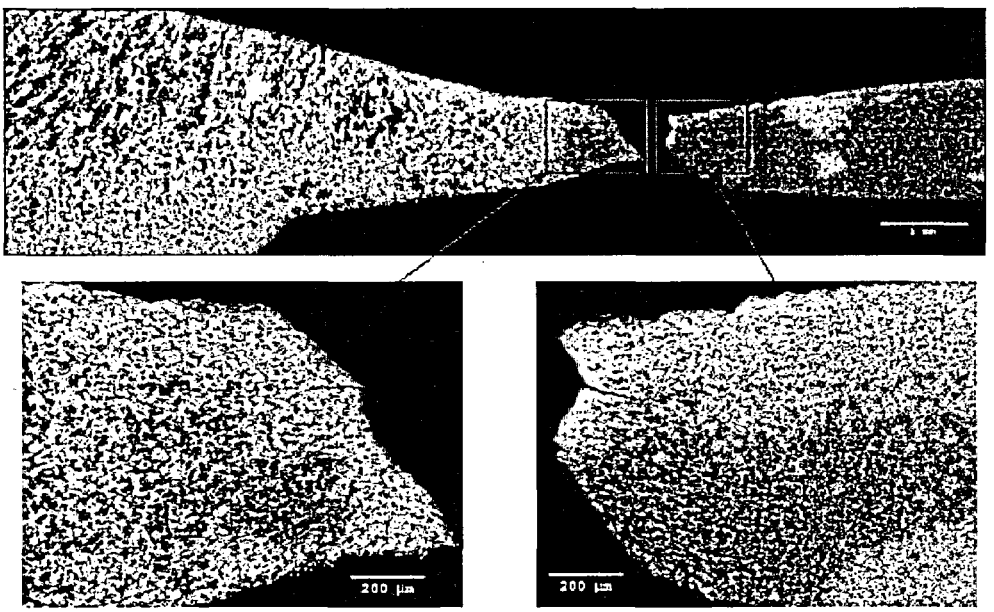

Figure 67. Metallographic cross section of tear #1 approximately 2 cm distant from the cross section shown in Figure 66. Note that failure occurred by more typical shear, and that microstructure shows evidence of substantial localized deformation having occurred prior to final separation. This represents an area removed from the lack of fusion defect where liner tearing occurred as the tear grew in length during testing of the structure. Tearing occurred through the fine grained portion of the heat affected zone.

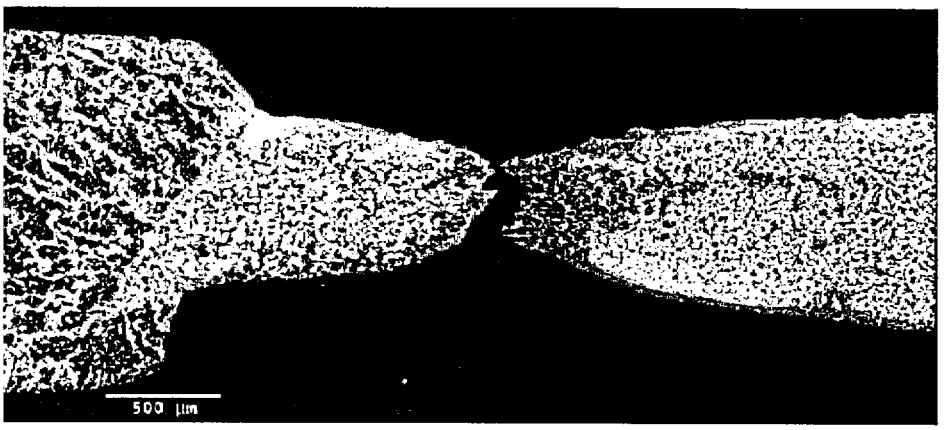

Figure 68. Metallographic cross section of tear #2-1. Tearing occurred in heat affected zone adjacent to repair weld. Note how grinding ends abruptly at edge of fusion zone, providing for measurement of as-ground liner thickness at edge of weld and close to location of tear. Tearing occurred in the adjacent heat affected zone.

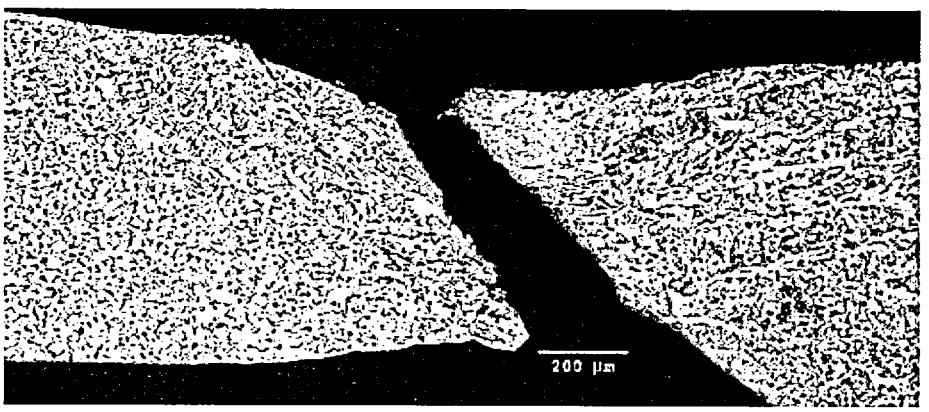

Figure 69. Metallographic cross section of tear #2-2. A very wide region (~29 mm) representing many sequential side-by-side welds was observed in this sample. The fusion zones of many of the early welds had been recrystallized by the heat input from subsequent welds, whereas many of the later welds retained the coarse columnar grain structures characteristic of single pass welds. Tearing occurred in by shear following substantial plastic deformation near the boundary between recrystallized weld metal and a region that could be either unrecrystallized weld metal or coarse grained heat affected zone.

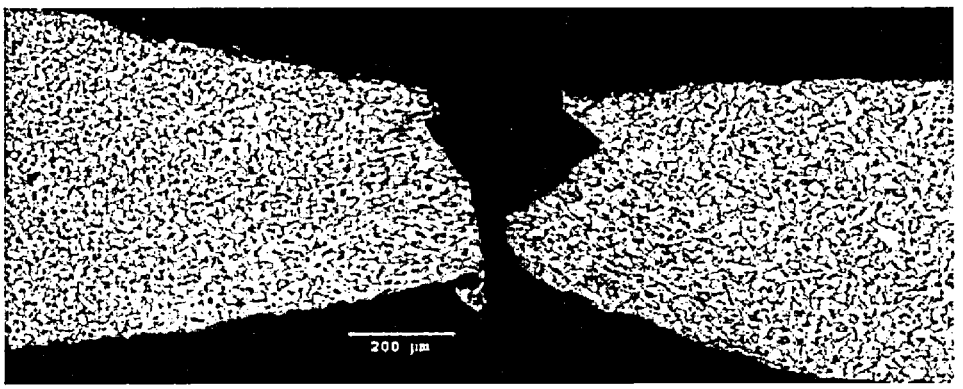

Figure 70. Metallographic cross section of tear #2-3. This sample was similar to #2-2, except that tearing occurred in a completely recrystallized fusion zone of an earlier weld. A portion of the fracture appears to have been mashed flat; this represents an artifact which occurred during unloading or when samples were being removed from the liner.

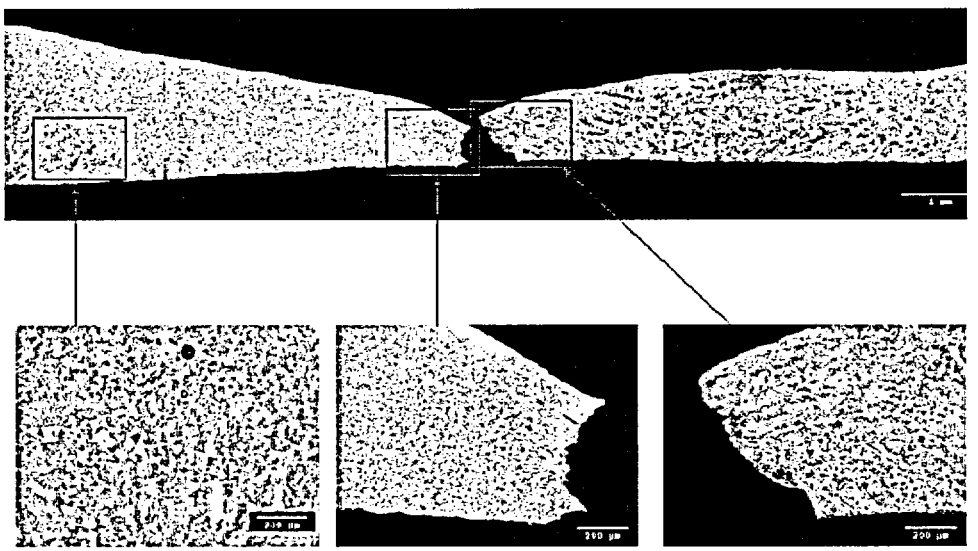

Figure 71. Metallographic cross section of tear #4-1. This sample was similar to #2-2, except that the region of sequential side-by-side welds was even wider, approximately 51 mm. Tearing occurred in an area of mixed recrystallized and unrecrystallized weld metal, and was accompanied by substantial localized plastic deformation.

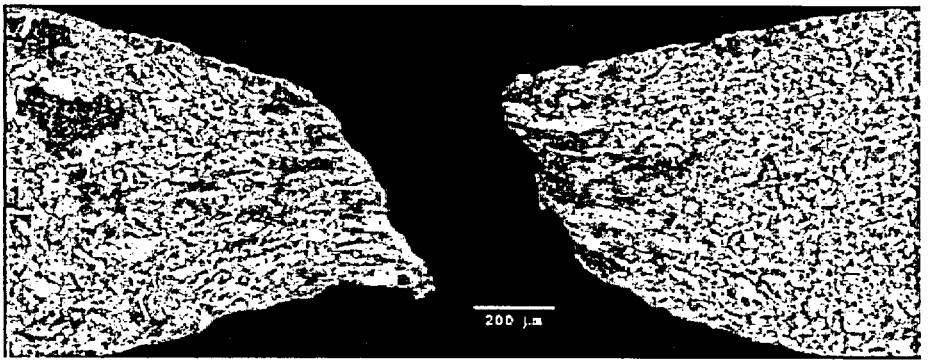

Figure 72. Metallographic cross section of tear #4-3. This sample contained the primary weld and several associated repair welds, plus a second weld approximately 25 mm in from the primary weld. This secondary weld was apparently made to repair the liner where it had been ground through when repairs were being made to the primary weld. Tearing occurred in a coarse grained region of heat affected zone between these two welds, and was preceded by extensive plastic deformation.

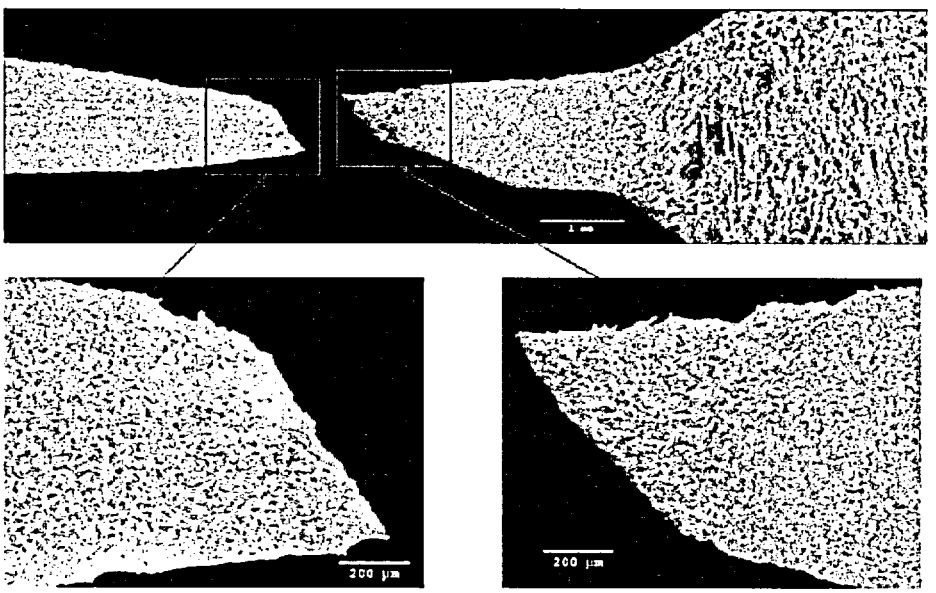

Figure 73. Metallographic cross section of tear #6-2. This sample contained a single repair weld. Grinding on the outside surface ended fairly abruptly at the edge of the back-up bar, resulting in a fairly deep but narrow region of liner thinning. Tearing occurred in the heat affected zone adjacent to the weld, and was accompanied by substantial localized plastic deformation.

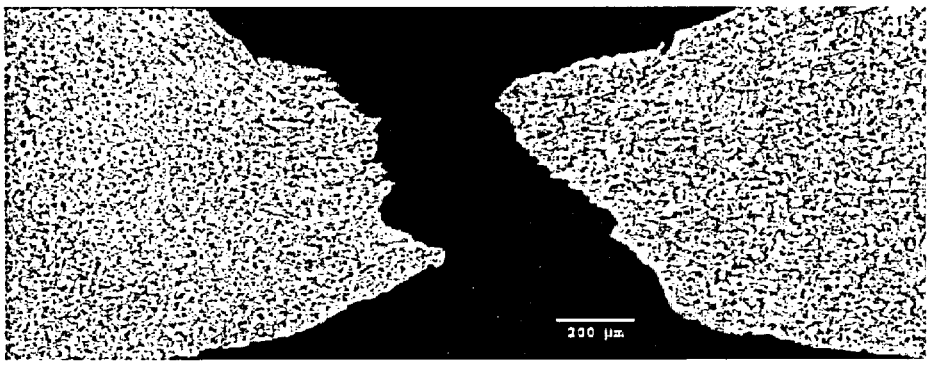

Figure 74. Metallographic cross section of tear #8-1. This sample contained a single repair weld surrounded by a region of recrystallized weld metal representing the original weld. Tearing occurred in either the recrystallized weld metal or the heat affected zone adjacent to the weld, and was accompanied by substantial localized plastic deformation.

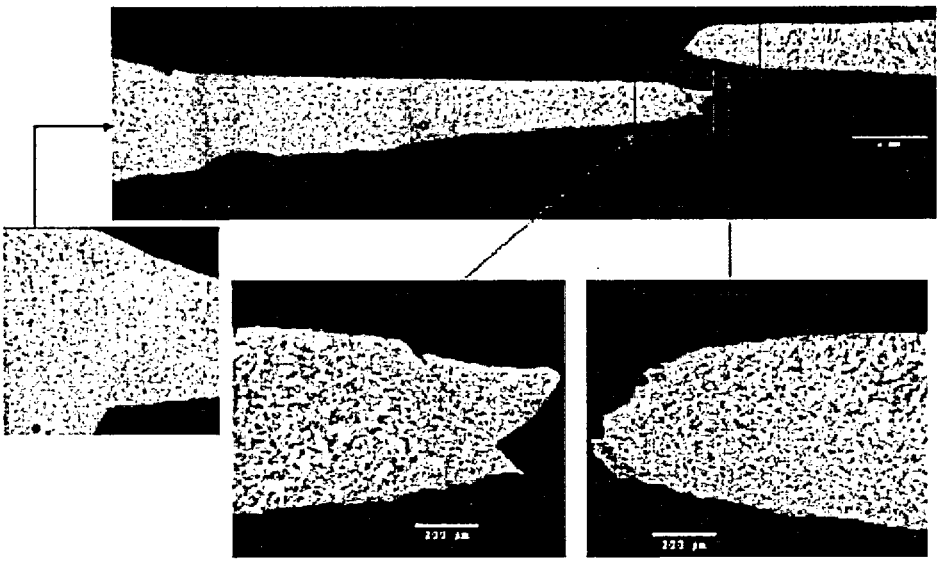

Figure 75. Metallographic cross section of tear #8-2. This sample contained the primary weld, plus a second weld approximately 13 mm in from the primary weld. This secondary weld was apparently made to repair the liner where it had been ground through when repairs were being made to the primary weld, similar to sample #4-3. Tearing occurred adjacent to the secondary weld in what appears to be recrystallized weld metal. Substantial localized plastic deformation accompanied tearing.

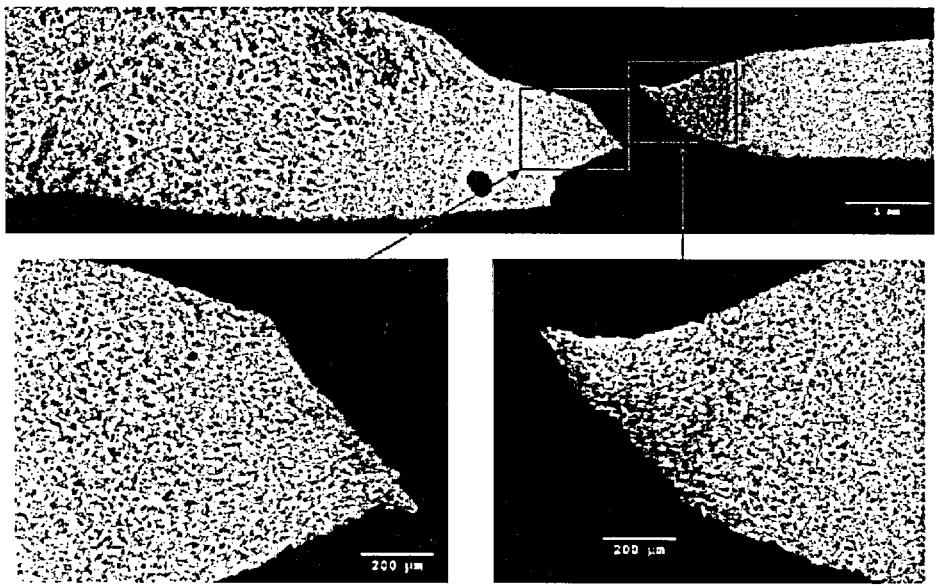

Figure 76. Metallographic cross section of tear #9. This sample contained a single repair weld. Grinding on the outside surface ended abruptly at the edge of the back-up bar, resulting in a deep but narrow region of liner thinning. Tearing occurred in the heat affected zone adjacent to the weld, and was accompanied by substantial localized plastic deformation.

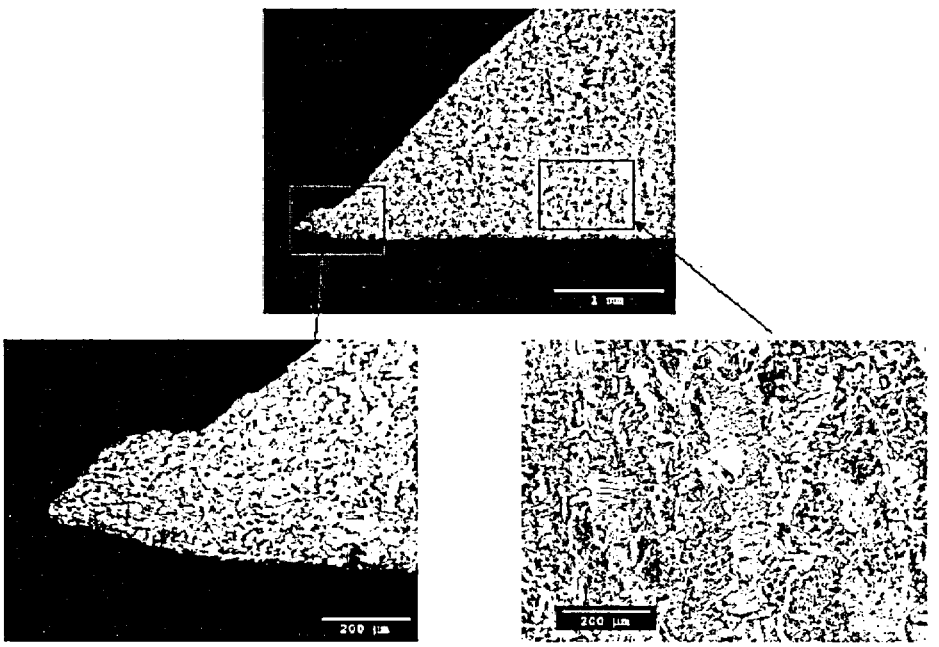

Figure 77. Metallographic cross section of tear #17. This shows the fusion zone of the primary weld, plus the tear adjacent to it. The tear appears to have occurred in a region of recrystallized weld metal from a previous weld. Tearing was accompanied by substantial localized plastic deformation.

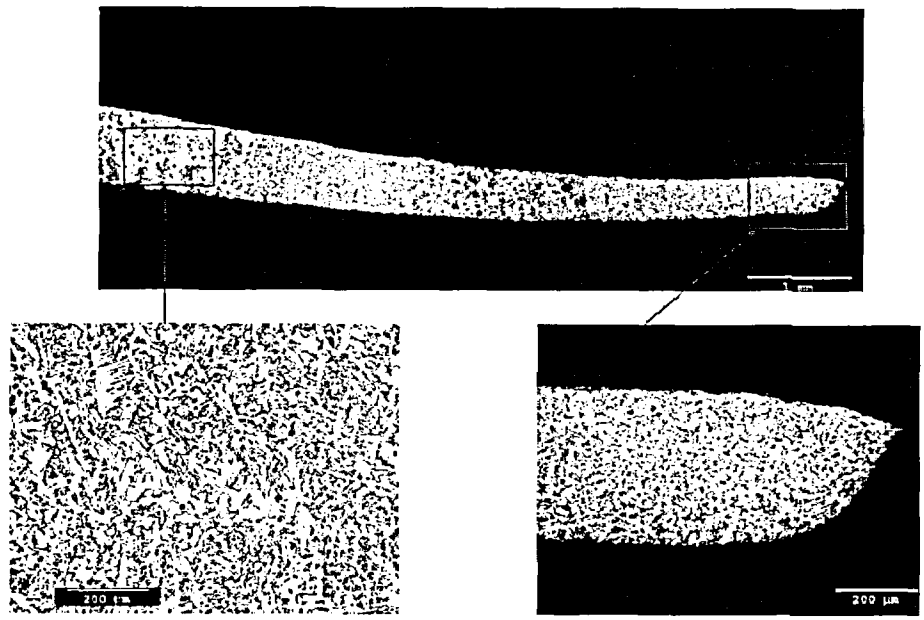

Figure 78. Region of tear #17 adjacent to that shown in Figure 77. Note columnar fusion zone at left; this corresponds to a secondary weld made to repair the liner where it had been ground through when repairs were being made to the primary weld, similar to samples #4-3 and #8-2. Note that the liner thickness was greatly reduced by grinding over the entire region pictured here.

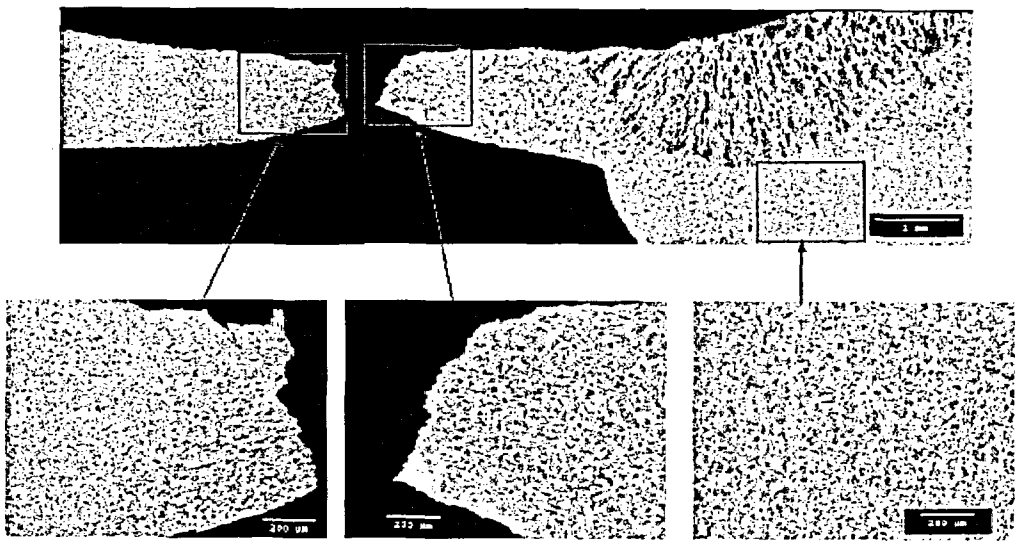

Figure 79. Metallographic cross section of tear #7. Columnar grained region represents repair weld; underlying recrystallized region represents earlier weld. Tearing occurred in heat affected zone adjacent to weld. Less shear and localized deformation appears characteristic of this tear, suggesting that it may have occurred due to more complex stresses.

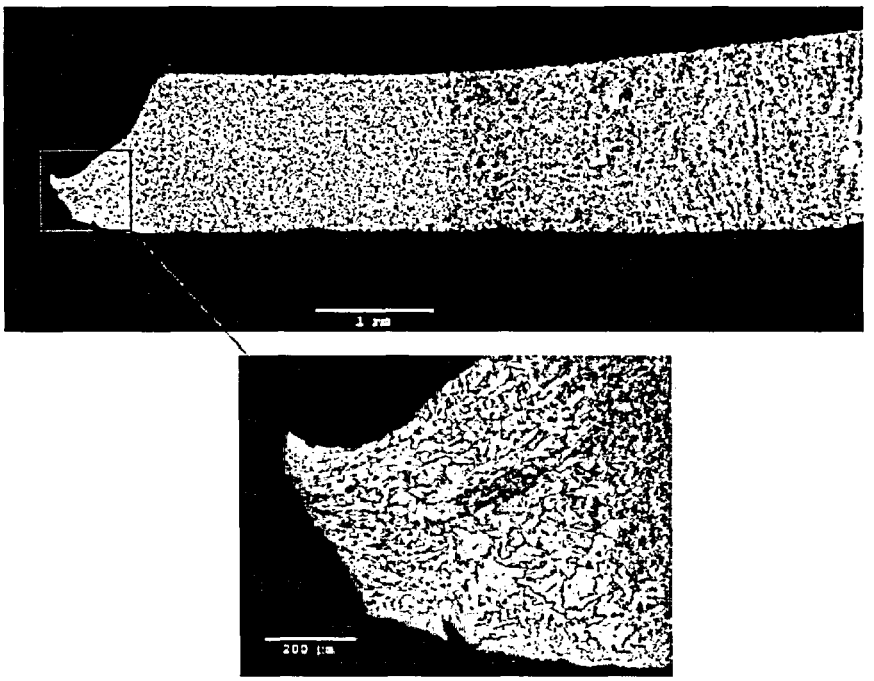

Figure 80. Metallographic cross section of tear #15. Region at right is columnar fusion zone of repair weld. Region at left is recrystallized fusion zone of former weld. Tear (at far left) occurred just left of where recrystallization stopped, either in unrecrystallized weld metal or coarse grained heat affected zone.

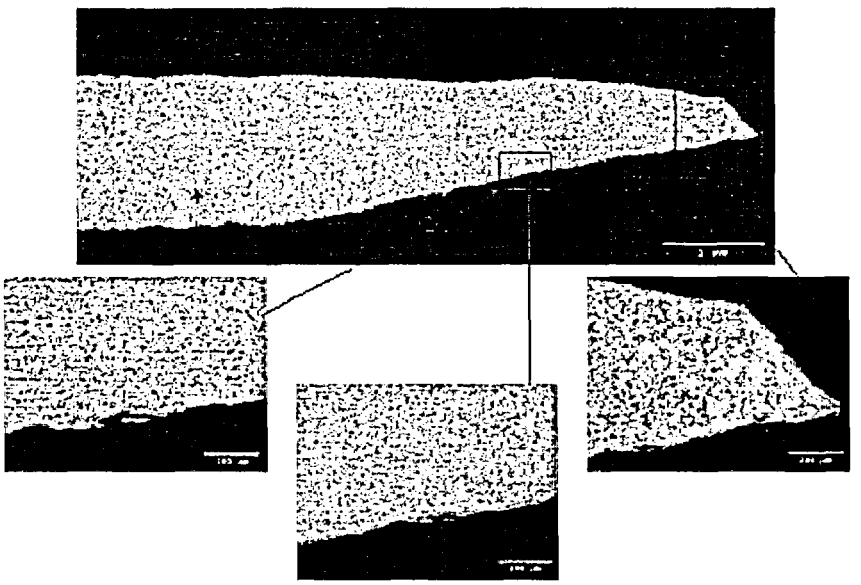

Figure 81. Region of tear #15 adjacent to that shown in Figure 80. Tear (at far right) occurred in coarse grained portion of heat affected zone. Note substantial angle between surface and segregation bands in metal, indicative of grinding in tapered area.

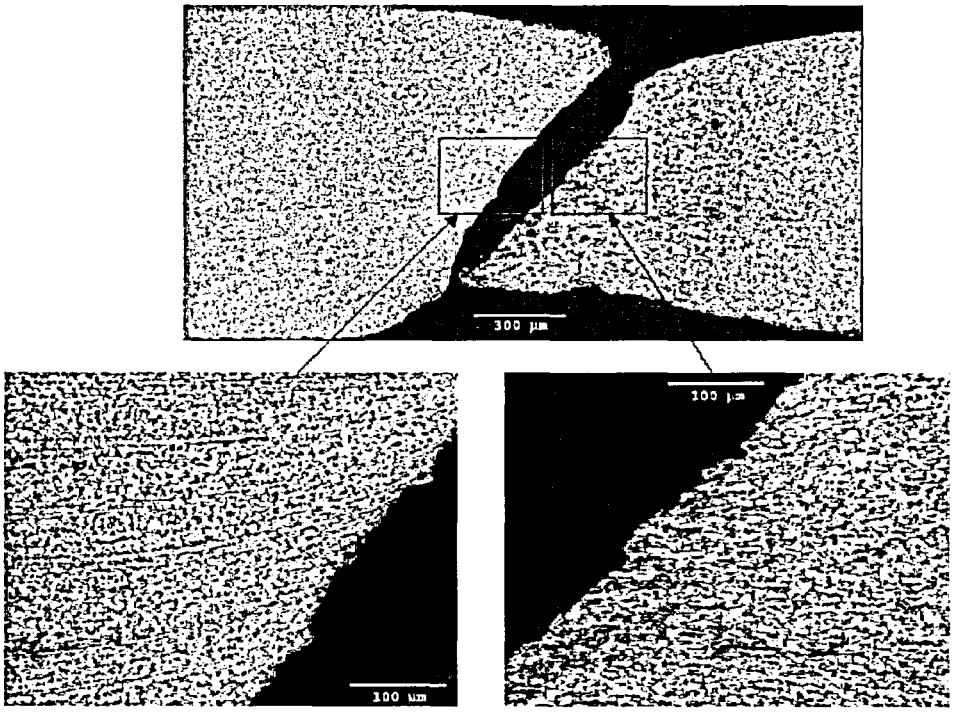

Figure 82. Metallographic cross section of tear #12. Tearing occurred in base metal (or perhaps far out in fine grained portion of heat affected zone). Note that two halves do not match perfectly across tear; this results in uncertainty regarding the amount of grinding done.

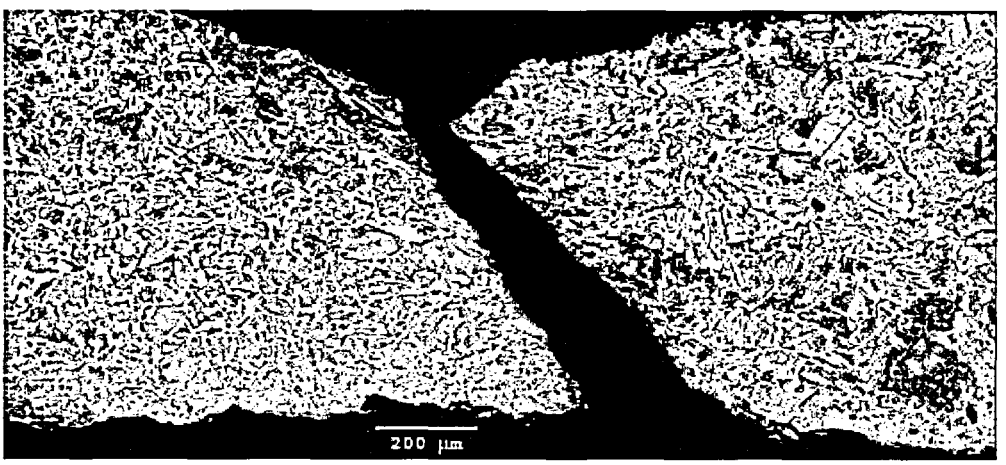

Figure 83. Metallographic cross section of tear #13. Tearing occurred in coarse grained portion of heat affected zone).

Determination of Grinding Reduction

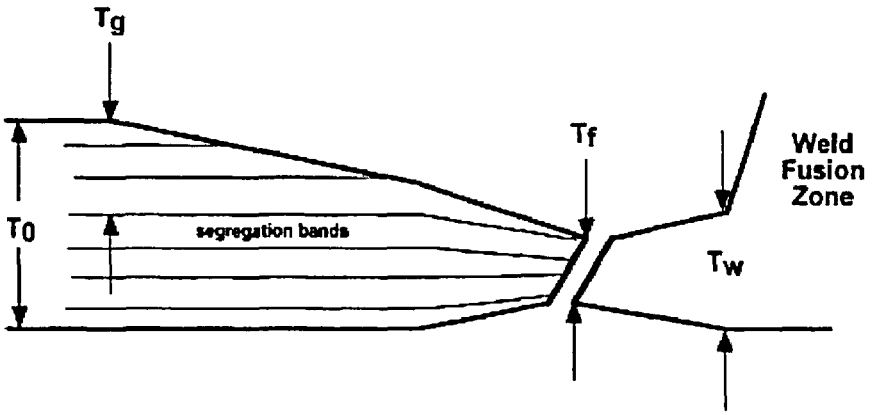

Thickness at Tear: % Grinding = $((T_0 - T_f/0.51) / T_0) \times 100$

Thickness at Weld: % Grinding = $((T_0 - T_w) / T_0) \times 100$

Segregation Bands: % Grinding = $(T_g / T_0) \times 100$

Figure 84. Illustration of three methods used to estimate extent of liner thickness reduction due to grinding from metallographic cross sections.

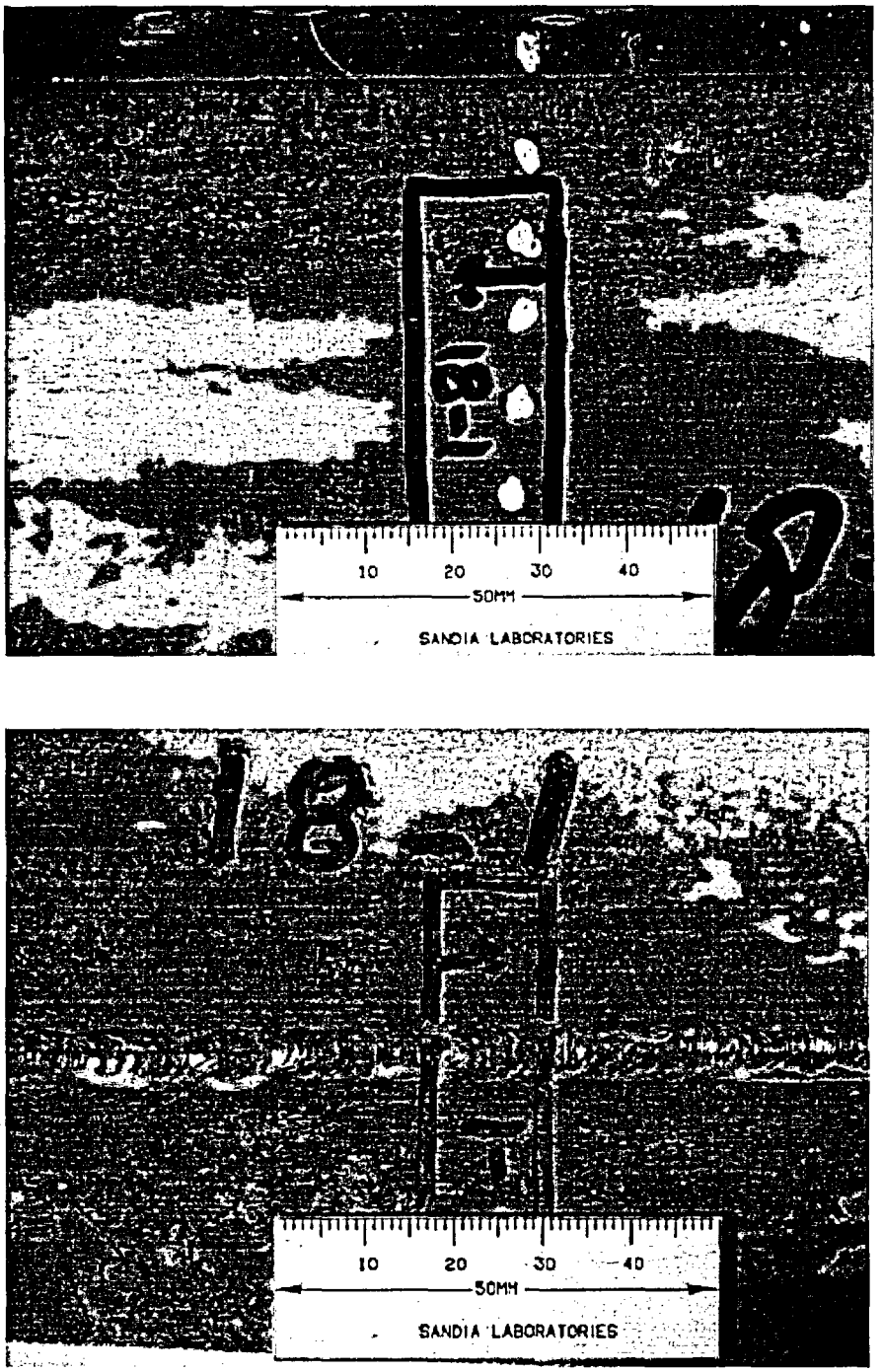

Figure 85. Details of inside (top) and outside (bottom) liner features in region #18-1 metallographic cross-section (arrows begin at plane of section and indicate view direction).

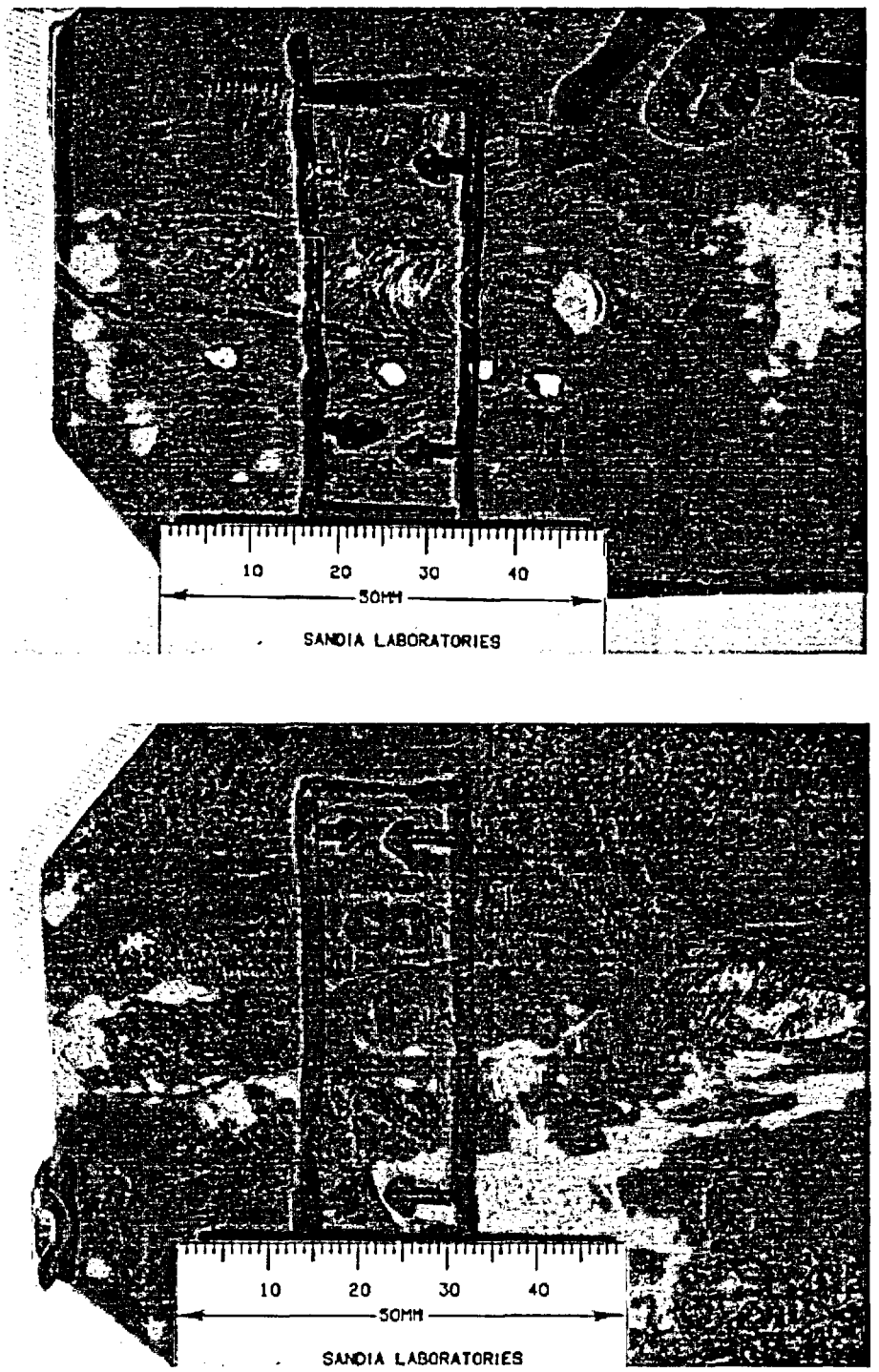

Figure 86. Details of inside (top) and outside (bottom) liner features in region #18-2 metallographic cross-section (arrows begin at plane of section and indicate view direction).

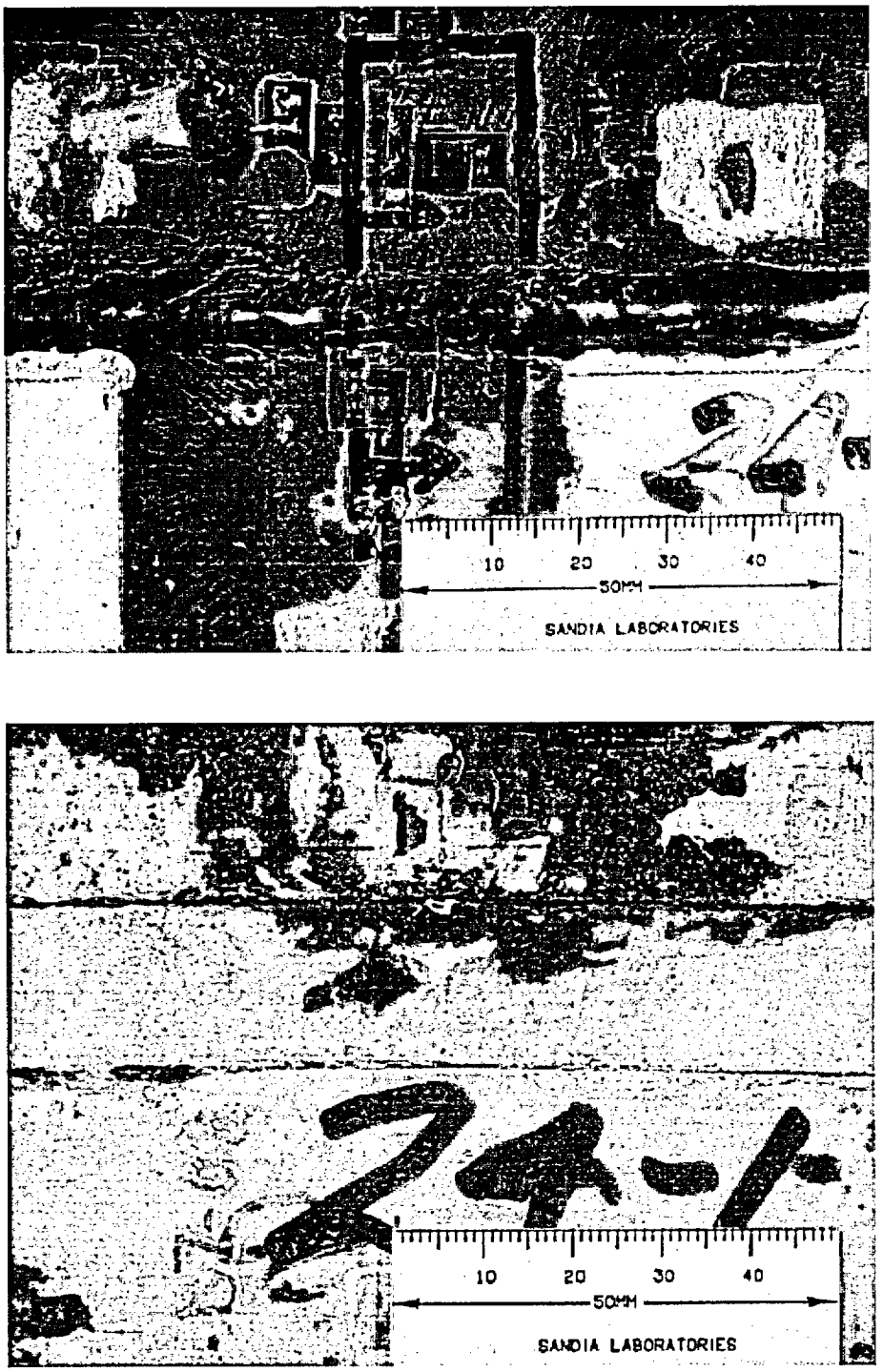

Figure 87. Details of inside (front) and outside (back) liner features in region #24-2 metallographic cross-section (arrows begin at plane of section and indicate view direction).

Figure 88. Details of inside (front) and outside (back) liner features in region #24-1 metallographic cross-section (arrows begin at plane of section and indicate view direction).

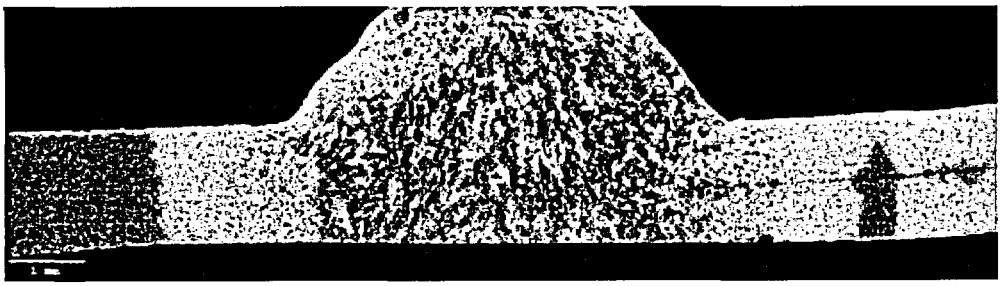

Figure 89. Metallographic cross section of region #18-1. Plastic deformation, but no tearing, occurred in this region. No evidence of repair welding or substantial grinding was found in this area.

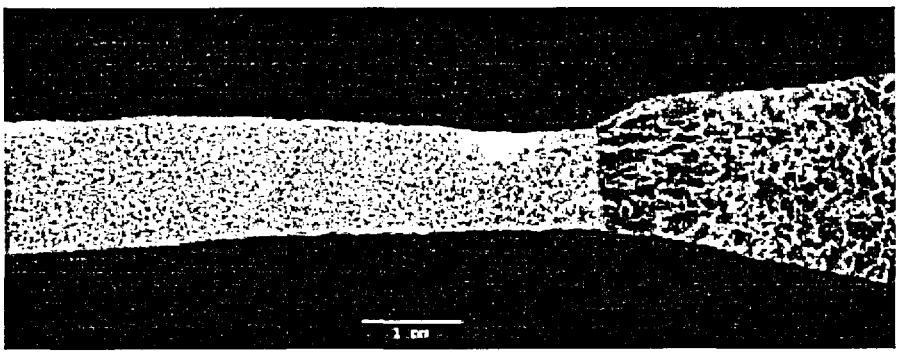

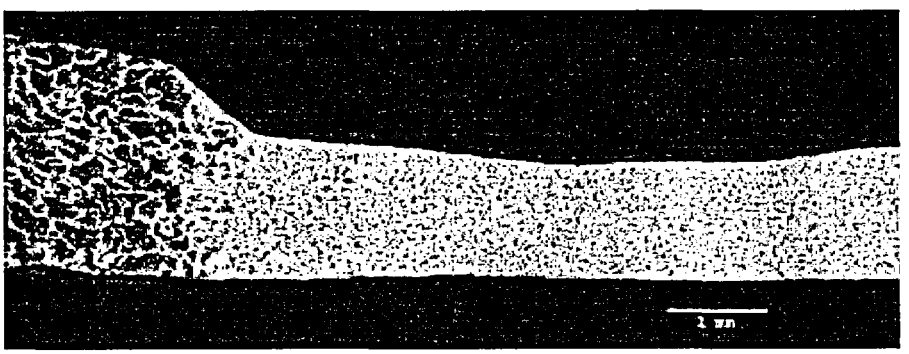

Figure 90. Metallographic cross section of region #18-2. Plastic deformation, but no tearing, occurred in this region. Evidence of repair welding and an undetermined amount of grinding was found in this area.

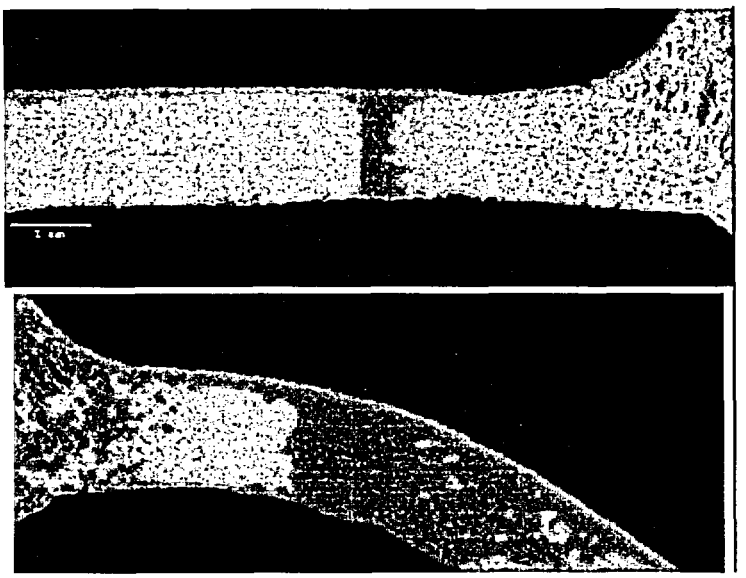

Figure 91. Metallographic cross section of region #24-2, where strain gauges recorded local strain of approximately 7%. No evidence of repair welding or substantial grinding was found in this area. Detailed observation of the surface "depressions" to the left of the weld suggested that they may correspond to surface defects in the plate. In particular, the bottom depression was filled with non-metallic particles, perhaps rolled-in oxide (too dark to be visible on this photo). These depressions may also correspond to the early stages of necking.

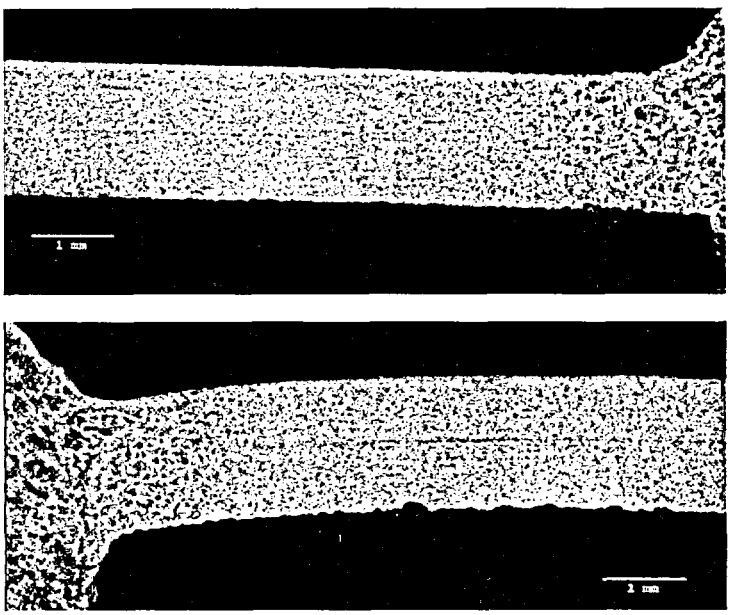

Figure 92. Metallographic cross section of region #24-1. Plastic deformation, but no tearing, occurred in this region. No evidence of repair welding or substantial grinding was found in this area.

NRC FORM 335 (2-89) NRCM 1102, 3201, 3202

U.S. NUCLEAR REGULATORY COMMISSION

BIBLIOGRAPHIC DATA SHEET

(See instructions on the reverse)

1. REPORT NUMBER (Assigned by NRC, Add Vol., Supp.. Rev., and Addendum Numbers, if any)
NUREG/CR-6810
SAND2003-0840P

2. TITLE AND SUBTITLE

Overpressurization Test of a 1:4-Scale Prestressed Concrete Containment Vessel Model

3. DATE REPORT PUBLISHED

MONTH	YEAR
March	2003

4. FIN OR GRANT NUMBER

Y6131

5. AUTHOR(S)

Hessheimer, M. F., Klamerus, E. W., Lambert, L. D., Rightley, G. S., Dameron, R. A.

6. TYPE OF REPORT

Technical

7. PERIOD COVERED *(inclusive Dates)*

6/91 to 6/02

8. PERFORMING ORGANIZATION – NAME AND ADDRESS *(If NRC, provide Division, Office or Region, U.S. Nuclear Regulatory Commission, and mailing address; if contractor, provide name and mailing address.)*

Sandia National Laboratories, P.O. Box 5800, Albuquerque, NM, 87185-0744

9. SPONSORING ORGANIZATION – NAME AND ADDRESS *(If NRC, type "Same as above", if contractor, provide NRC Division, Office or Region, U.S. Nuclear Regulatory Commission, and mailing address.)*

Nuclear Power Engineering Corporation
Systems Safety Department
Tokyo 105, Japan
under FIA DE-FI04-91-AL73734

Division of Engineering Technology
Office of Nuclear Regulatory Research
U. S. Nuclear Regulatory Commission
Washington, DC 20555-0001

10. SUPPLEMENTARY NOTES

NUPEC Project Manager: S. Shibata

NRC Project Manager: J. F. Costello

11. ABSTRACT *(200 words or less)*

The Nuclear Power Engineering Corporation (NUPEC) of Japan and the U.S. Nuclear Regulatory Commission (NRC), Office of Nuclear Regulatory Research, co-sponsored a Cooperative Containment Research Program. Overpressure tests of a prestressed concrete containment vessel (PCCV) model began in July 2000, culminating in a functional failure mode or Limit State Test (LST) in September 2000 and a Structural Failure Mode Test (SFMT) in November 2001. The PCCV model, uniformly scaled at 1:4, is representative of the containment structure of an actual Pressurized Water Reactor (PWR) plan (OHI-3) in Japan. The objectives of the internal pressurization tests were to obtain measurement data of the structural response of the model to pressure loading beyond design basis accident in order to validate analytical modeling, to find pressure capacity of the model, and to observe its failure mechanisms.

This report describes the design, construction, instrumentation and testing of the PCCV model. Detailed results of each test and posttest inspections findings are presented and all model response data is provided on the enclosed Data CD.

12. KEY WORDS/DESCRIPTORS *(List words or phrases that will assist researchers in locating the report.)*

Containment
Severe Accidents
Pressure Testing
Finite Element Analysis

13. AVAILABILITY STATEMENT

Unlimited

14. SECURITY CLASSIFICATION

(This Page)
Unclassified

(This Report)
Unclassified

15. NUMBER OF PAGES

16. PRICE

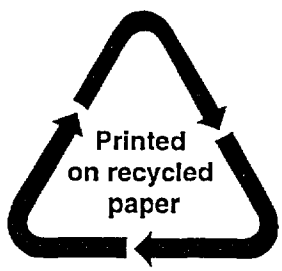

Federal Recycling Program

UNITED STATES
NUCLEAR REGULATORY COMMISSION
WASHINGTON, DC 20555-0001

OFFICIAL BUSINESS
PENALTY FOR PRIVATE USE, $300

(25 copies)

Dr. Costello
T-10 L1